

2003

Laboratory oxide coatings: Physical form and surface chemistry

Kea U. Duckenfield

College of William and Mary - Virginia Institute of Marine Science

Follow this and additional works at: <https://scholarworks.wm.edu/etd>



Part of the [Civil Engineering Commons](#), [Geochemistry Commons](#), and the [Ocean Engineering Commons](#)

Recommended Citation

Duckenfield, Kea U., "Laboratory oxide coatings: Physical form and surface chemistry" (2003).
Dissertations, Theses, and Masters Projects. Paper 1539616635.
<https://dx.doi.org/doi:10.25773/v5-h0kx-m428>

This Dissertation is brought to you for free and open access by the Theses, Dissertations, & Master Projects at W&M ScholarWorks. It has been accepted for inclusion in Dissertations, Theses, and Masters Projects by an authorized administrator of W&M ScholarWorks. For more information, please contact scholarworks@wm.edu.

**LABORATORY OXIDE COATINGS:
PHYSICAL FORM AND SURFACE CHEMISTRY**

A Dissertation

Presented to

**The Faculty of the School of Marine Science
The College of William and Mary in Virginia**

In Partial Fulfillment

**Of the Requirements for the Degree of
Doctor of Philosophy**

by

Kea U. Duckenfield

2003

APPROVAL SHEET

This dissertation is submitted in partial fulfillment of

the requirements for the degree of

Doctor of Philosophy



Kea Umstatt Duckyfield

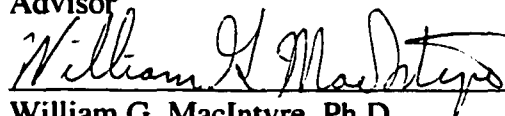
Approved, January, 2003



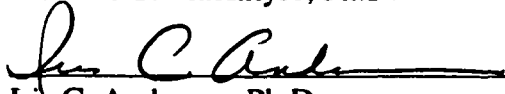
Rebecca M. Dickhut, Ph.D.
Committee Chairman/Advisor



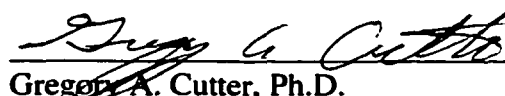
Catherine J. Chisholm-Brause, Ph.D.
Advisor



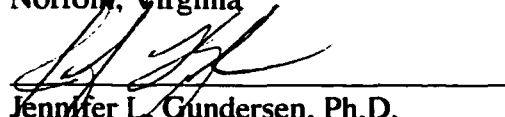
William G. MacIntyre, Ph.D.



Iris C. Anderson, Ph.D.



Gregory A. Cutter, Ph.D.
Old Dominion University
Norfolk, Virginia



Jennifer L. Gundersen, Ph.D.
U.S.E.P.A. Environmental Science Center
Fort Meade, Maryland

To Paul

Ithaka

C.P. Cavafy*

As you set out for Ithaka
hope your road is a long one,
full of adventure, full of discovery.
Laistrygonians, Cyclops,
angry Poseidon – don't be afraid of them:
you'll never find things like that on your way
as long as you keep your thoughts raised high,
as long as a rare excitement
stirs your spirit and your body.
Laistrygonians, Cyclops,
wild Poseidon – you won't encounter them
unless you bring them along inside your soul,
unless your soul sets them up in front of you.

Hope your road is a long one.
May there be many summer mornings when,
with what pleasure, what joy,
you enter harbors you're seeing for the first time;
may you stop at Phoenician trading stations
to buy fine things,
mother of pearl and coral, amber and ebony,
sensual perfumes of every kind –
as many sensual perfumes as you can;
and may you visit many Egyptian cities
to learn and go on learning from their scholars.

Keep Ithaka always in your mind.
Arriving there is what you're destined for.
But don't hurry the journey at all.
Better if it lasts for years,
so you're old by the time you reach the island,
wealthy with all you've gained on the way,
not expecting Ithaka to make you rich.

Ithaka gave you the marvelous journey.
Without her you wouldn't have set out.
She has nothing left to give you now.

And if you find her poor, Ithaka won't have fooled you.
Wise as you will have become, so full of experience,
you'll have understood by then what these Ithakas mean.

* From *C.P. Cavafy: Collected Poems*, ed. George Savadis (Princeton: Princeton University Press), 67-68.
Translation copyright 1975 by Edmund Keeley and Philip Sherrard.

TABLE OF CONTENTS

	Page
ACKNOWLEDGEMENTS.....	v
LIST OF TABLES.....	vi
LIST OF FIGURES.....	vii
LIST OF EQUATIONS.....	xi
ABSTRACT.....	xii
CHAPTER 1: INTRODUCTION.....	2
CHAPTER 2: PHYSICAL CHARACTERIZATION.....	14
CHAPTER 3: CU(II) SORPTION EXPERIMENTS.....	68
CHAPTER 4: NATURAL SEDIMENTS.....	122
CHAPTER 5: CONCLUSIONS.....	151
APPENDIX 1: BET Data.....	158
APPENDIX 2: EDS Data.....	162
APPENDIX 3: Batch Adsorption/Desorption Data.....	165
APPENDIX 4: Spline Fits	171
APPENDIX 5: Derivation of Partitioning Coefficients for Additive Models.....	175
LITERATURE CITED.....	179
VITA.....	188

ACKNOWLEDGEMENTS

This work was supported by the Dean's Office, the U.S. Environmental Protection Agency STAR Graduate Fellowship Program, the William G. Hargis Fellowship, the VIMS Associate's Scholarship, the VIMS Faculty Mini-grant Program, and the VIMS GSA Mini-grant program. I would particularly like to thank the Graduate Dean's Office and the Dean and Director's Office for their many instances of encouragement and support throughout my course at VIMS. I am profoundly grateful for the teaching, guidance, and mentorship provided by my major professors, Catherine Chisholm-Brause and Rebecca Dickhut. The members of my advisory committee each have given me support and advice in addition to their valuable critiques and suggestions. Field sediments and associated information were graciously provided by Dr. Jessica Kogel of Thiele Kaolin and Dr. John Seaman of the Savannah River Ecology Laboratory. Off-campus research facilities were made available by Dr. Ted Callender and Dr. Edward Landa at the U.S. Geological Survey, Reston, Virginia. Technical assistance and advice were given by many people, most notably Patrice Mason of VIMS's electron microscopy lab, and Carol Skeen, Mike Doughten, and Kathy Conko of the U.S.G.S. Dr. Mark Duckenfield suggested the normalization technique used in all f -plots.

All over VIMS, from the library and publications to grants administration and shipping and receiving, many hours have been sacrificed by many cheerful people to the completion of this degree. I would particularly like to recognize Cynthia Harris and Sue Presson for their years of help and advice. Finally, many thanks to the multitude of people – teachers, colleagues, friends and family – who have made the completion of this dissertation possible in a thousand other ways. It would be impossible to name every one, unfortunately, for they all deserve recognition. Steve Kuehl encouraged me to pursue this degree and has on several occasions helped me in the pursuit. Many fellow students have given advice, help, and companionship, including Ai Ning Loh and Krisa Arzayus. My fellow advisee, Christine Conrad, has been a reliable source of insight, and has unflinchingly helped me out of several tight logistical spots. Katie Farnsworth and Beth Waterson provided months of hospitality and friendly encouragement. Brian Block, Ruby Brown, and LaRynda Thoen spoke saving words at a critical moment. Thanks to my extended family for their enduring and multifaceted support, my parents for their enthusiasm and faith, and my brother Jordan for his calls, letters, and insights; to my sons, Jack and Chad, for their marvelous gifts, especially laughter. And, last and best, to my husband Paul, who has been and done all of the above over the course of a long seven and a half years, and who is simply the best thing that ever happened to me.

LIST OF TABLES

Table	Page
1. Experimental system.....	12
2. Summary of BET analysis.....	39
3. Summary of SSA analysis.....	41
4. Summary of comparison plot analysis.....	43
5. Criteria for evaluating variability of oxide distribution.....	55
6. Descriptive statistics for each solid sample set.....	56
7. Statistical significance of difference in mean %RSD between solids.....	62
8. Similarities in physical adsorption and desorption.....	64
9. Properties of the coated solids.....	71
10. Recipe for 10‰ synthetic estuarine water.....	76
11. Surface coverages bracketing the onset of dominant surface precipitation.....	94
12. N_{max} and log IAP for coated solids.....	97
13. Effect of normalizing sorption data to mass goethite.....	100
14. Summary of the effects of the null hypothesis tests.....	110
15. Characteristics of the natural materials studied.....	127
16. BET analysis of natural materials.....	133
17. t -plot, α -plot, and internal SSA analysis of natural materials.....	133

LIST OF FIGURES

Figure	Page
1. SEM photomicrographs of quartz and kaolinite.....	19
2. Typical BET behavior for N ₂ gas adsorption on a nonporous solid.....	23
3. Gas sorption hysteresis	24
4. Characteristic t- or α -plots.....	27
5. N ₂ adsorption and desorption isotherms for particulate goethite.....	34
6. N ₂ adsorption and desorption isotherms for quartz.....	34
7. N ₂ adsorption and desorption isotherms for kaolinite.....	35
8. N ₂ adsorption and desorption isotherms for K-chem.....	35
9. N ₂ adsorption and desorption isotherms for Q-chem.....	36
10. N ₂ adsorption and desorption isotherms for Kch-thick.....	36
11. Linear ranges and residuals analysis for quartz, kaolinite, and K-chem.....	37
12. Linear ranges and residuals analysis for goethite, Q-chem, and Kch-t _{thick}	38
13. t-plots.....	44
14. Harkins-Jura thickness (t_{HJ}) plots.....	45
15. f-plots : quartz, kaolinite, and goethite to each other and reference silica.....	48
16. f-plots comparing coated solids to their substrates and particulate goethite.....	49
17 f-plots comparing coated solids to each other	50

Figure	Page
18. SEM image and EDS Fe map for Q-chem.....	52
19. SEM image and EDS Fe map for K-chem.....	53
20. SEM image and EDS Fe map for Kch-t _{thick}	54
21. Distribution of $[\text{Fe}]_{\text{substrate}}$ for all spots sampled.....	58
22. Distribution of $[\text{Fe}]_{\text{substrate}}$ for faces vs. edges.....	60
23. Regression analysis of edge vs. face spots on Q-chem grains.....	61
24. Cu(II) speciation in 10‰ SEW at pH 7.4.....	74
25. Cu remaining in solution as a function of elapsed time.....	79
26. Schematic drawings of adsorption isotherms and Langmuir plots.....	82
27. Summary of the tests of the null hypothesis.....	85
28. Changes in θ as a function of loading.....	89
29. Changes in θ as a function of percent blocking.....	90
30. Cu(II) adsorption and desorption isotherms.....	92
31. Langmuir-type plots.....	93
32. Results for uncoated quartz.....	94
33. Desorption hysteresis in Cu sorption by bulk goethite and the coated solids.....	95
34. Inverse Langmuir-type plots and derivation of N_{max}	96
35. Adsorption isotherms normalized to the mass of goethite in the system.....	99
36. Directions in which the null hypothesis corrections work.....	101
37. Results of physical corrections to Q-chem.....	104
38. Results of physical corrections to Q-phys.....	105
39. Results of physical corrections to K-chem.....	106

Figure	Page
40. Results of physical corrections to K-phys.....	107
41. Results of Cu(II) sorption by coated solids in comparison to bulk goethite.....	110
42. N ₂ adsorption-desorption isotherms for crude kaolin and clean kaolinite.....	129
43. Residuals for crude kaolin and cleaned kaolinite.....	130
44. <i>t</i> -plots and Harkins-Jura thickness plots for crude kaolin and cleaned kaolinite.....	131
45. <i>f</i> -plot of crude kaolin vs. cleaned kaolinite.....	131
46. <i>f</i> -plots of crude kaolin and cleaned kaolinite vs. reference material and chemical coatings.....	132
47. N ₂ adsorption isotherms for subsurface material and surface soil.....	135
48. Residuals for subsurface material and surface soil.....	136
49. <i>t</i> -plots and Harkins-Jura thickness plots for subsurface material, surface soil, and bulk goethite.....	137
50. <i>f</i> -plot comparisons of crude kaolin, subsurface material, and surface soil to a nonporous reference material, quartz and kaolinite, and bulk goethite.....	138
51. <i>f</i> -plot comparisons of crude kaolin, subsurface material, and surface soil to Q-chem, K-chem, Kch-thick, and each other.....	139
52. Cu(II) adsorption isotherms and Langmuir plots for crude kaolin and cleaned kaolinite.....	140
53. Sorption hysteresis in crude kaolin and cleaned kaolinite.....	141
54. Comparisons of sorption-related quantities for cleaned kaolinite and crude kaolin relative to bulk goethite.....	142
55. Cu(II) adsorption isotherms and Langmuir plots for natural materials in comparison with bulk goethite.....	143
56. Cu(II) sorption hysteresis in subsurface material and surface soil.....	143
57. Comparisons of sorption-related quantities for crude kaolin, subsurface material, and surface soil relative to bulk goethite.....	145

Figure	Page
58. Cu(II) adsorption by subsurface material and Kch-thick in comparison to bulk..... goethite.	146
59. Cu(II) adsorption by natural materials and Q-phys in comparison to bulk..... goethite.	147

LIST OF EQUATIONS

Equation	Page
1. Linear BET.....	22
2. Specific surface area.....	24
3. Calculation of t	26
4. Calculation of α	26
5. Calculation of f	26
6. Calculation of SSA_p	28
7. Calculation of SSA_α	28
8. Calculation of t_{H_2O}	29
9. Calculation of SSA_{eq}	29
10. Predicted SSA for coatings.....	40
11. Calculation of estimated SSA for coatings.....	40
12. Example of a surface complexation reaction.....	70
13. Partitioning coefficient.....	83
14. Apparent equilibrium constant for an adsorption reaction.....	83
15. Derivation of N_{max} from adsorption data.....	83
16. Dissolution reaction for $Cu(OH)_2$	84
17. C_s calculated from Cu_{TOT} and K_d for additive models.....	87

ABSTRACT

The impact of dissolved trace metals on aquatic ecosystems and human health is controlled by sorption, or binding, to the surfaces of particles such as sediment grains. Chemical moieties on particle surfaces known as surface functional groups react with dissolved metal ions to form surface complexes, binding the metal ions to the particle. Capacity, binding strength, and reversibility of particle sorption is dependent on the physical properties of the surface and the chemical properties of the surface functional groups. Since many environmental particles are coated with highly reactive substances, such as Fe(III) oxides, and since discrepancies in trace metal sorption persist between oxides developed in the laboratory and those found naturally in field sediments, it was hypothesized that the physical form of oxide coatings may influence the chemical properties of the coated particle. Therefore, relationships between the physical forms of several different Fe(III) oxide coatings and the Cu(II) sorption behavior of the coated sediment grains were investigated.

Goethite (α -FeOOH) was coated onto quartz and kaolinite grains using two methods. Coating method and thickness were varied. The resulting coated solids were subjected to a variety of analyses to determine the physical and chemical properties of their surfaces. Physical properties were probed using multipoint N_2 (g) adsorption and desorption analysis (BET). The morphology of the particles was studied by scanning electron microscopy (SEM), and the uniformity of oxide distribution on the grain surfaces was assessed by energy-dispersive X-ray (EDS) analysis. Chemical properties were investigated via batch Cu(II) adsorption/desorption experiments.

Goethite physical form was found to vary with the method used to generate the coating and with the mineralogy of the substrate. Cu(II) sorption (uptake and release of dissolved Cu from goethite-coated particles) depended on the coating method, substrate, and thickness of the coating. Analysis of these variations indicated not only alterations in the physical form of the goethite coatings, but also interactions between goethite and substrate and changes in the surface chemical properties of one or both solid phases (goethite and substrate). The combined physical and chemical alterations in the properties of the solids produced distinct behavior in each of the coated solids studied.

A parallel set of experiments was conducted on three geologically related sedimentary materials. Several physical and chemical differences were observed between crude kaolin and a cleaned reference kaolinite. One laboratory-prepared goethite coating matched a surface soil at precipitation-dominated Cu loadings, and another coated solid matched a subsurface material at all Cu loading ranges sampled. These results suggest that more complex laboratory-prepared sorbent phases may better reflect trace metal sorption properties of environmental particles.

**LABORATORY OXIDE COATINGS:
PHYSICAL FORM AND SURFACE CHEMISTRY**

INTRODUCTION

The purpose of this study was to address one of the challenges in applying laboratory research to environmental issues – specifically, the differences between pure laboratory sorbent phases and natural sedimentary materials. This area of research is germane to the fate, transport, and availability of dissolved trace metals in aquatic ecosystems.

Many trace metals are both essential micronutrients and toxicants. Humans use trace metals such as copper, zinc, and tin in many ways, thereby perturbing their fate and transport. In turn, humans are affected by the cycling of trace metals through environmental compartments such as ground and surface water, terrestrial vegetation, and aquatic biota. An example of this interaction between humans, trace metals, and the environment can be seen in the Fal Estuary, U.K., as described in Bryan et al. 1987. The Carnon River, a major tributary of the Fal, drains a region that has contained Cu mines since the Bronze Age. In the mid-19th century, this area may have been the top producer of Cu and Sn in the world. One major operation was the Wheal Jane mine, opened in about 1740. In the mid-1800s green oysters began to be reported in the Fal, and in 1862 an export of these oysters (*Ostrea edulis*) to Rochefort, France, caused an outbreak of poisoning. Subsequent analysis revealed that each green oyster contained about 20 mg of “copper salt,” or roughly 3,000 mg Cu per g (dry wt).

By about the year 1900, production at the Wheal Jane mine had dropped to almost zero. However, a 1985 survey of sediment-associated Cu in the Fal indicated levels of up to 2,000 mg Cu g⁻¹ (dry wt.), increasing toward the mouth of the Carnon River. In addition, green *Ostrea edulis* in the Fal were sampled in 1921 and again in 1971, and their Cu contents remained consistently high (roughly 3,500 mg g⁻¹). Green oysters were still being reported in the Fal in 1987. Thus, 85 years after the source of dissolved Cu to the estuary had largely ceased, the sediments not only remained heavily contaminated but

the estuary had largely ceased, the sediments not only remained heavily contaminated but were acting as a continuous source of Cu to benthic organisms. This is because reactive sorbent phases in the sediment had removed dissolved Cu from the water column, concentrating it in the sediment, and were affecting its subsequent fate and transport by means of a physicochemical process known as *sorption*.

The term 'sorption' refers to the accumulation of dissolved substances at solid/water interfaces. This term encompasses several more specific mechanisms. For the uptake of trace metals by mineral phases such as iron oxides, important mechanisms of sorption include *adsorption*, *oligomer formation*, and *surface precipitation*.

'Adsorption' may occur by the formation of either weaker, more ionic 'outer-sphere' complexes, or stronger, more covalent 'inner-sphere' complexes, and metal ions may bind to one or two sorbent surface sites. These mechanisms are also sometimes called 'physisorption' and 'chemisorption,' respectively. 'Oligomer formation' describes the co-adsorption of more than one metal ion to the surface; these ions are often hydroxy-bridged. This is also known as 'cluster formation.' Metal ions may also form a precipitate phase (or 'surface precipitate') on the sorbent surface.

Many environmental sediments contain phases that strongly sorb dissolved trace metals. Iron oxides are a very common example of this type of phase. Conversely, many trace metals are highly particle-reactive. Thus, the sorption of trace metals to iron oxides is an environmentally relevant field of surface geochemistry. Much is known about metal/mineral surface reactions in the laboratory, where single, well-characterized minerals (called 'pure phases') are studied in simple electrolyte solutions carefully controlled for pH, ionic strength, and metal ion concentration (see below).

It has been hoped that the information gained from studying systems containing one or two pure phases could be used to understand environmental sorption (Davis and Kent 1990). This would bring the benefits of a thermodynamic description to the study of environmental systems (Honeyman and Santschi 1988; Davis and Kent 1990; Ioannou and Dimirkou 1997; O'Day et al. 1998), enabling the description of general processes and mechanisms in many different systems. It could also yield tools for predicting the extent

and duration of environmental impact such as that observed in the Fal estuary. Many studies have addressed this objective from various angles.

Comparative studies have uncovered qualitative similarities between the observed behaviors of natural solids and well-described systems (Lion et al. 1982; Zachara et al. 1989; Müller and Sigg 1990), suggesting that a theoretical approach is viable (Honeyman et al. 1988; Tessier et al. 1996; Davis et al. 1998). However, disparities persist between field- and lab-derived results. For example, an analysis of published data (Lion et al. 1982) found that binding constants derived from field samples were different from ones based on an analogous pure-phase system. Plots of field-derived sorption constants vs. pH were linear, and sorption constants for metal ions followed the same trends as in laboratory studies using pure iron oxides, but the values of the field-derived constants were different from those determined using pure oxides (Tessier 1993). Elsewhere, the general sorption behavior of synthetic goethite and freshwater particles was observed to be qualitatively similar despite distinct differences in quantitative affinity (Müller and Sigg 1990; Stumm and Morgan 1996).

The difficulties of achieving a theoretical understanding of environmental trace metal cycling have frequently been emphasized (Zachara, Resch, et al. 1994; Robertson and Leckie 1997; Lofts and Tipping 1998). Accordingly, some scientists have opted to continue pursuing empirical alternatives, such as calculating partitioning coefficients (Turner et al. 1993) and using selective extraction techniques to quantify metal sorption (Rule and Alden 1992). Such approaches often provide a satisfactory description of sorption in individual systems and can yield valuable information about trace metal cycling on a site-to-site basis. However, the results do not provide theoretical constants that could be used for modeling sorption in general, or reveal the mechanisms at work, which would contribute to a more fundamental understanding of trace metal behavior in natural systems.

Furthermore, despite the above-mentioned quantitative disparities, progress continues to be made toward increasing the theoretical understanding of environmental systems. Some studies have identified surface properties of binary oxide suspensions

distinct from those of the individual oxides (Anderson and Benjamin 1990). This is a crucial contribution to understanding sorption by complex assemblages of sorbent phases, such as occur in the environment. Others have improved the success of mechanistic models of environmental sorption by accounting for interactions between sorbents, such as competition between mineral and organic sorbents (e.g. natural organic matter, or NOM; Benedetti et al. 1996; Lofts and Tipping 1998). Pure-phase geochemists have begun to explore more multiple-phase systems (Anderson and Benjamin 1990; Meng and Letterman 1993; Murphy et al. 1994; Huang and Yang 1995) and to apply spectroscopic techniques to natural adsorbents (Morra et al. 1997; Xia et al. 1997a; O'Day et al. 1998). These and other studies have significantly advanced the development of pure-phase research that can provide accurate and useful knowledge of the processes and mechanisms governing trace metal cycling in aquatic systems.

Several approaches for modeling metal-ion sorption mechanistically using multiple sorbent phases have been developed over the past several decades. After it was established that natural systems should be modeled using multiple phases (Oakley et al. 1981), 'assemblage' models were developed based on the behavior of isolated phases. The first attempts assumed 'sorptive additivity,' i.e., that the net sorption behavior of a multiple-adsorbent system is equal to the weighted sums of the constituent adsorbents. Concerns were soon raised about the validity of modeling complex systems as sets of separately reacting phases (Davies-Colley et al. 1984). It was demonstrated that mixed-oxide systems do not behave additively (Honeyman 1984). However, studies of some natural systems suggested little or no nonadditive behavior (Tipping et al. 1983; Zachara et al. 1994). Nevertheless, some researchers warned that constants calculated based on additivity might be orders of magnitude off (Honeyman and Santschi 1988).

Subsequent investigations into the behavior of systems containing multiple sorbents (Davies-Colley et al. 1984; Anderson and Benjamin 1990a and b) produced more advanced concepts – for example, the 'mixed site distribution' model, in which a coated surface is considered to have an overall surface potential consisting of a mixture of the coating and substrate surface sites (Meng and Letterman 1993a and b).

Quantitative models fit empirical data assuming a finite number of site types (e.g., Robertson and Leckie 1998) or a site population with a continuous range of affinities (e.g., Buffle and Altmann 1987). A major advance was the introduction of surface complexation models ('SCMs'), which treat sorption as a set of chemical reactions analogous to aqueous complexation (e.g., Schindler and Stumm 1987). Another was the publication of an internally consistent data set describing sorption by Fe oxyhydroxide (Dzombak and Morel 1990). Increasingly sophisticated SCMs have been advanced to account for both chemical and electrostatic components of surface complexation reactions (Davis and Kent 1990).

Over time, two fundamental facts have emerged. First, the composition of natural sediments is so complex and diverse that accounting for each and every constituent's contribution to the net sorption behavior of the system seems unfeasible, if not impossible. Second, despite the great complexity of natural sediments, in many cases net sorption behavior may be governed by a few highly reactive phases (Davis and Kent 1990). This would make it unnecessary to describe the sorption behavior of every phase contained in environmental sediments. At present, there appear to be two major strategies favored by surface geochemists interested in complex solids: (1) treat natural assemblages as a single phase, and focus on the properties which dominate behavior (Tessier et al. 1996); or (2) attempt to sum up the properties of a complex system using individual, well-described pure phases (Davis et al. 1998). Similarly, while some modelers continue to pursue an assemblage approach, accounting for the effects of each reactive phase (Lofts and Tipping 1998), others attempt to identify a few predominant factors that control the bulk of behavior in complex systems (Davis and Gloor 1981). This study fell into the second of both groups: it proposed an approach for conducting more applicable pure phase studies using a few predominant phases, used it to elucidate potential reasons for the observed differences in trace metal sorption behavior between pure phases and environmental sedimentary materials, and evaluated its feasibility as a tool for understanding sorption in the environment.

The proposed approach was to make pure-phase research more descriptive of environmental sorption by investigating reactive mineral phases as they occur in the environment. Specifically, it was proposed that reactive phases should be studied as coatings. Coatings comprise an important difference between pure phases and environmental sedimentary materials. When surface geochemists study kaolinite, for example, they first subject it to several cleaning techniques to remove any coatings or other impurities. On the other hand, environmental particles are frequently coated with highly reactive materials such as oxides and organic matter (Holmén and Gschwend, 1997; Ransom et al., 1997). There are several other ways in which coatings are important with regard to sorption. Coatings have a high surface area-to-volume ratio, an important consideration for sorption, which takes place on surfaces. They lie on the surfaces of substrate particles, masking part of the substrate surface, and may in turn be affected by the surface properties of the substrate. Finally, coatings may take a variety of physical forms in environmental particles (Holmén and Gschwend, 1997; Ransom et al., 1997; Seaman et al., 1997; Ryan et al., 1999).

Information on Reactants

In this study, the iron oxide goethite (α -FeOOH) was chosen as the reactive coating phase of interest. The substrate minerals were silica quartz (α -SiO₂) and kaolinite (Al₂Si₂O₅(OH)₄), and the trace metal ion used in the sorption experiments was Cu(II). Substantial research has already been done on the uptake of trace metal ions by these and related minerals. This section summarizes that research.

Copper(II) as a Sorbate Ion. Copper was chosen for several reasons. It is both an essential micronutrient and a toxicant. It has been cited as one of the most hazardous trace metals (Stumm and Morgan, 1996), and the EPA has listed it as a 'toxic of concern.' It has a complex and interesting chemistry due to its electronic configuration (Heslop and Jones, 1976). It is highly particle reactive, and its fate and transport in aquatic environments has been shown to be linked to sedimentary biogeochemistry and transport

processes (Summerhayes et al., 1985; Bryan et al., 1987). Finally, a great deal of field and laboratory research has been done on copper, providing a rich context for this study as well as supporting information.

Sorption by Iron Oxides. Ferric iron (hydr)oxides ('iron oxides') are ubiquitous in sediments. Iron oxides are hydroxylated in aqueous solutions, and typically have a high density of surface hydroxyl groups (or SHGs; $8.80 \mu\text{mol}/\text{m}^2$ for goethite; Langmuir 1997). The relative abundance and charge of SHGs is a function of the pH of solution and the intrinsic charge of the solid; the distance between the groups is controlled by mineralogy. Since the SHGs of oxides are amphipathic, oxide surfaces in aqueous solution may be either positive or negatively charged depending on the pH of the solution. The pH at which the surface has a net zero charge is called the 'zero-charge condition' or 'point of zero charge' ('PZC'); the PZC for goethite is ~ 9 (Langmuir 1997; Robertson and Leckie 1997).

Iron oxides have a very strong affinity for copper and other trace metals, as demonstrated in many studies (Benjamin and Leckie 1981; Anderson and Benjamin 1990; Davis and Kent 1990; Dzombak and Morel 1990; Cowan et al. 1991). Metal cation uptake by iron oxides increases dramatically with pH over a narrow range (about 1 to 2 pH units). This phenomenon is related to the pH at which the first hydrolysis product of the trace metal becomes a major species in solution, since metal cations overwhelmingly bind with hydroxyl groups on the surfaces of the oxide. The pH range over which uptake increases is called the 'adsorption edge.' For Cu(II), the adsorption edge generally falls between pH 4.5 and 6.5 (Davis and Kent 1990). Since the PZC for most iron oxides is between pH 7 and 9 (Langmuir 1997), it appears that divalent copper cations are attracted to a net positively charged iron oxide surface. This attraction despite the same charge sign indicates the strong affinity of the cation for the oxide SHGs. In addition, changing the ionic strength of the solution has relatively little effect on copper uptake (Morel and Hering 1993). All of this suggests that copper (among other trace metals) forms a strong inner-sphere complex with iron oxide surface sites which is insensitive to changes in the

electrostatic environment near the surface. Such complexes are stronger and less readily removed than the more electrostatic outer-sphere complexes observed for other dissolved species.

Sorption by Silica Phases. Quartz is a member of the silica group of minerals and mineraloids. It is the only common stable crystalline silica at the Earth's surface and is also the most common mineral on Earth's surface. However, quartz has a relatively low surface reactivity for dissolved trace metals. The undisrupted quartz surface contains reactive SHGs, but they are widely spaced compared to iron oxides (O'Day et al. 1996). This limits the ability of octahedrally-coordinated transition metal ions to form the multidentate surface complexes (i.e., complexes in which the metal ion is bound to the surface by more than one chemical bond) preferred for inner-sphere complexation (Brown et al. 1995; O'Day et al. 1996; Christl and Kretzchmar 1999). Accordingly, dissolved copper ions are observed to bind more weakly to quartz than to iron oxides, and the net association is thought to be primarily electrostatic (i.e., mainly outer-sphere complexes). This low surface reactivity is further diminished in effect by the low surface area per unit mass of quartz (generally at least two orders of magnitude lower than those of iron oxides).

When inner-sphere complexes of Cu do form on the quartz surface, they appear to be monodentate and to use an axial Cu coordination site (Takahashi and Tanaka 1986; Cheah et al. 1998). Alternately, stronger multidentate bonds may form at steps or kinks, or at defect sites on the quartz surface; however, the abundance of such sites would be relatively low (O'Day et al. 1996). Copper forms large polymeric complexes and/or surface precipitates on silica (ostensibly amorphous silica, although this is not explicitly stated by the authors) at low surface coverages (\ll one monolayer) and in undersaturated solutions (Xia et al. 1997), much like the observed behavior of cobalt or iron on quartz (O'Day et al. 1996; Waychunas et al. 1999). In the case of quartz grains coated with goethite, the iron in the coating may occupy Cu-reactive sites on quartz (Ryan and Gschwend 1992), further reducing quartz's role as a copper sorbent.

Sorption by Kaolinite. Kaolinite is also a very common soil mineral. Kaolinite is a 1:1 clay mineral made up of alternating silanol and aluminol layers. Individual grains are platelike, with a characteristic hexagonal shape. Each grain has one silanol and one aluminol face (or basal plane). The silanol face is composed of fully saturated oxygens arranged around siloxane cavities; this face may have a very slight negative permanent structural charge due to occasional isomorphous substitutions of Al^{3+} for Si^{4+} (Ikhsan et al., 1999). The aluminol basal plane contains SHGs which are relatively unreactive due to their coordinative saturation (Davis and Kent, 1990). Unsaturated sites on the edges of grains (both aluminol and silanol) control most of the reactivity of kaolinite. This edge site reactivity is comparable to the strong copper adsorption of aluminum oxides (Huang and Yang 1995; O'Day et al. 1996); and accordingly, copper binds more strongly to kaolinite than to quartz. Kaolinite also has a higher surface area per unit mass than quartz (roughly two orders of magnitude higher). However, kaolinite's overall copper affinity is less than that of aluminum and iron oxides, in large part because of the paucity of edge surface area relative to the abundant, but relatively unreactive, basal plane surface area.

Surface Properties of Iron Oxide Coatings. Iron oxides are often present as coatings on mineral surfaces (Davis and Kent 1990). The SHGs of iron oxide coatings may be different from those of discrete oxide particles for several of the reasons mentioned above. In iron oxide coatings, some of the reactive surface groups may be engaged in the substrate-oxide bond. This would change the number of SHGs available for surface reactions, and since there are different types of SHGs, it might also change the proportions of reactive types. Also, the underlying substrate mineral may influence the morphology of the iron oxide coating. Iron oxide might be able to grow epitaxially (i.e., reflecting to some degree the structure of the underlying surface) on the basal alumina surfaces of kaolinite, due to the similarity in the spacing of oxygens occurring on the (110) crystallographic plane (which forms the dominant crystal face) in goethite and the

corresponding oxygen spacing on the basal aluminol kaolinite plane. This would affect the characteristics of the goethite coating on the aluminol planes. In contrast, the reactive sites on quartz are spaced differently than those on iron oxide surfaces, limiting the possibility of epitaxial growth of iron oxide on quartz. At low quartz surface coverages, iron oxide forms a monodentate bond with the quartz surface, whereas at higher coverages, iron oxide forms larger patches anchored to the quartz surface in a few places (Waychunas et al. 1999). Thus, a similar amount of goethite might form a patchier coating on quartz than on kaolinite. This could mean that the properties of goethite coatings are more strongly affected by a kaolinite substrate than by quartz.

Environmental Coatings and Synthetic Analogs. Iron oxides form at least two common types of coating on environmental particles. One type forms when dissolved iron precipitates out of solution onto the surfaces of mineral grains. For example, this may occur when acidic mine drainages mixes with an alkaline stream, causing an increase in pH and decreasing the solubility of Fe(III). Another example is the oxidation of Fe(II) to the less soluble Fe(III) in aquifers when reduced groundwater is oxygenated by mixing with recharge. These may be generally categorized as 'chemical coatings.'

A second common type of environmental iron oxide coating develops when already formed goethite particles come into contact with the surfaces of mineral grains and are attached by electrostatic forces. A good example is the aggregation of mobile colloids with quartz and clay particles in aquifers. This might be called a 'physical coating.'

Overview of Study

This study was divided into three parts:

- (1) Synthesis and physical characterization of a set of goethite coatings
- (2) Investigation of surface properties of the coated solids
- (3) Comparative studies of environmental sediments

Five synthetic goethite coatings were synthesized on quartz and kaolinite, using methods designed to simulate chemical and physical coatings. These are summarized in Table 1, along with the nomenclature that will be used throughout the text.

Cu(II) adsorption/desorption experiments were conducted in batch mode using the coated solids and individual pure phases (quartz, kaolinite, and bulk goethite).

Experiments were conducted in 10‰ synthetic estuarine water at room temperature and under air. The Cu-to-surface ratio (i.e. 'loading') was varied over an environmentally relevant range approximating Cu loadings in pristine (ca. 10 mg g⁻¹ dry wt.) to heavily polluted (ca. 4,000 mg g⁻¹) sediments, and focusing on contaminated to heavily contaminated loadings (ca. 100 to 1,000 mg g⁻¹).

TABLE 1. Summary and nomenclature of goethite-coated solids.

SUBST RATE	COATING METHOD		
	Physical	Chemical	Chemical
Kaolinit e	Thin physical coating on kaolinite: K-phys	Thin chemical coating on kaolinite: K-chem	Thick chemical coating on kaolinite: Kch-thick
Quartz	Thin physical coating on quartz: Q-phys	Thin chemical coating on quartz: Q-chem	x

Three environmental sediments were selected for comparison with the synthetic goethite coatings. These are primarily composed of quartz, kaolinite, and goethite; two contain little or no organic matter. All three are from the Southeastern Atlantic Coastal Plain sequence. The first is a crude kaolin mined by the Thiele Kaolin Company in Sandersville, Georgia. It shares the same parent material as the clean kaolinite used in this study as a substrate. The others were collected in Aiken, South Carolina; one is a sandy aquifer material and the other is a related surface soil (Vulava and Seaman, 2000). In the following chapters, these will be referred to as “crude kaolin” or “crude,” “aquifer material” or “aquifer,” and “surface soil” or “soil.”

Hypothesis

H₀: goethite coatings have the same surface properties as bulk goethite.

H₁: the physical form of goethite is related to its surface properties.

Organization of Dissertation

The first chapter provides background information and motives for the research and an overview of the study. Chapter 2 covers the synthesis and physical characterization of the three chemical coatings (thin chemical coatings on quartz and kaolinite and thick chemical coating on kaolinite). Chapter 3 describes the investigation of the relationships between the forms of all five coatings, their physical characteristics, and their Cu(II) sorption behavior. Chapter 4 covers the comparative studies of the physical and chemical properties of the environmental sediments, and Chapter 5 synthesizes the results of all of the investigations and offers some general conclusions. Raw data are given in the Appendices.

CHAPTER 2: PHYSICAL CHARACTERIZATION

Introduction

The sorption behavior of a dissolved metal ion varies from sorbent to sorbent (Benjamin and Leckie 1981). This is in part because sorption behavior is controlled by the particular physical and chemical properties of the sorbent. Additionally, the properties of a particular hydrous oxide may vary, such as the distribution of exposed crystallographic faces, which in turn may have different points of zero charge (PZCs) (Brown et al. 1995; Hiemstra et al. 1996). For example, the specific surface area (SSA) of synthetic goethite may range from 8 to 200 m² g⁻¹ (Larsen and Postma 2001), and commonly varies between 30 and 50 m² g⁻¹. Differences in the method and technique for synthesizing goethite lead to variations in specific surface area (Robertson and Leckie 1997; Randall et al. 1999; Rietra et al. 1999; Elzinga et al. 2001; Larsen and Postma 2001), degree of crystallinity (Collins et al. 1999; Randall et al. 1999; Larsen and Postma 2001), and crystal habit (Schwertmann and Cornell 1991; Larsen and Postma 2001).

Thus, even mineralogically identical sorbents may vary in their metal-ion sorption behavior as a function of their physical form. Moreover, the studies cited above examined bulk oxides; however, oxide coatings commonly occurring in natural soils and sediments may have a wider range of physical forms, influenced not only by formation conditions but also by thickness and the mineralogy of the substrate. This chapter explores physical properties of goethite coatings formed by surface precipitation on quartz and kaolinite phases for the purpose of elucidating the effect of substrate and thickness on coating surfaces.

All three minerals used in this study— quartz, kaolinite, and goethite – have distinct physical and surface chemical properties, as discussed in Chapter 1. These

differences may affect the nature of goethite coatings formed on quartz as opposed to kaolinite. The quartz-goethite complexes were anticipated to resemble patches of goethite anchored to the quartz surface by monodentate ligands (Waychunas et al. 1999). This is supported by models of quartz surface groups (Hiemstra et al. 1996) and adsorption studies of other octahedrally coordinated transition metal ions. For example, Co^{2+} was observed to form multinuclear and precipitate-like complexes at relatively low metal-ion surface coverages, proposed to be anchored to the quartz by mononuclear or small multinuclear bonds (O'Day et al. 1996). Similarly, although Cu(II) binding to silica has been determined to be relatively weak (Cheah et al. 1998), Cu(II) appears to bind to silica surface hydroxyl groups ('SHGs') with a one-site coordination (Takahashi and Tanaka 1986; Cheah et al. 1998), perhaps of an axial ligand (Cheah et al. 1998).

On the other hand, the crystal structure of kaolinite suggests that Fe oxide uptake may be both stronger and more uniform than that of quartz. The basal planes of kaolinite are composed of aluminum atoms coordinated octahedrally with six oxygen atoms. Iron oxides also contain this basic structural unit (with central Fe atoms), and the average Al-O and Fe-O bond length (for octahedral coordination) differs by only 6%; since they share similar bulk structures, aluminum and iron oxides might be expected to have similar surface structures and surface functional groups (Bargar et al., 1997).

Epitaxial growth of $\alpha\text{-Fe}_2\text{O}_3$ has been observed on $\alpha\text{-AlOOH}$ (Charlet and Manceau 1992). Investigators have compared the aluminol planes of clays to γ -alumina (Al_2O_3 ; Cheah et al. 1998), and have found similar metal-ion sorption environments on γ -alumina and kaolinite (Chisholm-Brause et al. 1990), and on δ -alumina and kaolinite (Schulthess and Huang 1990). Investigators have even suggested that alumina may be used as an analog for clay aluminol planes (Cheah et al. 1998). These lines of evidence suggest that the aluminol planes of kaolinite offer a more favorable surface for the uptake of Fe oxides. In addition, there should be some role played by the pH of association, since the basal planes of kaolinite sometimes have a small, permanent negative charge, while the amphoteric edge sites have variable charges dependent on solution pH (Saleh and Jones 1984).

Studies of goethite and ferrihydrite coatings on kaolinite show the importance of method and thickness of coating. When particulate ferrihydrite was mixed with kaolinite in suspension, association was greatest at pH 3 and not apparent at pH 9 (Saleh and Jones 1984). Such coatings were always associated with the basal planes of the kaolinite. It was inferred that the permanent charge of the basal planes was an important factor in controlling the formation of the coatings. The uniformity of the coating appeared to depend on thickness; coating morphology ranged from discrete particles at < 1% Fe to small dispersed areas at 1-2% Fe, to a complete coating at about 8% Fe (Jones and Saleh 1987). When Fe oxyhydroxide was precipitated in the presence of suspended kaolinite, chemisorption appeared to take place, although at the pH of reaction (pH 4) electrostatic attraction can not be ruled out (Arias et al. 1993), as kaolinite has a net negative charge (PZC \approx 2-4.6; Langmuir 1997) and Fe oxyhydroxides have a net positive charge (PZC \approx 9; Hiemstra et al. 1996; Robertson and Leckie 1997; Brown et al. 1999) at this pH. Such coatings maintained their association with the kaolinite despite increases in pH. Flocculation studies of the coated kaolinite suggested that some of the negative charge remained even for a 6.68% Fe solid. This may mean that some of the kaolinite surface remained exposed after coating. In addition, the coatings showed relatively less crystallinity upon aging than similar Al oxide coatings. Si poisoning of the Fe oxide crystallization process was ruled out; other results suggest that sorption to the silanol surfaces may place stoichiometric hindrance on the development of a crystalline form (Saleh and Jones 1984). However, this would not explain the higher level of Al crystallinity since Al is also thought to bind to both basal surfaces (Arias et al. 1993).

In summary, the quartz coatings are expected to be sparse and patchy in nature, with more goethite-like particles growing out from monodentate anchors to the quartz surface. It is expected that the method of coating will not make as much of a difference for quartz as for kaolinite, since in both cases uptake of goethite is expected to be relatively minor and produce similar types of association and crystallinity. In contrast, the degree of association, uniformity of coating, and perhaps even crystallinity may vary significantly with method and thickness of coating for kaolinite. The kaolinite basal

planes are expected to take up the coatings, and it seems possible that the aluminol planes may be both more reactive and more structurally similar to the coating phase, so that they may take up more than the silanol planes and allow for more crystallization with aging of precipitated Fe phases. It may even be possible for the goethite coating to grow epitaxially along the aluminol basal plane, because of the stoichiometric and surface charge similarity between the SHGs of the surface and those found on the (110) crystallographic face of goethite. The thin coating may leave parts of the basal planes exposed; however, the thick coating is expected to form a complete layer over the basal planes. In both cases, however, the reactive kaolinite edge sites are expected to remain available for uptake.

This chapter relates the results of the physical characterization of the three coatings formed by surface precipitation (i.e., the 'chemical' coatings): a thin chemical coating on quartz ('Q-chem'), a thin chemical coating on kaolinite ('K-chem'), and a thick chemical coating on kaolinite ('Kch-thick'; see Chapter 1, Table 1). Multipoint N₂ adsorption/desorption (BET) analysis was used to probe physical surface properties such as specific surface area (SSA) and porosity, and the spatial distribution of the coatings over the substrate surfaces was evaluated using energy-dispersive X-ray spectrometry (EDS). Unfortunately, these methods are inappropriate for characterizing 'physical' coatings formed by heterocoagulation of coating and substrate particles. The electrostatic bonds holding these solids together are notoriously fragile (Bertsch and Seaman, 1999). In particular they are vulnerable to alteration and disruption by drying, which is required in preparing samples for both N₂ adsorption/desorption and SEM/EDS analysis.

Materials

All reagents used were at least ACS-grade. Quartz was obtained from Unimin Corp, and then cleaned and size-fractionated using established procedures (O'Day et al. 1996). Specifically, the bulk of the finest grain-size fraction (< ≈ 2 μm) was removed by settling. The quartz was suspended in 4N HNO₃ and incubated at 95°C for 4 h, then decanted and rinsed with DDI water until pH reached ≈ 6. Next, it was suspended in 1N NaOH and allowed to settle for 1.5 h, then rinsed with DDI water until pH was ≈ 7-8 and

dried in a 90°C oven, where it was stirred periodically to minimize compaction. Grain-size distribution (GSD) analysis, determined by X-ray scattering using a Micromeritics SediGraph 5100 particles size analyzer, indicated a median diameter of 14.9 μm and a distribution of 6.4% sand ($> 50 \mu\text{m}$), 87.6% silt (2-50 μm), and 6.0% clay sized particles ($< 2 \mu\text{m}$). Figure 1a is a scanning electron microscope (SEM) photomicrograph of the cleaned quartz.

Kaolinite (KGa-1b) was obtained from the Source Clay Minerals Repository. It was cleaned, size-fractionated, and sodium-saturated, again following established procedures (Chisholm-Brause, 1997). Specifically, the kaolinite was centrifuged to select the 0.5-2 μm size fraction, and then subjected to a modified citrate-dithionate-bicarbonate (CDB) extraction, as follows: 50-g batches were suspended in 800 mL of 0.3M sodium citrate and 100 mL 1M sodium bicarbonate. Sodium dithionate (1.76 g) was slowly added to each batch and the suspension stirred overnight at room temperature. About fifty mL saturated sodium chloride solution was then added to induce flocculation and the suspension centrifuged; the supernatant was decanted. This procedure was repeated once. Then, each batch was suspended in ~ 100 mL of a 1M sodium acetate solution adjusted to pH 5 with acetic acid and 350 mL of 4.5% H_2O_2 were added, and the suspension was heated to 70°C for 30 min, then cooled partially. Fifty mL saturated NaCl was added and the suspension was centrifuged and decanted. This was repeated twice; after the third cooling, the pH was raised to 8 with sodium carbonate, the suspension was allowed to stand for 10 min, and excess H_2O_2 was boiled off. Fifty mL saturated NaCl was added, and the suspension was centrifuged and decanted. Finally, the batches were suspended in ~ 900 mL of 1M NaCl and stirred for 30 min, then centrifuged and decanted; the batches were consolidated and dialyzed against tap water for 1h, and then against DDI until the conductivity of the dialysis solution approached that of DDI water. The kaolinite was freeze-dried and stored in a tightly sealed Teflon jar. GSD analysis showed a fairly even split between the 1-2 μm and 0.5-1 μm fractions (52.6 and 47.4%, respectively). A photomicrograph of the kaolinite, showing the typical 'books of hexagons' habit, is shown in Figure 1b.



Figure 1. SEM photomicrographs of cleaned quartz (top) and kaolinite (bottom). Note the disrupted surfaces in quartz and the classic "books of hexagons" habit of kaolinite. Small ($< \sim 5 \mu\text{m}$) quartz grains were removed by size fractionation during the coating procedure.

Goethite was synthesized using a method based on Schwertmann and Cornell (1991). No glassware was used in order to prevent silica poisoning of the goethite. 50 g of solid ferric nitrate was weighed into a 1-L Nalgene jar. 800 mL of DDI water was added to dissolve the $\text{Fe}(\text{NO}_3)_3$. While stirring constantly, 200 mL of 2.5 M sodium hydroxide was slowly added. The jar was capped and placed in a 70-degree oven for 60 hours, occasionally agitated gently to resuspend the precipitate. These were allowed to settle the last 10 h in the oven, the jar was then removed and allowed to cool and settle further. As much of the supernatant as possible was poured off; the remainder was swirled to suspend the precipitate and both were poured into washed dialysis tubing clipped shut at one end. The other end was then clipped shut and the solids were dialyzed against DDI until the conductivity of the water outside the tubing approached that of DDI. The solids were transferred to pans and freeze-dried, then stored in a sealed Nalgene jar. XRD analysis confirmed the mineralogy of the solid as goethite.

Coating Methods

The method developed for forming goethite coatings on quartz and kaolinite was based on several found in the literature (Edwards et al. 1989; Schwertmann and Cornell 1991; Lai et al. 1994; Schmitt et al. 1996). 50 g of clean quartz were suspended in ~ 850 mL DDI and stirred for 2 days, then allowed to settle for ~ 90 min and poured off. This removed grains smaller than ~ 5 μm in diameter. The remaining quartz was resuspended in \approx 850 mL of 12.5 mM $\text{Fe}(\text{NO}_3)_3$ and stirred; a pH meter was placed in the suspension, and 150 mL of 150.5 mM NaOH was added very slowly and in small quantities (on the order of 100 μL) to minimize any areas of localized Fe hydroxide solid supersaturation in the suspension until the pH reached ca. 9.7. The solutions, still being stirred, were allowed to equilibrate at this pH level for about 15 minutes; they were then placed in a 50°C water bath for 5 d, being periodically shaken (several times the first day and at least once a day after that). The solids were allowed to settle out of solution; the supernatant was poured off and replaced with DDI, and the solids were resuspended. The suspension was filtered through a 3- μm Teflon filter; the solids on the filter were resuspended in ~

1000 mL of DDI water and allowed to settle for ~ 45 minutes. The cloudy, dark-orange solution was poured off. This rinsing was repeated several more times until the supernatant was transparent and nearly colorless. The solids were freeze-dried and stored in a Teflon container.

In the procedure for forming the thin coating on kaolinite, five g of clean kaolinite were suspended in dilute NaOH (pH = 8) overnight. The suspension was centrifuged and the supernatant poured off. The kaolinite was then suspended in 80 mL of dilute HCl (pH = 4), centrifuged, and the supernatant poured off. Next, the kaolinite was suspended in 80 mL of 12.5 mM Fe(NO₃)₃ solution and the pH allowed to stabilize at ≈ 3. Small quantities of concentrated NaOH (on the order of 100 μL) were added slowly while stirring to bring the pH up to ca. 8. The jar was capped and the suspension was stirred for another 15 min, then placed in a 50°C water bath and aged for 4 d (stirring continuously). The jar was removed from the bath and allowed to cool partially, and the solid was transferred to a 50-mL centrifuge tube and centrifuged. The slightly cloudy, untinted supernatant was poured off and replaced with 50 mL DDI water. This rinsing was repeated 4 more times, until the supernatant was clear and the solid began to flocculate as soon as agitation of the suspension ceased. The solid was freeze-dried and stored in a sterile polypropylene vessel.

The procedure for forming the thick coating on kaolinite is nearly identical to that for the thin coating with two exceptions: (1) the concentration of the Fe(NO₃)₃ solution was 50 mM instead of 12.5 mM; and (2) the process of suspending the solid in the Fe(NO₃)₃ solution, raising the pH, and aging the solution was repeated for a total of 3 times. Then the solution was allowed to cool partially, transferred to a 50-mL Corning centrifuge tube and centrifuged, and the supernatant was poured off. This was repeated only once, after which the conductivity of the supernatant was approximately that of DDI water. The solid was then freeze-dried and stored in a sterile polypropylene vessel.

All three coating procedures yielded grains with the same macroscopic and microscopic texture as the uncoated substrates. Q-chem and K-chem were a pale salmon color, and Kch-thick was a lighter shade of the ochre color characteristic of goethite. The

iron content of the coated solids was determined by extraction of the iron using a citrate-dithionate-bicarbonate ('CDB') extraction method (Jackson et al. 1986) for quartz and hot nitric acid extraction for kaolinite (approximately 4N HNO₃ at 80°C for 8 h), and analysis of the extractant by inductively coupled plasma optical emission spectrophotometry (ICP-OES) or graphite furnace atomic absorption spectrophotometry (GF-AA). The iron content was 0.13 wt % Fe for Q-chem, 1.3 wt % Fe for K-chem, and 11.3 wt % Fe for Kch-thick. No separate iron oxide crystals were found by inspection with optical and electron microscopy surveys, in addition to visual inspection of the whole samples.

Physical Adsorption Analysis

The volume of N₂ gas taken up by a solid over a range of relative pressures is a function of its specific surface area (SSA, m² g⁻¹). The Brunauer-Emmett-Taylor (BET) method uses this relationship to derive SSA from a series of measurements of the volume of gas adsorbed onto a solid at a given relative pressure (N₂ gas pressure, or P , normalized to saturation pressure, or P_o). This method is both accurate and reproducible, when performed correctly (Davis and Kent, 1990; Mayer, 1999); and although its precision can be low (Gregg and Sing, 1982), an estimate of method precision may be made by repeatedly measuring a reference material of known SSA.

Figure 2 is an example of a typical BET adsorption isotherm for a nonporous solid, with the volume of N₂ gas adsorbed (V_a) plotted versus relative pressure (P/P_o). The range from $P/P_o \approx 0.05-0.30$ is generally linear; in BET theory this is called the 'multilayer region,' where successive monolayers of gas are assumed to be forming on the solid surface (Gregg and Sing 1982). It is the data in this region from which SSA is derived, using the BET equation.

The linear form of the BET equation is as follows:

$$\frac{1}{V_a} \cdot \frac{x}{(1-x)} = \frac{(c-1)}{cV_m} x + \frac{1}{V_m}, \quad (1)$$

where $x =$ relative pressure (P/P_0), V_m is the volume of gas in a monolayer, and c is a dimensionless parameter related to the heat of adsorption (sometimes called C_{BET} or the BET parameter; Hiemenz and Rajagopalan 1997). To derive SSA, the left-hand side of the equation is plotted against x and a linear regression is performed over the multilayer region. The residuals of this regression are plotted in order to select the portion of the linear region with the steepest and most linear residuals, and to avoid any changes in residual inflection. A second linear regression is then performed on the optimal portion of the multilayer region, as indicated by analysis of the residuals (Mayer 1999).

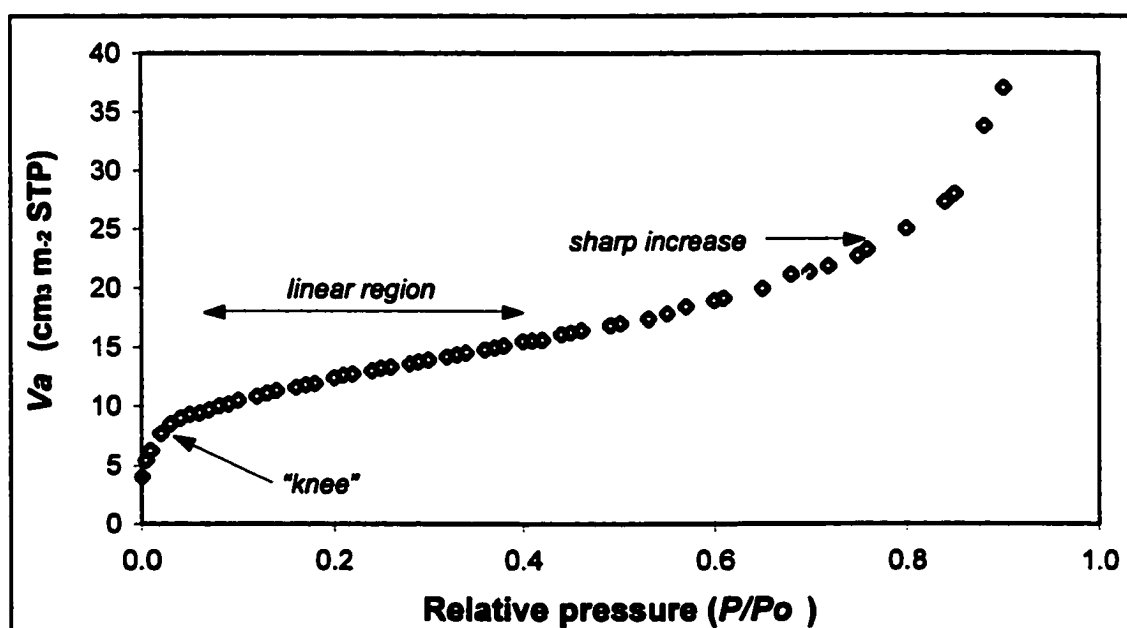


Figure 2. Typical BET behavior for N_2 gas adsorption on a nonporous solid. Some characteristic features of the isotherm: a 'knee' at $P/P_0 \approx 0.05$, as the hypothetical monolayer of adsorbed N_2 is reached; a linear region between $P/P_0 \approx 0.05$ - 0.30 called the 'multilayer region' (here, this region appears to extend to approximately 0.40); a continual increase in V_a with increasing P/P_0 past the multilayer region; and a sharp increase in V_a at $P/P_0 \approx 0.70$, as condensation of N_2 on the surface ensues. Data from Gregg and Sing, 1982, Table 2.14.

This technique is not necessary to obtain an accurate value for SSA, which is not sensitive to slight changes in the linear range chosen. However, it is a rigorous method

for choosing the most linear portion of the multilayer region for analysis and is especially useful for deriving c , which is extremely sensitive to the linear range used. The slope (m) of this second regression line = $(c-1)/cV_m$, and the y-intercept (b) = $1/cV_m$. The value of V_m is extracted algebraically and used to solve for surface area (A_{sp}):

$$A_{sp} = \frac{V_m N_A \sigma^o}{22,414}, \quad (2)$$

where N_A = Avogadro's number, σ^o is the area occupied by one N_2 molecule ($16.2 \times 10^{-20} \text{ m}^2$), and 22,414 = the volume of a mole of gas at standard temperature and pressure (cm^3). The region chosen for linear regression is crucial to obtaining accurate values for SSA and c . Although the region of $P/P_o = 0.05 - 0.30$ is generally fairly linear, there are usually some slight deviations from linearity. The region chosen should be as linear as possible but should also give a reasonable value for c , which is highly sensitive to the value of b (the y-intercept), especially for solids, including oxides, where b often approaches zero (including oxides). In such cases, a slight change in the equation may produce either a very high c value, which if real might preclude the use of BET analysis, or a negative one (which implies endothermic adsorption and is therefore unrealistic).

In addition to SSA, gas adsorption analysis yields several types of information about the porosity of a sample. One indication of porosity is hysteresis upon desorption. (Hiemenz and Rajagopalan 1997) In BET theory, the volume of gas taken up at any given relative pressure should be released at the same pressure, producing a desorption isotherm identical to the adsorption isotherm. This assumes that the solid surface takes up N_2 gas homogeneously, and does not consider the possibility of pores on the solid surface, which may trap N_2 molecules and retain them at relative pressures lower than those at which they entered the pores, or which may experience the onset of condensation before the nonporous areas of the surface (Gregg and Sing 1982). Figure 3 is a schematic drawing of gas sorption hysteresis.

A second indicator of porosity is the value of the c parameter. Some materials are known to have characteristic ranges for c ; for example, oxides tend to range from $c = 50-$

100, while organic materials typically have lower c values (Mayer 1999). Solids with extensive microporosity (pores with diameters of < 2 nm) generally have very high c -values, i.e., in the range of 700 (Davis and Kent 1990). Because in BET theory this implies a very high heat of adsorption, and because extensive microporosity might produce an atypical adsorption isotherm, solids with $c \geq 500$ are considered questionable candidates for BET analysis (Hiemenz and Rajagopalan 1997). An additional indicator of mesoporosity in BET plots include enhanced adsorption above $P/P_0 \approx 0.40$ (Gregg and Sing 1982; Davis and Kent 1990). Several features may be present in the case of microporosity, such as enhanced adsorption at very low P/P_0 , slight hysteresis near $P/P_0 = 1$, or a depressed mid-range adsorption isotherm (Gregg and Sing 1982; Davis and Kent 1990).

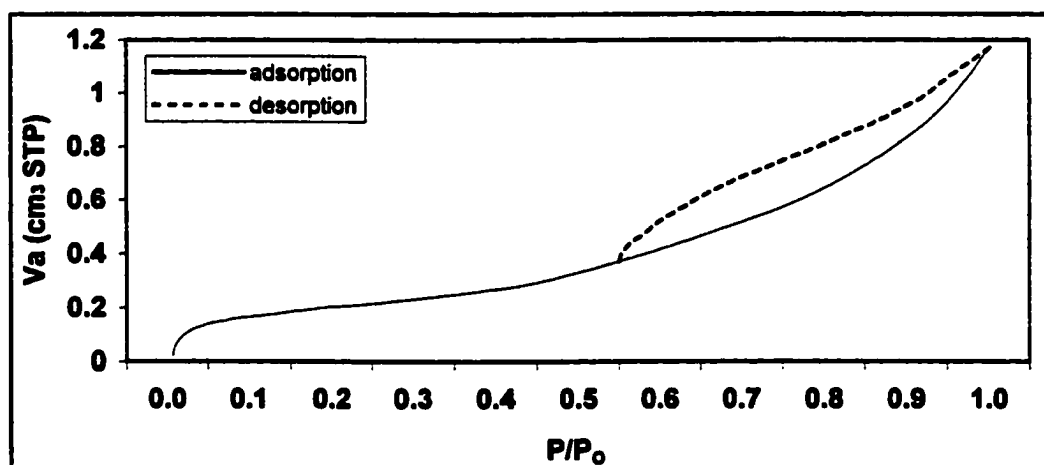


Figure 3. Gas sorption hysteresis. According to BET theory, a plot of V_a vs. P/P_0 should be the same whether relative pressure is increasing or decreasing. Hysteresis indicates a difference in the adsorption and desorption conditions – most often, the onset of capillary condensation in mesopores during adsorption.

In addition to hysteresis and the c parameter, comparison plots – such as t -plots, α -plots, and f -plots (described below) – may be used to assess porosity. If two materials take up N_2 gas in precisely the same manner, their adsorption isotherms will have the same shape, and only the vertical scale will vary with SSA. Thus, it is sometimes useful to compare the adsorption isotherm of a sample to that of a standard reference material or

another material under study, in order to assess any differences in isotherm shape that may point to porosity and other variations in surface properties (Gregg and Sing 1982). Several approaches for comparing adsorption isotherms exist, including t -plots, α -plots, and f -plots.

A t -plot shows V_a as a function of the statistical thickness (t) of the layers of adsorbed N_2 gas (t_1 , considered to be 3.54 Å for N_2 , assuming hexagonal close packing of the molecules) (Gregg and Sing 1982). To construct the plot, t is calculated for all values of P/P_0 of a reference material comparable to the solid under study:

$$t \frac{P}{P_0} = t_1 \cdot \left(\frac{V_a}{V_m} \right) \frac{P}{P_0} \quad (3)$$

V_a for the sample is then plotted against t for all P/P_0 . If the material takes up N_2 exactly like the reference material, the plot will be an increasing straight line intersecting the origin. An α -plot is similar to a t -plot and should yield a plot of similar shape (Gregg and Sing 1982). To derive α , V_a of the reference material is normalized to V_a for $P/P_0 = 0.4$:

$$\alpha \frac{P}{P_0} = \frac{V_a \left(\frac{P}{P_0} \right)}{V_{a(0.4)}} \quad (4)$$

Then V_a for the solid under study is plotted against α for all P/P_0 . Finally, an f -plot shows the ratio of V_a for two solids as a function of P/P_0 :

$$f \frac{P}{P_0} = \left(\frac{V_{a1}}{V_{a2}} \right) \frac{P}{P_0} \quad (5)$$

If the solids take up N_2 in the same manner, the plot will be a straight horizontal line (Gregg and Sing 1982).

In addition to highlighting differences in N_2 uptake, t - and α -plots can be used to evaluate porosity (Gregg and Sing 1982; Davis and Kent 1990). Microporous and mesoporous solids have characteristic t - or α -plot shapes (Figure 4). In addition, each

can be used to calculate SSA, although the results should be used only for comparison with the BET calculation. In the case of a mesoporous solid, the result will not agree well with the BET calculation (Davis and Kent 1990). Finally, micropore, and in some cases, mesopore volume may be estimated from these plots, and internal SSA can be derived (Gregg and Sing 1982).

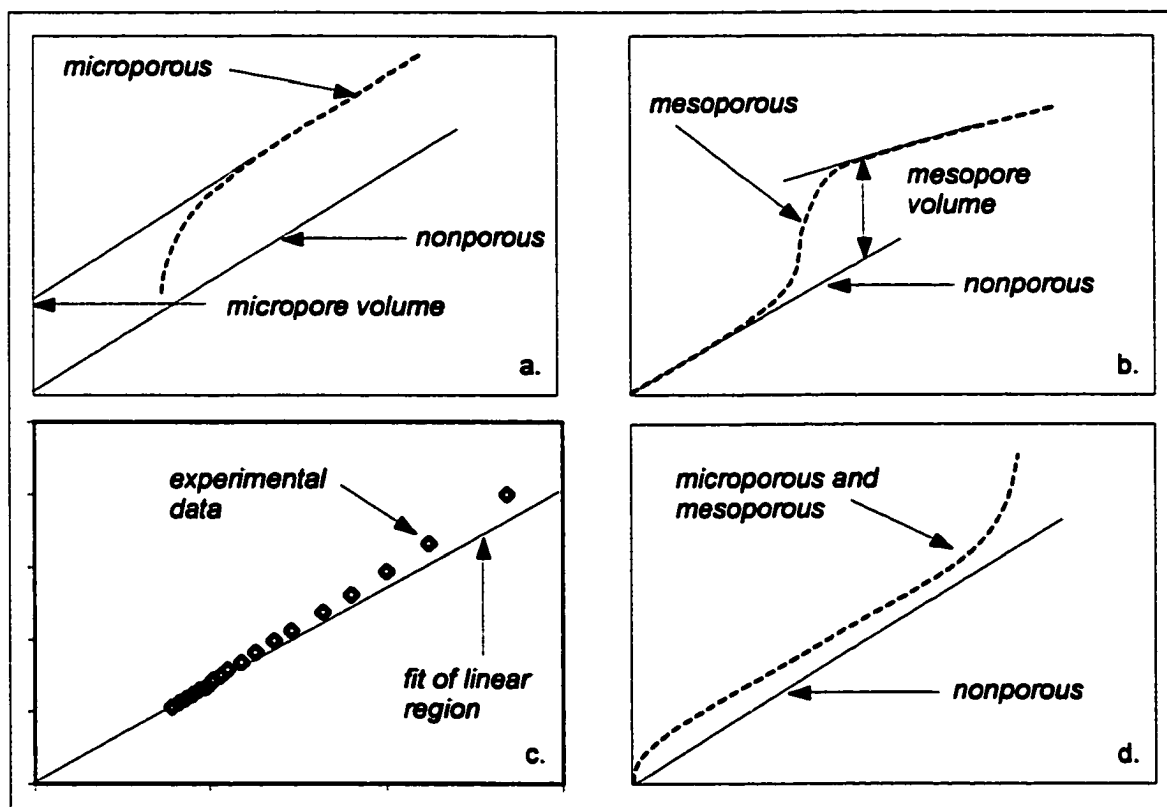


Figure 4. Characteristic t - or α -plots. X-axis is t or α , and y-axis is V_n .
a. Idealized microporous plot (no other significant surface area). Lower branch is non-linear. Upper branch is linear and parallel to nonporous line. Micropore volume is the y-intercept of the upper-branch line. **b.** Idealized plot of mesoporous solid with narrow range of pore sizes (no other significant surface area). Lower branch matches nonporous line. Upper branch is linear, but not parallel to nonporous line. Mesopore volume is equal to the rise of the upper branch from the lower branch. **c.** Experimental data for mesoporous goethite (x-axis is 0-1.5 nm, y-axis is 0-2.5 mmol g⁻¹). Lower branch matches nonporous line. Upper branch rises off the line, and does not return to linearity. Adapted from Figure 10, Davis and Kent, 1990. **d.** Schematic plot of microporosity occurring with mesoporosity. Both nonlinear lower branch (microporosity) and rising upper branch (mesoporosity) are evident.

It should be noted that Figure 4 shows plots for solids in which all substantial surface area is contained in micropores or mesopores (Figure 4, a and b). It is much more common for porosity to accompany significant external surface area, and both size classes of pores may be present in the same solid (Gregg and Sing 1982). In such cases, evidence of microporosity may be subtle; its occurrence with external surface area may produce an isotherm shape typical of a nonporous solid, and the data must be carefully inspected for signs of a steepened initial uptake region ($P/P_0 < 0.05$), an increase in c , and a shortened linear branch. Similarly, microporosity occurring with mesoporosity may yield an isotherm similar to that for mesoporosity alone (Gregg and Sing 1982). When all three are present, particular care is required to detect and assess their relative contributions to N_2 gas adsorption.

To calculate SSA using t - or α -plots, a linear region must be carefully selected. It is advisable to analyze several similar and overlapping sets of points in order to assess the stability of the value derived for SSA. The following expression may be used to derive SSA from a t -plot:

$$SSA_t = 15.392 \cdot m. \quad (6)$$

This calculation exploits the relationship between the volume of the first layer of N_2 and the specific surface area of the solid. (N.B. The expression given by Gregg and Sing, $SSA(t) = 3.45 \times 10^5 \cdot m$, is based on n_m , the number of molecules in the first layer, and has been corrected here using the molar volume of an ideal gas.) To calculate SSA using α , the following expression may be used:

$$SSA_\alpha = m(\alpha) \cdot 2.900. \quad (7)$$

(Again, Gregg and Sing's (1982) expression has been corrected to yield units of $m^2 g^{-1}$.) These values for SSA may be compared to BET-derived SSA to check for mesoporosity.

The linear fits may also be used to estimate pore volume. Micropore volume is equal to the y-intercept, and mesopore volume may be estimated for solids with a narrow

range of pore sizes (which return to linearity at high t) as the rise from the low branch to the high branch (Gregg and Sing 1982).

Internal SSA is calculated using a variation of the t -plot developed by Harkins and Jura (Webb and Orr 1997). Harkins and Jura collected adsorption isotherms on a broad variety of solids to obtain the following expression:

$$t_{HJ} = \left(\frac{A}{B - \log\left(\frac{P}{P^o}\right)} \right)^C, \quad (8)$$

where t_{HJ} gives the Harkins-Jura thickness for each P/P^o , and A , B , and C are empirical coefficients ($A = 13.99$, $B = 0.034$, and $C = 0.5$). V_a is plotted against t_{HJ} and a linear range is selected. External SSA is then calculated as follows:

$$SSA_{ext} = \frac{mD \cdot 10^{10}}{F \cdot 10^6}, \quad (9)$$

where m is the slope of the line, D is a liquid-to-gas density conversion ($1.547 \times 10^{-3} \text{ cm}^3 \text{ cm}^{-3}$), 10^{10} is a conversion from Å to m , F is a correction factor usually equal to 1 (for clays it is 0.975), and 10^6 is a conversion from cm^3 to m^3 . This value is subtracted from BET SSA to give internal SSA.

Solids were analyzed for specific surface area and porosity using a Micromeritics Gemini 2375 multipoint N_2 surface area analyzer. Solids were degassed for at least two hours with N_2 at 102°C and placed into the instrument for analysis immediately upon cooling. N_2 uptake onto the solid was measured at 42 relative pressures (P/P_o) rising from 0.05 to 0.96 and then falling back to 0.05. The instrument was calibrated using a reference kaolinite standard of known SSA at the beginning of each day's analysis (Micromeritics Part No. 004-16819-00, Lot No. 19672-19). Over the period in which the solids studied here were analyzed, 20 of these calibration analyses were sampled and the results used to assess the precision and accuracy of the analytical method for determining specific surface area. The SSA of the kaolinite was reported to be $16.4 \pm 0.8 \text{ m}^2 \text{ g}^{-1}$. The

mean value for the 20 sampled calibration analyses was $16.5 \text{ m}^2 \text{ g}^{-1}$, and the 95% confidence interval was calculated to be $\pm 0.1 \text{ m}^2 \text{ g}^{-1}$.

An analysis of the method's sensitivity to measurement uncertainties involved in sample preparation and analysis. Three solids were chosen to test the method's sensitivity to measurement error. The measured quantities considered were the mass of the sample, as it affects volume of gas adsorbed (given in units of $\text{cm}^3 \text{ gas g}^{-1} \text{ solid}$), and gas pressure, as it affects relative pressure (both gas pressure and atmospheric pressure) and volume of gas adsorbed. The uncertainty of the balance used is $\pm 0.02 \text{ mg}$; the manufacturer reports that the pressure resolution is better than 0.1 mmHg and the instrument supplies data with two decimals; therefore, the uncertainty for pressure measurements was estimated as 0.01 mmHg . The solids were chosen to represent the full range of SSA measured: quartz ($0.5 \text{ m}^2 \text{ g}^{-1}$), the reference kaolinite ($16.4 \text{ m}^2 \text{ g}^{-1}$), and goethite ($92.6 \text{ m}^2 \text{ g}^{-1}$ – not the goethite used elsewhere in this study). Mass and gas pressure were systematically varied, and wherever differences in relative pressure (P/P_0) and volume adsorbed (V_a) resulted, SSA was calculated using the affected quantities.

The changes in mass and gas pressure made no difference in either P/P_0 or V_a at the levels of uncertainty for quartz (and hence had no effect on SSA). Kaolinite and goethite values for V_a were altered in only two cases: low mass/high gas pressure, and high mass/low gas pressure. Goethite SSA values calculated using these quantities were not affected; kaolinite values changed by $0.01 \text{ m}^2 \text{ g}^{-1}$. This was considered a negligibly low level of sensitivity, since it constitutes 0.06% of the kaolinite SSA.

The largest change in atmospheric pressure over the course of an analysis observed was from 797.91 to 795.79 mmHg, or 2.12 mmHg, over 4.75 h. Saturation pressure was varied by this amount and SSA values calculated using the lowest and highest ranges of P/P_0 . Quartz and kaolinite SSA values were not affected; the goethite value decreased with decreasing P_0 by $0.2 \text{ m}^2 \text{ g}^{-1}$, or 0.2% of the goethite SSA. This was considered an acceptably low level of sensitivity. Nevertheless, as part of the quality assurance/quality control protocol, atmospheric pressure was measured at the beginning

of each day and monitored over time to ensure that changing atmospheric conditions did not require recalibration of the instrument for saturation pressure (P_o).

In order to further assure the accuracy and precision of BET analysis, several sets of points within the multilayer region were used to derive SSA, and the variations in SSA, m , b , and c were evaluated in comparison with each other and with published data. Using this information, the set considered optimal for analysis were selected and used to determine SSA and c .

Energy-dispersive X-ray Spectrometry (EDS)

This method yields information on the identification and spatial distribution of elements in a specimen by making use of the fact that atoms emit characteristic X-rays on bombardment with high-energy electrons. EDS analyzers are typically attached to scanning electron microscopes; the X-ray detector (a lithium-drifted silicon crystal) is placed near the surface of the specimen and measures characteristic X-rays emitted as the electron beam strikes the surface. These are converted to spectra of X-ray energy; peaks in the spectra are used to identify elements present in the specimen and quantify their abundance as a function of the magnitude of the peaks. Data for as many elements as desired may be collected at points ("spot counts"), along lines ("line scans"), or throughout a region ("element maps") (Goldstein et al. 1992).

Although a powerful analytical technique, widely applied in environmental geochemistry, EDS has some intrinsic limiting characteristics. One issue is the large number of analytical artifacts, such as escape peaks, which make accurate quantification difficult (Goldstein et al. 1992). Another is the relatively low spatial resolution of the method, which limits its usefulness for studying very small particles. The electron interaction volume for EDS analysis under typical conditions for studying geological materials has been estimated to be $1 \mu\text{m}^3$; hence, a spot counted on a particle smaller than this contains signals generated throughout the entire particle (Seaman 2000). This effect is ameliorated to some extent by the fact that signal efficiency decreases exponentially with depth in the sample; for the instrument used, ~ 90% of the signal is estimated to

originate in the top 0.1 μm of the specimen (IXRF Systems Inc. 2002). Nevertheless, EDS results must be carefully interpreted in light of these analytical limitations.

Investigations of the spatial distribution of the coatings on the surfaces of the quartz and kaolinite grains was performed using a LEO 435VP scanning electron microscope (SEM) with an IXRF EDS attachment. Particles of each solid were sparingly scattered across an adhesive carbon tab mounted on an aluminum stub and sputter-coated to a thickness of 20 nm with gold and palladium. Using a random sampling method, 10 grains of Q-chem were selected. On each grain, three spots on 'face' surfaces and three on 'edge' surfaces were chosen for analysis. 'Faces' refers to relatively smooth areas of the grains, while 'edges' are visibly disrupted regions of the grain surface, such as pits, cracks, and fracture scars. The flat grains of coated kaolinite could not feasibly be sampled for both 'face' (basal plane) and 'edge' spots, since they tended to lie either face-on or edge-on to the electron beam. For these solids, therefore, 10 face-on and 10 edge-on grains were selected, and three spots on each grain were analyzed.

Each spot chosen for analysis ($n = 60$ for each solid) were counted for Fe, Al, and Si. The specimen was tilted 10° from normal to the electron beam (EHT = 20 keV). The desired count rate was $\approx 4,000$ per second; beam current was adjusted between 200 and 400 picoamps to achieve this count rate. A live time fraction of 0.70 was sought by varying spot size. A total of 100 live seconds of data were collected for each spot. Then an element map of Fe was made of the sampling region, with a resolution of 512 pixels and a point dwell time of 20 ms.

The spot-count data was transformed into semiquantitative wt % values using the automatic standardless ZAF quantitation routine provided with the EDS manufacturer's software. 'Semiquantitative' here indicates that the data are considered useful for element identification, determination of presence or absence of the elements, and relative quantity in comparison with other spots. Because the Fe data are normalized to the substrate signal (Si for quartz and Al:Si for kaolinite), quantities can neither be compared between solids with different substrates nor used as an estimate of absolute Fe concentration.

Physical Adsorption Results

Figures 5-10 are N_2 adsorption/desorption isotherms for particulate goethite, quartz and kaolinite, and the three coated solids. All show typical BET behavior with increasing relative pressure (compare to Figure 1). (Note that data was not collected at $P/P_o < 0.05$, so that there is no “knee” visible in the isotherms.) Goethite showed a slight hysteresis above $P/P_o \approx 0.8$ (Figure 5). Quartz and kaolinite displayed no hysteresis upon desorption (Figures 6 and 7); likewise, K-chem showed no hysteresis (Figure 8); however, Q-chem exhibited desorption hysteresis between $P/P_o \approx 0.4$ and 0.8 (Figure 9), while for Kch-thick, hysteresis appears to persist throughout the desorption leg, notably above $P/P_o \approx 0.4$, and is greatest at highest P/P_o (Figure 10).

Figures 11 and 12 show the linear ranges and residuals for the BET adsorption isotherms of the solids studied. The linear ranges chosen for SSA calculation are shown along with the regression lines, equations, and correlation coefficients. As discussed above, choosing the set of points within the linear range from which to derive SSA is an iterative process: the entire linear range is subjected to a linear regression, and the residuals are plotted. The subset of points corresponding to the steepest and most linear part of the residuals function decreasing from left to right is selected, and regressions are performed on several groups from within this subset in order to find the set which strikes the best balance between linearity and the reasonableness and stability of the derived parameters. Known BET properties of similar materials are also taken into consideration.

Although the entire region tends to be relatively linear (see Figures 11 and 12), dramatic shifts in the values of the parameters may result from using slightly different sets of points; thus, relatively few points are generally used in the final set used to derive SSA (Mayer 1999). However, the use of residuals analysis to find the most linear subset of points and the intensive analysis of numerous linear fits to ensure relative stability and linearity somewhat ameliorates the scantiness of the final set of points used. The greatest number of points yielding a satisfactory result was chosen for each SSA derivation here.

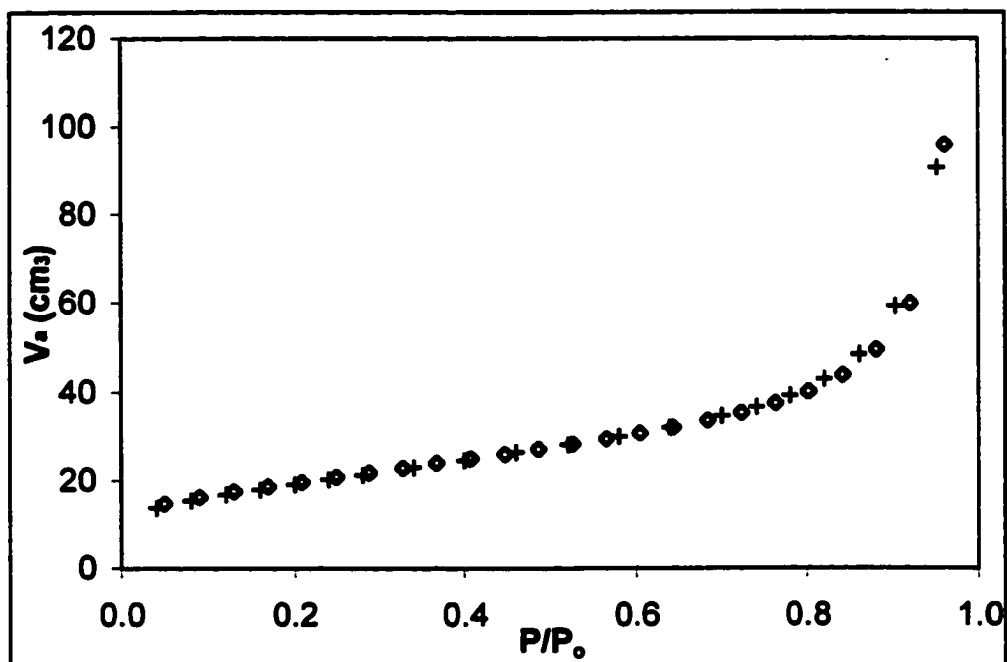


Figure 5. N₂ adsorption and desorption isotherms for particulate goethite. ' \diamond ' = adsorption; '+' = desorption. Note slight hysteresis at high P/P_o .

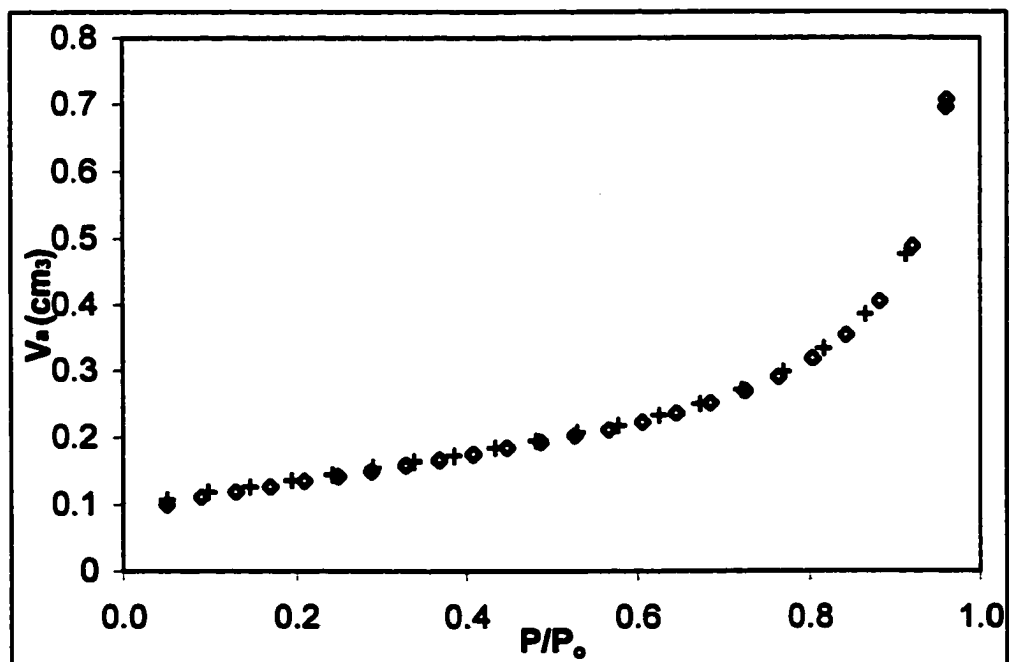


Figure 6. N₂ adsorption and desorption isotherms for quartz. ' \diamond ' = adsorption; '+' = desorption.

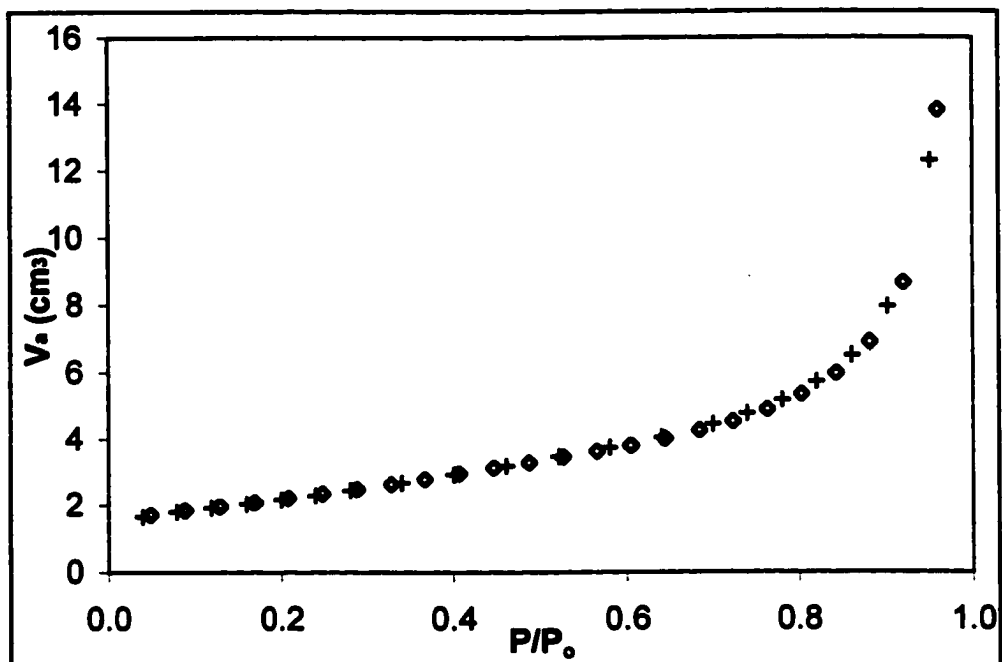


Figure 7. N₂ adsorption and desorption isotherms for kaolinite. '◇' = adsorption; '+' = desorption.

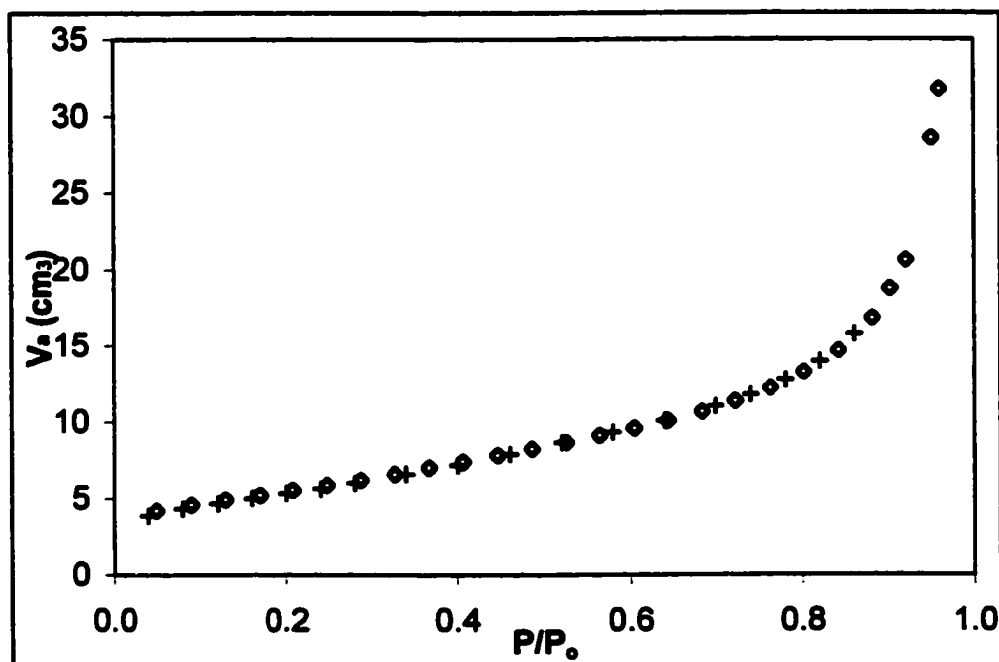


Figure 8. N₂ adsorption and desorption isotherms for K-chem. '◇' = adsorption; '+' = desorption.

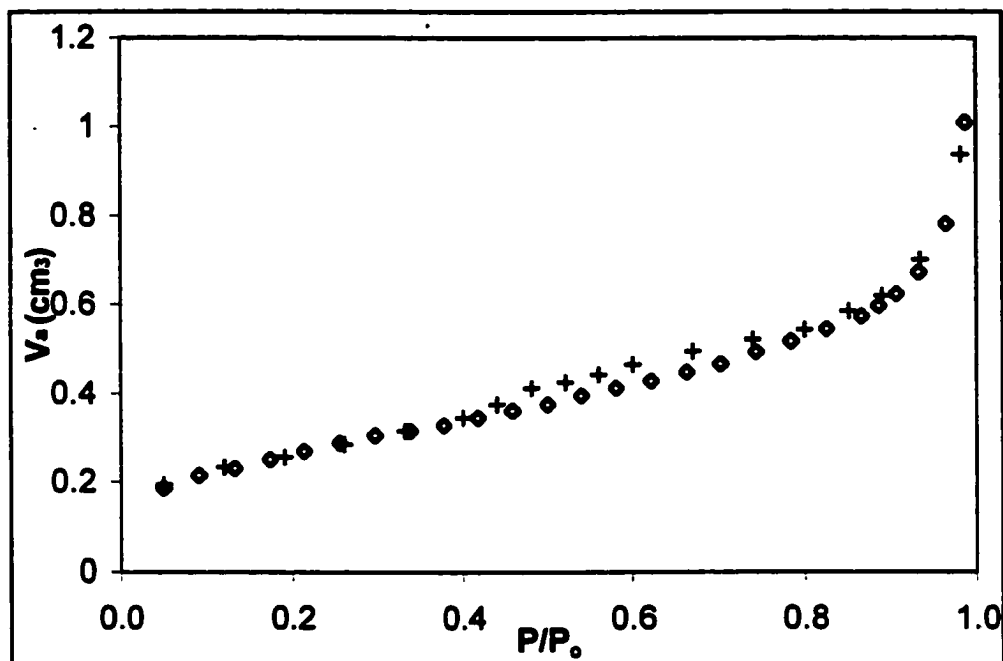


Figure 9. N_2 adsorption and desorption isotherms for Q-chem. ' \diamond ' = adsorption; '+' = desorption. Note hysteresis from $P/P_0 \approx 0.4$ - 0.9 .

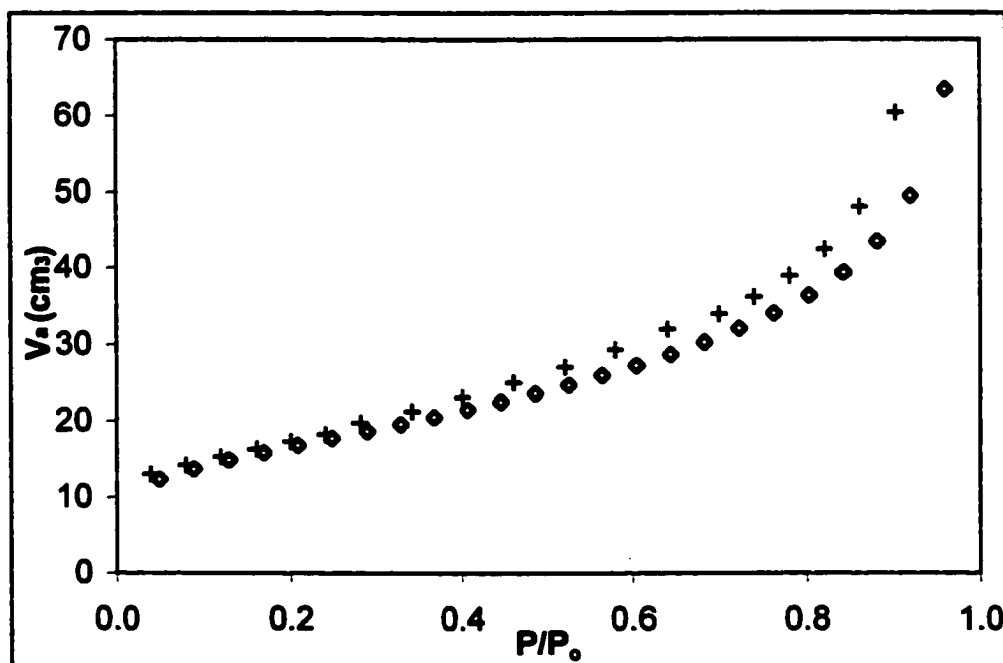


Figure 10. N_2 adsorption and desorption isotherms for Kch-thick. ' \diamond ' = adsorption; '+' = desorption. Note hysteresis over entire range of P/P_0 .

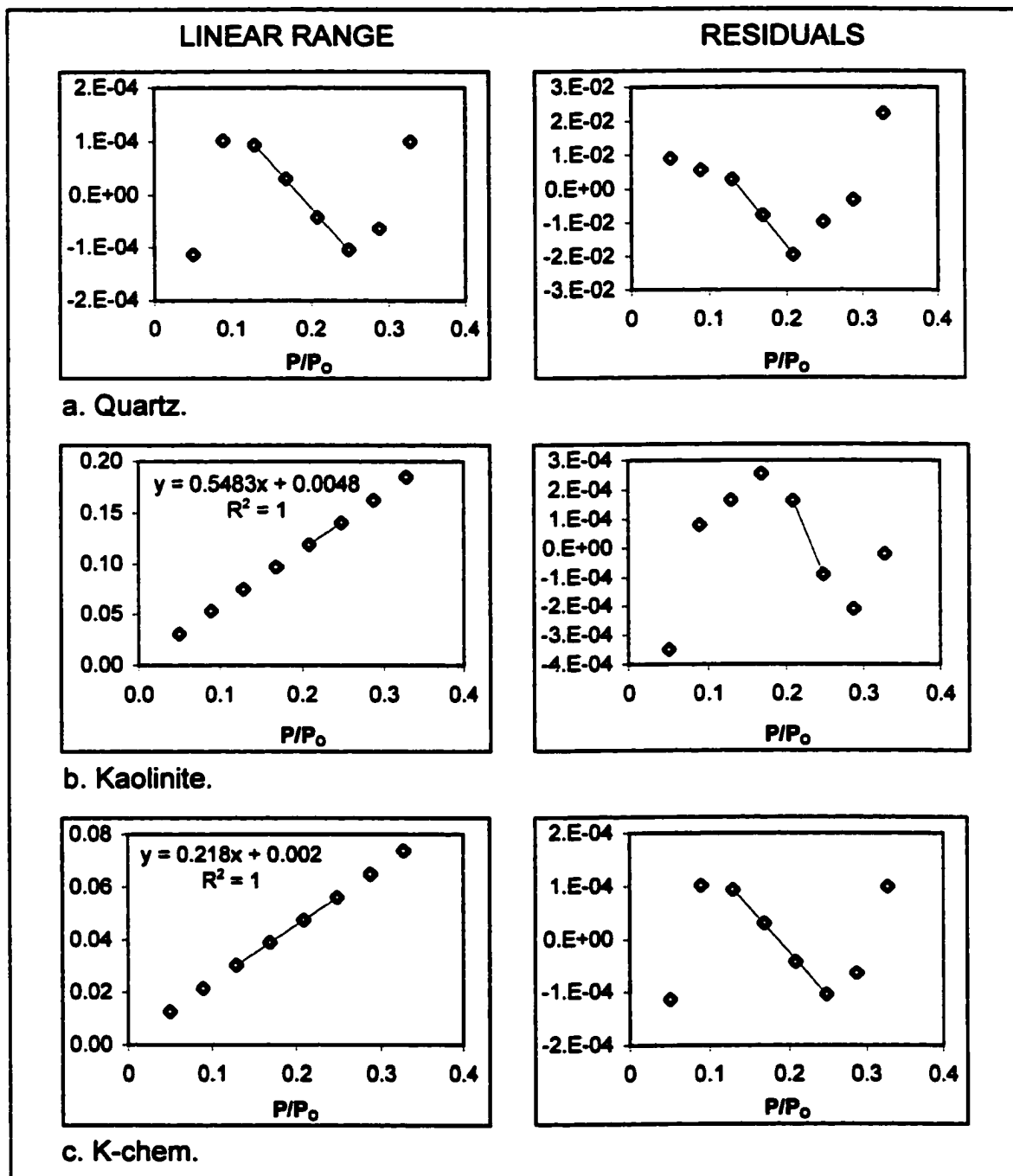


Figure 11. Linear regions of N₂ adsorption isotherms (left) and residuals of linear regression analysis (right) for quartz, kaolinite, and K-chem. The y-axis for the linear region plots is the left-hand side of the linear BET equation: $(1/V_a) \cdot (x/[1-x])$, where $x = P/P_0$. Lines and equations indicate the points selected for SSA analysis.

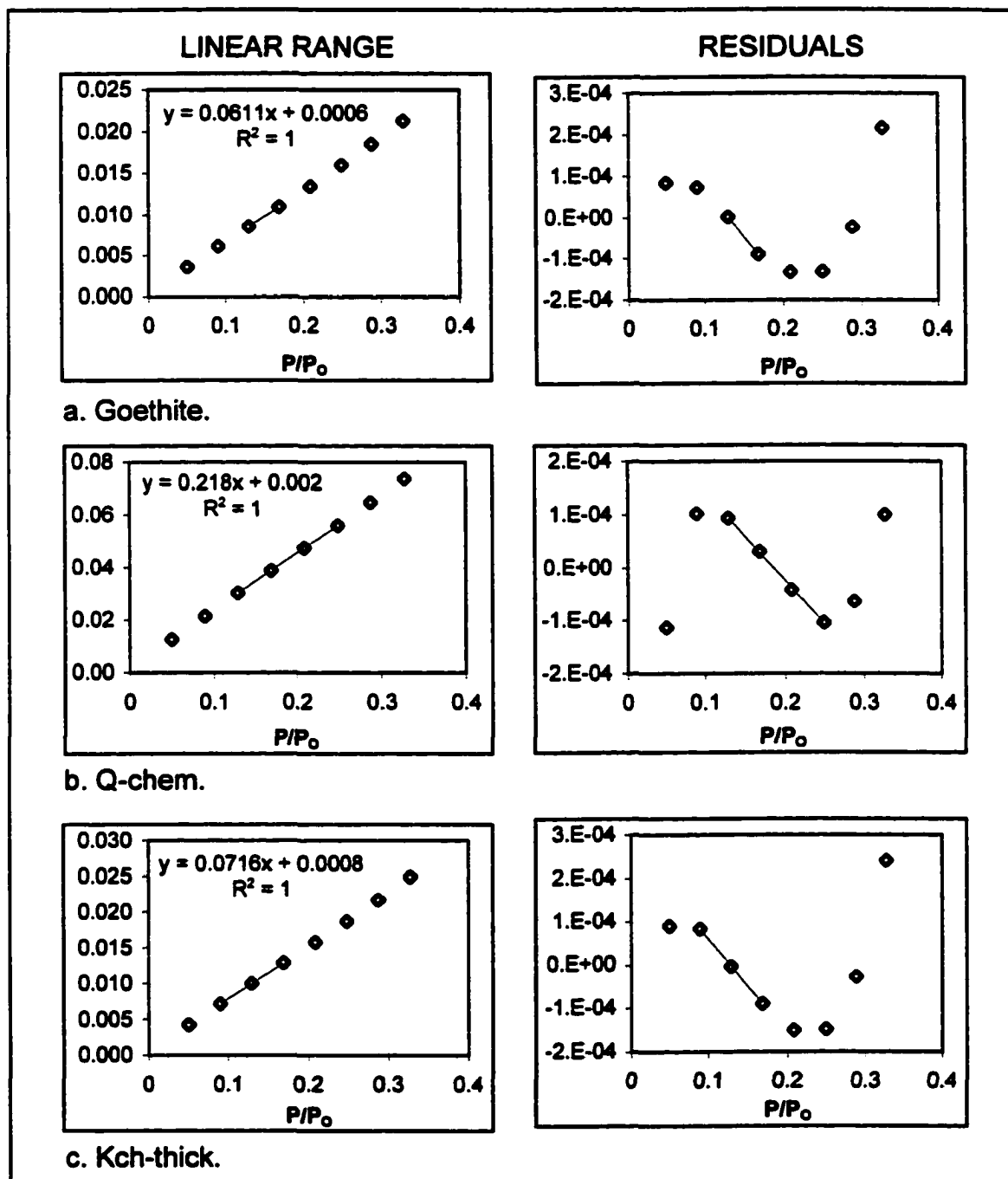


Figure 12. Linear regions of N_2 adsorption isotherms (left) and residuals of linear regression analysis (right) for goethite, Q-chem, and Kch-thick. The y-axis for the linear region plots is the left-hand side of the linear BET equation: $(1/V_a) \cdot (x/[1-x])$, where $x = P/P_0$. Lines and equations indicate the points selected for SSA analysis.

It is interesting to see that the shapes of the residuals trends can be split into two types: an “N-shaped” curve characteristic for oxide minerals (Mayer, 1999), seen in the quartz, kaolinite, and K-chem data (Figure 11); and a more ‘U-shaped’ curve, without the initial low residual point; solids exhibiting this trend are goethite, Q-chem, and Kch-thick (Figure 12). Note, however, that this may be an artifact of the data range, since very low ($P/P_o < 0.05$) data were not collected for this study. Thus, the entire linear range for the solid may not have been measured.

Table 2 summarizes the results of BET specific surface area analysis. The c values are all positive, within BET constraints, and near typical values for oxide minerals. The y-intercepts are all near zero; those for goethite and Kch-thick are the lowest, on the order of 10^{-4} , followed by kaolinite and K-chem on the order of 10^{-3} , and then quartz and Q-chem on the order of 10^{-1} . The typical range of P/P_o used for analysis was approximately 0.13 to 0.20.

TABLE 2. Summary of BET analysis.

Solid	SSA $\text{m}^2 \text{g}^{-1}$	Hysteresis	c	y-intercept
Quartz	0.5	—	91	1×10^{-1}
Kaolinite	7.9	—	115	5×10^{-3}
Goethite	70.6	$> \approx 0.8$	103	6×10^{-4}
Q-chem	1.0	$\approx 0.4-0.9$	46	1×10^{-1}
K-chem	19.8	—	110	2×10^{-3}
Kch-thick	60.1	entire range	91	8×10^{-4}

In all cases, the coated solids had a higher SSA than the corresponding uncoated substrates (see Table 2). The thin coatings had roughly double the SSA (1.0 versus $0.5 \text{ m}^2 \text{g}^{-1}$ for quartz, and 19.8 vs. $7.9 \text{ m}^2 \text{g}^{-1}$ for kaolinite); the thick kaolinite coating approached the SSA of particulate goethite ($60.1 \text{ m}^2 \text{g}^{-1}$ vs. $70.6 \text{ m}^2 \text{g}^{-1}$). (The particulate goethite analyzed was synthesized using the method of Schwertmann and Cornell (1991), which is very similar to that used in producing the coatings.) A high-SSA coating should increase the net SSA of a solid more than would be predicted from its mass, because it

has a higher surface-area-to-volume ratio than an equivalent amount of the same material occurring as a bulk particle, just as a bubble has a higher surface area-to-volume ratio than a drop of water. This can be tested by predicting the SSA that should be contributed to the solid by the coating material purely on the basis of its mass. Assuming that the substrate contributes its full SSA to the coated solid, and that the coating contributes all of the remaining SSA, then the difference between the SSA of the coated solid and the uncoated substrate should be due solely to the presence of the coating. The calculation of the predicted SSA for the coated solid is as follows:

$$SSA_{pred} = (SSA_{sub} * f_{sub}) + (SSA_{goet} * f_{goet}), \quad (10)$$

where SSA_{pred} is the predicted SSA for the solid, SSA_{sub} and SSA_{goet} are the measured SSA for the substrate and particulate goethite, respectively, and f_{sub} and f_{goet} are the fractions of substrate and goethite present in the solid (i.e., wt % /100). For example, the coating on Q-chem has a predicted SSA of $(0.5 \text{ m}^2 \text{ g}^{-1} * 0.9979) + (70.6 \text{ m}^2 \text{ g}^{-1} * 0.0021) = 0.6 \text{ m}^2 \text{ g}^{-1}$. As shown in Table 3 (“Predicted solid SSA”), this yields a comparable value for Q-chem, but underpredicts both kaolinite solids.

The SSA of the coating was estimated by subtracting the weighted substrate SSA from the measured solid SSA, and dividing by the fraction of goethite in the solid:

$$SSA_{coat} = \frac{(SSA_{meas} - [SSA_{sub} * f_{sub}])}{f_{goet}}. \quad (11)$$

This is given in Table 3 as “Calculated coating SSA.”

The calculated coating SSA values are much greater than that of particulate goethite. This is not very surprising; however, it is interesting that the estimates derived in this way for Q-chem and Kch-thick are relatively similar, while the value for K-chem is about twice as great. This suggests that the thin kaolinite coating exposes much more surface area on a per-mass basis. A simple conceptual model for converting particulate goethite surface area to coating surface area is to visualize the particulate goethite as a cube. The cube is then cut in half, and the two halves are placed end to end. This

increases the surface area in the system by a factor of 7/6, or 1.667. One may assign the measured SSA for goethite to the imaginary cube and make successive divisions until the calculated SSA for the coating is reached. For Q-chem, this requires approximately 8 divisions ($242.3 \text{ m}^2 \text{ g}^{-1}$); for Kch-thick, about 9 divisions are required ($282.7 \text{ m}^2 \text{ g}^{-1}$); and for K-chem, between 13 ($523.7 \text{ m}^2 \text{ g}^{-1}$) and 14 ($611.0 \text{ m}^2 \text{ g}^{-1}$) divisions.

It must be emphasized that these estimates are rough because of the underlying assumptions discussed above. In addition, although it is assumed that the SSA of the substrate remains the same throughout the coating process, the substrate surface may in fact be altered to some extent by equilibration in the Fe solutions prior to precipitation. Furthermore, although the substrate solids were cleaned and size-fractionated before coating, there were probably some residual fine particles in the cleaned materials. Some of these were lost during the coating process, so that the coated substrate probably had a slightly higher mean grain size than the uncoated mineral, and hence a slightly lower SSA. Finally, although the goethite sample used to represent the coating in the calculations was synthesized using an almost identical method, recently published SSA values for goethite range from 27 to $153 \text{ m}^2 \text{ g}^{-1}$ (Robertson and Leckie 1997; Randall et al. 1999; Rietra et al. 1999; Elzinga et al. 2001; Larsen and Postma 2001). Consequently, factors such as the age of the samples and the degree of crystallinity could have a significant effect on goethite SSA.

TABLE 3. Summary of SSA analysis ($\text{m}^2 \text{ g}^{-1}$).

Solid	Measured solid SSA	Measured substrate SSA	Predicted solid SSA^a	Calculated coating SSA^c
Q-chem	1.0	0.5	0.6	249.2
K-chem	19.8	7.9	9.2	584.1
Kch-thick	60.1	7.9	19.2	298.6

^a Predicted solid SSA = sum of the products of component SSA and component mass fraction. ^b SSA of goethite ($70.6 \text{ m}^2 \text{ g}^{-1}$) times mass of goethite in solid. ^c Value for coating SSA that yields the measured SSA of the solid.

Nevertheless, the large differences in the calculated and predicted SSAs demonstrate that the coating contributes disproportionately to the net SSA relative to what would be expected for two co-occurring mineral phases (such as quartz and goethite). In addition, the “Calculated coating SSA” values are considerably greater than those of typical or even high surface area ($153\text{-}200\text{ m}^2\text{ g}^{-1}$; Larsen and Postma 2001). The similarity in estimated coating SSA between Q-chem and Kch-thick, in contrast to K-chem, is also interesting. It would seem more likely either that all three goethite coatings would have similar SSAs; or that all three would be different; or that if two were similar, the kaolinite coatings would resemble each other in contrast to the quartz. This result suggests the possibility that the quartz coating and the thick kaolinite coating have some characteristic or characteristics in common.

Figure 13 shows the t -plots for the solids. Linear regions were chosen within $P/P_0 \approx 0.35 - 0.70$ (Davis and Kent 1990); several regions were analyzed for linearity as well as stability of slope and y-intercept values. One region was selected, based on these criteria, and used to calculate SSA_t . The typical linear range used was approximately $P/P_0 = 0.53\text{-}0.68$. The equations and correlation coefficients for the selected linear ranges appear on the plots with the line extended over the entire range of data; SSA_t values and micropore volumes (PV_t) are given in Table 4.

None of the t -plot curves appears to rise off the line at high t (Davis and Kent 1990). However, Q-chem appears to fall below the line at high t ; this could suggest mesoporosity within a restricted size range (Gregg and Sing 1982). Q-chem and Kch-thick also slightly resemble the idealized microporous profile in that the curves fall below the line at regions below the linear range. The SSA_t estimates generally agree reasonably well with those calculated by BET analysis; however, some analyses yielded negative y-intercepts ($'b'$; the solids were quartz, kaolinite, and K-chem; see Table 4). (Obviously, these are not useful estimates of pore volume.) No linear range tested gave a zero or positive value for b for these samples. In these cases, more weight was given to regions with stable and least negative values for b . To support these results, α -plots were also

constructed; the curves (not shown) resemble those for the t -plots. SSA_{α} and PV_{α} were calculated; these generally agreed well with t -plot analysis (see Table 4.)

Internal surface area (SSA_{int}) was estimated from plots of Harkins-Jura thickness (Figure 14). A linear range was selected and external SSA was calculated from the slope.

The correction factor F was set at 1 except in the case of kaolinite and K-chem; these were calculated using $F = 0.975$ (the correction factor for clays). The equations and correlation coefficients are given along with the linear fit extended over the entire range of data. SSA_{int} was calculated as the difference between SSA and external SSA. Results are given in Table 4. It should be noted that the apparent presence of internal SSA in kaolinite, with no other evidence of porosity, is thought to arise from the general level of BET method precision ($\approx 0.1 \text{ m}^2 \text{ g}^{-1}$ for this instrument) in combination with errors in analysis of the Harkins-Jura thickness plots. Kaolinite is known to lack porosity.

TABLE 4. Results of t -plot, α -plot, and internal SSA analysis.

Solid	SSA ($\text{m}^2 \text{ g}^{-1}$)	SSA_t ($\text{m}^2 \text{ g}^{-1}$)	SSA_{α} ($\text{m}^2 \text{ g}^{-1}$)	PV_t^a (cm^3)	PV_{α} (cm^3)	SSA_{int} ($\text{m}^2 \text{ g}^{-1}$)	% of SSA ^b
Quartz	0.5	0.6	0.6	-0.031	-0.021	0	0
Kaolinite	7.9	10.0	10.4	-0.453	-0.603	0.3	3.6
Goethite	70.1	68.4	68.8	1.569	1.547	17.8	25.8
Q-chem	1.0	0.8	0.8	0.070	0.080	0.2	23.1
K-chem	19.8	25.1	26.1	-1.107	-1.471	0	0
Kch-thick	60.1	61.3	64.0	2.681	0.624	9.9	16.5

^a PV = pore volume, equal to the y-intercept for the linear region of the plot. ^b Internal SSA as a percentage of BET-calculated SSA.

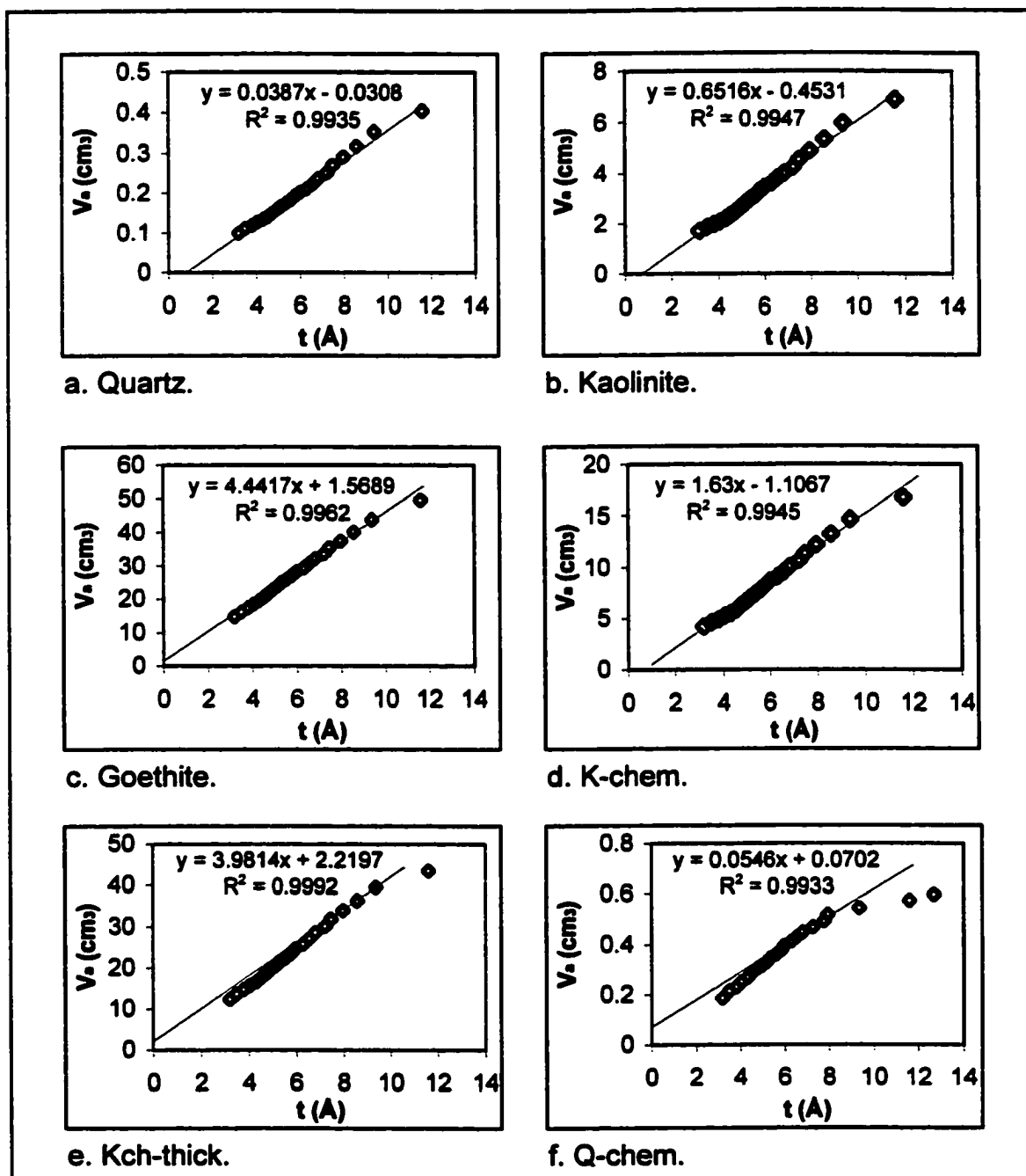


Figure 13. t -plots. Lines are extended from the selected linear range (typically $P/P_0 = 0.53$ - 0.68 , i.e. $t = 5.97$ - 7.24) over the entire data range and correspond to the equations and correlation coefficients given in the plots. Quartz, kaolinite, and K-chem appear to have a slight minimum at $t \approx 4.5$. Q-chem and Kch-thick drop slightly below the line at low t , and Q-chem also drops at low and high t .

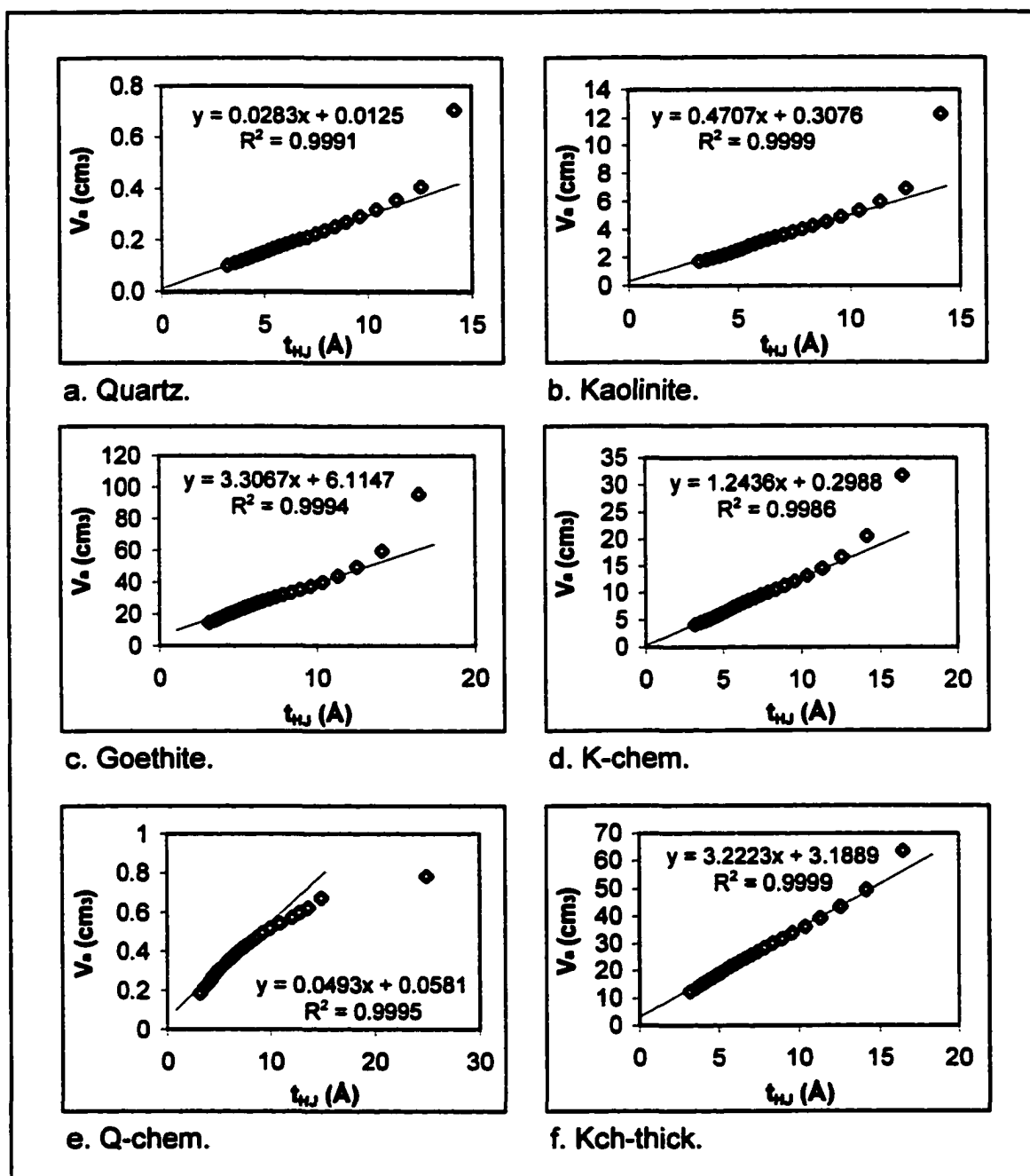


Figure 14. Harkins-Jura thickness (t_{HJ}) plots. The linear ranges chosen varied within the range $P/P_0 \approx 0.37-0.69$. The equations and correlation coefficients for the lines are given on the plots; the lines are extended over the entire range of t_{HJ} . The slope of the line is used to calculate external SSA.

Pairwise comparison of the adsorption isotherms by f -plot analysis required normalization of the data in order to eliminate the disparity in vertical scales, which approached three orders of magnitude. In f -plots, V_a of one solid of interest is divided by V_a of the other, and this ratio is plotted against relative pressure. If the shape of the isotherms is identical, this yields a straight horizontal line. This technique is useful for assessing differences in the shapes of two isotherms. The normalization approach used resembles residuals analysis: for each set, the mean and standard deviation of the ratios was calculated, and the difference of each point from the mean was plotted in standard deviation units (e.g., a difference equal to the standard deviation is assigned the value of positive or negative 1, depending on the direction of deviation from the mean). This process preserves the shape of the f -plot while allowing a consistent vertical scale to be chosen for comparing f -plots, and indicates where the ratio falls relative to the mean.

The following sets of comparisons were made: (1) quartz, kaolinite, and goethite to each other and to the reference silica; (2) each coated solid to its substrate; (3) each coated solid to particulate goethite; and (4) pairs of coated solids. The results are shown in Figures 15-17. In the discussion below, the notation "X:Y" indicates an f -plot in which V_a for X was divided by V_a for Y for each relative pressure.

Figure 15 shows comparisons between quartz, kaolinite, goethite, and the reference silica. The f -plots for quartz and kaolinite compared to the reference silica are similar: they begin below the mean and rise to cross the mean at $P/P_0 \approx 0.4-0.5$; they rise to a sharp maximum at ≈ 0.8 before dropping at the final point. Likewise, the goethite:reference f -plot begins below the mean and also dips before rising as P/P_0 increases; however, above ≈ 0.4 it appears to vacillate near the mean before dropping sharply at the final point. Comparisons of quartz and kaolinite to goethite resemble those to the reference silica in general shape and trend. The quartz:kaolinite f -plot, however, exhibits a concave-down shape with two rounded maxima, one at ≈ 0.2 and the other at ≈ 0.7 . This trend drops sharply at $P/P_0 > 0.8$.

Although it might be expected that the nonporous quartz and kaolinite would behave most like the reference nonporous silica, the f -plot for goethite:reference silica

appears to reflect the closest match (except for the final point), in that many of the points fall onto a horizontal line, and the variability of the ratio is relatively small, implying a relatively straight line. This observed similarity in the isotherms for goethite and the reference silica helps explain the also unexpected similarities between the reference silica and goethite comparisons for quartz and kaolinite – if goethite and the reference silica isotherms are similar, comparisons to each should yield similar curves.

Figure 16 shows *f*-plots comparing each coated solid to its substrate and to particulate goethite. In both cases, Q-chem exhibits a concave-down curve beginning near the mean, which appears to drop off linearly after $P/P_0 \approx 0.75$. The range of variability (i.e., the number of SDs from the mean) is similar for all four plots. The *f*-plots for Kch-thick also evince a characteristic shape, in this case resembling that seen in the quartz:kaolinite plot (Figure 15). The plots for K-chem, however, vary: the substrate plot resembles that for Kch-thick, but the K-chem:goethite plot is similar to the kaolinite:goethite plot. Comparisons between the coated solids did not suggest any striking similarities between any pair (Figure 17). Both Q-chem plots exhibited the same curve seen in comparison to quartz and goethite, and the Kch-thick:K-chem plot also resembled the substrate and goethite plots. (The remaining three plots, not shown here, are inversions of the plots in Figure 17: the goethite-kaolinite solids compared to Q-chem, and K-chem:Kch-thick.)

Given the level of precision of physical adsorption analysis techniques (Gregg and Sing 1982; estimated in the Methods section), it is difficult to distinguish details of intrinsic variability from real differences in reactivity in these plots. However, from the general shape of the plots, some observations about how the isotherms vary can be made. The repetition of characteristic curves is interesting, as is how they track the solids in each pair. The single-maximum curve appears in all plots containing Q-chem, while the double-maximum curve appears in all Kch-thick curves except that with Q-chem. On the other hand, the K-chem plot shapes appear to be controlled more by the other solid in the ratio.

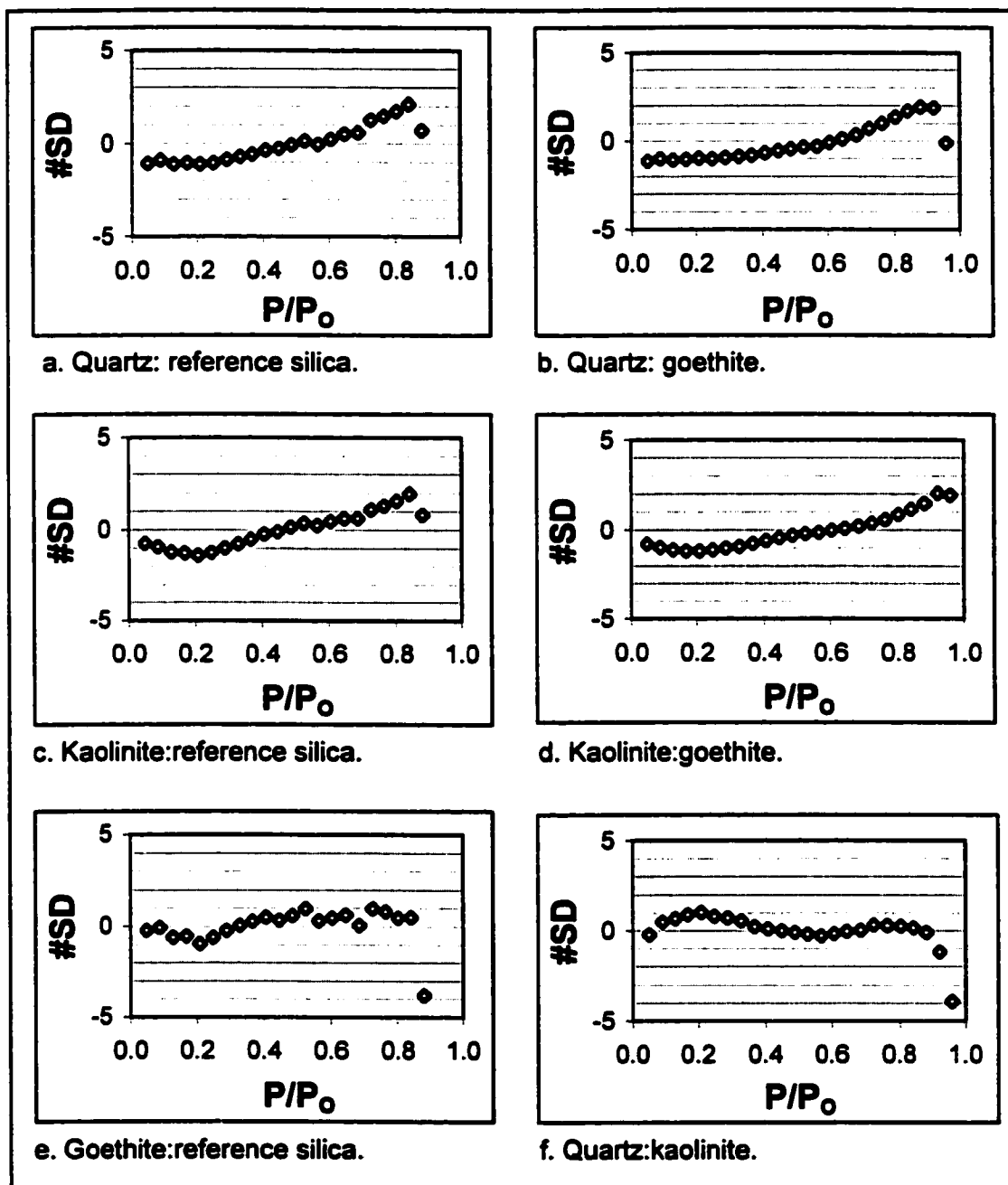


Figure 15. *f*-plot comparisons of quartz, kaolinite, goethite, and reference silica. The plots of quartz and kaolinite compared to the reference silica are similar to those comparing quartz and kaolinite to goethite, while the goethite:reference silica plot suggests a relative degree of similarity in their adsorption isotherms. The quartz:kaolinite plot is distinct from the rest, with its concave-down shape, two maxima, and early positive deviation from the mean ($P/P_0 \approx 0.2$). "#SD" is the number of standard deviations from the mean.

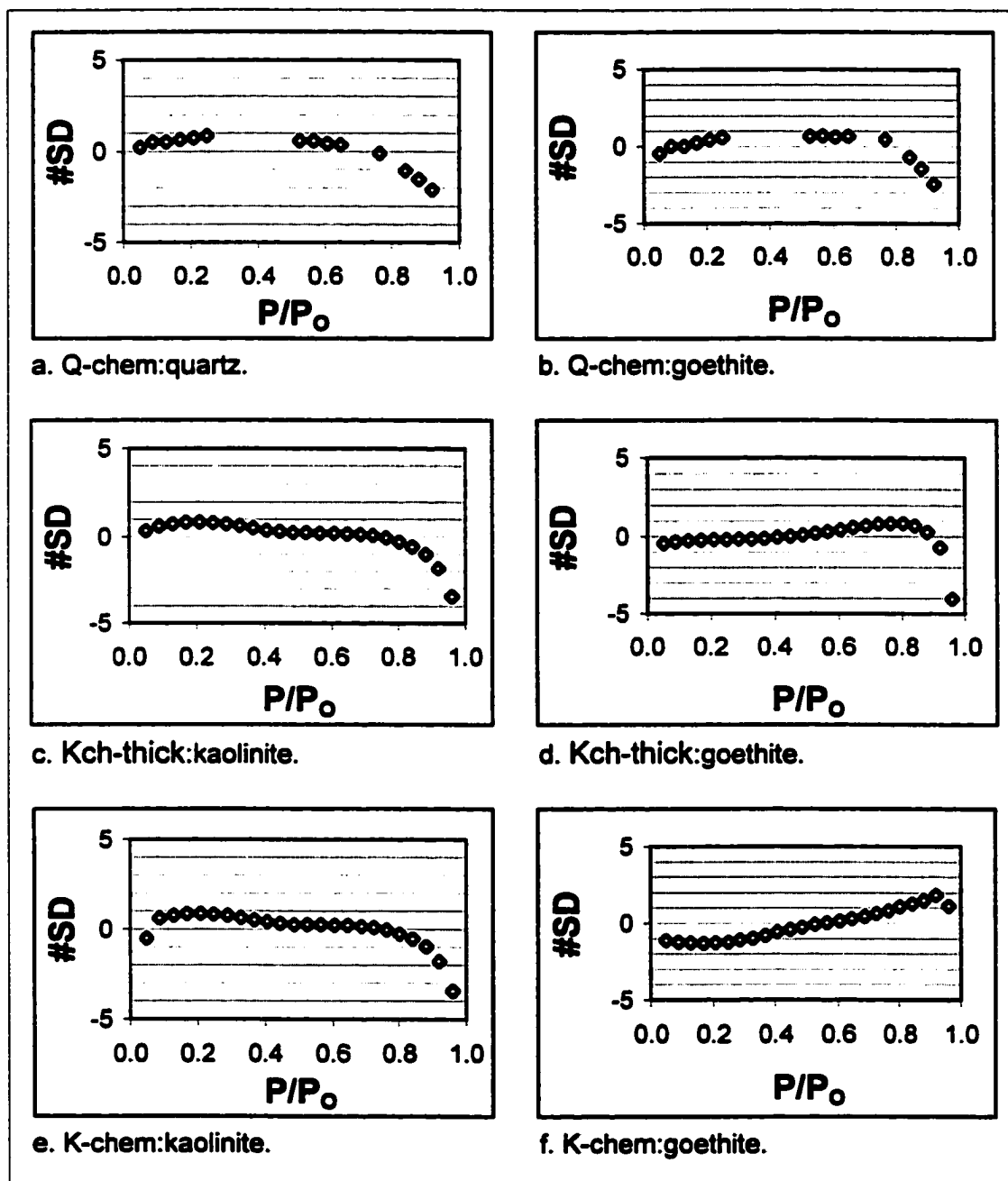


Figure 16. f -plot comparisons of coated solids to their substrates and to particulate goethite. Gaps in Q-chem data occur where V_s was measured at slightly different P/P_0 than the other solids. Note the suggestion of linearity in the high- f drop in Q-chem, and the similarity of quartz and kaolinite plots compared to substrate and goethite. In contrast, although the K-chem:kaolinite plot is similar to Kch-thick:kaolinite, the K-chem:goethite plot is more like kaolinite:reference silica.

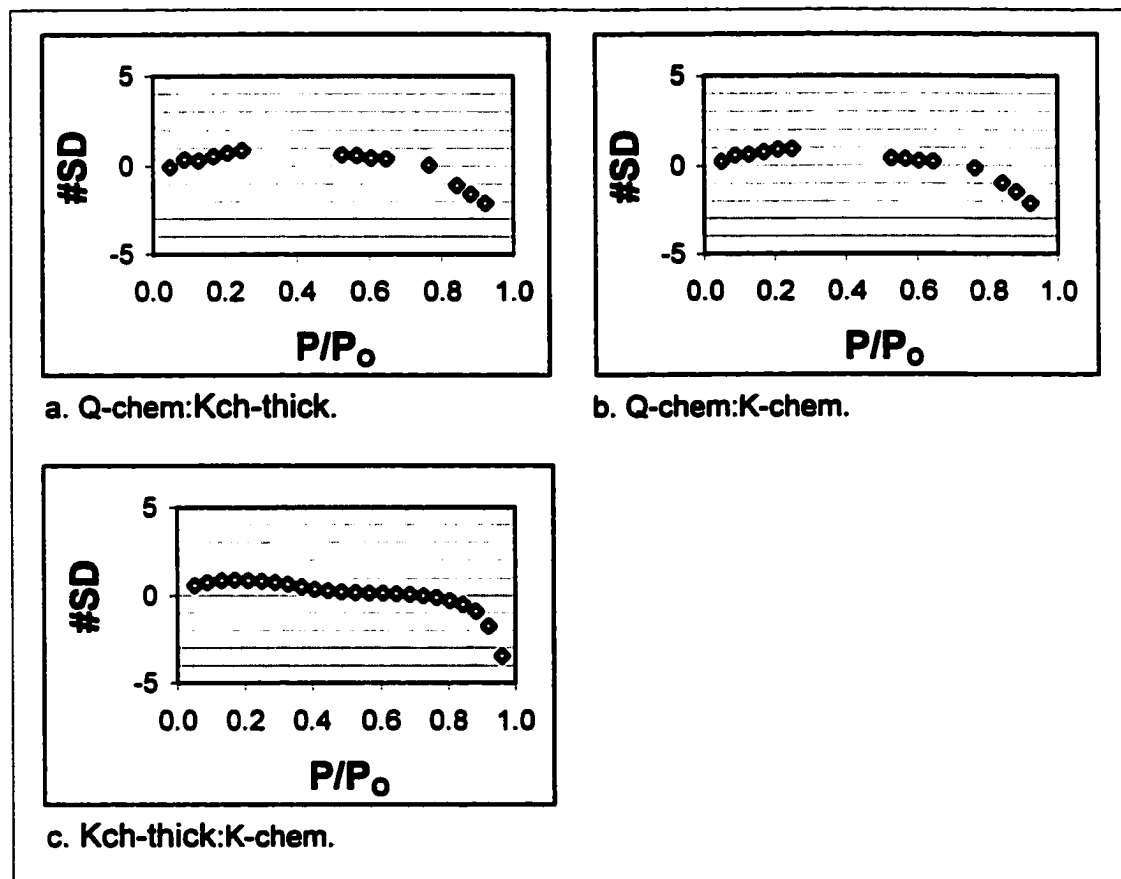


Figure 17. f -plots comparing coated solids to each other.

It is also interesting to consider the relatively slight degree of variability in the f -plots: most of the points in all plots fall within one standard deviation of the mean. It is only at high P/P_0 ($> \approx 0.8$), where one solid is likely to reach the level of condensation before the other, that large variations in the ratio appear. In some cases these are limited to the last point or two in the plot. At other P/P_0 regions, the degree of deviation is generally echoed from plot to plot, and so are features such as the values of P/P_0 where deviation changes sign.

EDS Results

Figures 18-20 show the samples and element maps for each solid included in this study. Because statistical information about the coating distributions for the entire solid

was desired, a random sampling method was employed to avoid any bias in selecting grains. The sample size ($n = 60$, comprising 10 sets of edge spots and 10 of face spots, with three spots per set) was designed to be reasonably representative while remaining feasible in terms of instrument time and resources required. Element maps were not collected until after spots had been sampled and analyzed.

Several features of Fe distribution are evident on the Q-chem element map (Figure 18). Fe signals are indicated in red. The apparently low and even distribution of Fe across the image (including regions containing only the adhesive carbon tab on which the solids were mounted for analysis) occurs in all maps and appears to be a background signal; it is well below the method detection limit ('MDL'), i.e., the concentration of Fe which is detected with confidence in the context of the experimental method. Below the MDL, an analyte signal cannot be confidently distinguished from background noise or analytical artifacts. An MDL depends on such factors as the instrument model and setup, the method of sample preparation, and the composition of the sample; the Fe MDL for this study is 2 wt % (Powell 2000; IXRF Systems Inc. 2002).

Detectable Fe occurs only occasionally, and it tends to be localized. In some cases it follows disruptions in the quartz surface, and in others, appears to coat small projections, or possibly discrete grains. Comparison of the grains chosen to the element map reveals that only one sampled grain, #6, contains edge spots that correspond to a local concentration of Fe. The others either were sampled at locations with no strong Fe signal or the spots did not capture the signal. The K-chem map shows less localization of Fe; however, there is a slight suggestion of small, linear regions of high Fe concentration (Figure 19). This should not be given too much weight, however, partly because during the collection of the element map image focus degenerated to some extent. The Kch-thick map shows a generally higher Fe content and also suggests some degree of localized concentration; however, this is difficult to correlate with grain features, again in part because image focus is less than ideal (Figure 20).

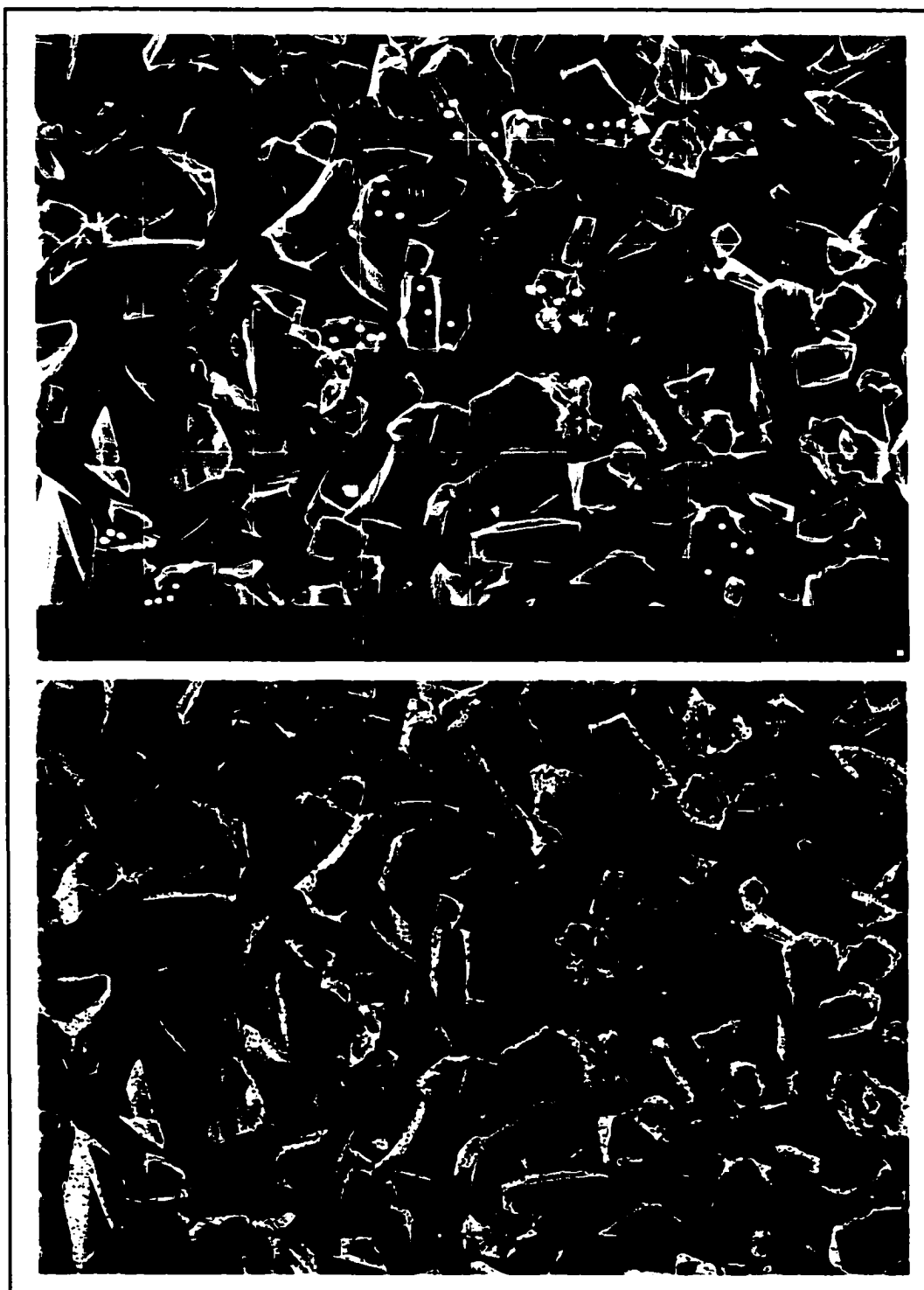


Figure 18. SEM image (top) and EDS Fe map (bottom) of GQc. Fe is indicated by colored dots. The low-level distribution of Fe throughout the image is a background signal and may be system contamination. Note the localized concentration of Fe in small areas of some grains.

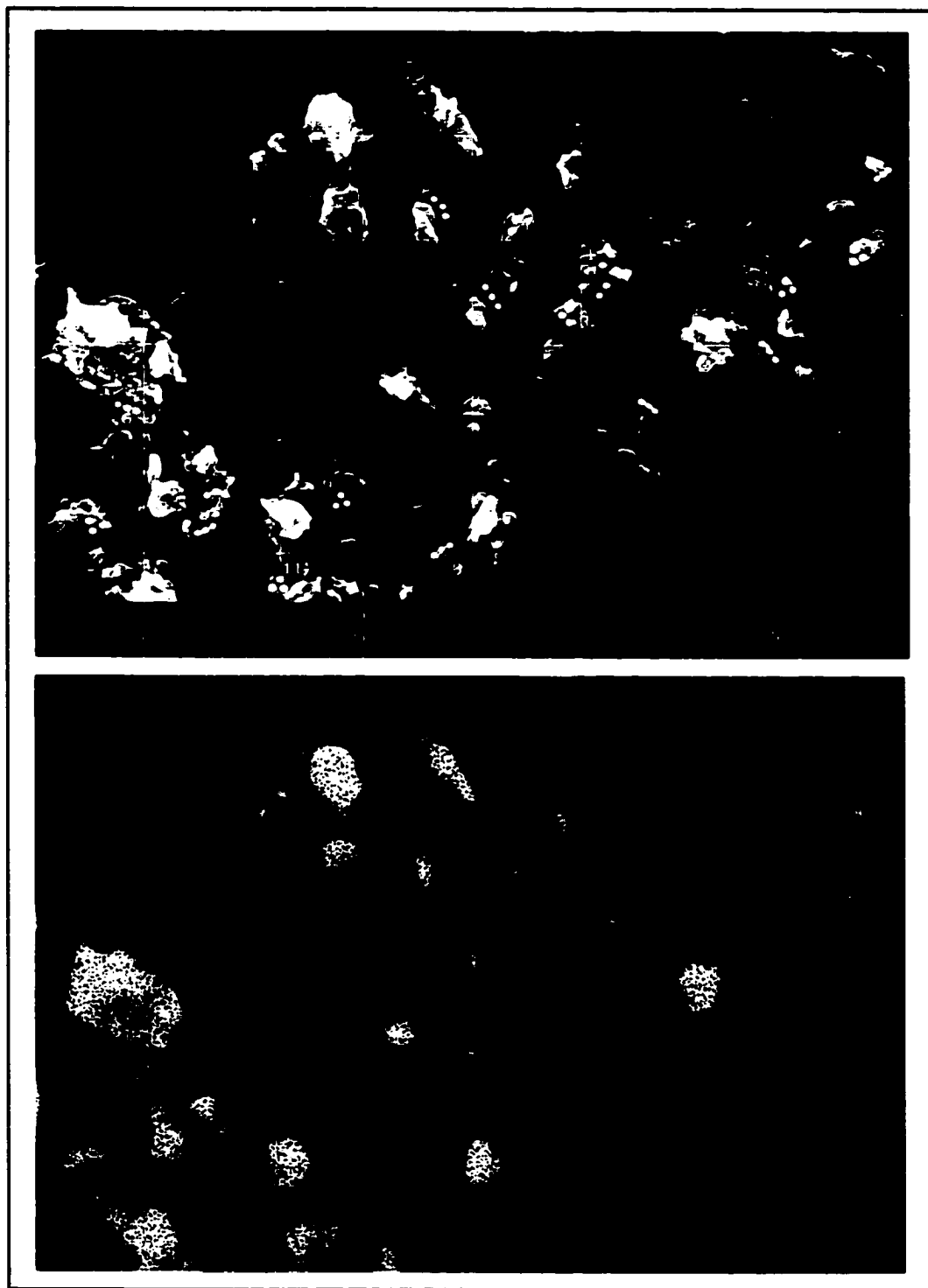


Figure 19. SEM image (top) and EDS Fe map (bottom) of GKc-thin. Fe appears more uniformly over the grains.

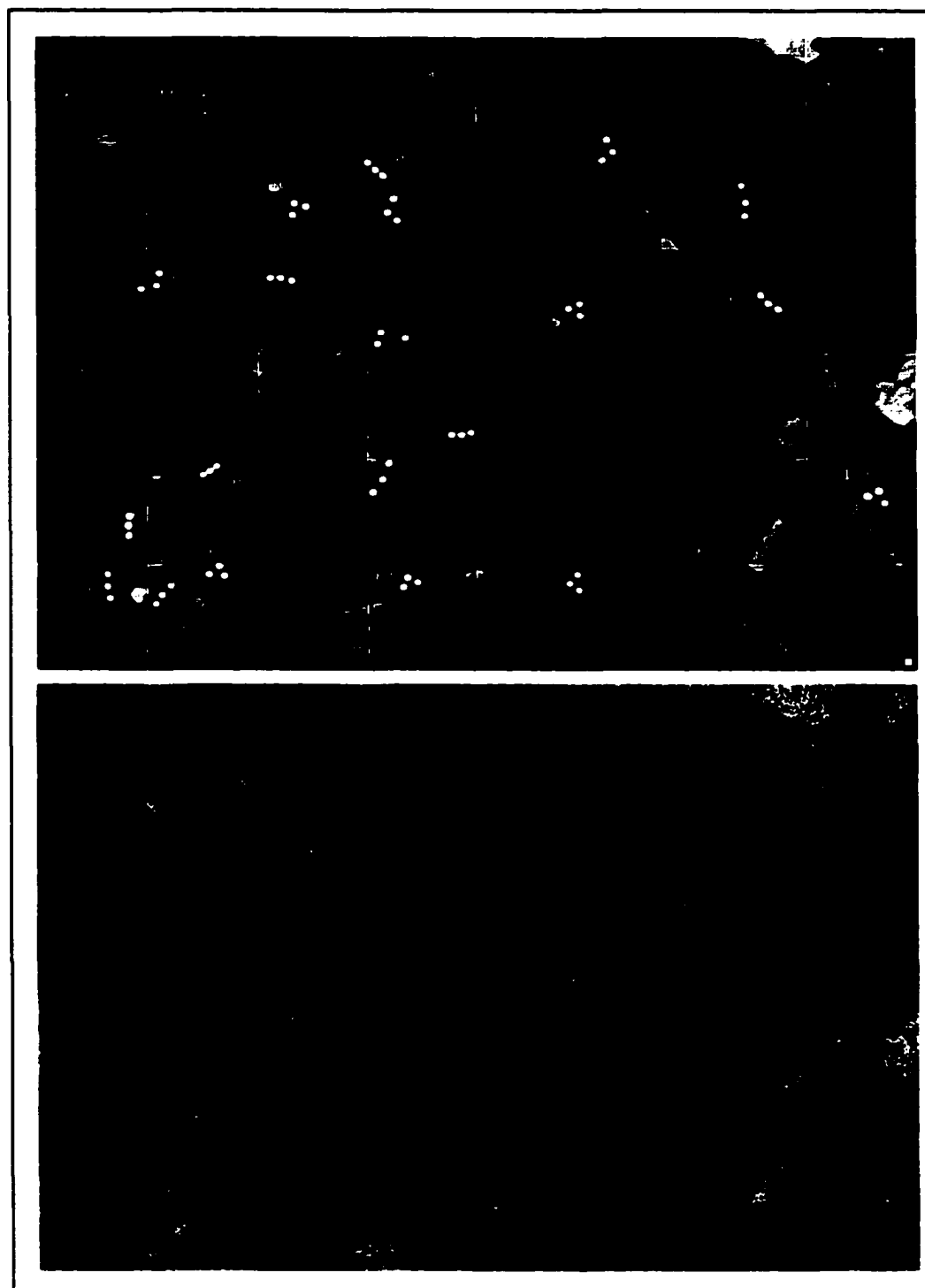


Figure 20. SEM image (top) and EDS Fe map (bottom) of GKaoC_{thick}. There appears to be a generally higher Fe content compared to GKaoC, and there is some suggestion of occasional localized concentrations.

Four potential controls on coating uniformity were examined using EDS: (1) the mineralogy of the substrate; (2) differences between the grains of each substrate; (3) surface properties of edges versus faces; and (4) variability within each facet sampled (edge or face). For each solid, the 60 spots sampled were grouped into subsets: all spots counted ('solids'), all spots on a grain, all edge spots, and all face spots. Spatial distribution was evaluated statistically in terms of the *variability* of results within and between subsets (faces, edges, grains, and solids). Relative Fe content, and the variability of that content, was used to evaluate the spatial distribution of the coatings. Descriptive statistics were used to address uniformity qualitatively. Variability was represented quantitatively by changes in Fe concentration and by the relative standard deviations (%RSDs) of each sample set; these were compared directly and, where appropriate, tested for statistically significant difference. A number of criteria were selected to describe the uniformity of each coating, both within each solid and in relation to the other solids. These are summarized in Table 5.

TABLE 5. Criteria for evaluating the variability of iron oxide distribution.

Variability	Sample sets	Descriptive statistics	t-tests	Other analyses
Within solids	spots, grains, edges, faces, edge v. face	histograms of [Fe], mean, median, 2σ , mean %RSD	[Fe] _{Substrate} , edge v. face; %RSDs, edge v. face	Q-chem only: linear regression analysis of relationships between edges and faces of grains
Between solids	grains, faces, edges	–	%RSDs (pairwise comparisons)	Kaolinite solids only: t-test ([Fe] _{Substrate}), thin v. thick: spots, edges only, faces only.

It is worthwhile to emphasize two points here. First, the purpose of the study was to assess distribution, not concentration, of the coating. Therefore, a semi-quantitative method was employed and [Fe] is expressed as a ratio of Fe to element(s) representing

the 'substrate signal' (i.e., $[\text{Fe}]_{\text{substrate}}$). For the quartz substrate the ratio is Fe:Si, and for kaolinite it is Fe:(Al/Si). This means that the data cannot be considered a quantitative measure of the Fe content at each spot. Second, because the substrate signal is different for quartz and kaolinite, the Fe content data for Q-chem cannot be compared directly to those for the kaolinite solids.

The descriptive statistics evaluating variability within each solid suggest that the K-chem coating is the most uniform in distribution and Q-chem the most variable. Descriptive statistics for each solid are given in Table 6. Figure 21 shows the distribution of $[\text{Fe}]_{\text{substrate}}$ for all spots sampled in each solid. Mean, median, and standard deviations are marked on the histograms. Perhaps the first notable result is the paucity of Q-chem spots containing detectable Fe (18 of 60 spots). In contrast, Fe was detected at all spots sampled (60 of 60 spots) for both kaolinite solids.

TABLE 6. Descriptive statistics for each solid sample set.^a

Solid	Sample set	n	Mean	σ	%RSD	Median	Δ^b	% Δ^c
Q-chem ^d	Spots	18	0.092	0.065	71	0.073	-0.019	-27
	Grains	8	0.066	0.055	83	0.061	-0.006	-8
	Edges	9	0.129	0.074	58	0.123	-0.006	-5
	Faces	9	0.056	0.022	40	0.042	-0.014	-33
K-chem	Spots	60	6.9	1.2	18	6.7	-0.2	-3
	Grains	20	6.9	1	14	6.6	-0.3	-4
	Edges	10	7.0	1.4	20	6.6	-0.4	-6
	Faces	10	6.8	1	15	6.7	-0.1	-1.1
Kch-thick	Spots	60	9.8	3.5	35	8.7	-1.1	-11
	Grains	20	9.8	3.2	33	8.8	-1	-11
	Edges	10	10.0	4.2	42	8.1	-1.9	-19
	Faces	10	9.6	2.6	27	9.3	-0.3	-3.3

^a Values are Fe intensity normalized to Si intensity for Q-chem and Al/Si for K-chem and Kch-thick (i.e., $[\text{Fe}]_{\text{substrate}}$) ^b ' Δ ' is the median-mean difference ^c '% Δ ' is $(\Delta/\text{mean}) \times 100$ ^d Q-chem data include only spots containing detectable Fe

All three histograms tail off to the right; otherwise, the kaolinite histograms are more similar to each other than either is to Q-chem. In both kaolinite samples, every spot

sampled contained detectable Fe, and the results exhibit a histogram suggestive of statistically uniform sample distribution (i.e., a Poisson-shaped sample distribution). K-chem is more narrowly distributed and the median is closer to the mean; σ is lower and there are points falling further from the mean (one is more than 5σ above the mean, in contrast to Kch-thick, where all points are less than 3σ from the mean). However, Kch-thick has four points more than 2σ above the mean, versus the two observed for K-chem. K-chem has no point more than 1σ below the mean, and Kch-thick has no points more than 2σ below the mean.

Since the 'edges' and 'faces' in each solid might be expected to have distinct surface characteristics (e.g. unsaturated edge sites, as opposed to fully coordinated face sites), the results for edges and faces were contrasted for each solid. Two-sample t-tests were performed comparing relative $[\text{Fe}]_{\text{substrate}}$ and mean %RSD for faces and edges.

Figure 22 gives the Fe contents of spots broken into surface types (faces and edges). As in Figure 21, there is more apparent difference between the face and edge sample sets in Q-chem in relation to the other two solids. Of the 42 spots with no detectable Fe (not shown in Figure 22), 21 were from faces and 21 from edges; four faces and four edges contained no detectable Fe in any of the three spots sampled. The $[\text{Fe}]_{\text{substrate}}$ of edges is significantly higher than that of faces for Q-chem ($P > 99.5\%$). In addition, the highest $[\text{Fe}]_{\text{substrate}}$ value in the set (more than 3σ above the mean for all spots sampled) is on an edge. In K-chem, face and edge spots appear to have similar distributions, although, like Q-chem, the highest spot (5σ above the mean for all spots sampled) is on an edge. On the other hand, Kch-thick edge spots appear to contain slightly less Fe than face spots, although no statistically significant difference was found ($P < 90\%$). Nonetheless, the descriptive statistics suggest other differences between edge and face spots for Kch-thick. Specifically, edge spots have a broader spread, higher %RSD and % Δ , and all of the spots falling $> 2\sigma$ from the mean of all spots sampled are edge spots.

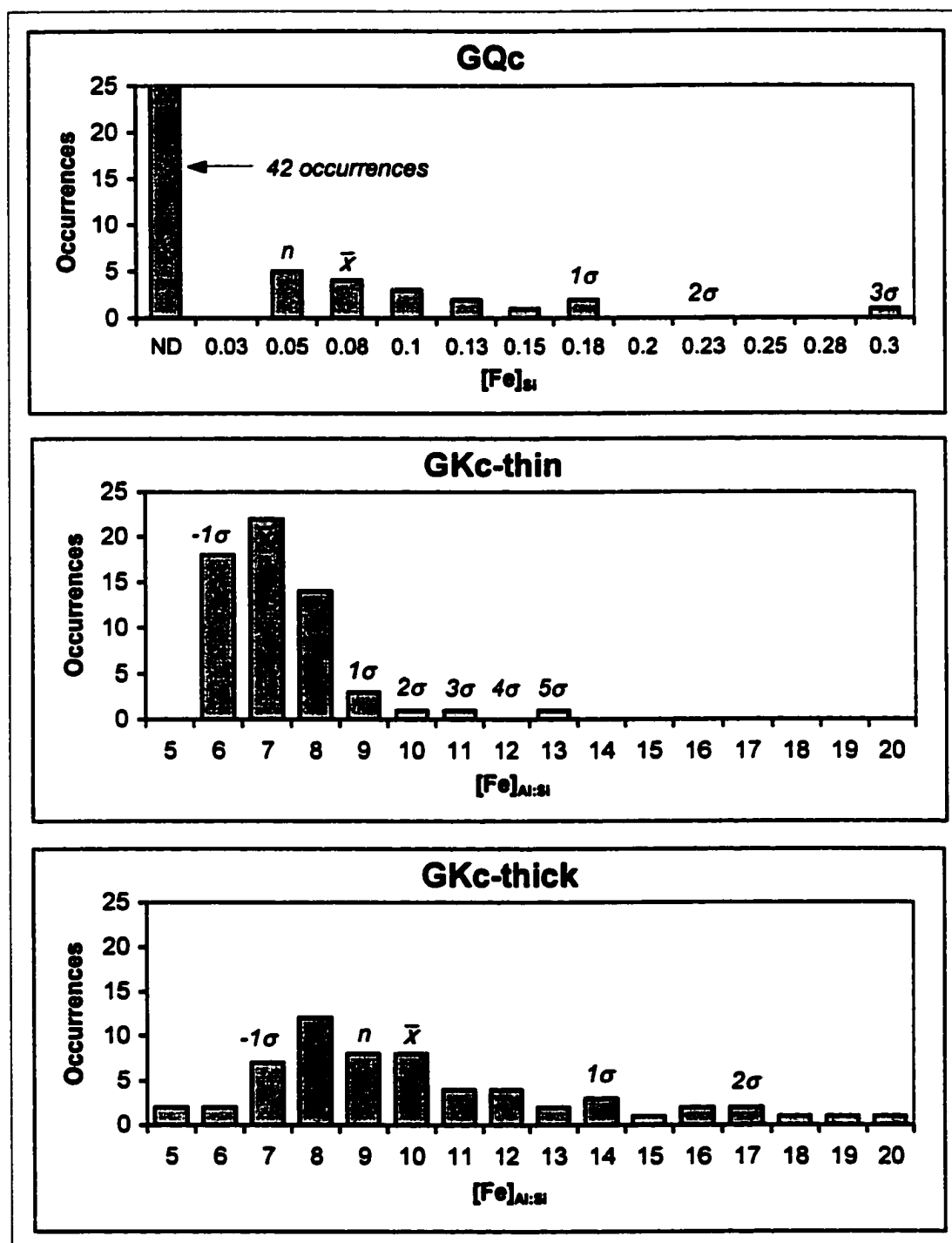


Figure 21. Distribution of $[\text{Fe}]_{\text{substrate}}$ for all spots sampled. ' \bar{x} ' indicates the location of the mean; ' n ' indicates the median; ' σ ' is standard deviation. These are calculated only for spots with detectable Fe; note that 42 spots in the Q-chem set fell below the Fe detection limit.

There might be a relationship between the variability of edges and faces of the same grain. For instance, one grain might have particularly favorable surfaces for binding goethite due to a relatively weathered surface. This could be tested in the case of Q-chem, where one edge and one face were sampled on each of 10 grains. For each Q-chem grain, the edge values were plotted against the face values, and a linear regression analysis was performed. If some characteristic of individual grains was controlling both edge and face coatings, there should be some relationship between edge values and face values. Figure 23 shows the results for the analysis of paired edge and face spots on Q-chem grains. No correlation was found between edge and face values for Fe content, %RSD, or number of spots containing detectable Fe. In addition, Fe did not consistently occur on both surfaces of a grain, or on one particular surface type, and, when detected on a surface, Fe frequently occurred in only one spot (8 out of 12 surfaces with Fe had only one Fe-bearing spot). This includes the highest $[\text{Fe}]_{\text{substrate}}$ value observed.

First, the depth of electron beam penetration is approximately $1\mu\text{m}$ (Goldstein et al. 1992). This means that characteristic X-rays are generated throughout the thickness of the face-on grains (and a large proportion of the edge-on grains). Although efficiency of detection of these X-rays decreases exponentially with depth, and ~ 90% of the signal comes from the top $0.1\mu\text{m}$ of the specimen (IXRF Systems Inc. 2002), this is still sufficient to collect X-rays generated throughout the face-on grains. The resulting signal is an average value of the entire thickness of the grain (for Si and Al), and both surfaces (for Si, Al, and Fe). Second, the electron interaction volume, i.e. the volume of specimen within which atoms interact with both incident electrons and the products of these primary interactions, is an estimated $1\mu\text{m}^3$ (depending on the specimen material and operating variables such as beam energy; Seaman 2000). This means that the signal is collected from a region greater than the volume of one kaolinite grain.

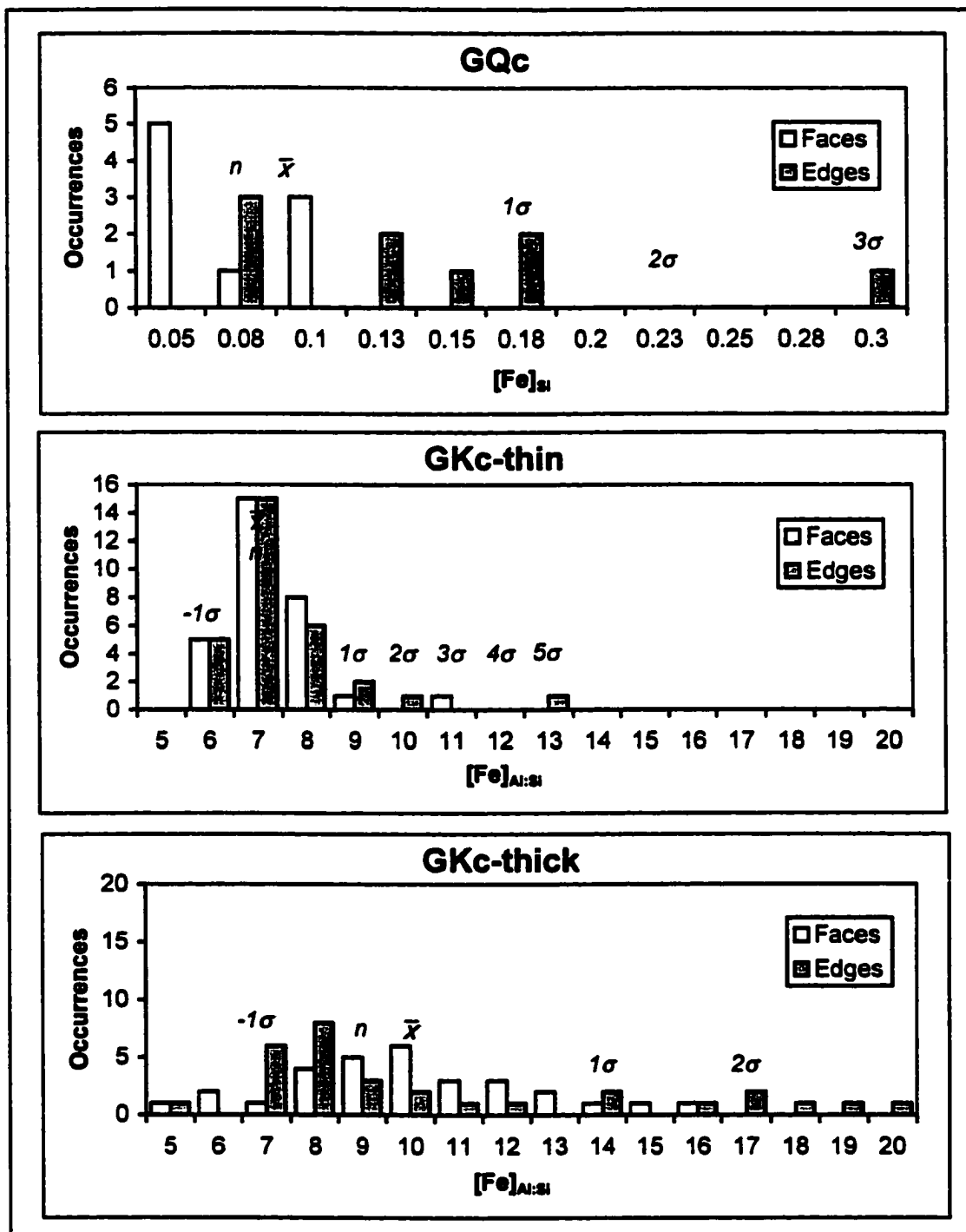


Figure 22. Distribution of $[\text{Fe}]_{\text{substrate}}$ for faces vs. edges. For Q-chem, only spots with detectable Fe are shown; nine face spots and nine edge spots. All spots on both kaolinite solids had detectable Fe. Mean $[\text{Fe}]_{\text{substrate}}$ for Q-chem edges is significantly higher than that for faces ($P > 99.5\%$).

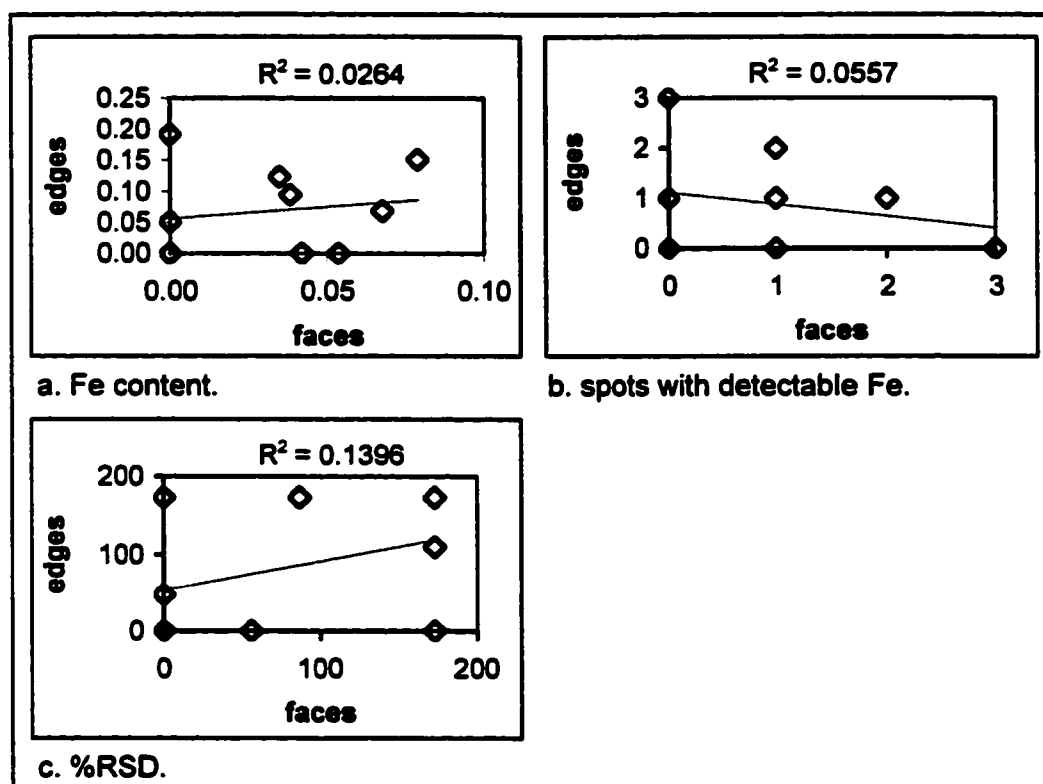


Figure 23. Regression analyses of correlations between edges and faces of Q-chem grains. **a.** Fe content. Two grains lie at (0,0). **b.** Number of spots containing detectable Fe. Two grains lie at (0,0) and two at (1,1). **c.** %RSD. Two grains lie at (0,0) and two at (173,173).

Thus, the data are not as well resolved as the locations of spots indicated in Figures 18-20 imply. For Q-chem, this effect is not of as much concern, since the grains are generally large enough and separate enough, and the spots far enough apart, for the signal to remain relatively confined to each spot sample. However, the interpretation of the kaolinite data must take account of the fact that the signal is an average value for both sides of a face-on grain, most or all of the depth of an edge-on grain, and some of the area surrounding the target grain. There are some ameliorating circumstances: for K-chem, the grains are relatively dispersed on the stub, forming small clumps with few grains stacked in layers; this means that even if the beam completely penetrated a face-on grain, it was unlikely to encounter several more grains underneath. In addition, the SEM image indicates that grains in the K-chem clumps tended to have similar orientations, so that the

region around an 'edge-on' grain, for example, was likely to contain other edge-on grains. This is less true for Kch-thick, and may be one reason for the greater observed spread in the data. However, this 'smoothing' effect should make edges and faces look more alike (assuming some of each were orientation were near any given spot). But the data actually appear to indicate more dissimilarity between edges and faces for Kch-thick as opposed to K-chem (see Figure 21 and Table 6).

Another positive consideration is the uniformity of the kaolinite grain size distribution. Half of the kaolinite grains were 0.5-1 μm in diameter, and the other half was 1-2 μm . The 1-2 μm fraction may be larger still due to the loss of smaller particles during the coating process. In addition, the specimens were sputter-coated with Au/Pd rather than C, which improves spatial resolution (Seaman 2000).

To quantify variability between solids, a series of two-sample t-tests were conducted comparing mean %RSD. Pairwise comparisons were made by grain, surface, edge, and face. (It should be reemphasized that for kaolinite solids, "surface" and "grain" refer to the same sample set, since one surface was sampled on each grain.) Table 7 shows the results.

Table 7. Statistical significance of difference in mean %RSD between solids.

Sample set	P		
	Q-chem v. K-chem	Q-chem, v. Kch-thick	K-chem v. Kch-thick
Grains	> 99.5%	> 99.5%	> 95%
Surfaces	> 99.5%	> 99.5%	> 95% ^a
Edges	> 99.5%	> 99.5%	< 90%
Faces	> 99.5%	> 99.5%	> 90% ^b

^a The 'grains' and 'surfaces' sets are the same for the kaolinite solids. ^b Estimated level of statistical significance = 5.25%.

It might have been anticipated from the descriptive statistics that Q-chem would show a highly significantly different degree of variability from the G-Kao solids for all subsets considered. It is more interesting to see that Kch-thick grains are significantly

more variable than K-chem grains. In addition, there is a distinction between how edge variability and face variability differ in the kaolinite solids: edge variability shows no significant difference ($P < 90\%$), but face variability is different at the 94.75% confidence level ($P \approx 5.25\%$). Taken together, these statistics suggest a difference in the spatial distribution of the coating as a function of thickness. Finally, t-tests showed that Kch-thick coatings contained significantly more Fe than K-chem, not only as a whole but on the basis of edges as well as faces ($P > 99.5\%$ for all three sample sets).

Discussion

Table 8 summarizes the similarities and differences between the physical sorption results for the three solids, their substrates, and particulate goethite. The physical sorption results suggest that the Q-chem solid takes up and releases N_2 (g) like particulate goethite and not like quartz. The similarities to goethite agree with the conceptual model of the coating as small particles of goethite bound to the quartz surface. Note that although the quartz surface is largely exposed, the SSA of quartz and other properties of this mineral are overwhelmed by the high SSA (3 to 4 orders of magnitude greater) of the goethite coating (see Table 3). Although the BET y-intercept values and the residuals plot shape are similar for quartz and Q-chem, these are slight similarities compared to those shared by goethite and Q-chem. The EDS results for Q-chem bolster this 'patchy' model: the goethite coating was found to be highly variable in its distribution both within and between surfaces and grains (see Figure 18 and Table 6), and the Fe content of edges is significantly higher than that of faces (see Figure 22).

The fact that few of the localized concentrations of Fe, and none of the high-Fe areas visible in Figure 18, fell within the random sampling suggests that there may be more than one population of Fe coating patches on Q-chem. At the lowest level, a small quantity of Fe adsorbate ions may form monodentate, mononuclear complexes with the widely spaced quartz SHG sites; these would fall well below the EDS method detection limit, and the term 'patches' would perhaps be better reserved for more extensive structures. In other cases, there may be a balance between the topography of a particular

region – i.e., the number and proximity of sites – and the adsorbate:surface ratio, which determines where and at what Fe levels larger, more bulk-goethite-like patches form. Thus, there might be some particularly rough or disrupted regions that could form enough monodentate surface species close enough together to promote surface precipitation at relatively low Fe concentrations, while particularly smooth grains might take up little Fe until aqueous Fe began to approach saturation levels.

Such a balance between region topography and adsorbate concentration would produce a diverse set of patches, the degree of diversity depending on the heterogeneity of the quartz grains. This ought to be reflected in a correlation study such as is shown in Figure 10. However, since this study did not sample any of the highest Fe regions indicated by the element map, it may not be representative of the entire range of patch characteristics. Given the low total Fe content of Q-chem, a larger sample may be necessary to represent this range accurately.

Table 8. Similarities in physical adsorption and desorption.

Solid	Substrate	Bulk Goethite	Q-chem
Q-chem	<i>b</i> (BET), residuals shape	Hysteresis, pore volume, residuals shape, dip in low $t_{H,U}$ plot, similar SSA_{int}	–
K-chem	No hysteresis, <i>b</i> (BET), <i>c</i> (BET), residuals shape, <i>f</i> -plot shape, lack of SSA_{int} , general <i>f</i> -plot shapes, shape of K-chem: goethite	–	–
Kch-thick	<i>f</i> -plot shape	Hysteresis, <i>b</i> (BET), <i>c</i> (BET), residuals shape, microporosity, pore volume, SSA_{int}	Hysteresis, residuals shape, estimated coating SSA, microporosity, pore volume, SSA_{int}

In contrast to Q-chem, K-chem showed N_2 adsorption and desorption behavior more like that of the substrate than the coating material (Table 8). There was no hysteresis and no evidence of porosity; the c values and BET y-intercepts were similar; and the shapes of the linear BET residual plots, the t -plots, and the f -plots are similar. On the other hand, the estimated coating SSA was about twice as high as that for the other two solids. Perhaps, then, the K-chem coating occurs in a form that exposes a great deal of the external area of goethite crystallites without allowing the development of the porosity seen in bulk goethite. For example, crystallites might be growing epitaxially or topotaxially along the aluminol surface. This is supported by the lack of apparent porosity, which would correspond to a two-dimensional surface structure. Such a flat coating might preserve some of the structural features of the underlying substrate, producing some adsorption behavior similar to that of uncoated kaolinite.

Other studies have indicated that ferric oxides precipitate from solution as patches on the basal surfaces of kaolinite which grow and coalesce into a uniform layer when the Fe content reaches several wt % of the oxide (Arias et al. 1993; Saleh and Jones 1984). In this study, EDS analysis of K-chem indicates a uniform level of Fe on all edges and faces sampled, and no significant difference between edge and face $[Fe]_{\text{substrate}}$ (Figure 22). Here, the relatively low spatial resolution of the data must be kept in mind. Patches occurring on the basal planes would be averaged with uncoated regions of the surface; at best they might produce slightly higher values; and EDS edge results include some characteristic X-rays from nearby grains, as well as some signal from the basal planes. However, no evidence of patchy coatings was found. Also, patches would exhibit a more heterogeneous Fe distribution on a per-grain basis, unless each grain had uniform numbers and sizes of patches, which would seem unlikely.

Although the studies cited above assert that Fe oxyhydroxides precipitating from solution bind only to the basal surfaces of kaolinite, it does not seem unreasonable to suppose that aqueous Fe(III) ions might complex reactive kaolinite edge sites, leading to the development of coatings on the kaolinite edges as well as the faces. The kaolinite-like physical adsorption behavior of K-chem might reflect a strong substrate influence on

the surface properties of the relatively uniform, thin coating, rather than the preservation of the reactive kaolinite sites in the solid. This is also more reasonable given that the much higher SSA of the goethite coating (2 to 3 orders of magnitude greater; Table 3) is likely to overwhelm the sorption behavior of any uncoated kaolinite surfaces in the solid, as it does in Q-chem.

The physical sorption behavior of Kch-thick is in marked contrast to that of K-chem. It resembles that of Q-chem and particulate goethite, and does not resemble that of uncoated kaolinite. The BET results indicate a porous, three-dimensional solid phase. The properties of the kaolinite substrate – and probably the substrate surface itself – are masked by a coating whose properties are approaching those of bulk goethite. Kch-thick has a SSA comparable to particulate goethite, and it shows evidence of microporosity and mesoporosity, though its total internal surface area is somewhat less than that of goethite and Q-chem. Its t -plot most resembles that of Q-chem, and the increase in estimated coating SSA per g of goethite added is similar to that for Q-chem.

On the other hand, the EDS results for Kch-thick are much more similar to K-chem than Q-chem, although it has a higher overall Fe content and slightly more variability in $[\text{Fe}]_{\text{substrate}}$ (Figure 21, Table 6) than K-chem. There is more variability from grain to grain in Kch-thick and a slight, but not statistically significant, separation between $[\text{Fe}]_{\text{substrate}}$ for faces and edges (Figure 22), unlike K-chem. All spots falling more than 2σ above the mean are edges, and Kch-thick edge sites appear to be more variable than K-chem. This may spring from the iterative coating method employed: the procedure used once to coat K-chem was repeated twice more for Kch-thick. A second contributing factor might be the variably reactive suite of kaolinite edge sites (aluminol and silanol sites and Lewis acid sites). Perhaps the initial complexation of Fe oxyhydroxides on these sites produces a relatively heterogeneous coating surface (in comparison to the basal coating) that is propagated through the second and third coating iterations.

In summary, EDS analysis of Kch-thick indicates that the distribution of goethite is relatively uniform, and in some ways statistically indistinguishable, from that on K-

chem. However, the physical sorption behavior of Kch-thick is distinct from that of K-chem, and resembles those of Q-chem and particulate goethite. This suggests that the thick coating is more like particulate goethite than the thin coating, despite similarities in the spatial distribution of the kaolinite coatings. The tenfold-greater quantity of goethite in Kch-thick corresponds to roughly 16 monolayer equivalents ('M.E.'), compared with about one and a half to two M.E. of goethite in K-chem; this likely constitutes enough coating thickness for any kaolinite-like characteristics of the coating surface in the first M.E. or few to be buried under the next ten or so layers of goethite.

In conclusion, the same goethite-coating method, applied to two different substrates, produced two different coatings. The quartz coating appears to be comprised of occasional thick, uneven patches with similar N₂ adsorption/desorption characteristics as bulk goethite, along with a more widespread, low-Fe population of surface complexes. The kaolinite coating seems to be very thin and flat, with no porosity, and some kaolinitic N₂ adsorption/desorption properties reflected despite the suggestion of a complete covering of the kaolinite surface. Making the kaolinite coating thicker appeared to eliminate the influence of the substrate on N₂ adsorption/desorption behavior and yielded a porous surface that appears to be distributed evenly over the kaolinite grains. These results show that the physical form of an Fe oxide coating may depend on the thickness of the coating and the properties of the substrate surface.

CHAPTER 3: Cu(II) SORPTION

Introduction

Physical and chemical surface properties are closely related in oxide minerals. The surface structure of an oxide mineral is determined by the crystal structure, crystal habit, roughness, and other physical properties of the mineral. In turn, the surface structure dictates the coordination and spatial distribution of surface hydroxyl groups (SHGs), and thus the geometry and stoichiometry of adsorption surface complexes (Katz and Hayes 1995; O'Day et al. 1996; Brown et al. 1999). This is especially true for a mineral like goethite, which has several different primary crystallographic faces, as well as a variety of different SHGs on each surface (Davis and Kent 1990).

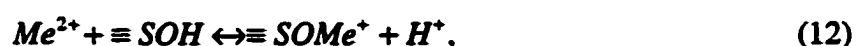
The relationship between oxide mineral physical form (hence physical properties) and surface properties (hence sorption behavior) is even stronger for oxide mineral coatings, where much more of the material occurs on the surface. For example, approximately 1.7% of the Fe atoms in bulk goethite are coordinated to SHGs; in contrast, an estimated 20% of the Fe atoms may occur at the surface in Fe oxide coatings (Davis et al. 1998). The (110) crystallographic face is known to dominate the surface properties of bulk goethite, largely because it is the primary exposed face (Hiemstra et al. 1996; Alcacio et al. 2001) and therefore comprises the majority of the surface area of the solid. There is evidence suggesting that Cu^{2+} is also taken up by sites on the (001) and (021) crystallographic faces (Alcacio et al. 2001 and Randall et al. 1999, respectively). The relative importance of these faces and associated site populations may vary with the physical form of the coating. For example, if a goethite coating had a lower degree of crystallinity (i.e. was composed of smaller crystallites), the proportion of (021) to (110) surface area per mass of goethite would be higher, since there would be more, shorter, crystallites in the same amount of goethite, and hence more (021) terminations.

The inclusion of a small number of high-affinity sites, perhaps those that occur at steps, kinks, and other crystallographic defects, substantially improves the fit of a surface

complexation model (or 'SCM,' a thermodynamic approach to modeling adsorption in which chemical reactions between adsorbate species and surface functional groups are treated as analogous to aqueous complexation reactions; see Chapter 1) for Cu^{2+} uptake onto goethite (Robertson and Leckie 1997). The occurrence of such defects might be expected to vary with the physical form of a coating – for example, a patchy coating might have more edge and step defects than a uniform coating; or a very thin coating might reflect the topography of its substrate, producing a different set of surface defects from those observed in particulate goethite.

The thesis of this study is that there is a correlation between the physical forms of goethite coatings and their surface chemical properties. It has been shown that the physical properties of a goethite coating vary with its thickness and with the mineralogy of the substrate (see Chapter 2). It is also expected that the manner in which an iron oxide coating forms may affect its physical characteristics. Changes in the surface area-to-volume ratio and the blocking of surface sites, due to the formation of chemical bonds with the substrate and/or masking of available surface area as a result of the coating/substrate association are likely, and these will affect the coating's ability to take up and release adsorbate species. Furthermore, there may also be significant variations in the number, type, and affinity of reactive surface sites of different coatings as a result of the coating method, coating thickness, and substrate properties.

One method of probing the chemical properties of surfaces is by exposing them to surface-reactive aqueous chemical species in adsorption/desorption experiments. Many dissolved substances are particle-reactive – i.e., associate preferentially with solid surfaces. In some cases, this association takes the form of a chemical reaction between the dissolved substance and one or more of the solid's surface chemical moieties (called 'surface functional groups' or "SFGs," of which surface hydroxyl groups, 'SHGs,' are a common subset on hydrous oxides). Such reactions are viewed as analogous to aqueous complexation reactions; for instance:



where $\equiv SOH$ represents a surface functional group. In controlled experiments, these reactions can be used to collect information about the chemical properties of a solid surface. The capacity and affinity of the adsorbent surfaces are measured as a function of one or more master variables – typically pH, ionic strength, or surface loading (i.e., adsorbate-to-surface ratio). This yields information about the quantity of binding sites, the presence of different types of sites, and their relative affinity for the adsorbate in the context of the chemical system chosen.

In this study, batch Cu(II) adsorption/desorption experiments were conducted on five solids consisting of a goethite (α -FeOOH) coating on either a quartz or kaolinite substrate. The five solids studied encompass the three independent variables mentioned above: coating method, coating thickness, and substrate properties. Iron oxide coatings in nature are thought to form primarily by two means: (1) surface precipitation, i.e., adsorption of Fe(III) to surfaces and subsequent formation of a surface precipitate (Ryan and Gschwend 1992); and (2) heterocoagulation of positively charged colloidal iron oxide particles with negatively-charged surfaces, such as clays and quartz (Boymel et al. 1981; Saleh and Jones 1984; Arias et al. 1993). The first method produces primarily covalent chemical bonds between the substrate and coating materials; the bonds created in the second method are more electrostatic in nature, and the physical form of the iron oxide particles is preserved. In this study, coatings formed by surface precipitation are represented by the three “chemical” coatings characterized in Chapter 2: a thin chemical coating on quartz and one on kaolinite, and a thicker chemical coating on kaolinite. Coatings formed via heterocoagulation are represented by two “physical” coatings: one each on quartz and kaolinite. Details of the methods for creating chemical coatings are given in Chapter 2; methods for creating physical coatings are given below in “Methods and Materials.” The properties of the five solids are given in Table 9.

It should be noted that only the three chemical coatings (Q-chem, K-chem, and Kch-thick, as described in Table 9) were physically characterized in Chapter 2. The methods used (N_2 gas adsorption/desorption and SEM/EDS analysis) are inappropriate for studying the physical coatings, where relatively weak electrostatic bonds are formed

in solution between goethite and substrate. One principle obstacle is the requirement of complete drying of the solid in preparation for analysis; another is the transference of the sample through a funnel and into a narrow tube for N₂ analysis, and the dissemination of a sparing sample across an aluminum stub for SEM/EDS analysis. The bonds in physically-associated assemblages are highly vulnerable to disruption and change; both air drying and physical disturbance have been observed to change the surface charge properties of natural materials containing analogous solids composed of goethite and clay particles associated with larger quartz grains in comparison with those of the same solids handled gingerly and maintained in field moist conditions (Bertsch and Seaman, 1999).

TABLE 9. Properties of the coated solids.

Solid	Substrate	Coating method	[Fe] (wt%)	Γ_{Fe}^a ($\mu\text{mol m}^{-2}$)	M.E. ^b (18 $\mu\text{mol m}^{-2}$)
Q-chem	Quartz	chemical	0.13	49	~ 2
K-chem	Kaolinite	chemical	1.3	30	~ $\frac{2}{3}$
Kch-thick	Kaolinite	chemical	11.3	313	~ 17
Q-phys	Quartz	physical	0.05 (5%) ^c	19	~ 1
K-phys	Kaolinite	physical	0.54 (14%) ^c	12	~ $\frac{2}{3}$

^a ' Γ ' denotes surface coverage, i.e. adsorbate bound per unit adsorbent. ^b 'M.E.' stands for 'monolayer equivalent,' corresponding to the approximate surface coverage if the surface was completely covered by a single layer of hydroxy-bonded octahedrally coordinated transition metal ions. This is conventionally estimated to be 18 μmol of adsorbate per m^2 of adsorbent. ^c This is a mean value for all samples, which were measured out individually ($n = 22$ for Q-phys and 16 for K-phys); the parenthetical value is the relative standard deviation of the mean.

The adsorption/desorption experiments were conducted in synthetic estuarine water (SEW; recipe follows) at room temperature and under ambient atmosphere. The master variable chosen was surface coverage; pH and ionic strength were held constant. (Details are given in Methods and Materials.) Desorption was induced by replacing the adsorption solution with fresh SEW containing no copper (i.e., 'desorption by dilution'). A desorption stage was included in the batch experiments for two reasons. First, one of

the more important environmental questions regarding trace metal/sediment cycling is that of reversibility – i.e., once bound by the sediment, might trace metals subsequently be released back into the water? Second, desorption provides further insight into the mechanisms controlling sorption at different surface coverages, by indicating how readily the sorption bonds are broken in response to a shift in balance between sorbed and dissolved Cu. Desorption was initiated by dilution (with solution of the same ionic strength), rather than by lowering pH, because this was considered more applicable to an estuarine setting, where pH is relatively stable, but dissolved Cu concentration may not be. For instance, events such as dredging or storm events might abruptly bring Cu-contaminated sediment into contact with relatively Cu-free waters.

System Constraints

The experiments were designed to focus on variability in Cu uptake behavior with the form of goethite coatings over a range of Cu surface coverages, keeping all other solution conditions as consistent as possible. Because there is evidence that sorption results may vary over broad ranges of particle concentration (Honeyman and Santschi 1988), the ratio of solid to solution was constrained to 0.4 - 5 g L⁻¹. Cu is relatively insoluble in seawater, which limited the concentration range of the Cu solutions. A study of Cu solubility in the solution matrix, indicated that 160 μM (10.2 ppm) dissolved Cu, the highest concentration used in the batch experiments, remained in solution in synthetic estuarine water (SEW) at pH 8.8 (well above the maximum allowed range for the experiments, i.e., 7.0 to 8.0) for at least two days. To further guard against any possibility of Cu precipitation from solution before or during the experiments, Cu solutions were made up as close to the time of experiment as possible.

The desired pH of reaction was set at 7.4 as a compromise between the actual pH of the matrix solution (8.0), the decreasing solubility of Cu in saltwater with increasing pH, and the location of the Cu(II) adsorption edge. The adsorption edge is a phenomenon of aqueous ion uptake onto oxide surfaces that arises from the amphoteric nature of SHGs. For cations, fractional uptake (i.e., the percent of total cation concentration

adsorbed, sometimes denoted as ' θ ') is low at low pH, when SHGs tend to be positively charged, hence less amenable to binding with positively charged ions, and increases rapidly with pH over one to two pH units, after which fractional uptake remains high. The region of rapid increase in fractional uptake with pH is the adsorption edge, and its location depends mainly on the identity of the adsorbate ion at constant adsorbate-adsorbent ratios.

It was desired that the adsorption/desorption reactions take place above the Cu adsorption edge for two reasons. First, this is the region of maximum adsorption; and second, working above the edge would minimize the impact of small, inadvertent variations in pH on fractional uptake. In general, the adsorption edge for Cu(II) falls well below pH 7 in many aqueous solutions, including full-strength major ion seawater (Barrow et al. 1981; Benjamin and Leckie 1981; Balistrieri and Murray 1984; Bourg 1987; Dzombak and Morel 1990). Although the exact location of the edge depends to some extent on the type of solid and the surface coverage (Balistrieri and Murray 1982), a review of fractional Cu(II) uptake over a range of pH values for the systems studied here indicated that the top of the edge typically occurs between $\text{pH} \approx 6.5 - 7$. Additionally, a thermodynamic simulation of speciation in SEW using MINTEQA2 (Allison et al., 1991) for a broad range of Cu(II) concentrations and pH values indicated that, for a given pH, Cu(II) species distribution is fairly consistent over the range of Cu concentrations used (see Figure 24 for an example). Thus, the adsorption process should not be significantly affected by minor variations in solution speciation over the range of concentrations studied here. Finally, to further control for pH-driven effects, the experimental results were evaluated critically in conjunction with MINTEQA2 speciation models to probe for unforeseen variability with pH. As a result, the data were grouped into two subsets by $\text{pH} = 7.0-7.5$ and $\text{pH} = 7.5-8.0$ for separate consideration. This was a conservative measure; the results did not indicate pH-related effects within the experimental range. Samples whose equilibrium pH fell outside this range were discarded due to concerns about either the proximity of the adsorption edge (for samples at $\text{pH} < 7.0$) or shifts in the equilibrium species distributions (for samples at $\text{pH} > 8.0$).

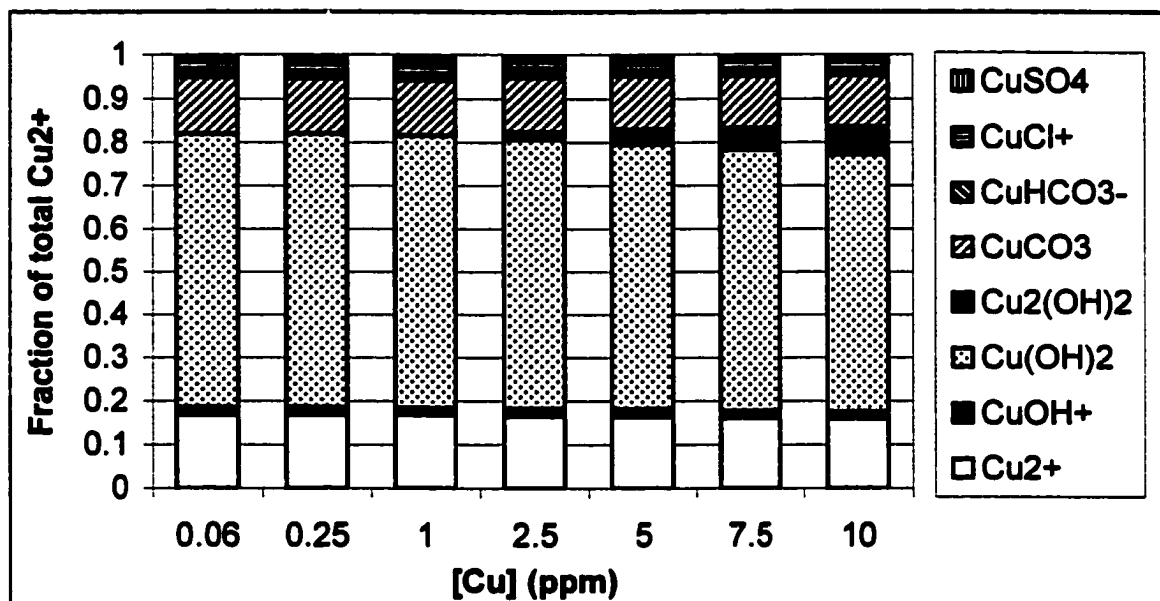


Figure 24. Cu(II) speciation of 10‰ SEW at pH 7.4 for the range of Cu concentrations used in the batch experiments. The general consensus in the literature is that one or more of the hydroxylated Cu species are the most important in reactions with surface hydroxyl groups. Note that these species (CuOH⁺, Cu(OH)₂, and Cu₂(OH)₂) make up approximately two-thirds of total Cu over the entire range of Cu concentration. The free Cu concentration (Cu²⁺) also remains consistent.

Surface coverage was varied over a range considered germane to environmental and surface-chemical issues, i.e. ~ 0.05 to ~ 20 μmol Cu m⁻² solid. The range between 0.05 and 5 μmol m⁻² was given particular attention. First, it reflects levels of Cu observed in uncontaminated to heavily polluted environmental sediments (10¹ – 10³ ppm; Bryan and Langston, 1992), assuming a general SSA of 10 m² g⁻¹ for field sediments. Second, it is expected to encompass the continuum of uptake mechanisms with increasing adsorbate-to-adsorbent ratio for Cu(II), beginning with specific, monomeric adsorption to high-affinity sites, and ending with surface precipitation (Brown et al. 1995; Katz and Hayes 1995; O'Day et al. 1996).

Finally, whenever possible, the volume of solution was held to 50 mL in order to maximize the consistency of both reaction vessel conditions (composition, cleanliness, history, etc.), and the measuring devices used (pipettes, volumetric flasks, etc.).

Methods and Materials

Quartz and kaolinite were prepared as described in Chapter 2. The particulate goethite used in the physical coatings is the same as that characterized in Chapter 2. The “chemical” coatings (Q-chem, K-chem, and GKc-thick) were prepared as described in Chapter 2 by precipitating Fe(III) oxyhydroxide from solution in the presence of quartz or kaolinite and aging the suspensions for 96 h at 50-60° C. The “physical” coatings were synthesized sample by sample immediately before the experiments by combining particulate goethite with quartz or kaolinite and suspending them in SEW for 24 h, which has been shown to result in goethite deposition on the substrate (Boymel et al. 1981; Saleh and Jones 1984; Arias et al. 1993).

All reagents used in preparation and batch experiments were at least ACS-grade, and all water was double-deionized and had a typical resistance of 18 MΩ. High-concentration Cu stocks (500 to 2000 ppm) were prepared using solid $\text{Cu}(\text{NO}_3)_2$ dissolved in double-deionized water (DDI); solutions were then prepared from these stocks for use in the batch adsorption experiments. The Cu solutions were made up in SEW and ranged in Cu concentration from 50 ppb to 20 ppm (see Appendix 3). Immediately before initiating the adsorption reactions, the pH of the Cu solutions was adjusted using 5% NaOH as necessary to approach the desired experimental pH of 7.4. (Cu solution adjustment was always in the direction of higher pH, and was not necessary for solutions containing less than ≈ 60 ppb Cu.) During the initial uptake phase (i.e. the first few hours of reaction), pH was monitored using a pH meter, and very small amounts (~ 25 μL at a time, or $\sim 0.05\%$ of total volume) of NaOH, HCl, or HNO_3 were added to maintain sample pH within the allowable range (7.0 to 8.0). Samples were rotated continuously during reaction, and agitated immediately after the addition of acid or base.

The synthetic estuarine water (10‰ salinity) was prepared using a recipe based on Lyman and Fleming's (1940) formula for full-strength synthetic seawater (see Table 10).

TABLE 10. Recipe for 10‰ synthetic estuarine water.

Compound (solid)	Mass (g) ^a
NaCl	67.0743
MgCl ₂	14.2314
Na ₂ SO ₄	11.1914
CaCl ₂	3.1486
KCl	1.8971
NaHCO ₃	0.5486
KBr	0.2743
H ₃ BO ₃	0.0743
SrCl ₂	0.0686
NaF	0.0086

^a Made up to 10L in DDI water.

The ratios of constituents were the same as for synthetic seawater, but more water was added to lower the overall salinity. No organic compounds were included, since these would be likely to complex dissolved Cu and coat the mineral surfaces, obscuring the reactions between Cu and the mineral SHGs. SEW was made up in 10-L batches as needed by dissolving the ingredients in DDI in a 10-L Nalgene dewar used only for this purpose. The pH of SEW was 8.0. This solution was repeatedly analyzed for Cu contamination; no detectable Cu was found in any batch.

Whenever possible, sterile Corning 50-mL polypropylene centrifuge tubes were used for reaction vessels, solution storage, dilution for analysis, etc. Sterility was important, since bacteria can produce organic compounds that react with both Cu and mineral surfaces, and bacterial cell walls can take up Cu (Jackson et al., 1999). In cases where a larger volume was required, acid-washed Nalgene polypropylene jars were used. Cu spikes and standards were made up and stored in acid-washed glass volumetric flasks or Nalgene polypropylene jars. Analytical samples were run in new polycarbonate or polypropylene autosampler vials.

In preparation for each batch experiment, the solids were weighed out into the reaction vessels and one half of the reaction volume (typically 25 mL) of SEW was added. The sample suspensions were rotated for 24 h to fully hydroxylate the solid in equilibrium with SEW. At the start of the adsorption stage, one-half of the reaction volume of Cu solution was added and the samples rotated. After ~ 1 h the pH was checked and adjusted as necessary to ~ 7.4. Because of the adjustment of the Cu solution to yield approximately the desired pH range immediately before beginning the experiments, pH at + 1h was rarely more than 0.5 pH units outside the allowable final pH range (7.0 to 8.0).

After 24 h, the sorption samples were centrifuged to separate the solids from solution prior to measurement of pH and Cu. Samples were centrifuged for at least 20 minutes at approximately 5,000 rpm, until the particles formed a coherent pellet and the supernatant was clear. The amount of centrifugation required varied from solid to solid. Because it usually took at least 2 h to centrifuge all the samples in a batch, samples were stopped in sets of 6 over a time period bracketing the 24-h sorption and desorption marks. Samples were considered “stopped” after having been centrifuged, and since pH measurement of the final solution was often time-consuming, some batches experienced a lag of a few hours or less between the ending of the sorption and beginning of the desorption stages.

Final pH was then measured. The pH measurements were made while the solution remained in contact with the reaction vessel and sedimented particles using an Orion 210A portable pH meter with a Ross combination electrode. Results were periodically double-checked using litmus paper or another pH meter. The final pH was generally 7.4 ± 0.2 (see Appendix 3). Samples were grouped into subsets falling between pH = 7.0 and 7.5, and between 7.5 and 8.0, in order to ensure against any unforeseen pH-related effects arising from changes in Cu speciation. Samples falling outside this pH range were excluded from consideration.

Following pH measurement, the supernatant, called the ‘sorption solution,’ was replaced with 50 mL of SEW, initiating the desorption stage of the experiment. The solid

was resuspended, the samples were rotated for an additional 24 h and then centrifuged, with the 'desorption solution' removed for analysis.

All batch samples were run in duplicate. A method precision study was performed in which six identical samples were run and the standard deviation for the method derived. The 95% confidence interval for the method is 0.12% of the absorbance value. Container-loss was measured for three samples using a 60 ppb Cu solution, and the average loss, 0.38% (range = 0 to 1.05%), was accounted for in data reduction. Experiments were started as near 24 h after the solids were wetted as possible and run for the next 48 h, after which samples were analyzed as promptly as possible, usually within a week. Solids wetted and not reacted within 2 d were discarded. In cases where supernatants were not analyzed for an extended period of time, small quantities (~ 100 μL , or ~ 0.2% total volume) of concentrated HNO_3 were added 24 h before analysis.

A mass balance study was conducted in which a set of six samples were run through the batch experimental procedure. The initial Cu added, Cu in solution after adsorption, Cu in solution after desorption, and Cu extracted from the solids (using 2N HCl extraction at room temperature) were measured using GF-AA. All six samples had a balance between 2.8 and 4.5 ppb Cu, or +0.9% and +1.4% (mean: +1.2%; relative standard deviation 15%). The method detection limit for the GF is 2 ppb Cu, and the GF samples were diluted 1:6, further increasing uncertainty.

Strong specific adsorbents such as Cu^{2+} typically exhibit two sorption steps: a fast step, in which adsorbate ions bind specifically with surface sites; and a slow step, during which adsorbate ions may rearrange on the surface to form more stable complexes or even diffuse into the adsorbent (Charlet and Manceau 1992; Waychunas et al. 1993; Cheah et al. 1998). The time scale for fast sorption is a few hours; slow sorption occurs over greater time scales. The batch experiments were targeted at the fast step of adsorption; the goal was to allow fast sorption to approach completion, then stop the reaction before significant post-sorption rearrangement occurred. (In addition, since the experiments took place under atmosphere and at room temperature and pressure,

concerns about bacterial activity in the reaction vessels made it desirable to avoid durations of more than a few days.)

A time series study was performed in which Cu(II) adsorption by goethite was initiated and then stopped at 10 min, 2 h, 8 h, 24 h, 48 h, and 72 h. Sorption appears to have neared equilibrium within 8 h and was fairly steady for the remainder of the period (Figure 25). Other authors have suggested a minimum equilibration time for batch adsorption of 16 to 24 h (Dzombak and Morel 1990; Brown et al. 1995). 24 h was set at the reaction time for this reason, and for several others as well. A 24-h window would ensure that all solids had reached the end of the fast-sorption stage, while preventing much slow sorption. At the same time, allowing 24 h for hydrolyzation, adsorption, and desorption (72 h total) would not allow the development of much bacterial activity. Logistically, 24 h was also favored by laboratory facility regulations.

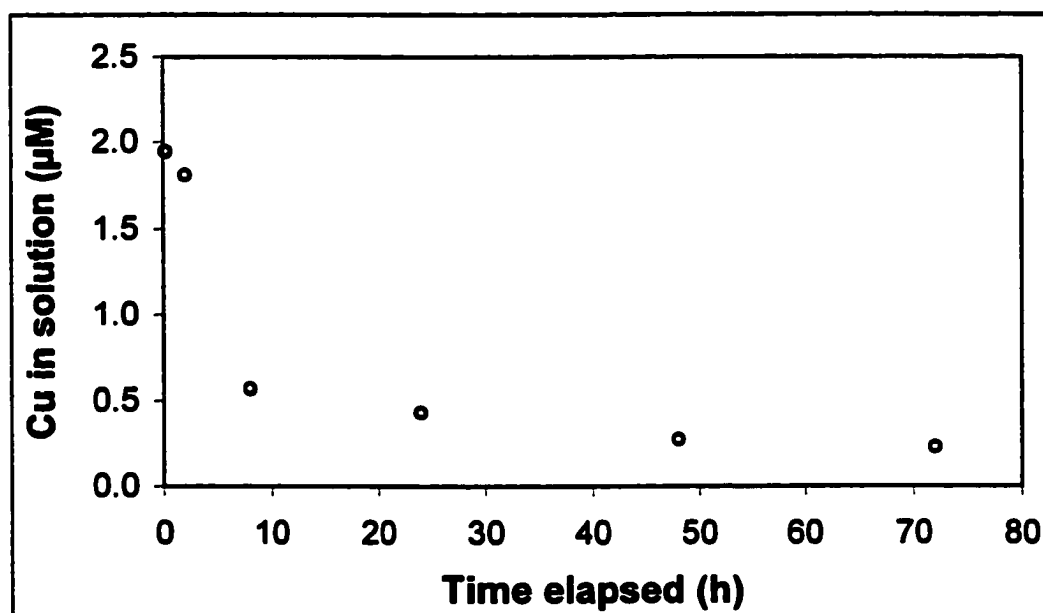


Figure 25. Cu remaining in solution as a function of elapsed time in batch adsorption experiments with goethite. Initial [Cu] was 2 µM; 2.6% was removed at 10 min.

Total Cu in the sorption and desorption solutions was measured using graphite furnace atomic absorption (Varian SpectraAA 300/400 or Perkin-Elmer GF-5100 GF-AA)

or inductively-coupled plasma atomic emission spectrophotometry (Perkin-Elmer P2 or Optima 4300DV ICP-AES). Cu removed during sorption was calculated as the difference between initial Cu added and concentration of Cu in the sorption solution, corrected for adsorption to reaction vessels. The Cu concentration of the desorption solution was interpreted to be the amount of sorbed Cu which was released from the solid during desorption. In some cases, analytical samples were diluted to fall within the linear range for the GF-AA, or to reduce the high ionic strength for ICP-AES analysis. For GF-AA analysis, matrix modifiers were used to eliminate interference and signal suppression effects caused by the high Na and Cl concentrations: 10% NH_4NO_3 or 15 μg Pd + 10 μg $\text{Mg}(\text{NO}_3)_2$. The matrix and modifier together proved relatively corrosive to the graphite tubes; these were frequently cleaned with isopropyl alcohol and DDI and changed as necessary, typically after 10 to 20 hours of analysis. The graphite contacts were also cleaned regularly, and the optic path monitored for cleanliness.

An instrument precision study was performed for the Varian instrument: a standard was run 18 times and the 80% and 95% confidence intervals were calculated ($\pm 1.4\%$ and 2.2% , respectively). The precision of the ICP-AES was not tested in this way; however, their general performance in terms of drift, linearity, and long-term consistency of standard reference materials analysis indicates that their precision was markedly better than that of the Varian. The Perkin-Elmer GF drift and linearity were superior to those of the Varian, and its recovery of SRMs was relatively consistent. During Cu analysis, three replicates of each analysis were performed and the mean value used. In each analytical run, reagent and solution blanks were run (DDI and SEW, as appropriate) along with an acid blank (0.5% HNO_3 , i.e. the instrument rinse solution) and a matrix modifier blank for GF-AA runs. A variety of external standards were also run in the analysis sets, including SLRS-3 (Riverine Water Reference Material for Trace Metals, NRC), CRM-ES (Estuarine Sediment, High-Purity Standards), and standards prepared by colleagues. Recoveries varied: for the Varian, 62-148%, mean 105%; for the Perkin-Elmer GF, 64-89%, mean 77%; for the Optima ICP, 92-114%, mean 101%; and for the Perkin-Elmer ICP, 89-112%, mean 101%.

Interpretation and Modeling

Analytical approaches to the data. The goal of this study was to determine the effect of surface coating physical form on the chemical properties of goethite coatings via Cu adsorption/desorption experiments. A series of null hypotheses were tested by correcting the observed results for each solid according to a set of assumptions that permitted no change in surface chemistry as a function of physical form. In addition, several quantities related to the uptake and release of adsorbates at the solid/water interface were compared between solids: fractional uptake, surface coverage, solution concentration, the partitioning coefficient, total site occupancy, and the ion activity product.

Two conventional approaches to interpreting batch sorption data where pH is held constant are plots of fractional uptake vs. adsorbate added, here called *adsorption isotherms*, and plots of equilibrium concentration on the solid (or surface coverage) vs. equilibrium concentration in solution, here called *Langmuir plots*. In adsorption isotherms, fractional uptake, or ' θ ,' is the amount removed by the solid divided by the amount added, such that 0 = no uptake and 1 = complete uptake. Total adsorbate added (' Me_{TOT} ') is usually expressed in terms of moles of adsorbate added per unit solid (in mass, surface area, or moles of sites). Surface coverage (' C_s ' or ' Γ ') is expressed in the same units as Me_{TOT} and solution concentration (' C_A ') is in molar units. Schematic drawings of a typical adsorption isotherm and Langmuir plot are presented in Figure 26.

These two types of plots provide numerous clues to the surface chemical properties of the solid. Uptake capacity and desorption hysteresis may be probed using θ vs. Me_{TOT} plots, while C_s vs. C_A plots test for conformation to well-described theories of adsorption. These plots also provide two lines of evidence regarding the effect of surface coverage on the proposed predominant uptake mechanism in the system (e.g., adsorption by high-affinity sites, or surface precipitation). These were supplemented by analysis of the partitioning coefficient, total site occupancy, and the ion activity product (for the precipitation region). Note that while all solids studied generally exhibit the trends described, molecular-level information about the sorption complexes is needed to confirm these assignments.

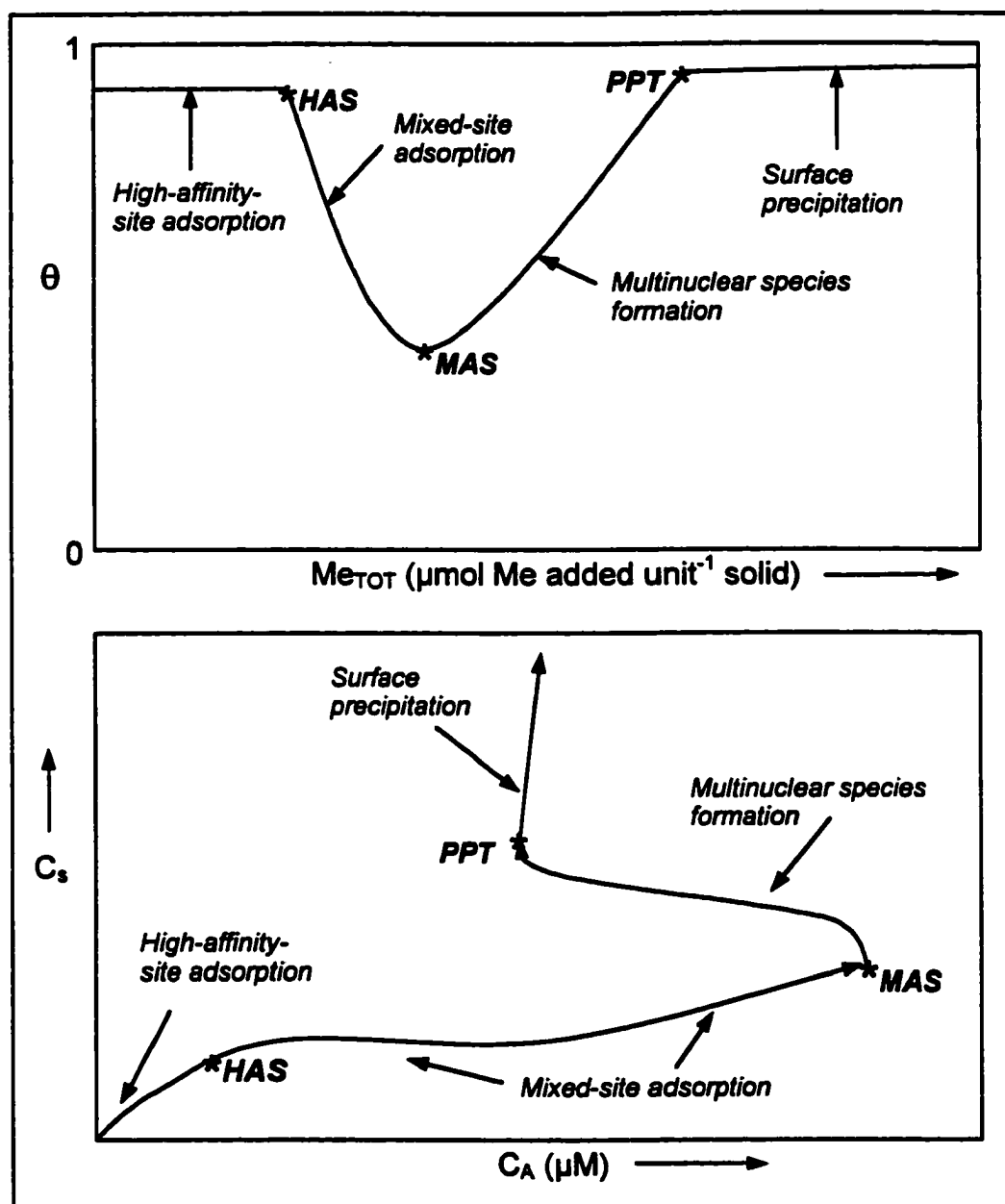
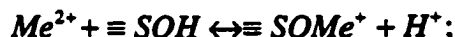


Figure 26. Schematic drawings of adsorption isotherms (plots of fractional uptake (θ) vs. total adsorbate added (Me_{TOT}) and Langmuir plots (surface concentration (C_s) vs. solution concentration (C_A) at equilibrium). Me_{TOT} and C_s are expressed in the same units. The arrows in the trend line of C_s vs. C_A indicate the direction of increasing surface coverage. The points where shifts in dominant uptake mechanism are suggested are noted on both plots: *HAS* = high affinity to mixed sites, *MAS* = mixed sites to multinuclear species formation, and *PPT* = multinuclear species formation to surface precipitation.

The partitioning coefficient, or K_d , is the ratio of adsorbed to dissolved metal:

$$K_d = \frac{C_s}{C_A} = \frac{\{ \equiv S O M e^+ \}}{[M e(aq)]} \quad (13)$$

It bears some resemblance to an apparent equilibrium constant for the adsorption reaction



$$K_{app}^* = \frac{\{ \equiv S O M e^+ \} [H^+]}{\{ \equiv S O H \} \{ M e^{2+} \}} \quad (14)$$

where $\equiv S O H$ represents a surface functional group, and it can, with caution, be used to interpret and model sorption data. However, it is highly dependent on the specific solution conditions (especially pH) and, like the Langmuir model, it makes assumptions known to be false for the systems – in particular, that there is only one adsorption reaction with one site type. In this study, pH is fairly constant, as is the ratio of $M e^{2+}$ to $M e(aq)$ (see Figure 24); in addition, at adsorption-dominated loadings, unreacted surface sites are in excess and their concentration can therefore be considered relatively constant. Under these conditions, K_d and K_{app}^* are roughly proportional.

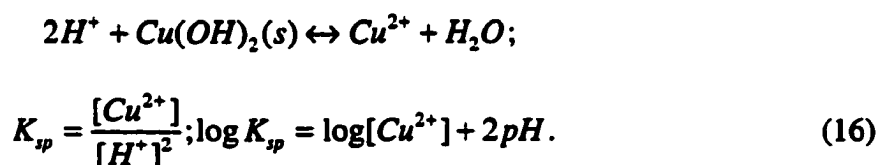
Total site occupancy (N_{max}) is also known as the limit of mononuclear adsorption. It is the surface coverage at which a complete monolayer of adsorbate would theoretically form (given Langmuirian conditions), or in other words, the point at which all adsorption sites are occupied. It is derived from an “inverse Langmuir plot,” in which $1/C_s$ is plotted vs. $1/C_A$:

$$\frac{1}{C_s} = \frac{1}{N_{max}} \cdot \frac{1}{C_A} + \frac{1}{b N_{max}} \quad (15)$$

where b is an empirical value. Only the coverages exhibiting Langmuir behavior are plotted (i.e. the initial linear increase and the plateau, or up to MAS in Figure 26), which is transformed into a line in the inverse plot. The y-intercept is the inverse of N_{max} . Like

K_{ϕ} this is a useful empirical value but, given the theoretical constraints of Langmuirian behavior, does not necessarily indicate the actual number of adsorption sites present.

The quantities listed above are intended to describe adsorption. The combination of sorption mechanisms operating at moderate coverages (adsorption, polymeric complex formation and growth, and surface precipitation) makes it more difficult to elucidate surface properties. However, at coverages where surface precipitation appeared to dominate uptake (i.e., fractional uptake was independent of coverage, and C_A remained roughly constant), the ion activity product ('IAP') of the systems was calculated. The precipitate was taken to be cupric hydroxide ($\text{Cu}(\text{OH})_2$) and the dissolution reaction for this solid was written:



The IAP for the system is the same as K_{sp} , without the assumption of equilibrium conditions. If the precipitate formed on all coatings is the same, the IAP for all systems should be the same. However, if different precipitates form (e.g., different degrees of crystallinity), then the IAP should differ.

Expression and testing of the null hypothesis. The null hypothesis is that the surface chemistry of a goethite coating is not related to its physical form. Therefore, changing the physical form of goethite should have no correlative effect on Cu sorption behavior arising from the chemical properties of the surface – specifically, the surface site density, the properties of sites, and the relative proportions of different site types. Any change in sorption should therefore be removed by considering non-chemical surface effects and/or normalization of the data. The assertions and tests of the null hypothesis are presented in the form of a flow chart in Figure 27.

H₀: Physical form does not affect surface chemistry.

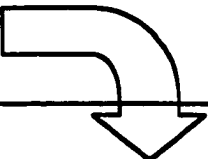
Assumption	Assertion	Test	Alternative
1. Goethite controls all sorption.	Goethite form has no effect on Cu(II) sorption.	→ <i>normalize for mass of goethite</i>	→ Physical form has some effect
	The effect is due only to changes in SA:V.	→ <i>normalize for SA:V</i>	→ The effect is not only due to SA:V; substrate must be considered
2. Substrate interacts only with Cu.	The effect is due only to substrate sorption of Cu.	→ <i>model additively</i>	→ Apparent nonadditivity is due to SA:V
	The effect is due to SA:V and substrate sorption.	→ <i>correct SA:V and model additively</i>	→ Substrate must affect goethite
3. Substrate interacts only with goethite.	The effect is due only to goethite site blocking.	→ <i>correct for site blocking</i>	→ Apparent non-site-blocking effect is due to SA:V
	The effect is due to SA:V and site blocking.	→ <i>correct SA:V and site blocking</i>	→ Substrate interacts with Cu and goethite
4. Substrate interacts with Cu and goethite.	The effect is due to substrate sorption and site blocking.	→ <i>correct for site blocking and model additively</i>	→ Apparent nonadditivity is due to SA:V
	The effect is due to SA:V, site blocking, and substrate sorption.	→ <i>Correct for SA:V and site blocking, and model additively</i>	→ 
<p>There appears to be an effect on sorption behavior other than those related to SA:V ratio, substrate sorption of Cu, or site blocking. <i>Reject null hypothesis.</i></p>			

Figure 27. Summary of the tests of the null hypothesis.

The null hypothesis is broken into a series of assertions that may be tested in turn. Each assertion springs from an assumption about the reactivity of the sorbent or sorbents, and leads to two tests of the data. First, it is assumed that Cu sorption in the systems can be described in terms of goethite sorption alone – i.e., that the substrate does not play a significant role in the net sorption of the system. This is a reasonable starting assumption, since the substrates are relatively unreactive compared to goethite. If true, then all solids should exhibit the same amount of Cu sorption when normalized to the amount of goethite present. It may also be necessary to account for the difference in the surface area-to-volume ratio ('SA:V') of a coating as opposed to a bulk phase. As stated above, an estimated 20% of the Fe atoms in a goethite coating occur at the surface, in contrast to about 1.7% in bulk goethite. It could be that although the properties and types of sites remain identical, the sheer increase in their number produces any observed variation in Cu sorption. If so, then there should be a correction factor to account for this change in SA:V. (It should be noted that such a correction should only be necessary for the chemical coatings, since the physical coatings are composed of goethite particles.) The correction factor for SA:V was based on the difference between the measured SSA and the estimated SSA of the chemical coatings (Chapter 2, Table 3).

If variations persist despite normalization to goethite, this implies either a change in the properties of the goethite surface and/or the possibility that the substrate plays a role in the behavior of the system. Since the null hypothesis does not admit a change in goethite surface properties, the role of the substrate is considered. The substrate may interact with Cu, or with goethite, or both. The second assumption, then, is that the only substrate role in controlling sorption is that of direct sorption of Cu by the substrate. If true, then the systems could be modeled following the principle of additivity, which assumes that each sorbent acts as it would in the absence of any other sorbent phase. The additive model should be run without, and then with, corrections for SA:V, in order to check for a combined effect.

The conceptual model of additive sorption assumes that when more than one sorbent phase is present, each reacts as if in isolation. This precludes any interaction

between the sorbent phases affecting the net sorption of the system. For instance, if both goethite and quartz are present, the net sorption according to the additive model is equal to the sum of the amounts goethite and quartz each would take up if it were the only phase present. This can be compared to a set of aqueous complexation reactions in a system containing one cation and two anions.

In order to determine how much Cu each phase would take up at a given coverage, it was necessary to formulate an equilibrium constant for the complexation reaction. Since the solution conditions are held constant in all cases, the partitioning coefficient, K_d , was used in place of a conditional equilibrium coefficient, as discussed previously. Separate values for K_d would be necessary for each coverage and for each phase; these were estimated from the data for the single-phase systems (see Appendix 5). Because the bulk of the discrepancies in Cu uptake were observed in MAS and OLG regions, these were the focus of the additive corrections.

The amount of Cu sorbed at a given coverage by one phase was calculated as follows:

$$\frac{Cu_{TOT}}{(1 + \frac{1}{K_d})} = C_s. \quad (17)$$

The additive models were run using MINTEQA2, an aqueous speciation program published by the USEPA (Allison et al., 1991). Each sorbent was assigned one aqueous component and given the K_d calculated for the sorbent at the coverage. The values for Cu_{TOT} , goethite, and substrate for each solid sample were input, and the pH and ionic strength were fixed, and precipitation was not allowed. In order to verify the model, it was tested using data from the goethite system. The sample run at a coverage of $0.660 \mu\text{mol m}^{-2}$ total produced a value for the surface complex of $0.6593 \mu\text{mol m}^{-2}$ total, which was within 0.2% of the observed experimental value of $0.6579 \mu\text{mol m}^{-2}$ total. This was considered a satisfactory degree of accuracy given the simplicity of the additivity model.

If the additive model failed to fit the data, then the substrate would appear to have some sort of effect on sorption of Cu by goethite. Therefore, the third assumption is that

the substrate's role is to affect Cu uptake by goethite. However, this need not involve a change in goethite's surface chemistry. For example, the blocking of goethite surface sites as a result of the two phases association as coating and substrate may require consideration. The association may remove sites from availability by occupying them with chemical bonds between the solids, or it may prevent some sites from complexing Cu ions by physical proximity, creating electrostatic or steric hindrances to sorption. Such hindrance of sites from complexing Cu would not change the chemical properties of the goethite surface, but it would alter its reactivity. The relative influence of surface blocking varies with loading – i.e., the amount of available surface relative to the amount of adsorbate (Figure 28). If there is an excess of surface area, and a small fraction is physically blocked, it has slight effect on uptake; however, if there is an excess of adsorbate, the same degree of blocking would affect uptake more.

The effect of blocking also varies with surface site density ("SSD") – i.e., the number of sites per unit surface area (Figure 29). This is a nonlinear function, making it difficult to model blocking in experimental data. Also, the precise SSDs of mineral grains have been a challenge to determine – the current best estimate for goethite is 2 – 20 sites per nm² (Robertson and Leckie, 1997). For quartz, recent estimates place the SSD between 1 and 3 sites per nm² (Hiemstra, 1996; Langmuir, 1997), and kaolinite estimates vary between 1 and 6 (Davis and Kent, 1990; Langmuir, 1997; Kretzchmar, 1998). This also makes quantifying the effect of physical surface blocking difficult.

Although a quantitative assessment of the effect of site blocking on Cu sorption is thus beyond the scope of this dissertation, scientific reasoning can be applied to evaluate the likelihood and relative degree of physical blocking of the goethite surface in the different solids. For example, in the physical coating of goethite on kaolinite (K-phys), it is expected that goethite particles will not associate with edge sites due to steric and electrostatic charge considerations. If all goethite particles lie flat on the basal planes of the kaolinite, then roughly half of their (110) planes will be turned toward the kaolinite surface and should not be available for Cu complexation. This is a reasonable maximum range to set on the proportion of goethite sites likely to be blocked in K-phys. Even if

some goethite does associate with the edges, it will not be able to lie flat. In addition, some particles associated with the basal planes may not lie flat; hence, any different arrangement of goethite particles in association with kaolinite grains should result in less than 50% of the sites being blocked. The experimental results for K-phys may then be compared to those for goethite, and the relative differences weighed in light of the known effects of surface blocking on apparent fractional uptake (Figures 28 and 29).

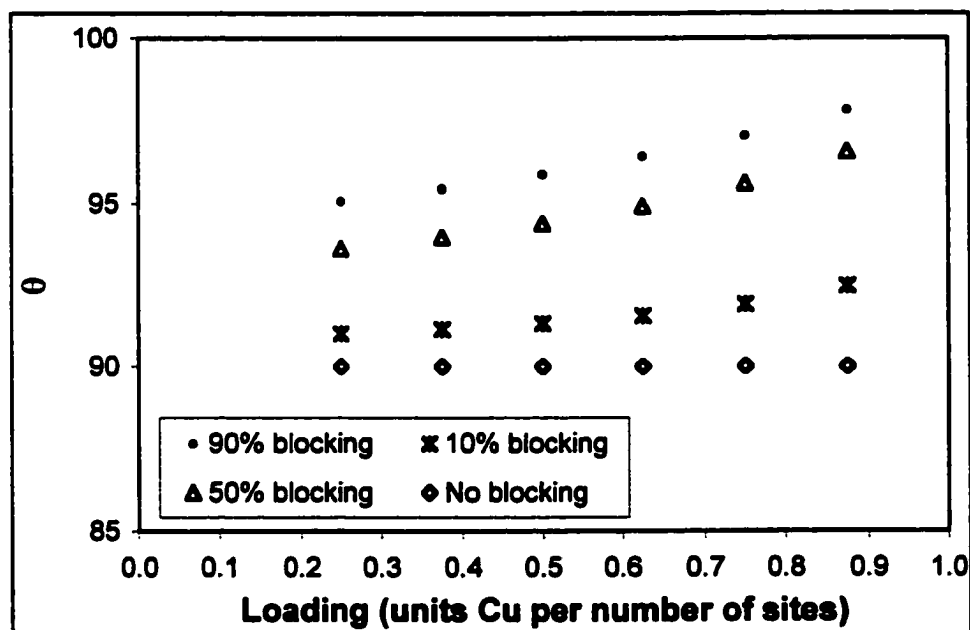


Figure 28. Changes in corrected fractional uptake as a function of loading. In this example, the amount of fractional uptake where no surface is blocked is set at 0.90. The other three series show the estimated actual uptake for a solid which appears to take up 90% of the adsorbate but which is partially blocked. Corrected uptake is estimated using the partitioning coefficient observed in the unblocked solid. Note that the effect of blocking on apparent fractional uptake increases with increasing loading.

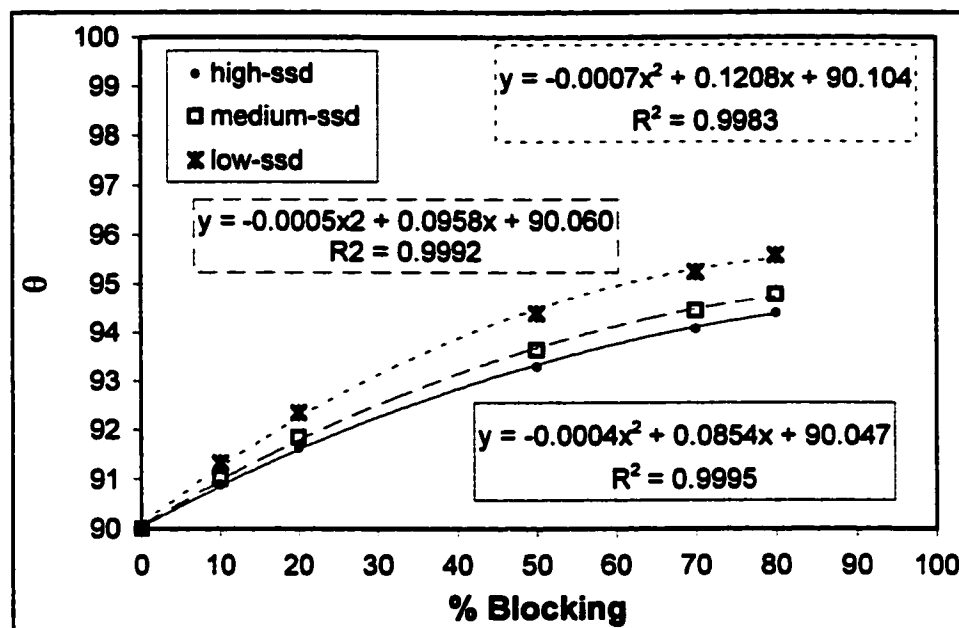


Figure 29. Changes in corrected fractional uptake as a function of the degree of surface blocking. Note that the effect of blocking is inversely related to SSD, and that this effect is nonlinear.

In addition to correcting only for site blocking, the attempts already made to eliminate apparent discrepancies in sorption between the coatings and bulk goethite may be applied in combination with site blocking. For example, if all variation is not reconciled by factoring for site blocking, the corrected data may be modeled additively to check for substrate sorption in addition to site blocking. If none of the tests of the null hypothesis explain variations in Cu sorption behavior as a function of the form of the goethite coating, an effect on sorption behavior other than those related to normalization to the amount of goethite, the surface area-to-volume ratio, uptake of Cu by the substrate, or surface site blocking by the substrate is implied – that is, an effect on the chemical properties of the solid surface, such as the types and abundances of different surface site types. This would mean that the null hypotheses asserting no changes in surface chemical properties should be rejected.

Results

The results of the Cu sorption/desorption experiments on bulk goethite and the coated solids are presented as isotherms and Langmuir plots (Figures 30 and 31). Cu sorption to uncoated kaolinite is plotted in Figures 30b and d; however, Cu sorption to uncoated quartz was both distinct in trend and much lower in reactivity than the other systems, as shown in Figure 32. The trends shown in Figure 26 are observed in all systems. However, the isotherms indicate differences in the observed range of fractional adsorption and desorption as well as the coverages at which inflections in the trends appear. In addition, the coated solids exhibit a broader range of fractional uptake than bulk goethite. Desorption is generally slight – the largest fraction of sorbed Cu released by any solid was about 12% – but coated solids generally released more sorbed Cu than bulk goethite (Figure 30c and d). In general, coverages where the least amount of Cu was sorbed also experienced the greatest release upon dilution (Figure 30c and d). Finally, the coverages at which surface precipitation begins to drive uptake varied; these are given in Table 11. Bulk goethite reached dominant precipitation at lower loadings than either of the substrates or any coated solid except for Kch-thick.

The Langmuir plots (Figure 31) also indicate differences in Cu sorption between the systems, especially those containing kaolinite. One variable is the maximum C_A reached in the plateau region of the plots, and another is the value of C_s in the plateau region. The quartz-bearing systems, in contrast, appear to agree with the bulk goethite data relatively well (Figure 31a), and all five solids appear to behave similarly at the lowest range of coverages, i.e. the range in which adsorption to relatively high-affinity sites is expected to dominate uptake. The desorption Langmuir plots of quartz-bearing solid data also appear to resemble that for bulk goethite, in contrast to the kaolinite-bearing solid data (Figure 31c). (It should be noted that although the data are plotted using the same units as conventional Langmuir plots in Figure 31, Langmuir-type behavior is exhibited only at the lowest loadings, where adsorption sites are in excess.)

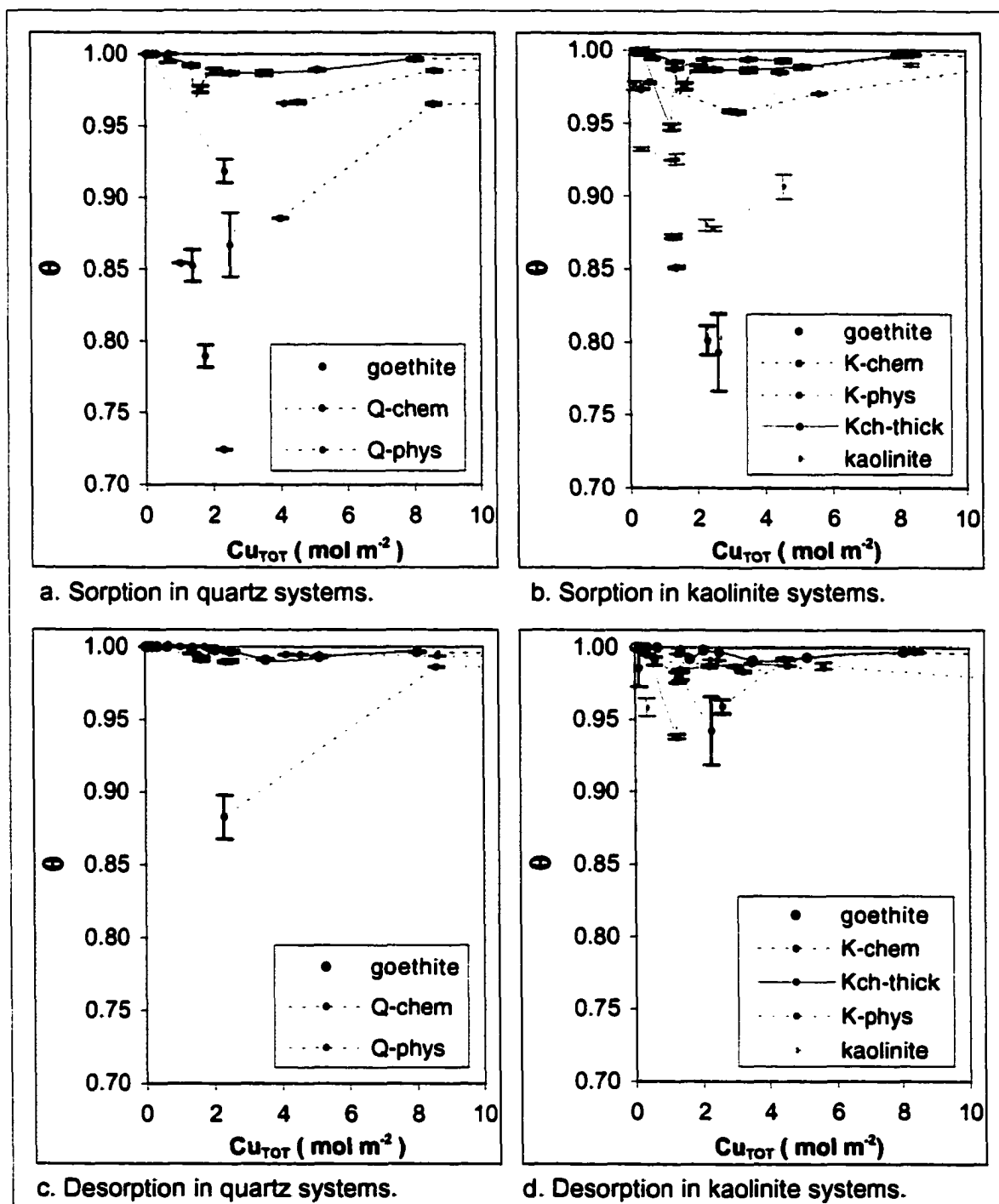


Figure 30. Cu(II) sorption and desorption isotherms for the goethite-coated solids in comparison with bulk goethite and uncoated kaolinite. Results for uncoated quartz are presented in Figure 32. Cu_{TOT} is in $mol\ Cu\ m^{-2}$ solid. Error bars show the range of the sample duplicates. Dashed lines between data points are to aid visual interpretation.

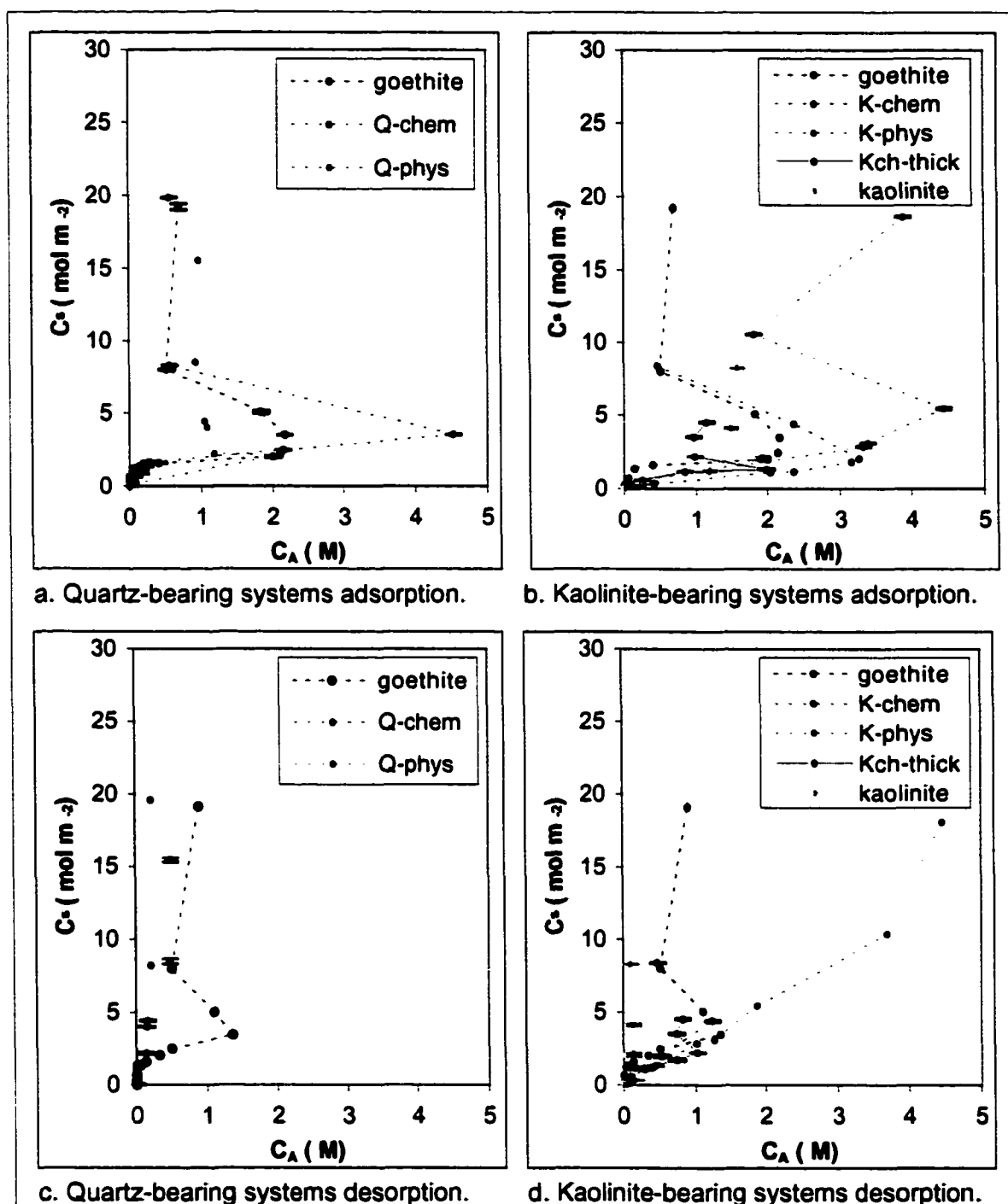


Figure 31. Langmuir-type plots of Cu(II) sorption and desorption by the goethite-coated solids in comparison with bulk goethite and uncoated kaolinite. C_s is mol Cu m^{-2} solid. Error bars show the range of the sample duplicates. Dashed lines between data points are to aid visual interpretation.

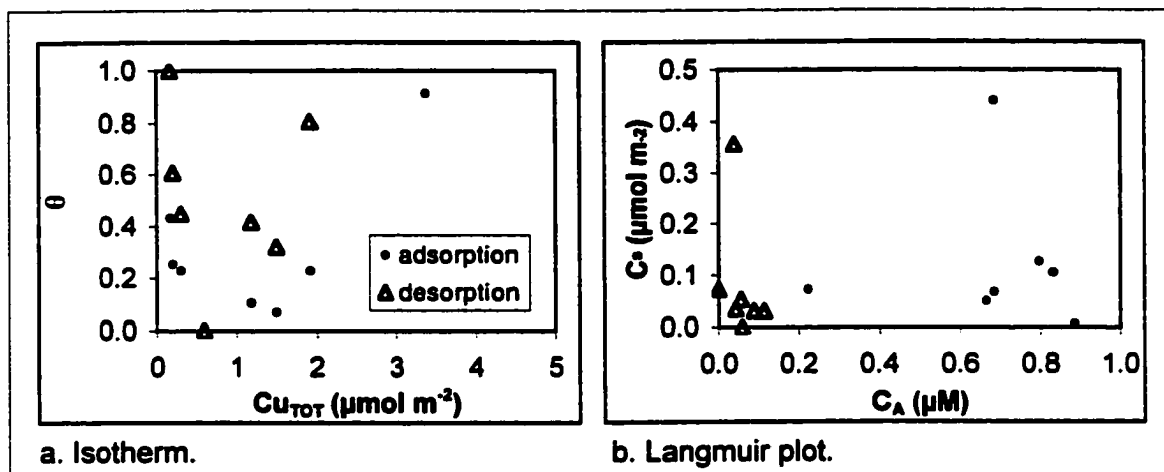


Figure 32. Results for uncoated quartz.

TABLE 11. Surface coverages bracketing the onset of dominant surface precipitation.

Solid	Cu_{TOT} $\mu\text{mol m}^{-2}$
Kch-thick	1.34 – 2.23
Goethite	1.63 – 2.51
Quartz	1.92 – 3.38
Q-phys	2.49 – 4.15
K-chem	2.61 – 4.48
K-phys	3.26 – 5.62
Q-chem	4.00 – 8.61
Kaolinite	4.55 – 8.37

Desorption hysteresis is observed in the adsorption range for all systems (Figure 33). Hysteresis occurs in cases where the uptake of an adsorbate is not fully reversible in the time allowed. As seen with N_2 adsorption in Chapter 2, this results in a deviation of the desorption trend from the adsorption trend (see Figure 3). In the case of Cu sorption from solution, Langmuir-type plots may be used to illustrate desorption hysteresis (Figure 33). Hysteresis is generally not observed at the lowest coverage ranges, although in many cases it may have fallen below the method detection limit.

The desorption data generally fall to the left of the adsorption trends and form a steeper slope, indicating that at least some of the bonds formed during uptake are irreversible over the time allowed.

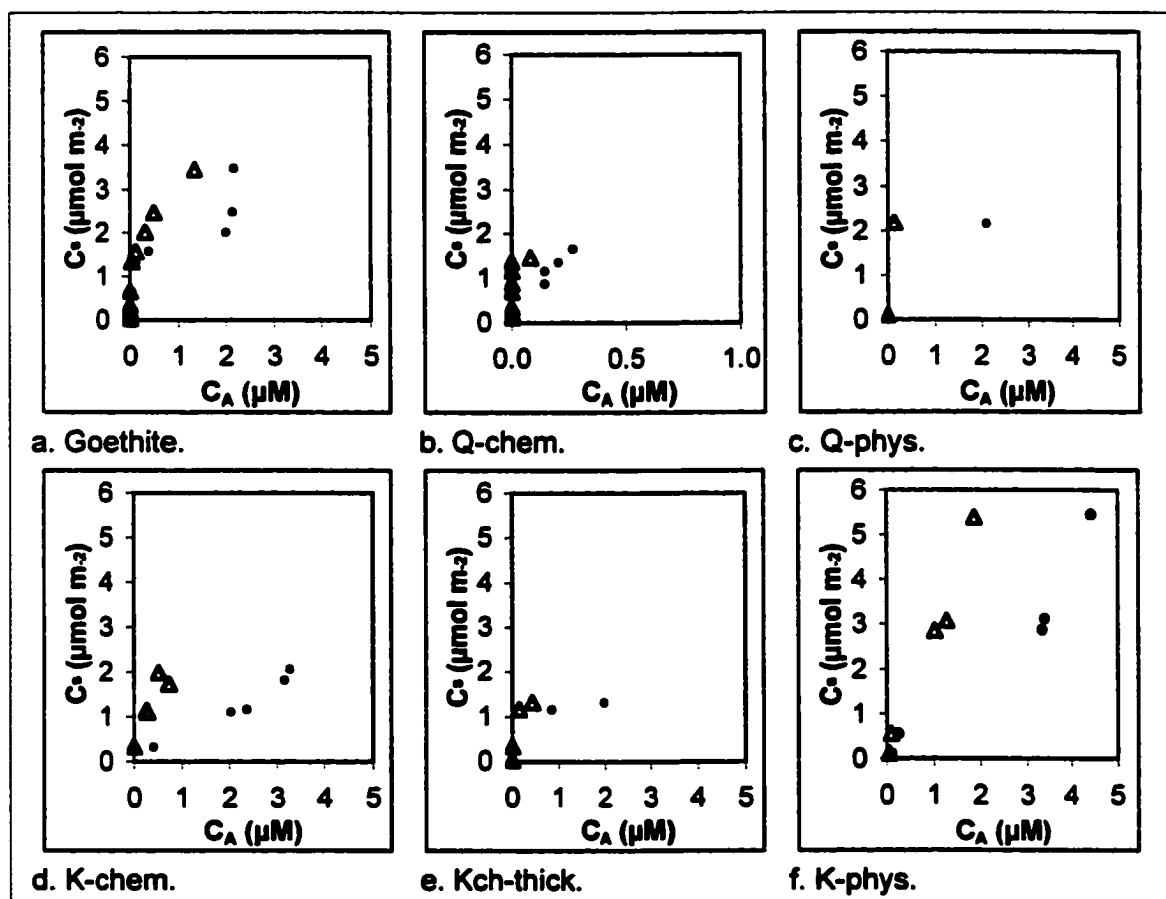


Figure 33. Desorption hysteresis in Cu(II) sorption by bulk goethite and the coated solids. Note the different x-axis scale for Q-chem.

Figure 34 shows the inverse Langmuir-type plots for bulk goethite, uncoated kaolinite, and the coated solids except for Q-phys (due to the lack of data in the pertinent loading range). N_{max} was calculated from these plots using Equation 15. A value for N_{max} could not be derived for uncoated quartz because it does not display Langmuir behavior (see Figure 32). Table 12 gives the values for N_{max} and also log IAP for bulk goethite, the substrates, and the coated solids. Log IAP was calculated for the precipitation-dominated loading ranges using Equation 16.

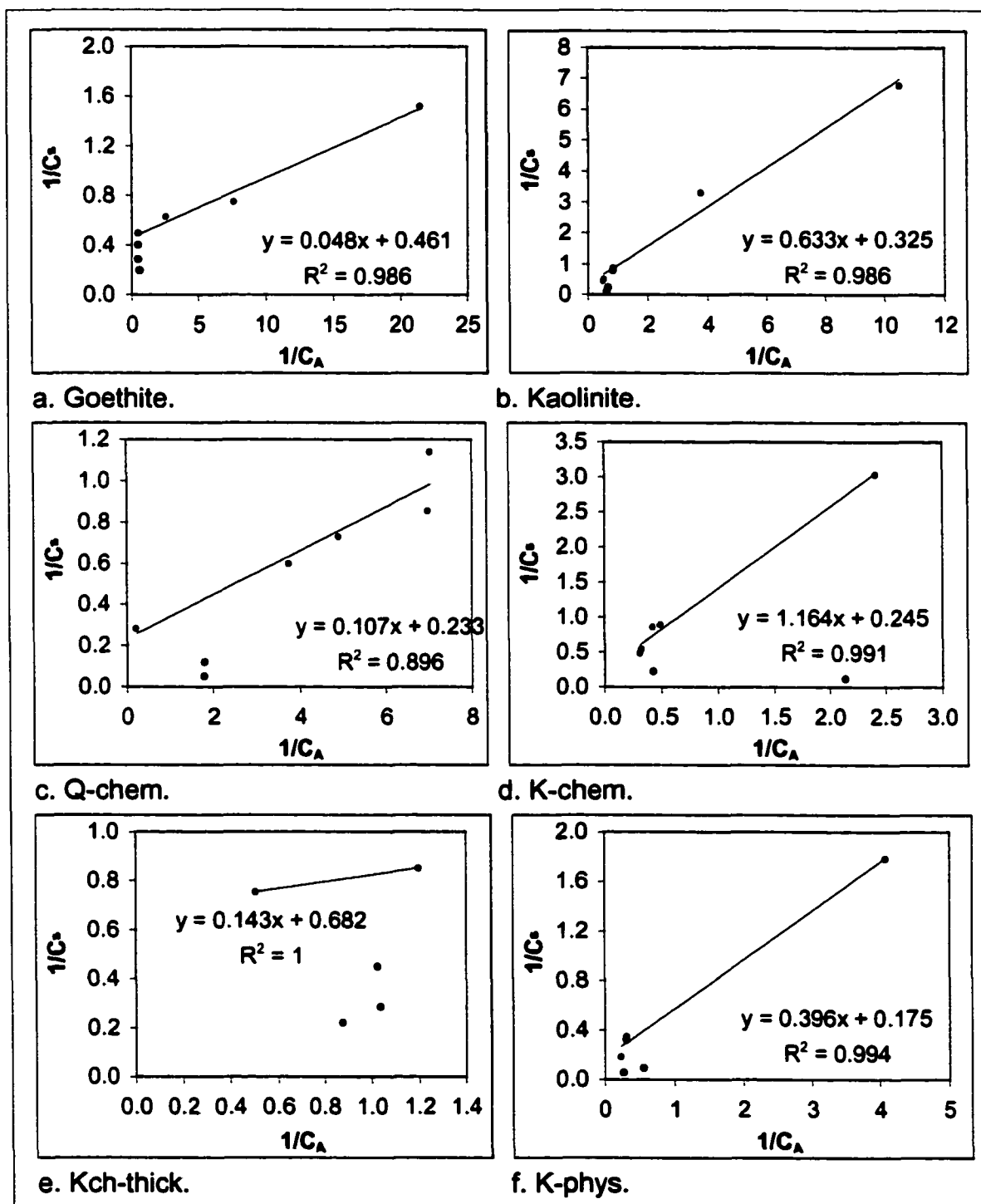


Figure 34. Inverse Langmuir-type plots showing the range of points used to calculate N_{max} (plotted in red).

TABLE 12. N_{max} and log IAP for coated solids.

Solid	N_{max}	C_s of $\theta_{\mu v}$ $\mu\text{mol m}^{-2}$	log IAP
Kch-thick	1.47 ^b	1.24	8.38
K-chem	4.08	2.61	8.81
K-phys	5.72	3.26	9.02
Goethite	2.17	1.63	9.16
Q-chem	4.29	2.30	9.23
Q-phys	x^c	2.49	9.46
Kaolinite	3.08	2.48	10.03

Tests of the null hypothesis. All eight tests compare the behavior of the solids to bulk goethite. If after applying the test the solids data lie within the error range of the goethite data points, or the error bars of the solids data overlaps the spline fit, the test is considered to have succeeded. If the data do not match bulk goethite, but more closely resemble it in any of several qualitative or quantitative ways, the correction is considered an improvement. If the application of a test increases the discrepancy between a solid and bulk goethite, the test is considered to fail.

The first test, assuming that goethite alone controls Cu sorption in the system, is to normalize the data to the amount of goethite present in the system. Because at this point physical form is asserted to have no effect whatever on Cu sorption, a simple correction for the mass of goethite present is applied. This normalization affects only C_s and Cu_{TOT} ; it is not present in the terms for C_A (units = μM) and is cancelled out in the calculation of θ ($\mu\text{mol Cu sorbed g}^{-1}$ goethite divided by $\mu\text{mol Cu added g}^{-1}$ goethite). Thus, the data in the isotherm plots are shifted only along the x-axis as a function of the mass of goethite present in the coated solid. Since θ also varies among solids (Figure 30), it is not possible for this single correction to remove all observed variations in sorption behavior. However, the test may produce an improvement if the observed inflections in the trends are brought into horizontal alignment.

The plots of sorption normalized to mass goethite are given in Figure 35. It is immediately apparent that this does not yield a common range of coverages. To evaluate whether the correction brings the data sets closer together, or closer to each other, a table was drawn up of the coverages at which the minimum value for θ was observed in each system (Table 13). In the first row, this coverage is given in terms of $\mu\text{mol m}^{-2}$ total, and the second row shows the factor by which each coverage differs from that for bulk goethite. The third row shows the coverages of the observed minimum θ in $\mu\text{mol g}^{-1}$ goethite, and the factor difference from goethite is given below that. This factor is uniformly larger for the mass-normalized data. Therefore, normalization to mass goethite is not considered a success, and the assertion that the form of goethite has no effect whatever on its sorption behavior is contradicted.

The next step is to consider corrections for the remainder of the null hypothesis asserting that there are no differences in the chemical properties of the surfaces of the goethite coatings. Some of these corrections can be discarded without testing them on the basis of what is already known about the coatings. In particular, none of the non-chemical alterations in the goethite surface should apply to the thick chemical coating on kaolinite (Kch-thick), where the surface of the goethite coating lies on a dozen or more layers of goethite and none of the kaolinite surface is exposed. This makes the surface analogous to the surface of a bulk goethite phase in terms of physical form; therefore, if this goethite phase is different only physically from bulk goethite, it should not be necessary to correct for a change in the surface area-to-volume ratio, since the SSA of the solid is essentially that of the goethite coating. For similar reasons, blocking of goethite surface area should not apply to Kch-thick, and additivity is not relevant since the kaolinite surface is completely buried and should not be able to take up any Cu. For the four thin coatings, the SA:V correction is not applicable to the physical coatings, which consist of discrete goethite particles attached to the substrate surface, and do not undergo a change in SA:V, and additivity is not expected to occur in K-chem, since the physical characterizations indicated that, like Kch-thick, the kaolinite surface is completely masked.

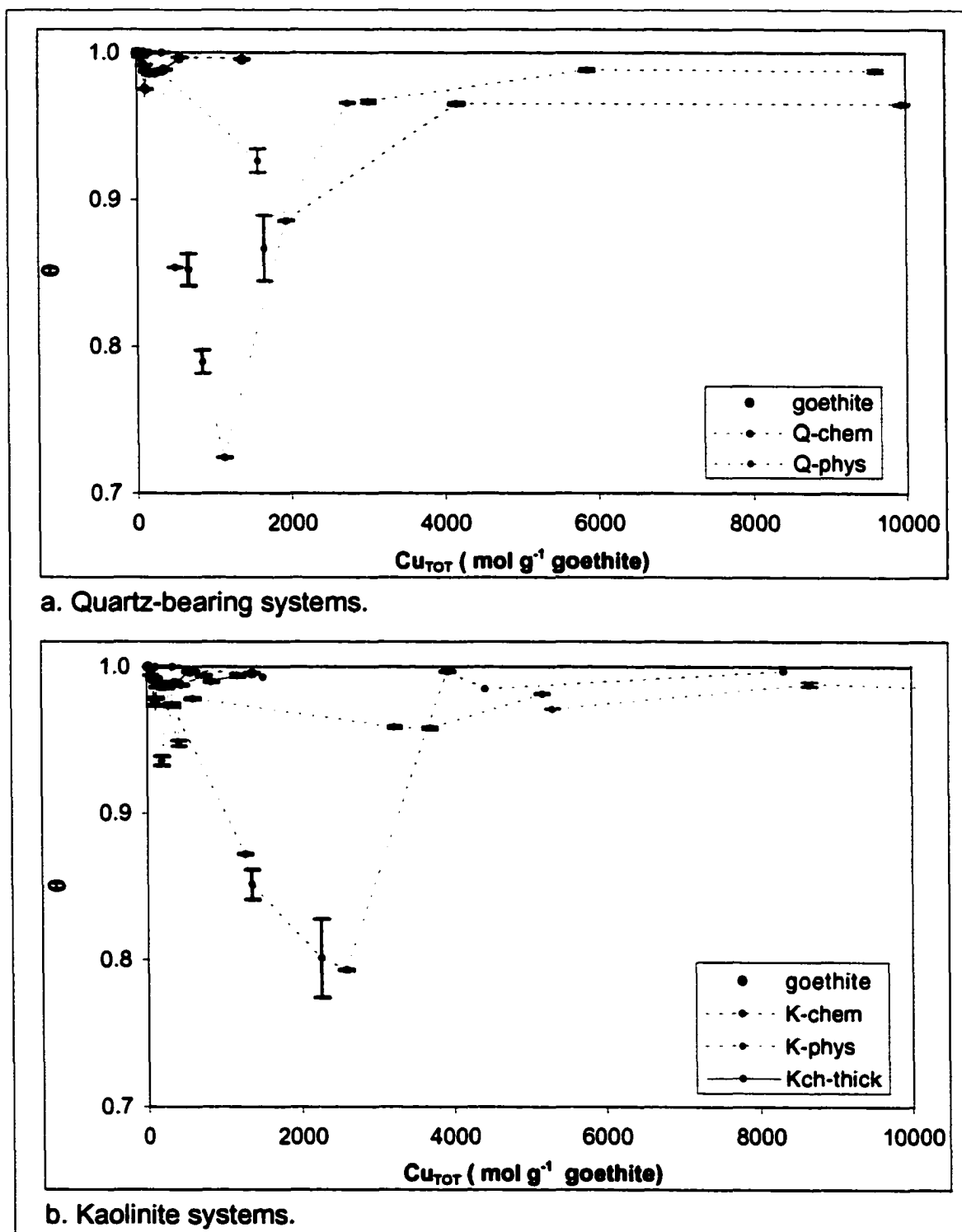


Figure 35. Cu(II) adsorption isotherms normalized to the mass of goethite in the system, in comparison with particulate goethite.

TABLE 13. Effect of normalizing sorption data to mass goethite and SA:V.

	Goethite	Q-chem	Q-phys	K-chem	Kch-thick	K-phys
Min θ , $\mu\text{mol m}^{-2}$ total	1.63	2.30	2.49	2.61	1.24	3.26
Ratio to goethite	(1)	1.4	1.5	1.6	0.76	2.0
Min θ , $\mu\text{mol g}^{-1}$ G	115.	1110.	1650.	2580.	411.	3690.
Ratio to goethite	(1)	9.7	14	22	3.57	32
Min θ , SA:V	1.63	4.46	x	4.41	1.38	x ^a
Ratio to goethite	(1)	2.7	x	2.7	0.85	x

^a 'x' indicates that the correction in question was not applied to the solid.

Additionally, before testing the remainder of the null hypotheses, the ways in which the corrections affect the data may be compared to the actual corrections required to match the coated solids to the bulk goethite. In the isotherm plots, the data for all four thin coatings falls below and to the right of the bulk goethite curve; in other words, it must be shifted up and to the left in order to match bulk goethite (Figure 30). None of the three corrections (SA:V, blocking, and additivity) would accomplish this alone (Figure 36). SA:V corrects for uptake by unaccounted extra surface area; therefore corrected uptake moves down on a per-unit solid basis; and Cu added is terms of area, so this term is reduced by correction for actual surface area. Site blocking corrects for blocked surface area; therefore corrected uptake moves up (corrected to reflect available SA); and the loading term is increased by the correction. In addition, site blocking is only relevant to data that falls below bulk goethite, while several points in the coated solids data falls above bulk goethite (Figure 30). These cannot be explained by blocking. Additive modeling corrects for additional uptake by second phase; therefore corrected uptake (on goethite alone basis) moves down, and the surface area of the second phase increases total surface area, so the loading term is decreased.

Furthermore, the degree of difference between the coated solids and bulk goethite trends varies throughout the range of loadings sampled – it is least in the HAS range, greatest in the MAS and OLG ranges, and closer in the PPT range. This nonlinearity in the discrepancies from bulk goethite requires either a nonlinear correction or a combination of corrections. The SA:V correction is linear because it preserves the number and types of sites per unit area. Additivity is variably nonlinear

because of the constantly changing affinity of the surface with changing Cu loading (due to the multiple mechanisms of uptake and site types, which in turn vary between solids). Blocking is nonlinear, and its effect increases continually with increasing loading. If there is a large excess of surface area available for adsorption, partial blocking has less effect on uptake than it does when the ratio of Cu to surface increases. This means that blocking cannot completely account for the observed discrepancies, which tend to be less at HAS and PPT loadings and greater at MAS and OLG loadings (Figure 30).

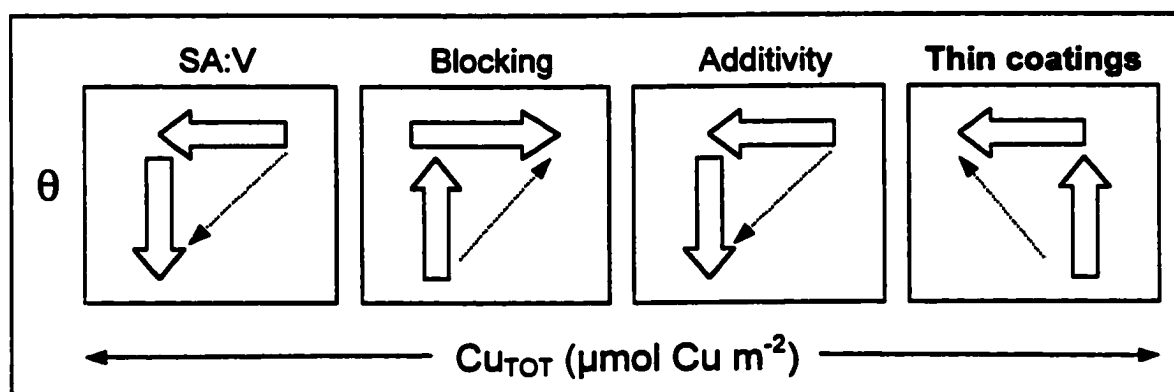


Figure 36. Directions in which the null hypothesis corrections work (SA:V, blocking, and additivity), and directions needed to match data for thin coatings to bulk goethite.

A combination of SA:V and additivity corrections cannot remove the discrepancies from bulk goethite because they both shift the data in the same directions. SA:V and blocking work in opposite directions, but since one is linear and the other becomes stronger with increasing loading, they cannot correct the data at higher loadings, where the coated solids data tend to become more similar to bulk goethite. This leaves additivity and blocking, which are both nonlinear and work in opposite directions. However, these corrections are applicable only to Q-chem and the two physical coatings. Thus, before testing the remainder of the null hypotheses, it can be discarded for two of the five solids (K-chem and Kch-thick), and for the remaining two (Q-chem, Q-phys and K-phys), only one combination of corrections has the potential to account for all discrepancies from bulk goethite.

Although alone they cannot explain all of the observed differences in Cu(II) sorption between bulk goethite and the coated solids, changes in SA:V or blocking may still be responsible for some of the differences; therefore, these factors should be considered. In addition, the substrate may take up Cu directly; thus the possibility of additive behavior, with or without blocking, also needs to be considered. Figures 37 through 40 summarize the results of correcting for the factors applicable to each of the four thin coatings. (As a reminder, none of them is applicable to the thick coating, Kch-thick.)

The goethite data alone, accounting for SA:V change or blocking, cannot describe Cu sorption to the chemical coating on quartz. As shown in Figure 37b, the chemical coating on quartz, Q-chem, is overcorrected to the left by SA:V, as based on the estimated SSA of the coating (see Chapter 2, Table 3). The general direction in which blocking would correct the data (up and to the right) does not match the direction of required change (up and to the left; Figure 37d), and blocking would alter the data at all loadings, while Q-chem matches bulk goethite in the HAS region. The Q-chem data also cannot be modeled by a simple combination of sorption to goethite and quartz. The additive model underpredicts the observed results for Q-chem (Figure 37c); however, the additive principle states that the addition of a second phase should increase the amount of sorbent available and therefore increase net uptake. This suggests that uptake by Q-chem exceeds the sum of the uptake by goethite and quartz separately. Last, since the additive model underpredicts the data, adding a blocking correction would further increase the discrepancy between the model and the data; thus, the null hypothesis is rejected for this solid.

Similarly, the observed results for Q-phys are not described by sorption to goethite with or without a blocking correction (Figure 38a,d); adding a blocking correction would shift the data up and to the left, while the required correction is up and to the right (Figure 38d). (The SA:V correction is not applicable for Q-phys, because the surface area of the goethite in the coating is known.) Also as for Q-chem, the additive model underpredicts the observed results for Q-phys (Figure 38c), and again,

combining additivity and blocking could only increase the discrepancy. Thus, the null hypothesis is precluded for both quartz-bearing solids.

It has already been determined that the null hypothesis cannot hold for K-chem, since no single correction or applicable combination of corrections can shift the data in the required direction. Remember that since the substrate is masked by the Fe coating, and thus, the additivity model is inappropriate, the goal of these corrections is to test whether bulk goethite adequately describes Cu sorption to the thin chemical coating on kaolinite (K-chem). As for Q-chem, the SA:V correction shifts the data too far to the left (Figure 39b). Blocking fails because it would not only work in the wrong direction but also apply over the whole loading range (Figure 39d). Cu(II) adsorption behavior on K-chem deviates from bulk goethite substantially only in the MAS and OLG ranges yet mimics bulk goethite at the highest and lowest loadings. Specifically, the K-chem goethite coatings more weakly binds Cu over low to moderate coverages than bulk goethite. This strongly suggests that at least a subset of the SHGs of the K-chem goethite coating are chemically different from those of bulk goethite.

As for K-chem, Cu sorption to K-phys cannot be described by sorption to bulk goethite with or without a blocking correction (Figure 40a, d). Since there are discrepancies from bulk goethite throughout the range of loadings sampled, and blocking operates at all loadings, it is feasible that blocking plays some part in the sorption behavior of the solid. However, the effect of blocking increases monotonically with loading (Figure 29), yet the difference between K-phys and bulk goethite decreases at the highest loadings (Figure 40a). Thus, even with a blocking correction, goethite alone cannot represent the behavior of K-phys. However, the kaolinite surface is partially exposed in K-phys, and thus additivity may be considered. The additive model brings the K-phys data closer to those of the coated solid (Figure 40c), although it still overpredicts sorption to K-phys (as does bulk goethite). Here again, blocking moves in the correct direction, but the degree of shift would be incorrect; compare, e.g., the 0.1 and 0.6 $\mu\text{mol m}^{-2}$ data points in Figure 40c. Thus, additional factors must be contributing to the net sorption behavior, and the null hypothesis is rejected.

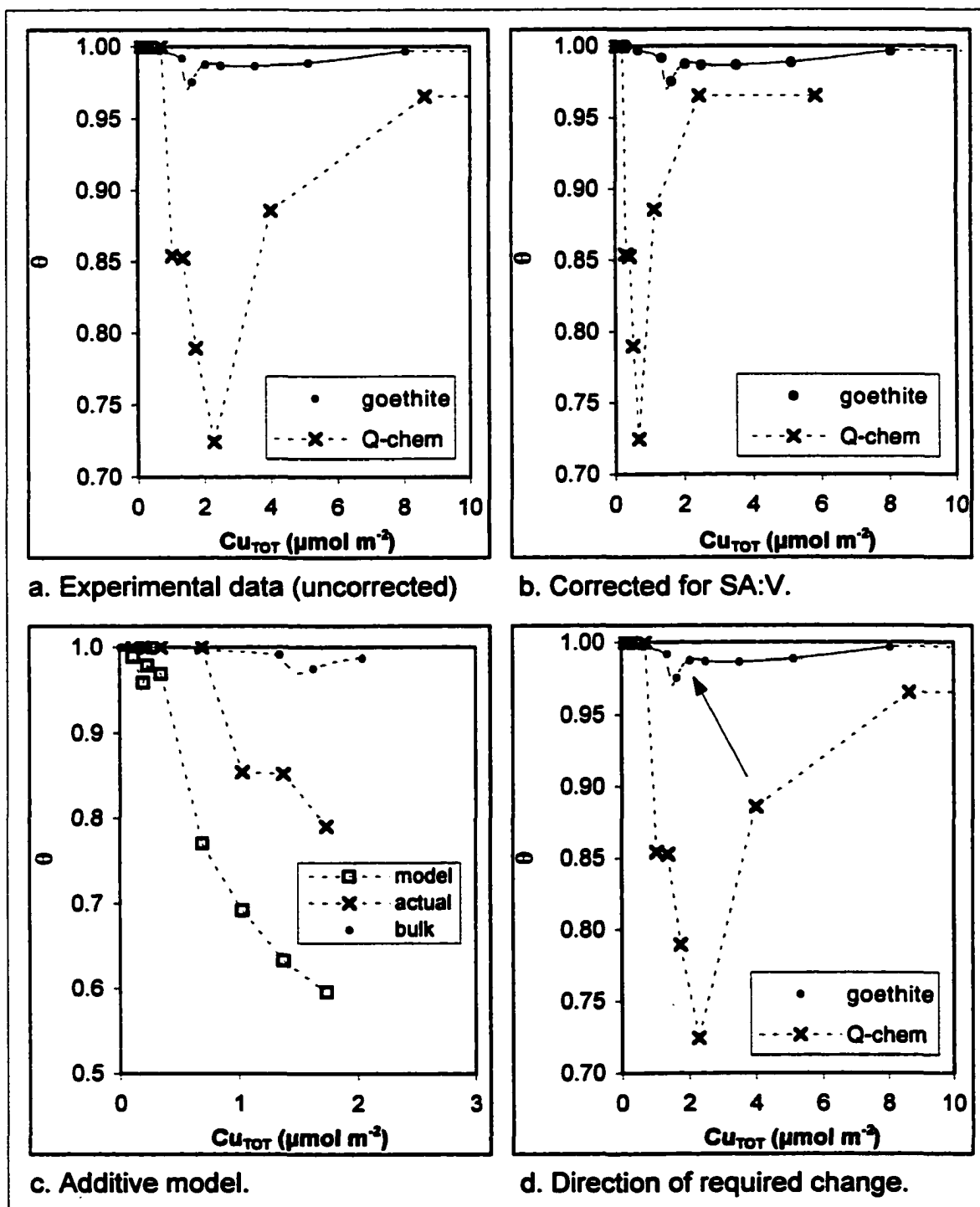


Figure 37. Results of applicable corrections for physical changes in goethite form for Q-chem in comparison with bulk goethite. Plot d shows the general direction in which the uncorrected Q-chem data would have to be shifted in order to match the bulk goethite data. Note the different x-axis scale for 37c.

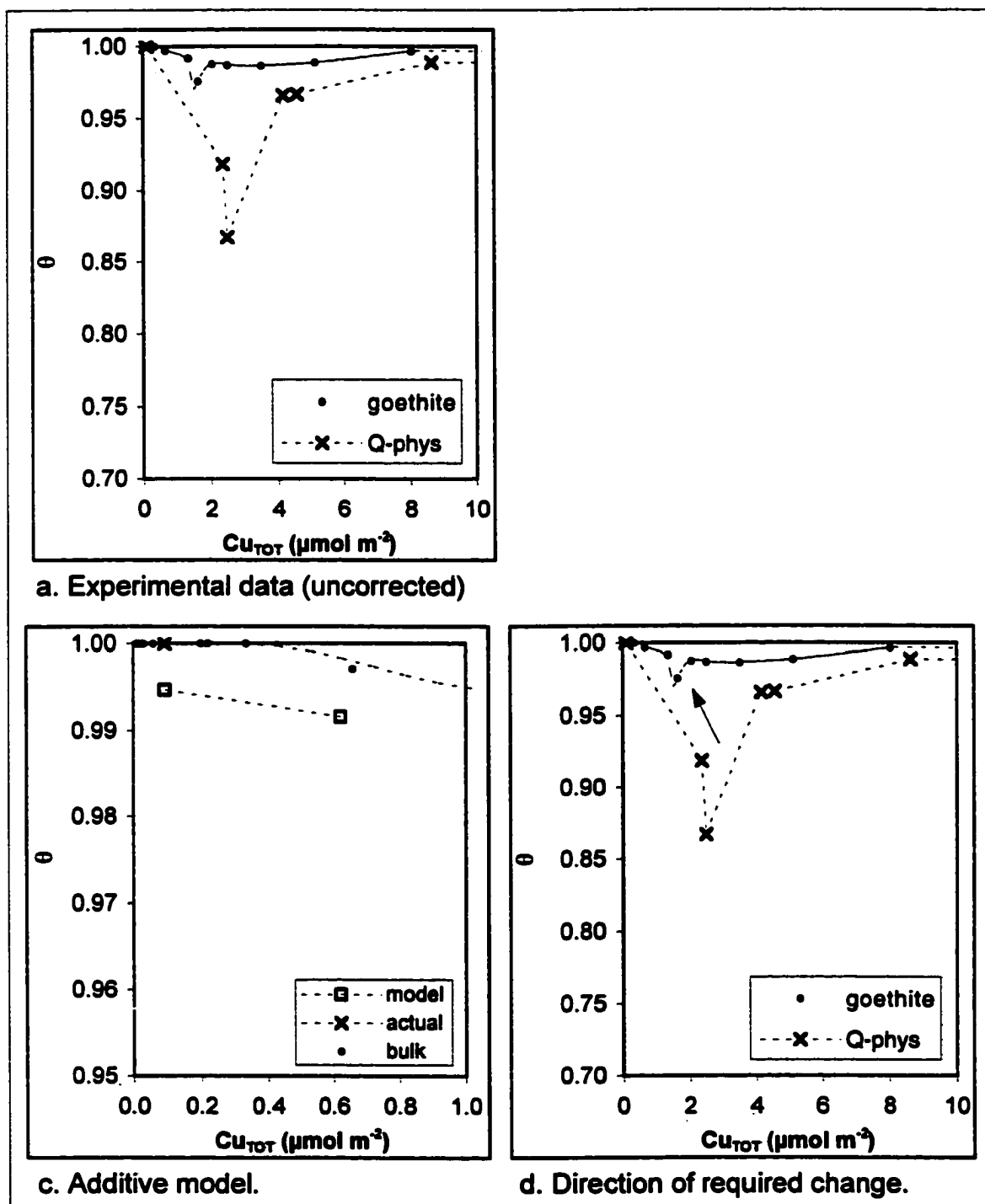


Figure 38. Results of applicable corrections for physical changes in goethite form for Q-phys in comparison with bulk goethite. Note that the correction for SA:V is inapplicable to this solid.

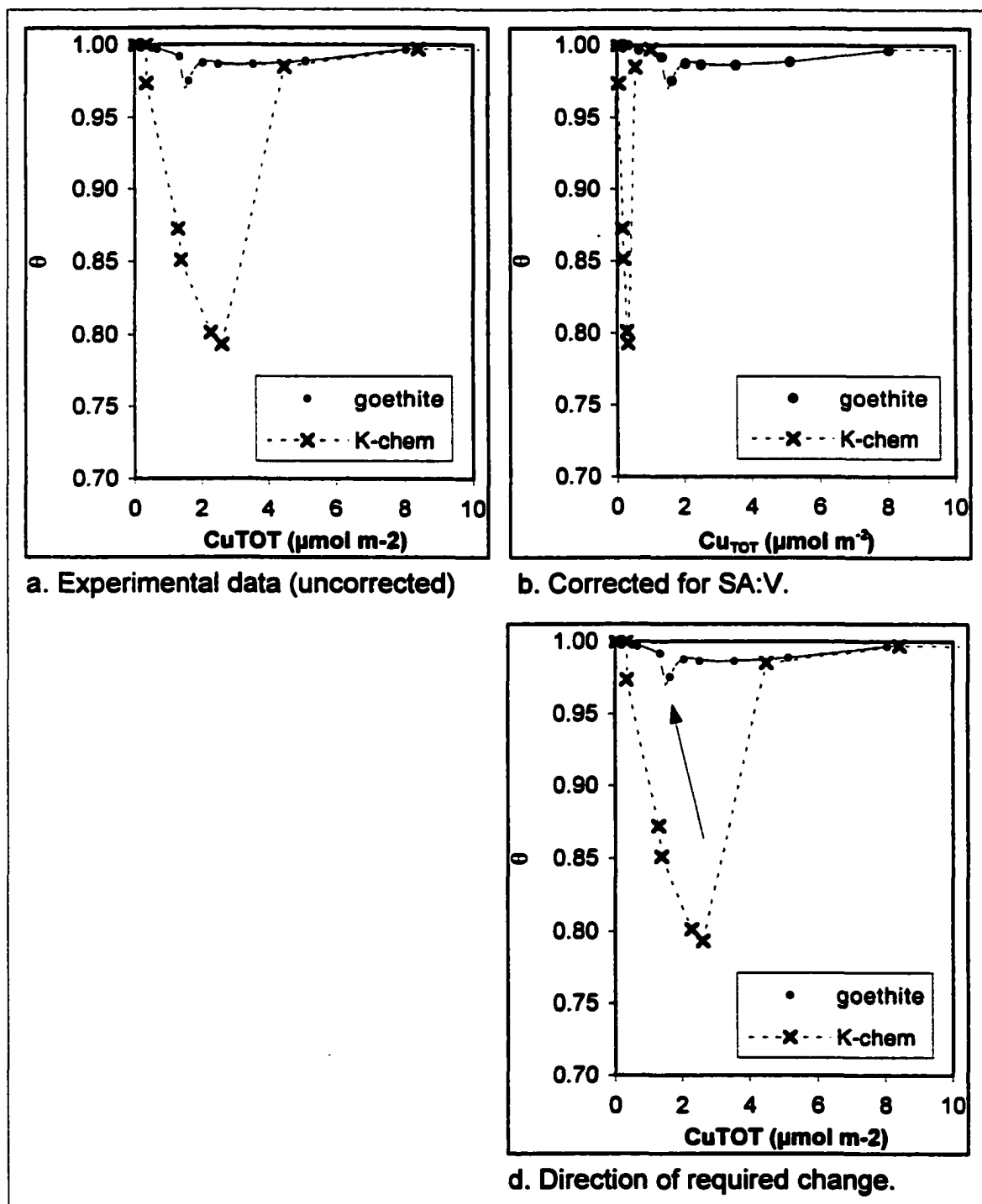


Figure 39. Results of applicable corrections for physical changes in goethite form for K-chem in comparison with bulk goethite. Note that the additive model is inapplicable to this solid.

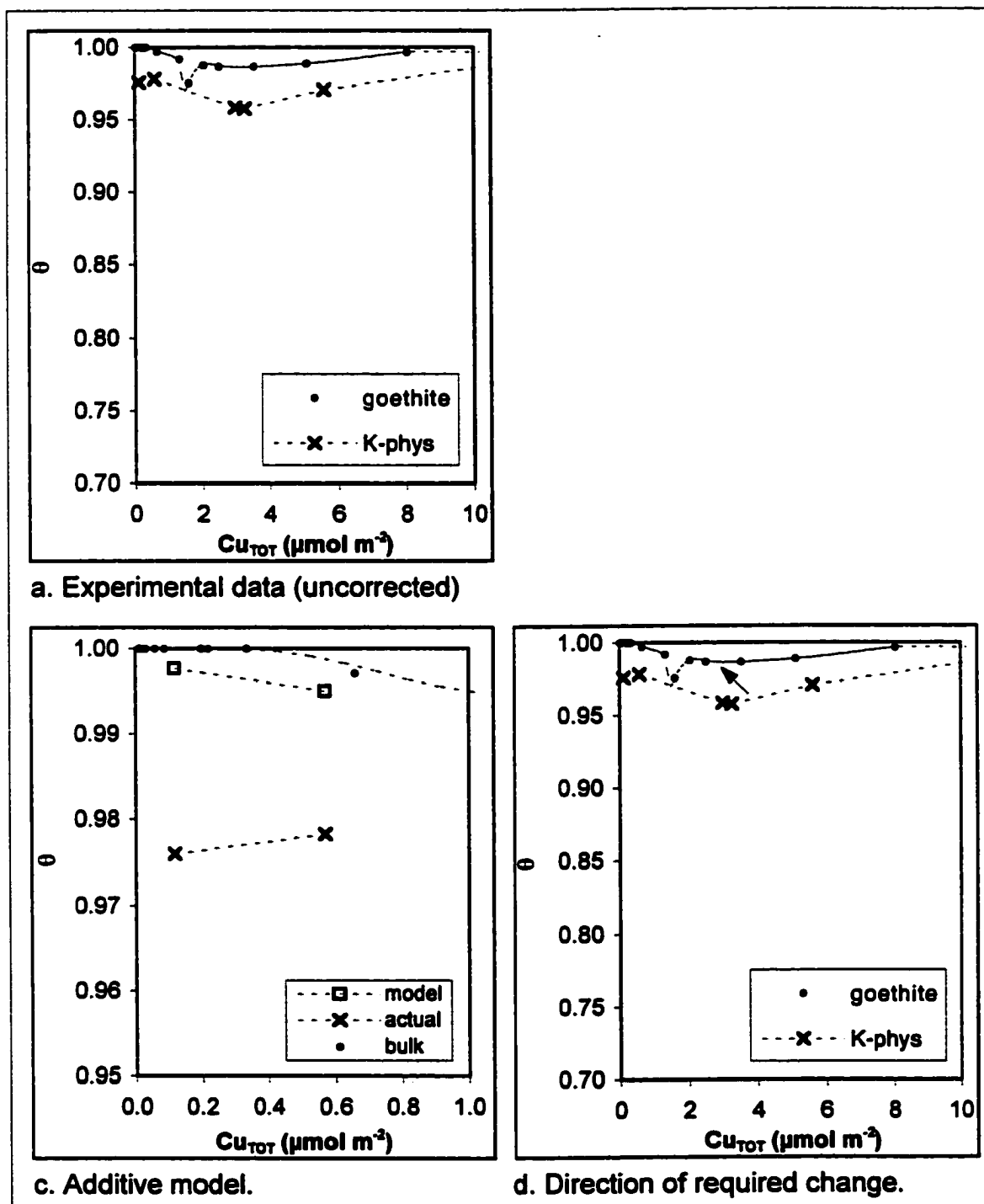


Figure 40. Results of applicable corrections for physical changes in goethite form for K-phys in comparison with bulk goethite. Note that the correction for SA:V is inapplicable to this solid.

Thus, although the null hypothesis is rejected for all five solids, some of the corrections suggest that physical alterations in the form of the goethite coating may be influencing Cu(II) sorption by the coated solids. Although SA:V alone shifts the Q-chem and K-chem data to the left of the bulk goethite data, this may be balanced by some chemical change – for example, a decrease in surface site density (SSD) would shift the data back toward the right. Nonetheless, no single or combination of physical corrections (SA:V, i.e., different SSAs of goethite coatings versus bulk goethite; blocking, i.e. masking of a fraction of the available surface area; and additivity, or the presence of a second Cu-sorbing phase) can adequately explain Cu sorption to the coated solids over the entire range of loadings studied.

Discussion

Each of the five goethite-coated solids had distinct Cu sorption characteristics, and none consistently behaved like bulk goethite. Figure 41 summarizes the similarities and differences of several different quantities related to Cu(II) sorption and desorption as a function of loading. Some general conclusions may be made from this figure. First, the Cu_{TOT} at which inflections in fractional uptake occurred were generally higher for the coated solids than for goethite (Figures 41a and b; Table 11), while fractional uptake (θ) was often lower, especially the minimum observed θ . Q-chem exhibited the first decrease in fractional uptake at a higher loading than bulk goethite (Figure 41a); this implies a greater abundance of high-affinity sites. (Note that the gap in data in this range for the physically coated solids precludes direct comparison.) Similarly, all of the thinly coated solids reached their observed minimum fractional uptake at a higher loading than bulk goethite (Figure 41b). This agrees with the lower observed minimum uptake for all coated solids relative to bulk goethite (Figure 41c). These results suggest that the onset of oligomer formation was delayed in these systems, which may be the result either of a greater abundance of total adsorption sites or a suppression of oligomer formation relative to bulk goethite.

The maximum observed C_A after adsorption is another clue to the transition between adsorption and oligomer formation. It is located at the end of the Langmuir plateau, before the trend begins to roll upward and backward; the greater the value of C_A , the higher the loading at which the transition between mixed-affinity-site adsorption and oligomer formation occurs. Maximum observed C_A for Q-chem, K-chem, and K-phys were higher than that for bulk goethite (although again, this transition is not always well-constrained due to the lack of data points); Q-phys and Kch-thick were generally similar and slightly lower (Figure 41d). This agrees with the values for N_{max} (Figure 41e). However, the surface Cu concentration (C_s) at maximum observed C_A (Figure 41f), another estimate of total site abundance, shows a different trend: Q-chem appears to have a similar abundance of sites, K-phys more sites, and the other three fewer sites.

Fractional uptake during dominant precipitation is similar for all solids, as is fractional release in these ranges (Figures 42g and h). However, the loadings at which dominant precipitation begins is variable (Table 11). Again, only Kch-thick appears to reach dominant precipitation before bulk goethite. Finally, despite the similarities in Cu(II) fractional uptake in precipitation-dominated ranges between the coated solids and bulk goethite, an examination of log IAP values suggests that the solubility of the precipitate phases is related to the substrate: both quartz-bearing solids had a higher log IAP, while all three kaolinite-bearing solids had a lower log IAP (Figure 41i).

Attempts to account for these discrepancies in terms of physical changes to the surfaces in the systems were unsuccessful (Table 14). If the coatings behaved like goethite and controlled all sorption, normalizing to mass should have removed all difference; if this was true, but the higher specific surface area (SSA) of the coatings relative to bulk goethite was important, correcting for the surface-area-to-volume ratio would have done so. If the blocking of goethite surface area was the only source of difference, then the data for the coated solids should have deviated from the bulk goethite data across the complete range of loadings and lain below and to the left on a plot of fractional uptake versus loading. Last, if the differences were due to additional uptake by the substrate, then the solids should have been amenable to additive modeling.

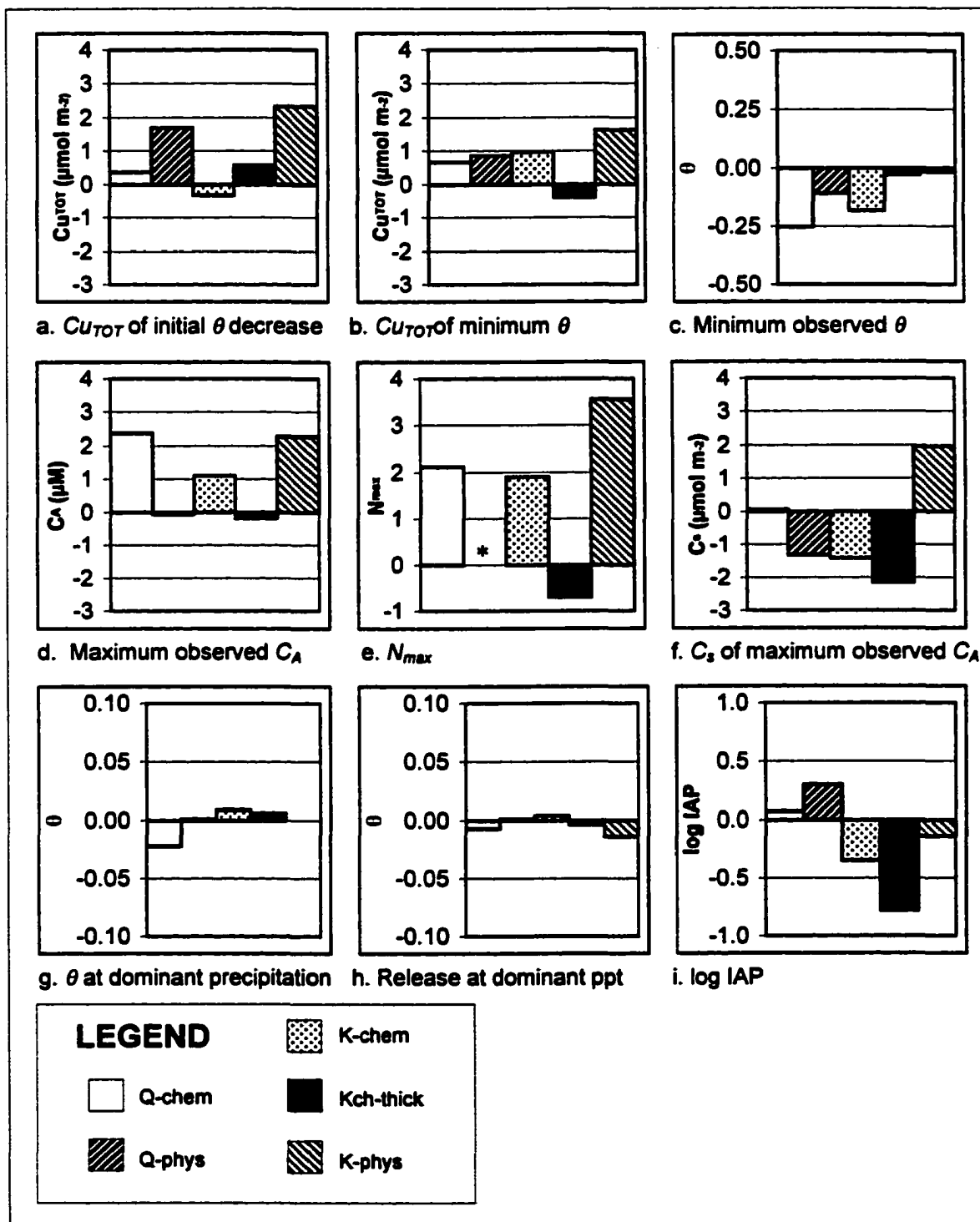


Figure 41. Summary of the results of Cu(II) sorption by coated solids in comparison to bulk goethite (set to zero). Note that N_{max} for Q-phys was not calculated. For comparison, $\log IAP$ for the proposed solid precipitate phase, $Cu(OH)_2(s)$, is 8.64, or 0.52 less than the precipitate phase on bulk goethite.

With the rejection of the null hypothesis, it becomes necessary to consider that the sorption properties of the coated solid may be related to the association of the substrate and coating. It is well established that multiple sorption mechanisms are possible and may operate to different extents simultaneously; however, the relative importance of different mechanisms may vary as a function of the identity and form of the sorbing phase(s). For example, while surface precipitation is favored thermodynamically by the supersaturation of the solution with Cu relative to the phase, the presence of a nucleating surface may promote surface precipitation at lower solution concentrations, even when high-affinity sites are available. In the case of surface precipitation, interfacial solution conditions such as pH and [Cu] may be higher than that for the bulk solution, so that surface precipitation may occur under conditions which appear (based on pH and Cu measurements) to be undersaturated. These interfacial surface conditions depend on the chemical properties of the surface; thus, different minerals such as goethite, quartz, and kaolinite exhibit distinct log IAP values.

TABLE 14. Summary of the effects of null hypothesis tests.

Solid	Mass	SA:V	Additivity	Blocking	Block + Add'y	Conclusion
Q-chem	↓ ^a	↓	x	↓	infeasible	H ₀ rejected
Q-phys	↓	NA	x	↓	infeasible	H ₀ rejected
K-chem	↓	↓	NA	↓	NA	H ₀ rejected
Kch-thick	↓	NA	NA	NA	NA	H ₀ rejected
K-phys	↓	NA	*	*	*	Insufficient; H ₀ rejected

^a Symbols: ' ↓ ' = worsens fit; ' x ' = overcorrects; ' * ' = improves fit.; "NA" = not applicable to this solid.

All the sorbents studied here -- bulk goethite, kaolinite, quartz, and the five goethite-coated solids -- exhibit sorption/desorption behavior suggestive of multiple sorption mechanisms. However, the transitions between dominant mechanisms occur at distinct surface coverages for each solid (Figure 41), even though the predominant sorbent phase present is always goethite. This suggests that each coating has distinct surface properties, which may be elucidated from the differences between the solids and in comparison with the individual phases present (goethite, quartz, and/or kaolinite).

Kch-thick. This solid might have been expected to have the most similarities to bulk goethite. It has a goethite coating roughly 17 M.E. thick; it adsorbs N₂ gas much like goethite; the Fe phase is distributed fairly uniformly across all surfaces, and the estimated number of monolayer equivalents present suggest that no underlying substrate is exposed. Because only goethite surfaces are present, no correction for mass goethite should be necessary; the surface area of the coating is that of the particles. The trends in sorption/desorption do not resemble those of the substrate kaolinite, as clearly seen by comparisons of the isotherms, Langmuir plots, or K_d vs. Cu_{TOT} , or N_{max} and log IAP. Yet *Kch-thick* does not behave exactly like bulk goethite. It experiences the complete range of uptake mechanisms and is forming surface precipitates at coverages where bulk goethite is still primarily filling low-affinity adsorption sites ($1.34 \mu\text{mol m}^{-2}$). The Langmuir and isotherm plots confirm this (see Figures 29b and 30b), as do the lower N_{max} and IAP values (Table 14). In addition, *Kch-thick* exhibits a lower observed minimum θ than bulk goethite (Table 11), indicating a lower affinity of Cu, and more Cu is removed from solution when surface precipitation dominates (Figure 41c).

Taken together, these facts suggest that *Kch-thick* essentially has a goethite coating with some different properties than the bulk phase, and that the kaolinite substrate is not exposed and thus not directly sorbing Cu. The high-affinity sites overall are less reactive, and the coating favors precipitation over adsorption once the high-affinity-site range has been passed. These results may indicate different abundances and reactivities of surface sites, especially with regard to low-affinity sites, since

sorption complexes do not appear to be favored at moderate coverages. They may alternately, or additionally, spring from some alteration of the goethite surface which promotes precipitation at relatively low coverages. This might be caused, for example, by a higher PZC relative to bulk goethite, which would result in a higher surface pH and hence favor precipitation.

The differences in reactivity of bulk goethite and Kch-thick could in part result from Kch-thick's relatively high porosity (Chapter 2). The internal environment within the pores is known to be different from that on exterior surfaces due to the close proximity of electrified surfaces. In addition, the pores could contain a different array of surface site populations; for example, if the coating is composed of an assemblage of microcrystals, the pores might include the spaces between groups of microcrystals, i.e. high proportions of (021) crystallographic faces. Finally, the close proximity of SHGs within the pores could result in higher effective local concentrations of Cu. This might also favor the onset of surface precipitation in pore spaces when the total average surface coverage was still relatively low.

The sorption/desorption behavior of Kch-thick is in contrast to the other four solids studied, where more of the substrate influence is indicated. For example, all the other solids have a greater Cu_{TOT} of observed minimum θ than bulk goethite, a greater maximum C_A , and a greater N_{max} (Figure 41b, f, and h). The middle coverage ranges exhibit more marked deviation from bulk goethite sorption, especially Q-chem (Figure 41). The coverages at which adsorption becomes limited and at which precipitation takes over are greater as well, suggesting that more adsorption sites, some with properties distinct from goethite, are available in these systems. Finally, the values for IAP appear to be controlled by the substrate (Table 14): all the kaolinite systems fall below the goethite value, and the quartz systems fall above it. Despite their common differences from both Kch-thick and bulk goethite, however, each of the other four coated solids exhibits distinct sorption/desorption behavior, indicating variations in substrate and coating interactions in each case.

Q-chem. Like Kch-thick, this solid might be expected to share many surface characteristics of bulk goethite. It sorbed N_2 much like bulk goethite, and SEM-EDS analysis indicated a coating resembling particles of goethite anchored to the relatively unreactive quartz substrate (Chapter 2). Its sorption behavior is distinct from uncoated quartz (Figure 41), particularly in the low- and mid-coverage ranges, and closely resembles bulk goethite at low coverages (Figures 29-31). It is in the middle ranges of coverage that most of the divergence from bulk goethite behavior is observed. Q-chem appears to have a greater abundance of high-affinity sites, as it continues to remove all detectable Cu up to at least $0.692 \mu\text{mol m}^{-2}$ (compared to $0.66 \mu\text{mol m}^{-2}$ for bulk goethite). This is followed by a sharp drop in θ , well below the minimum observed for bulk goethite, but an increase in the persistence of dominant adsorption as loading increases (to at least $2.30 \mu\text{mol m}^{-2}$ vs. 1.63 for goethite). This suggests an overall increase in the number of adsorption sites, both high- and low-affinity, and a relative favoring of adsorption over precipitation at higher coverages compared to both goethite and uncoated quartz. One key to these observed differences may be the manner in which Fe is bound to the quartz surface.

Transition metal ions are often observed to cluster at low coverages on quartz and silica surfaces. O'Day et al. (1996) observed precipitation of Co^{2+} on quartz surfaces at $0.63 \mu\text{mol m}^{-2}$, and Benjamin and Leckie (1980) at $\sim 1\%$ of complete coverage (this is taken to mean 1% of the monolayer equivalent coverage, or $\sim 0.18 \mu\text{mol m}^{-2}$, but could also be 1% of the titratable surface sites, or $< 0.02 \mu\text{mol m}^{-2}$). Other investigators have reported the formation of Cu dimers on amorphous silica at $0.03 \mu\text{mol m}^{-2}$ (Cheah et al., 1998), and Cu(II) hydroxide clusters at $0.055 \mu\text{mol m}^{-2}$ on fumed silica (Xia et al., 1997). Similarly, Waychunas et al. observed polymerization of Fe complexes on quartz surfaces above ca. 3% monolayer coverage (1998), and found small hematite-like and goethite-like precipitates on highly perfect quartz surfaces at roughly 5% coverage (Waychunas et al. 1999). As stated above, this early onset of precipitation does not necessarily indicate that quartz has few adsorption sites, but that the mechanism of precipitation is favored over adsorption at relatively low levels due to

the low affinity of the sites. In fact, the surface site density of quartz is estimated to be 1-3 sites per nm², which is comparable to that of kaolinite (1.2-6 sites nm⁻²; Langmuir, 1997).

In the case of iron oxide coatings on quartz, the findings of Waychunas et al. (1999) and Davis et al. (1998) suggest that during the coating procedure Fe is complexed at a low level by quartz sites throughout the surfaces of the grains, in addition to forming Fe oxide precipitates growing away from the quartz surface. Since precipitation of the adsorbate phase is observed at about 1% M.E. coverages, while Q-chem was coated to a thickness of about 2.5 M.E., it seems plausible that the quartz SHGs are overwhelmingly occupied by Fe as either molecular sorption complexes or iron oxide precipitates anchored to the surface at one or more SHG. Widespread, low-Fe complexes would not substantially increase the surface site density of the solid, but they could alter the affinity of the sites for Cu and/or compete with Cu for the quartz SHGs. In other words, Q-chem may contain two distinct classes of Fe-bearing surface sites – the goethite clusters controlling uptake at low coverages, and the Fe(III) ion-complexed quartz SHG sites controlling sorption at higher coverages.

This hypothesis is consistent with the results of the corrections applied to account for physical changes in goethite affecting its reactivity. If not all of the Fe in the system was present as goethite, the correction for the mass of goethite present would be thrown off (Figure 35). The presence of two distinct classes of sites would have lent itself to additive modeling had the second class of sites been unoccupied quartz sites; however, their modification prevented modeling as quartz sites (Figure 37c). Finally, if an additional population of sites was operating, it would not be possible to correct the data only for blocking (Figure 37d).

Evidence of a separation of sorption dominance by two classes of sites as a function of surface coverage is bolstered by the fact that at least some of the lower-affinity sites in Q-chem (i.e., the low-Fe surface complexes) appear to have higher binding strengths than bulk goethite sites occupied at comparable coverages. A comparison of Cu(II) adsorption and desorption by bulk goethite (Figure 30) shows that

as soon as fractional uptake began to decrease between 1.34 and 1.63 $\mu\text{mol m}^{-2}$, desorption upon dilution began to be detectable. In contrast, although between 1.03 and 1.73 $\mu\text{mol m}^{-2}$ fractional uptake is dropping in Q-chem, the solid releases no detectable Cu upon dilution at these coverages. On the other hand, in precipitation ranges, Q-chem not only removes a smaller fraction of Cu from solution than goethite, but also releases more of the sorbed Cu on dilution. This suggests that Q-chem has a lower affinity and binding strength for Cu(II) than bulk goethite in the precipitation-dominated range of Cu(II) uptake.

K-chem. Like Q-chem, K-chem behaves like bulk goethite at low coverages (Figure 29b). It also mimics bulk goethite in the precipitation range ($> 4.48 \mu\text{mol m}^{-2}$). In contrast, it resembles uncoated kaolinite in some of its behavior in the intermediate range of coverages (Figure 30b and 42a,b,f, and g). However, the coverage of the observed minimum θ (2.61 $\mu\text{mol m}^{-2}$) is greater than either goethite (1.63 $\mu\text{mol m}^{-2}$) or kaolinite (2.48 $\mu\text{mol m}^{-2}$), and so is N_{max} (4.08, compared to 2.17 and 3.08, respectively; see Table 12). Most interestingly, the observed minimum θ is less than that for either goethite or kaolinite (0.793 $\mu\text{mol m}^{-2}$ vs. 0.976 and 0.878, respectively; see Table 11). Again, this suggests that oligomer formation is suppressed, and hence adsorption continues to dominate uptake at higher coverages than is observed for bulk goethite.

Approximately two monolayer equivalents of goethite was coated onto kaolinite to form K-chem (see Table 9). The analyses described in Chapter 2 indicated a very thin, two-dimensional (non-porous), rather uniform distribution of goethite over the entire kaolinite surface (edges and faces) – apparently resulting in complete coverage by goethite. Since the porosity of particulate goethite is likely one important factor in determining its sorption behavior, some deviation might be expected in the sorption of Cu by K-chem due simply to its lack of porosity. In addition to this, if the goethite grew epitaxially, or even topotaxially, along the basal planes, the distribution of crystallographic surfaces and hence surface sites would be distinct for this coating

compared with bulk goethite and, perhaps, some goethite characteristics might be lost and kaolinitic traits propagated into the coating surface.

It is known that the substitution of Fe for Al in oxides increases surface reactivity; hence, the basal coating might behave much like basal kaolinite sites with an increased affinity for Cu. Similarly, Fe complexation with aluminol and silanol edge sites might result in the masking of the kaolinite site with one of greater affinity. However, the number and positioning of the sites would remain similar to that of the uncoated kaolinite. The coating would have a much greater surface-area-to-volume ratio than particulate goethite or the other two chemical coatings; however, correction for this or for the mass of goethite would yield misleading results since, as with Kch-thick, the surface of the solid consists predominantly, if not completely, of coating (see Figures 32 and 33 and Table 11.)

Again, the adsorption phase of uptake extends to higher coverages than in bulk goethite, and N_{max} is higher, which suggests that the surface sites of the chemical coatings have an increased ability to sorb Cu. There may also be a factor related to porosity in the case of K-chem. While the thick chemical coating is more porous than bulk goethite, the thin coating is nonporous. The hypothesis that porosity favors earlier transitions from adsorption to oligomer formation and precipitation would help explain why, for those solids with exclusively Fe oxide surfaces (Kch-thick, bulk goethite, and K-chem), the loadings at which transitions between dominant uptake mechanisms change appear to be directly related to porosity.

Q-phys. The chemical and physical coatings on quartz resemble each other in several aspects. First, while recalling that the low-coverage behavior is difficult to interpret due to the lack of samples in this region, the coverage at which fractional uptake is lowest is similar to that of Q-chem (2.49 vs. 2.30 $\mu\text{mol m}^{-2}$, in contrast to goethite's 1.63), as is its general isotherm trend (Figure 29c) and its difference from bulk goethite with increasing coverage (Figure 40a). Also, additive models underpredicted the results for both solids (Figures 37c and 38c)

However, there are also some differences between the two coatings on quartz. Sorption is less suppressed for the physical coating: the minimum observed uptake is lower for Q-chem than Q-phys (Figure 41c), and precipitation-range reactivity in Q-phys is similar to that of bulk goethite, in contrast to Q-chem, which both removed less Cu at precipitation coverages and released more of the precipitated Cu upon dilution (Figure 30). Additionally, Q-phys has higher Cu_{TOT} at and value of the minimum observed θ than Q-chem (Figure 30), and a lower C_i at maximum observed C_A , which suggest differences in the capacity and binding strengths of the surface sites. These differences could reflect the contribution of the quartz adsorption sites, which are exposed in Q-phys but masked or altered in Q-chem by sorbed Fe. Finally, the log IAP for Q-phys is higher than that for Q-chem, suggesting a less soluble precipitate phase forms on Q-phys.

Q-phys is relatively similar to bulk goethite in the precipitation range, which could indicate that goethite sites dominate in this loading range; the alternative hypothesis, that the precipitation phases on quartz and goethite sites are similar, is contradicted by some of the other data – for instance, the high fractional release of Cu upon dilution in the quartz system (Figure 32). Generally speaking, it appears that the chemical and physical coatings on quartz are relatively similar, except that Q-chem's quartz sites have been modified by Fe.

K-phys. The basal planes and edges of kaolinite have distinct electrical and binding properties. For instance, the PZC for the basal planes is between 2.8 and 4.8 (Arias et al., 1995; Swartz and Gschwend, 1997), while that for the edges is between 5.8 and 7.3 (Arias et al., 1995; Kretzchmar et al., 1998). Only the edges can bind metal ions coordinatively, but basal planes provide large flat surfaces for binding positively charged entities (at pH levels above their PZC). Therefore, in K-phys, the lathlike goethite particles were expected to attach to the basal planes of the kaolinite grains, while the edges would remain largely unassociated with goethite for steric and electrostatic reasons. This would produce a solid whose behavior is a combination of partially-blocked goethite and kaolinite surfaces. Correcting for mass would yield an

inaccurate result, since kaolinite is also reactive, and a surface area correction should be irrelevant. However, such a binary phase might be expected to behave relatively additively, allowing for some loss of available surface area (i.e., the areas of contact between the goethite and kaolinite particles).

This hypothesis is confirmed by the K-phys results. K-phys's fractional uptake as a function of Cu_{TOT} falls between those of goethite and kaolinite (Figure 29b); its Langmuir curve tracks goethite at low coverages, then deviates toward the kaolinite curve at higher coverages (Figure 30b). K-phys's log IAP is close to that of goethite (Figure 41i), suggesting that, as with Q-phys, the solid's surface precipitation is controlled by the goethite coating rather than the kaolinite substrate. Altogether, this suggests that interactions between the goethite and kaolinite have preserved some of the character of each sorbent, although the relative influence of each phase may vary with loading.

This would suggest that the physical corrections – specifically, a combination of additivity and blocking – would be most successful with this solid. Indeed, this was the only coated solid where additive modeling more closely approximated the observed results, and where blocking would further improve the fit. This may be because the goethite particles do indeed lie flat on the surface of the kaolinite (further suggested by the fact that a relatively large correction for blocking would have to be made to Cu_{TOT} in order to fit the data to bulk goethite; Figure 40d). Nonetheless, a certain amount of discrepancy persists beyond the physical corrections, since blocking would overcorrect the data at high loadings (Figure 29).

In summary, the thick chemical coating on kaolinite (Kch-thick) completely masks the underlying kaolinite surface, resulting in the exposure of only goethite surfaces for Cu(II) sorption. However, Kch-thick behaves differently from bulk goethite, reflecting an inherent difference in surface reactivity, likely due to different abundances, distribution, and/or inherent reactivity of surface sites, and possibly affected by the increased porosity of the goethite coating of Kch-thick relative to bulk goethite. The thin chemical goethite coating on kaolinite (K-chem) also appears to cover the

kaolinite substrate completely, so that the solid's surface contains only Fe surface hydroxyl groups, as in bulk goethite. Yet Cu(II) sorption on K-chem is markedly different from that on bulk goethite in the MAS and OLG regions, indicating that at least a subset of the Fe SHGs of the coating are chemically different from those on bulk goethite.

Even for those solids whose surfaces are not completely coated by goethite (Q-chem, Q-phys, and K-phys), there is evidence of altered chemical reactivity of the goethite and/or substrate surfaces. Both Q-phys and Q-chem are more reactive than the weighted sum of their constituent phases (i.e., the additivity model underpredicts Cu(II) sorption). However, each exhibits distinct sorption behavior. This may be related to the presence of a second class of Fe-bearing sites on the Q-chem quartz surface, which could alter or mask the quartz SHGs and react with Cu differently from the unaltered quartz sites on Q-phys. Finally, the thin physical coating on kaolinite (K-phys) reacted most additively, and a blocking correction was a feasible explanation for some of the deviation from bulk goethite sorption behavior, unlike the rest of the coated solids; however, physical corrections alone are not sufficient and hence there must be some inherent chemical difference in the surface properties of the coated solid relative to the separate component phases.

It is clear from these results that both physical and chemical surface properties vary with the form of the goethite coating, and that the mineralogy of the substrate, the method of coating, and the thickness of the coating are all factors influencing the surface properties of the coated solid. Furthermore, in each of the solids observed, a different type of change appears to be foremost in driving the observed variations in uptake behavior, whether it be a difference in porosity, the structural influence of the underlying substrate on the coating, the synthesis of an additional class of surface sites, the blocking of substrate sites, or the joint contributions of each solid phase to the net behavior of the system. There may be more changes still unobserved or minor in comparison to these. Examination of sorption in these systems by molecular-level analysis techniques are

necessary to identify the precise nature of both changes in surface chemistry and associated mechanisms of uptake as a function of surface coverage.

In addition, these experiments appear to emphasize the persistence of multiple mechanisms of uptake throughout the continuum of adsorption. Where one mechanism appears to predominate, others are nevertheless operating, and a change in any of several properties of the surface may result in a shift in the primary mechanism. There is a balance between the abundance and affinity of adsorption sites and the degree of saturation of the solution relative to the surface precipitate; this results in a competition between mechanisms not unlike those occurring among chemical species in solution. When exploring the effect of physical form on surface chemistry, therefore, the interrelated effects of changes in physical properties and chemical properties must be considered.

CHAPTER 4: NATURAL SEDIMENTS

This research was conducted as a first step in applying laboratory-derived knowledge to environmental sorption processes. The experimental design was to make synthetic sorbent phases more like those observed in nature – specifically, to prepare a set of goethite coatings analogous to ones commonly found in aquatic systems such as aquifers and estuaries. These synthetic sorbent phases were characterized and their Cu(II) sorption behavior was compared to that of bulk goethite. It was established that the form and properties, including Cu(II) sorption behavior, of synthetic goethite coatings varied from those of bulk goethite and depended on the coating method, substrate, and thickness. The next objective was to assess whether the distinctions observed between the coatings and bulk goethite reported in Chapters 2 and 3 were similar to observed differences between bulk goethite and natural sediments. In other words, it was desired to know whether the fact that goethite occurs in different forms in environmental particles might help explain the discrepancies between field and lab studies of trace metal sorption; and if so, whether synthetic coatings might be better representative surrogate phases for natural goethite.

Background Information

As discussed in Chapter 1, environmental particles are frequently coated with reactive phases (Ransom et al., 1997; Nelson et al., 1995). Conversely, reactive phases such as Fe oxides and humic acid frequently occur as coatings in environmental sediments (Warren and Haack, 2000; Mayer, 1999). In addition, coatings have a high surface area to volume ratio relative to the bulk phases typically used to represent them in laboratory studies, and they lie upon the surfaces of other potentially reactive solids in natural sediments. Thus, coatings must play a major role in environmental sorption processes (Warren and Haack, 2000); and since sorption is a dominant factor controlling the fate, transport, and bioavailability of trace metals in aquatic systems, particle

coatings must be important in regard to trace metal cycling and environmental impact.

Particle coatings influence and are impacted by biological processes in the environment. In addition to toxic substances, particle coatings remove some nutrients essential for primary production, such as phosphate, from the dissolved phase (Yao and Millero, 1996). Conversely, the uptake of bacterial cells on solid surfaces is enhanced by the presence of an Fe oxide coating (Truesdail et al., 1998), affecting cell growth (Nelson et al., 1996) as well as fate and transport, and also influencing the growth and development of biofilms on particle surfaces (Nelson et al., 1996). Fe oxide coatings accumulated on bacterial cell walls have been observed to take up more dissolved Cu and bind it more strongly than uncoated cell walls (Jackson et al., 1999). In the sediment, Fe oxide coatings are involved in microbial redox reactions that result in their reductive dissolution. Fe(II) released via microbially-mediated redox reactions migrates above the redox boundary, then oxidizes to Fe(III) and forms a new coating on the sediment grains.

Fe oxide coatings can also affect the surface charges of particles. They contribute positive charge regions to particle surfaces at many environmental pH levels (Johnson et al., 1996), and in some cases, may change the sign of the net surface charge from negative to positive (Zhuang et al., 2002). This would enhance attraction to and aggregation with other, more negatively charged, suspended particles in the water column, changing the physical dynamics of the particles and hence their interactions with biota in the water column and at the bottom. In sediments and aquifer materials, the more positive net surface charge causes the coatings to act as an electrostatic 'cement,' holding together colloidal solids in the matrix between larger grains as well as binding the larger grains more firmly together (Swartz et al., 1997).

Although particle coatings are common in the environment, they are rare in laboratory experiments. Mineral phases are routinely subjected to cleaning procedures designed to remove any oxide and organic coatings, revealing the clean, homogeneous mineral surface desired for traditional pure-phase studies. Investigations of natural coatings themselves have been infrequent; most of these have focused on their structure and composition (e.g., Swartz et al., 1997), or the processes by which they may be removed (e.g., Swartz and Gschwend, 1998). These studies have yielded valuable

information about the forms of Fe oxide coatings commonly occurring in natural settings. As discussed in Chapter 1, these tend to include 'chemical' coatings, formed when dissolved Fe precipitates onto the surfaces of grains, and 'physical' coatings, in which already-formed oxide particles are attracted to other surfaces by electrostatic forces.

Several descriptions of the structure and composition of Fe oxide coatings on environmental particles may be found in the literature. An example of physical and chemical coatings occurring together is reported in a Southeastern Coastal Plain aquifer sand collected in Georgetown, South Carolina (Swartz et al., 1997). Quartz, kaolinite, and goethite phases (with small amounts of other minerals) appeared to be cemented together by amorphous silica. About 95% of the Fe was present as discrete goethite crystals aggregated among kaolinite grains between the larger quartz grains, while the remaining 5% appeared to be an amorphous Fe phase distributed throughout the aquifer matrix and "intimately associated" with clay particles. In contrast to this material, an aquifer sand collected in Falmouth, Massachusetts, was found to contain primarily chemical coatings (Davis et al., 1998). Two types of chemical coating were observed on quartz grains: a thin (10 to 30 nm), ubiquitous, and extremely resistant form, and a much thicker (up to 5 μm) and patchy form concentrated on the rough surfaces of the quartz and filling in surface irregularities such as fractures. Finally, in a more complex material from a tropical environment, quartz grains were found to be chemically coated with well-crystallized, nearly pure Fe oxides occurring along the edges of the grains, along with more extensive, porous coatings in which several mineral phases were incorporated, including aggregated Fe oxide crystals and layers of kaolinite plates as well as small pockets of an Al-rich phase thought to be gibbsite (Padmanabhan et al., 1996).

Few investigators have prepared and studied synthetic coatings. In a study of the sorption of Pb(II) to bulk $\gamma\text{-Al}_2\text{O}_3$ versus a 20 nm thick, nonporous $\gamma\text{-Al}_2\text{O}_3$ coating on a metal support (i.e. a 'planar' oxide), sorption behavior was found to be similar in terms of coverage with increasing Pb(II) solution concentrations and adsorption edge shifts with increasing metal-surface ratios. However, Pb bonded preferentially to the bulk phase, perhaps because of a different population of site types and abundances on the planar oxides (Conrad et al., 2002). Another research group has made several studies of

“diagenetic Fe/Mn oxyhydroxides” (e.g., DeVitre et al., 1991). These were formed by placing Teflon sheets in the top sediment layers of oxic lakes for several weeks. The oxides formed on the Teflon as redox reactions in the sediment promoted the dissolution, migration, and precipitation of Fe and Mn phases. The resulting oxide phases were very poorly ordered and incorporated some organic material and sorbed trace metals. The concentrations of the trace metals and the sediment fractions they were associated with were measured using selective extraction techniques. Finally, in a study of relationships between Fe oxide coatings and the development of biofilms, physical coatings of colloidal Fe oxides together with biofilms on glass slides were prepared and their sorption of Pb(II) was investigated (Nelson et al., 1995). No toxic effect of Pb(II) to the bacteria in the system (*P. cepacia*) was observed in samples including the Fe oxide coating, and Pb(II) uptake in these systems was reported to be comparable to previously published adsorption isotherms for amorphous Fe oxyhydroxide (Nelson et al., 1995). In addition to these studies, some experiments of trace metal sorption in systems containing two oxide mineral phases have identified some important coating/substrate interactions affecting sorption behavior, such as site masking (Anderson and Benjamin, 1990a), the crystallinity of coating minerals (Davis and Kent, 1990), and the surface charge modifications involved (Holmén and Gschwend, 1996).

Objectives

In this study, three natural materials – a crude kaolin clay, a sandy subsurface material, and a sandy surface soil – were subjected to the same types of N₂ and Cu(II) adsorption/desorption experiments that were conducted using individual pure phases (quartz, kaolinite, and bulk goethite) and the goethite-coated solids, as described in Chapters 2 and 3. The first objective was to compare the properties of the cleaned and purified kaolinite used as a substrate for the synthetic coatings to the untreated kaolin clay, in order to identify potential sources of difference between pure phase and natural material behavior. The second objective was to compare the properties of bulk goethite, the synthetic goethite coatings, and the natural materials, in order to assess whether

goethite coatings might be a better surrogate phase for natural goethite in laboratory studies than the traditionally used bulk goethite.

Materials and Methods

A set of three increasingly complex sedimentary materials was compiled. These were composed primarily of quartz, kaolinite, and goethite; little or no organic matter was desired. The three materials were a crude kaolin and a pair of highly weathered, uncontaminated, coarse soil materials. The kaolin was mined by Thiele Kaolin Company (Sandersville, Georgia). It is from the Buffalo Creek formation and is classified as a high-Hinckley Index, soft kaolin (Kogel, 2002). Its composition is given in Table 15. The bulk of the Fe in the kaolins in the Thiele mine is structural Fe in the kaolinite; a small percentage of Fe is associated with accessory minerals, most commonly goethite and hematite occurring as coatings on kaolinite and anatase (Kogel, 2002). This material is from the same formation as the source clay mineral (KGa-1b) used as the substrate in this study and is similar compositionally, the major difference being that KGa-1b has been processed to remove some of the impurity phases (Kogel, 2001). (The sample used in this study was further cleaned using established methods as described in Chapter 2.)

The other two soil samples were collected at the Department of Energy's Savannah River Site (SRS) in Aiken, South Carolina, approximately 80 miles northeast from Sandersville, GA. Their compositions are also given in Table 15. Both have similar parent materials (i.e., weathered Southeastern Atlantic Coastal Plain sediments; Vulava and Seaman, 2000). One was a subsurface material from the Tobacco Road formation. It is a vadose zone sediment typical of the materials found in the deep soil, vadose zone, and first confined aquifer on the SRS. It has the physical appearance of sand stained orange with iron oxide. The other sample from the SRS is a surface soil of the Orangeburg Series collected from a coniferous/deciduous forested area. It is somewhat finer and grayish in color. Both are composed primarily of quartz, with the primary clay mineral being kaolinite, and almost all of the Fe oxides present are crystalline in structure, as indicated by extraction with the citrate-dithionate-bicarbonate method (Vulava and Seaman, 2000). XRD analysis of the clay-sized fraction confirmed

the presence of goethite (Seaman, 1998). The surface soil has less Fe oxide and some organic matter content (Table 15).

TABLE 15. Characteristics of the natural materials studied.

	Crude kaolin^a ("Crude")	Subsurface sediment^b ("Subsurface")	Surface soil^b ("Soil")
Grain-size distribution			
sand		94.9%	85.5%
silt		0.8%	7.8%
clay	= 60%	4.3%	6.6%
Mineral composition			
quartz	1-2%	95.7%	93.3%
kaolinite	95%	"primary" ^c	"primary" ^c
CDB Fe oxides	"trace"	0.74g Fe/100g	0.19 g Fe/100g
oxalate Fe oxides	"trace"	0.19 g Fe/100g	0.03 g Fe/100g
other minerals	anatase	mica	gibbsite, HIV
TOC	0.01-0.03%	0.02%	0.76%

^a (Kogel, 2001) ^b Grain-size distribution determined by the pipet method. Sand = 2000-50 μm ; silt = 50-2 μm ; clay = <2 μm . Clay-size fraction mineralogy determined by X-ray diffraction (XRD). Crystalline Fe oxide content determined by citrate-dithionate-bicarbonate (CDB) extraction; XRD of clay-sized fraction confirms the presence of goethite in subsurface sediment (Seaman, 1998). Amorphous iron oxide content determined by ammonium oxalate extraction. (Vulava and Seaman, 2000) ^c The term "primary" is taken to refer to the relative intensity of the kaolinite peaks in XRD analysis of the clay fraction, i.e., that these peaks were the dominant feature in the XRD spectrum. In a separate publication the author indicates that the clay fractions of the SRS materials are composed "mainly" of kaolinite (Seaman, 1998).

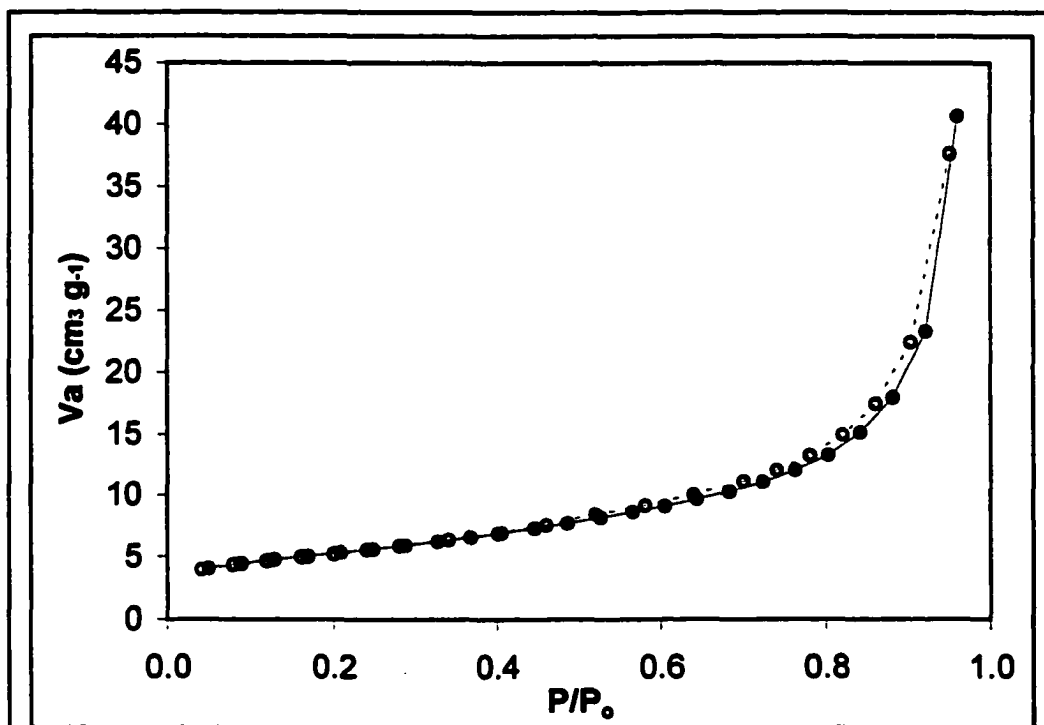
Flow-through sorption experiments have been conducted on the SRS materials. Acidic Pb solutions were injected into columns packed with the aquifer material or surface soil. The soil removed more Pb from solution, and less was released upon flushing with artificial groundwater (9% from the soil column compared to 30% from the subsurface column). This was proposed to be the result of different amounts of Fe oxide, clay mineral, and soil organic matter in the two materials, a hypothesis supported by the fact that two organic extractants removed more bound Pb from the soil than the subsurface material (Vulava and Seaman, 2000).

The materials were subjected to N₂ adsorption and batch Cu(II) sorption experiments, as described in Chapters 2 and 3. Because the goal of the experiments was to assess how well synthetic oxide coatings matched the sorption behavior of the natural sediments, in comparison to bulk goethite, no pretreatment beyond the initial hydroxylation in synthetic estuarine water was done. The results of these experiments were compared to bulk goethite, the laboratory oxide coatings, and to each other. In addition, because of their very close resemblance in source and characteristics, the crude kaolin and the clean kaolinite used in this study were compared to determine what differences in surface properties and behavior the cleaning and size fractionation procedures made. These results will be discussed first.

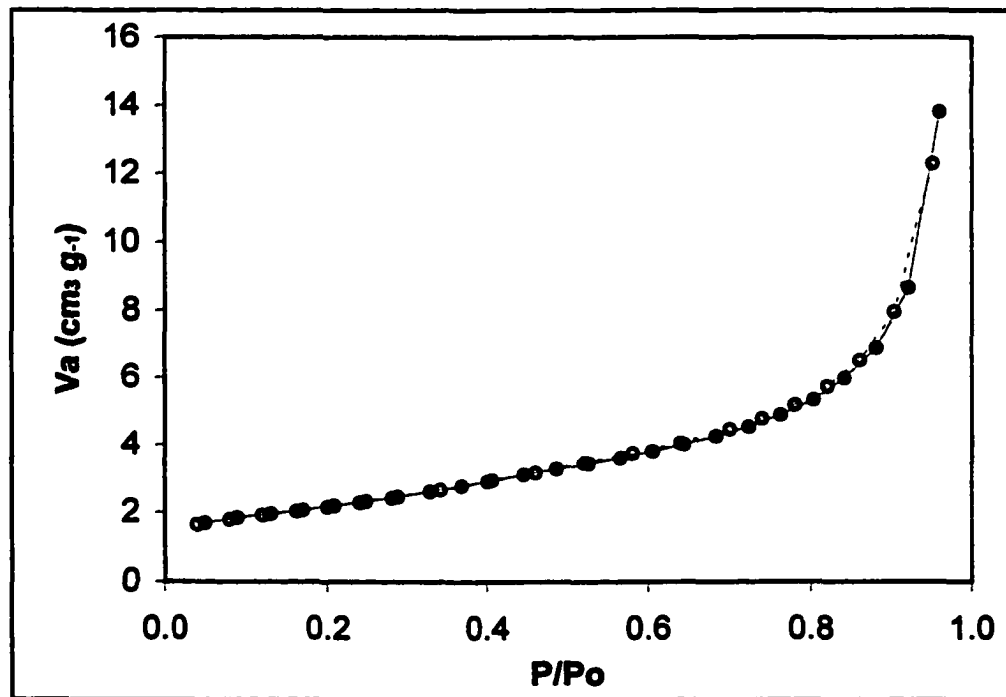
N₂ Adsorption/Desorption Results

Crude kaolin versus clean kaolinite. Figure 42 shows the N₂ adsorption-desorption isotherms for crude kaolin and cleaned kaolinite. There is an indication of mesoporosity (expressed as desorption hysteresis) in crude kaolin similar in range and extent to that observed in bulk goethite (see Chapter 2, Figure 5), but the hysteresis extends to lower relative pressure than in bulk goethite. Figure 43 shows the residuals analysis used to select the linear range for calculating SSA. The shapes of the residuals trends are dissimilar.

As discussed in Chapter 2, a t -plot shows the volume of N₂ adsorbed by the solid as a function of the statistical thickness (t) of the layers of adsorbed N₂ gas. These plots may be used to assess the porosity of the solid being studied (see Chapter 2, Figure 4, for examples of porosity exhibited in t -plots). In addition, a variation of the t -plot, the Harkins-Jura thickness plot, may be used to calculate the external SSA of a solid (see Chapter 2, Equations 8 and 9). It was observed in the Chapter 2 results that these plots also reflected similarities and differences between the solids; therefore, t -plots and Harkins-Jura thickness plots for the natural materials were also compared to the individual phases (see Figure 44). In contrast to the cleaned kaolinite, the crude kaolin trend rises above the linear fit at high t , corroborating the indication of mesoporosity seen in the N₂ isotherm.



a. Crude kaolin.



b. Cleaned kaolinite.

Figure 42. N_2 adsorption-desorption isotherms for crude kaolin and clean kaolinite. Black circles connected with a black line indicate adsorption; open circles with a dashed line indicate desorption.

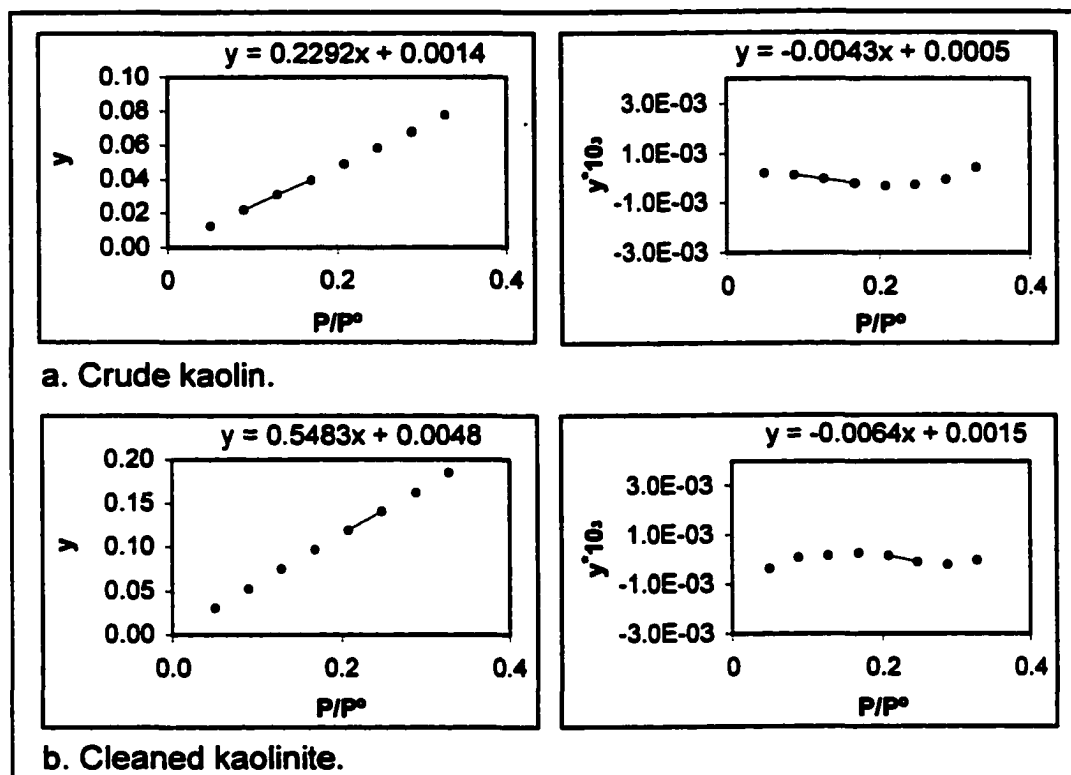


Figure 43. Residuals for crude kaolin and cleaned kaolinite used to select the linear range for SSA calculation using BET analysis.

As discussed in Chapter 2, an f -plot shows the ratio of adsorbed volume for two solids as a function of P/P_0 ; if the solids take up N_2 in the same manner, the plot will be a straight horizontal line (Gregg and Sing 1982). Figure 45 shows an f -plot comparing the crude kaolin isotherm to that of cleaned kaolinite. The isotherms appear to be somewhat dissimilar in shape at low relative pressure, as the trend swings from positive to negative standard deviations from the mean value for crude kaolin; however, the difference does not exceed two standard deviations (indicated with dashed lines) until P/P_0 reaches 0.76, when the isotherms are beginning to rise rapidly in response to the onset of condensation on the solid surfaces. At this point the difference between the two isotherms becomes marked, approaching 20 standard deviations at the highest relative pressure point.

Figure 46 shows a set of f -plots comparing crude kaolin and cleaned kaolinite against the chemical coatings and the nonporous reference material. Note that with the exception of the middle relative pressure range ($P/P_0 = 0.5 - 0.7$), in which a double

concavity appears in cleaned kaolinite, the two solids are qualitatively similar to the reference material and the two chemical coatings on kaolinite.

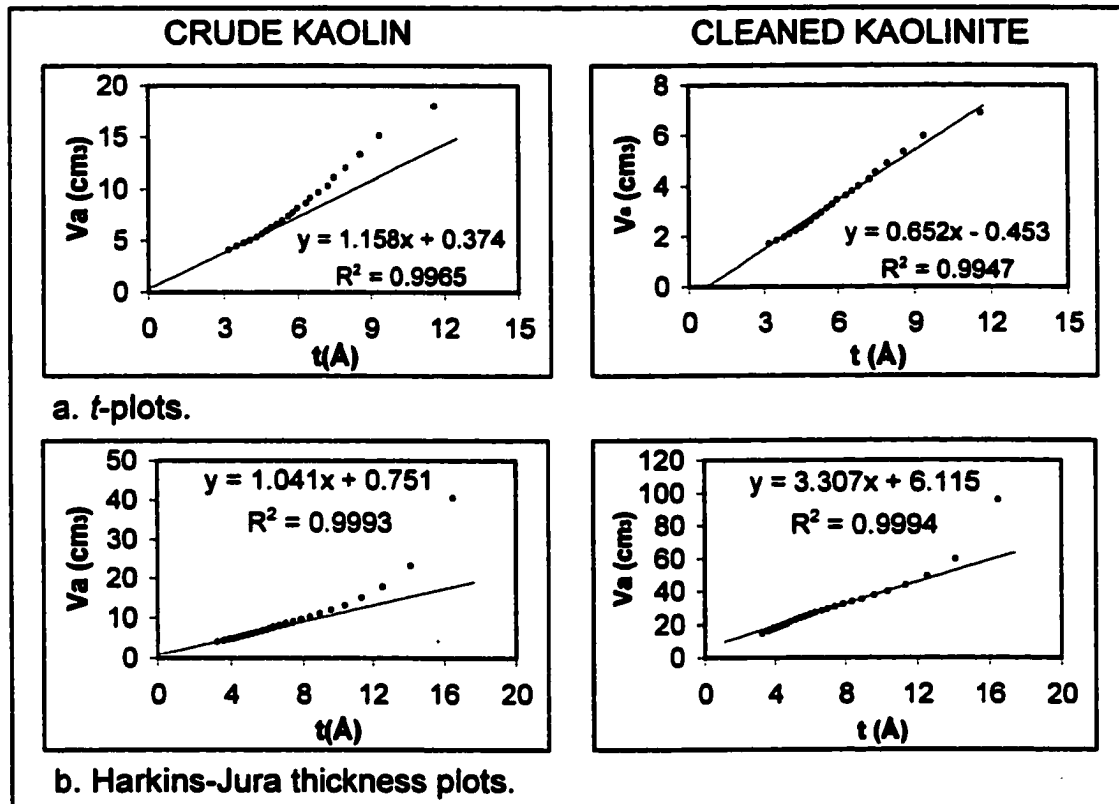


Figure 44. t -plots and Harkins-Jura thickness plots for crude kaolin and cleaned kaolinite.

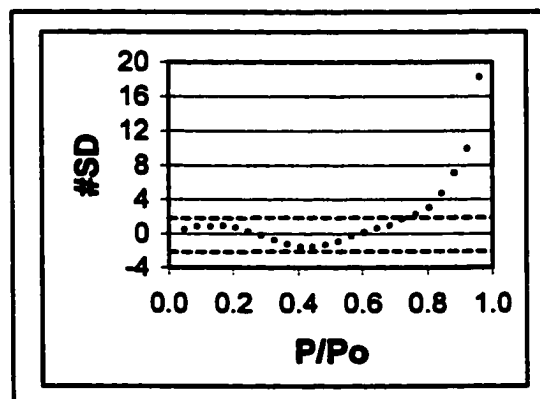


Figure 45. f -plot of crude kaolin vs. cleaned kaolinite.

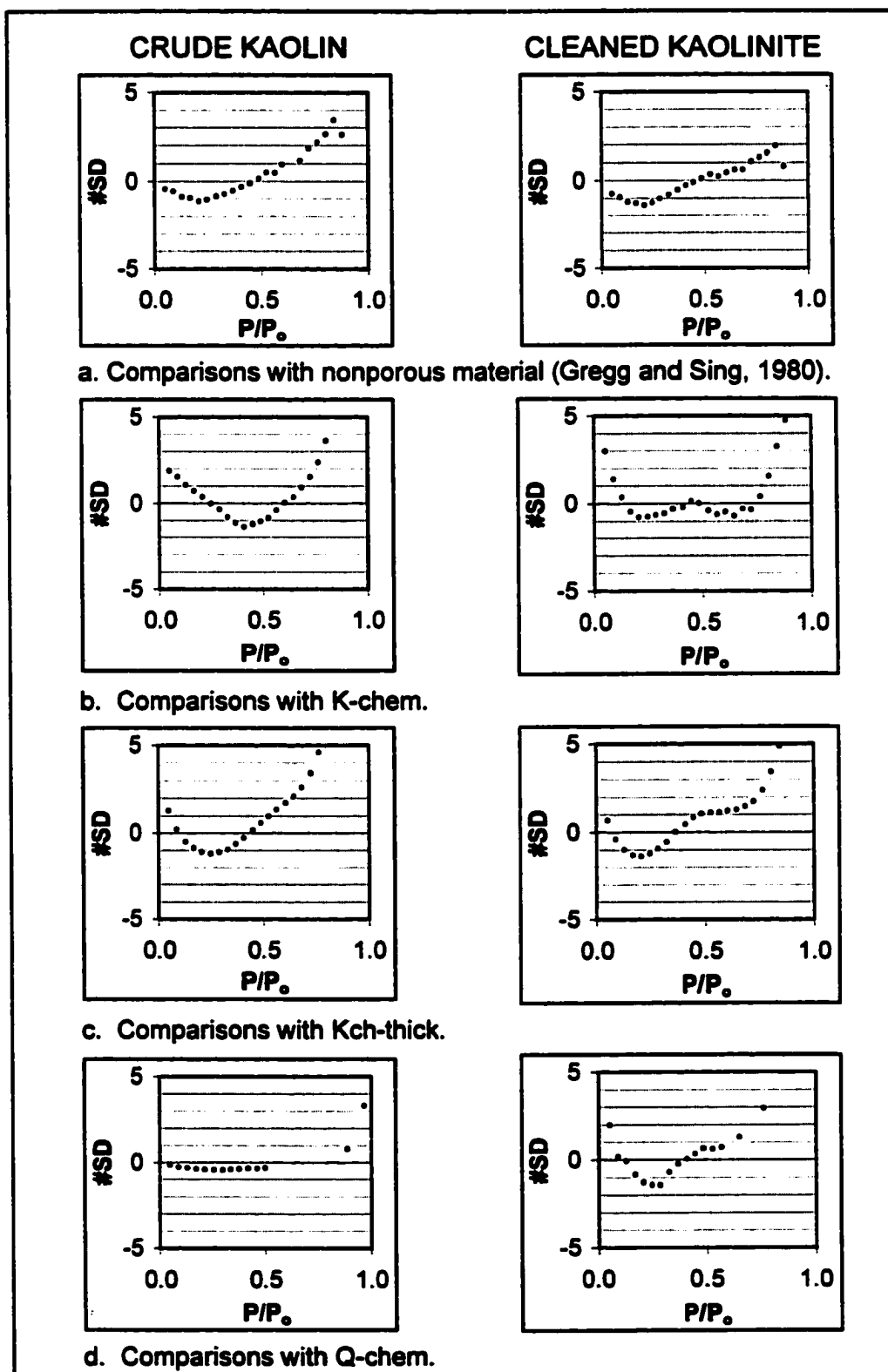


Figure 46. *f*-plot comparisons of crude kaolin and cleaned kaolinite to a nonporous reference material and the chemical coatings.

Tables 16 and 17 summarize the results of BET and SSA analysis for the natural materials, as described in Chapter 2, with the results for cleaned kaolinite and bulk goethite for comparison. The crude kaolin has more than twice the specific surface area than the cleaned kaolinite. The porosity indicated in Figures 43 and 45 is confirmed by the calculation of pore volumes from the t and α plots and internal surface area from the Harkins-Jura plot (Table 17).

TABLE 16. Summary of BET analysis.

Solid	SSA $\text{m}^2 \text{g}^{-1}$	Hysteresis	c	y-intercept
Crude kaolin	18.9	> ~ 0.4	165	1×10^{-3}
Subsurface	8.7	> ~ 0.5	117	4×10^{-3}
Soil	5.0	> ~ 0.4	143	6×10^{-3}
Kaolinite	7.9	—	115	5×10^{-3}
Goethite	70.6	> ~ 0.8	103	6×10^{-4}

TABLE 17. Results of t -plot, α -plot, and internal SSA analysis.

Solid	SSA ($\text{m}^2 \text{g}^{-1}$)	SSA _{t} ($\text{m}^2 \text{g}^{-1}$)	SSA _{α} ($\text{m}^2 \text{g}^{-1}$)	PV _{t} ^a (cm^3)	PV _{α} (cm^3)	SSA _{int} ($\text{m}^2 \text{g}^{-1}$)	% of SSA ^b
Crude kaolin	18.9	17.8	18.6	0.374	0.174	2.4	12.6
Subsurface	8.7	8.2	8.3	0.138	0.107	-1.2	—
Soil	5.0	4.8	4.8	0.064	0.025	0.5	10.4
Kaolinite	7.9	10.0	10.4	-0.453	-0.603	0.3	3.6
Goethite	70.6	68.4	68.8	1.569	1.547	17.8	25.8

^a PV = pore volume, equal to the y-intercept for the linear region of the plot. ^b Internal SSA as a percentage of BET-calculated SSA.

Natural materials versus bulk goethite and coatings. Figure 47 shows the N_2 adsorption-desorption isotherms for the subsurface material and surface soil (i.e., the Savannah River Site, or 'SRS,' materials). The hysteresis in both plots resemble that seen in bulk goethite (Chapter 2, Figure 5), but it is more extensive (i.e. the desorption trend falls further from the adsorption trend) and extends to lower relative pressures than bulk goethite. They are

distinct from the Q-chem coating, which exhibits little hysteresis above $P/P_0 \approx 0.9$ (Chapter 2, Figure 9), and Kch-thick, in which hysteresis is apparent throughout the entire P/P_0 range sampled. However, like Kch-thick, the subsurface material also appears to show increasing hysteresis at higher P/P_0 ranges (Chapter 2, Figure 10).

Figure 48 shows the residuals for the SRS materials, with those for bulk goethite for comparison. The subsurface residual trend is not unlike that of bulk goethite, but the surface soil residual exhibits a different shape and more vertical range.

Figure 49 shows the t -plots and Harkins-Jura thickness plots for the SRS materials and bulk goethite. There is more indication of mesoporosity in the SRS materials t -plots, in which the points rise further off the linear fit at high t . The Harkins-Jura plots for the SRS materials are more similar to each other.

Figure 50 shows four sets of comparison f -plots for crude kaolin and the SRS materials: against the nonporous reference material data given in Gregg and Sing (1980), uncoated quartz, uncoated kaolinite, and bulk goethite. The natural materials do not appear to have similar isotherms to the nonporous reference material, nor to quartz or kaolinite; however, the SRS materials (subsurface material and surface soil) show a high degree of similarity at low and middle P/P_0 ranges. This suggests that the surfaces dominating N_2 adsorption in the SRS materials have properties similar to those of bulk goethite. Interestingly, in three of the four sets of f -plots, the crude kaolin and subsurface aquifer trends appear qualitatively similar, while the surface soil trend is distinct, except in the case of bulk goethite, in which case the crude kaolin is distinct.

Figure 51 shows a second set of comparison f -plots with the three chemical coatings (Q-chem, K-chem, and Kch-thick) and comparisons between the natural materials. All three appear to be similar to Q-chem at $P/P_0 < 0.5$ (although the lack of data points from $P/P_0 \approx 0.5$ to 0.8 must be kept in mind), and there are also some similarities in the broad shapes of the plots comparing the natural sediments to both kaolinite coatings. The comparisons between the materials shows first, that no pair appears to have similar N_2 adsorption isotherms; and second, that the crude kaolin and subsurface material appear to have similar variances from the soil isotherm (compare subsurface/soil plot to the crude/soil plot in Figure 51d).

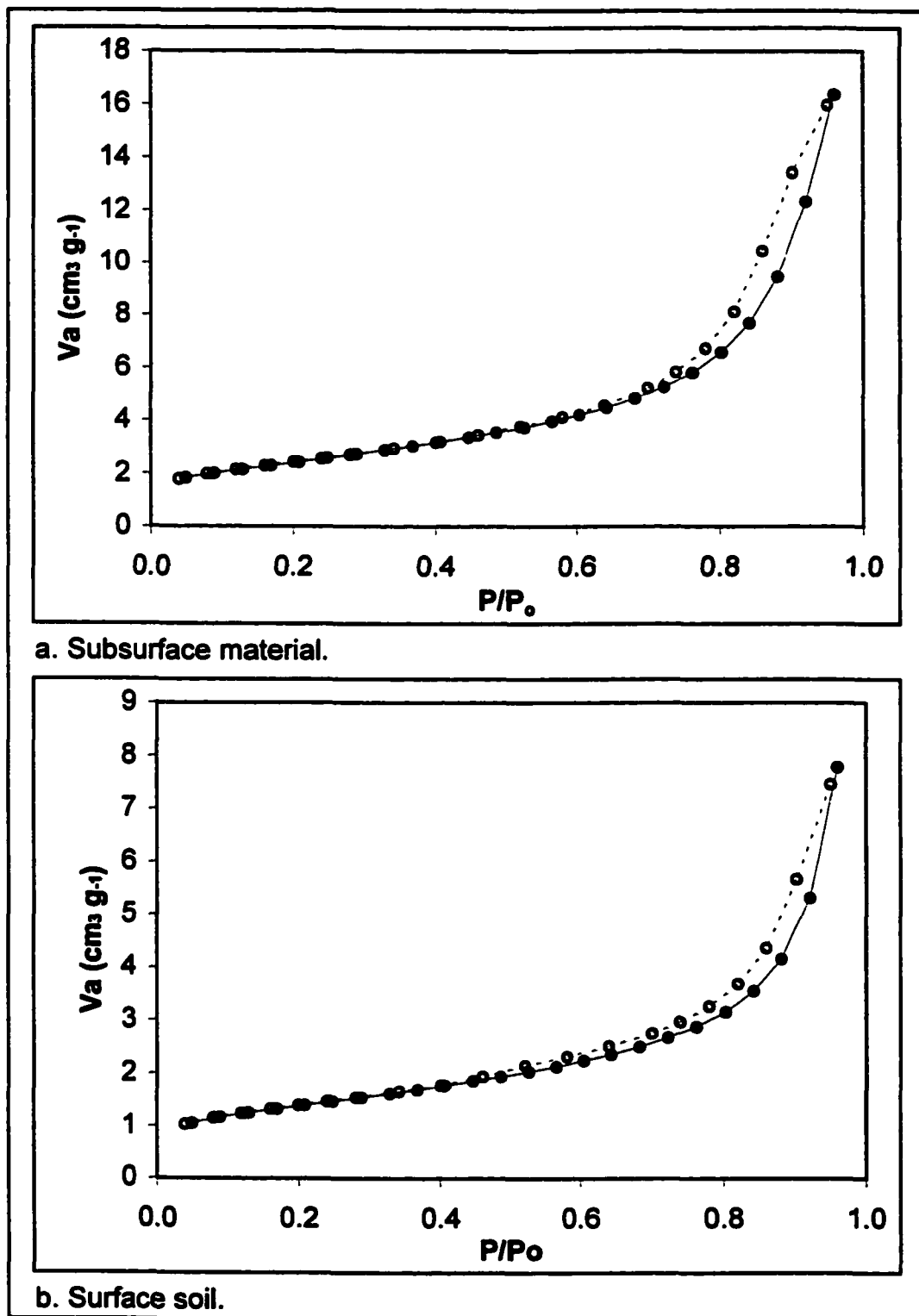


Figure 47. N_2 adsorption isotherms for subsurface material and surface soil. Black circles connected with a black line indicate adsorption; open circles connected with a dashed line indicate desorption.

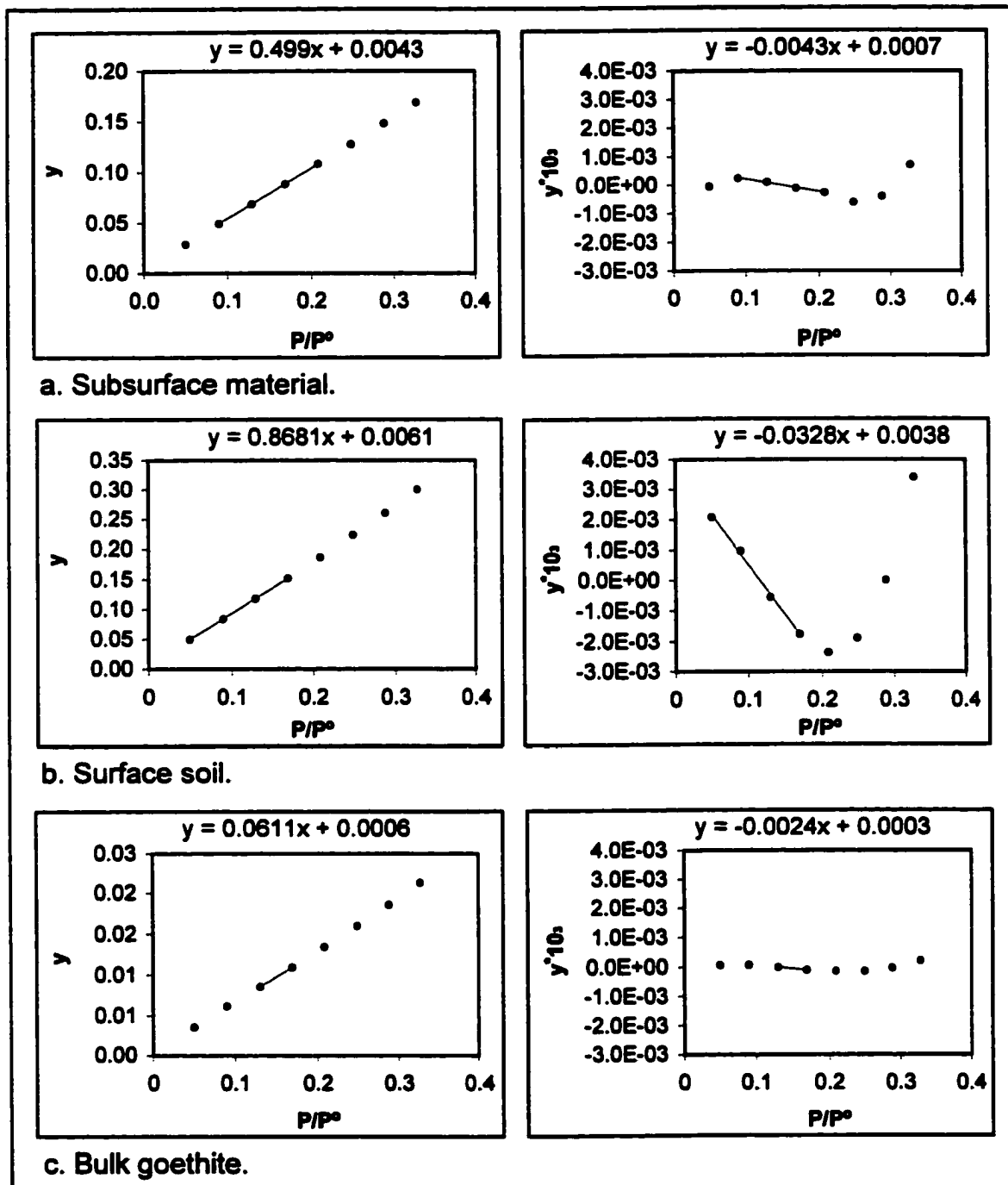


Figure 48. Residuals for subsurface material and surface soil used to select the linear range for SSA calculation using BET analysis.

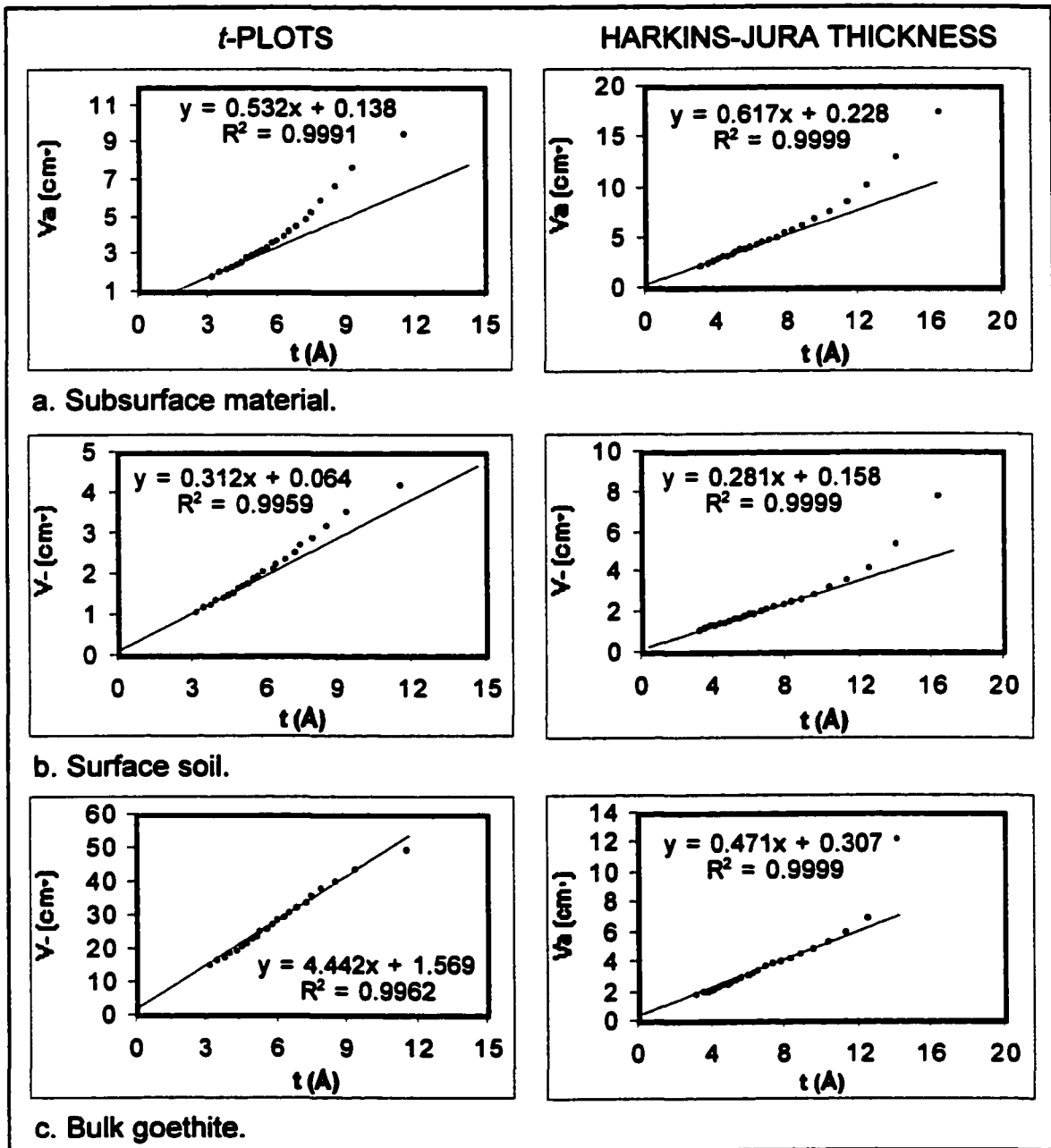


Figure 49. t-plots and Harkins-Jura thickness plots for subsurface material, surface soil, and bulk goethite.

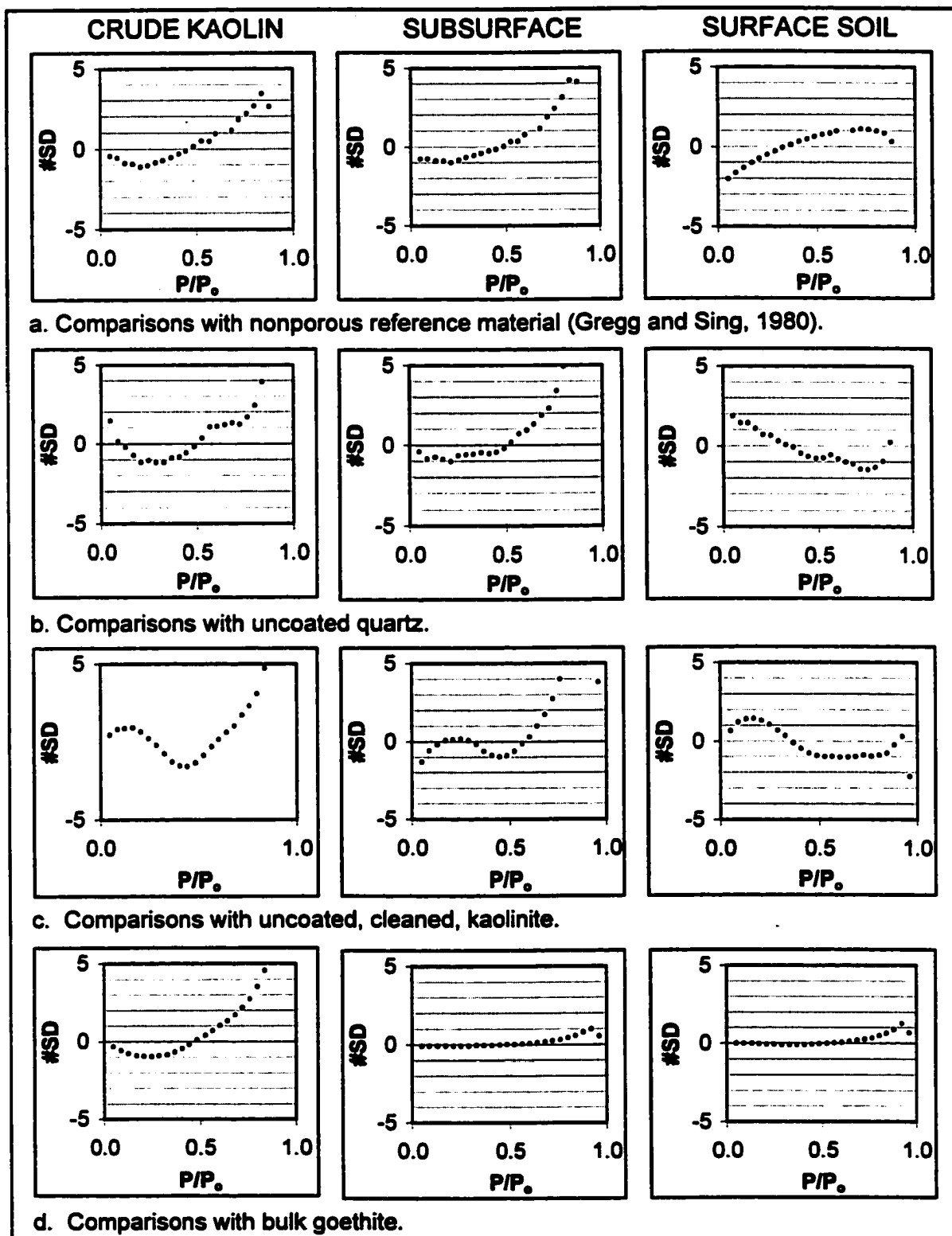


Figure 50. *f*-plot comparisons of crude kaolin, subsurface material, and surface soil to a nonporous reference material, quartz and kaolinite, and bulk goethite.

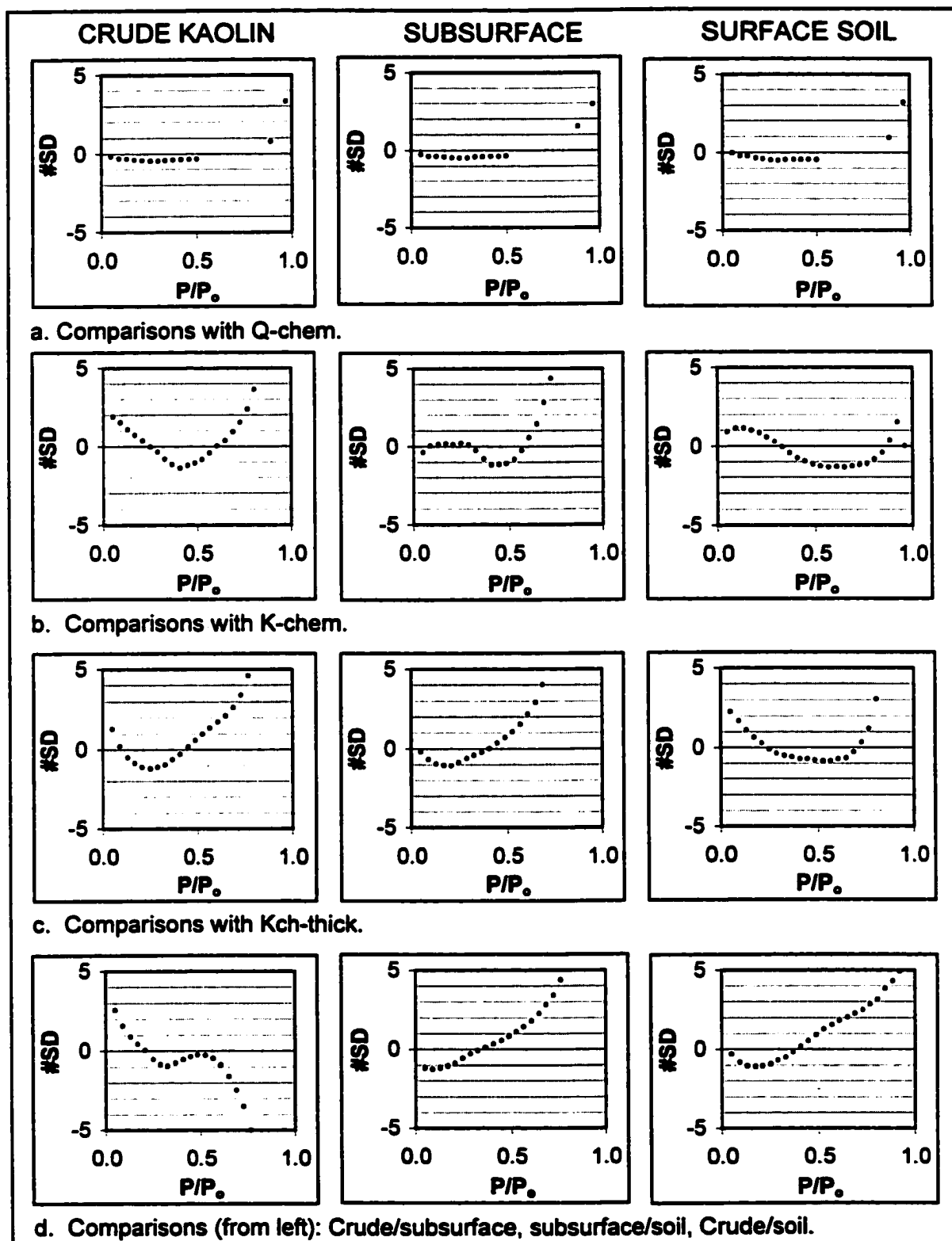


Figure 51. *f*-plot comparisons of crude kaolin, subsurface material, and surface soil to Q-chem, K-chem, Kch-thick, and each other.

Cu(II) Adsorption/Desorption Results.

Crude kaolin versus clean kaolinite. Figures 52 and 53 show the uptake of Cu(II) on crude kaolin and cleaned kaolinite. Both plots indicate differences in Cu(II) sorption behavior as a function of loading, particularly in the mixed-site adsorption and oligomer formation regions.

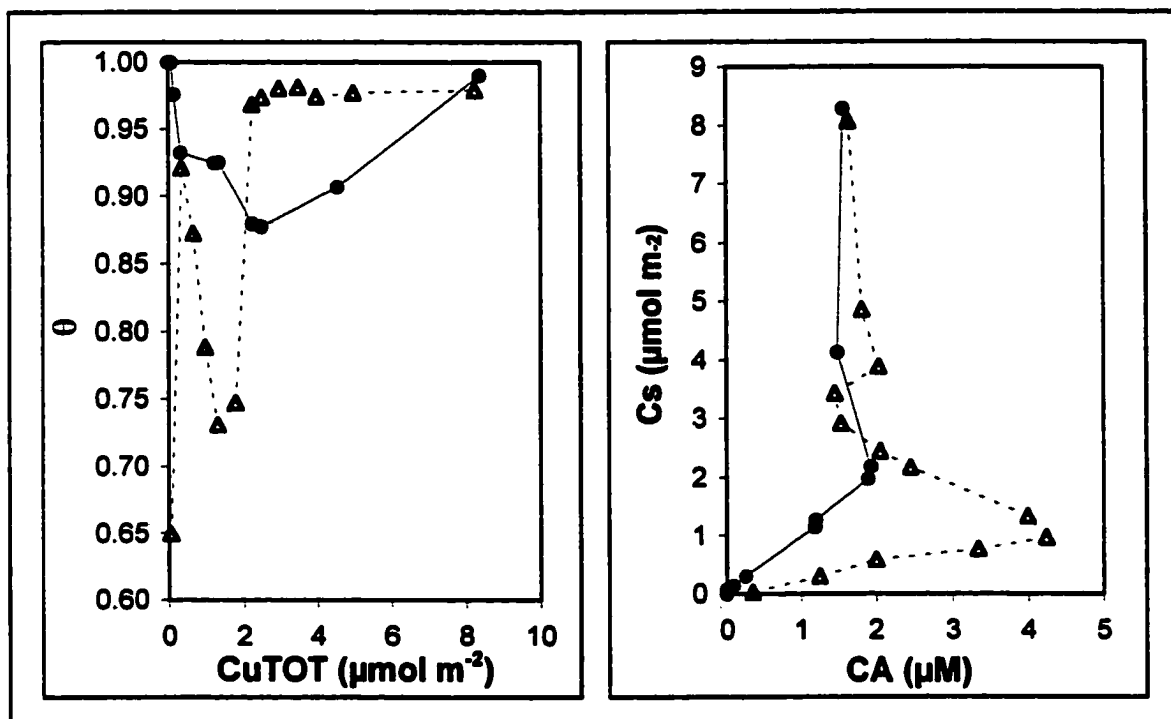


Figure 52. Cu(II) adsorption isotherms and Langmuir plots for crude kaolin (open triangles) and cleaned kaolinite (black circles).

Figure 53 shows that both solids exhibit sorption hysteresis. However, while crude kaolin retains all detectable Cu at all adsorption region samples, cleaned kaolinite releases detectable amounts of Cu at all but the lowest two loadings sampled.

Figure 54 is a series of bar charts comparing sorption-related quantities of crude kaolin and cleaned kaolinite to bulk goethite (set to zero). These confirm that while the two solids have similar numbers of high-affinity sites (Figure 54a), the transition from dominance by mixed-site adsorption to oligomer formation occurs at different loadings (Figure 54b, d, and f), and that it is delayed in cleaned kaolinite not because of a higher

abundance of adsorption sites, but by some other means (Figure 54e). Though precipitation behavior is more similar, the log IAP for the precipitate phases is quite different, suggesting that the cleaned kaolinite takes up a more soluble Cu precipitate phase.

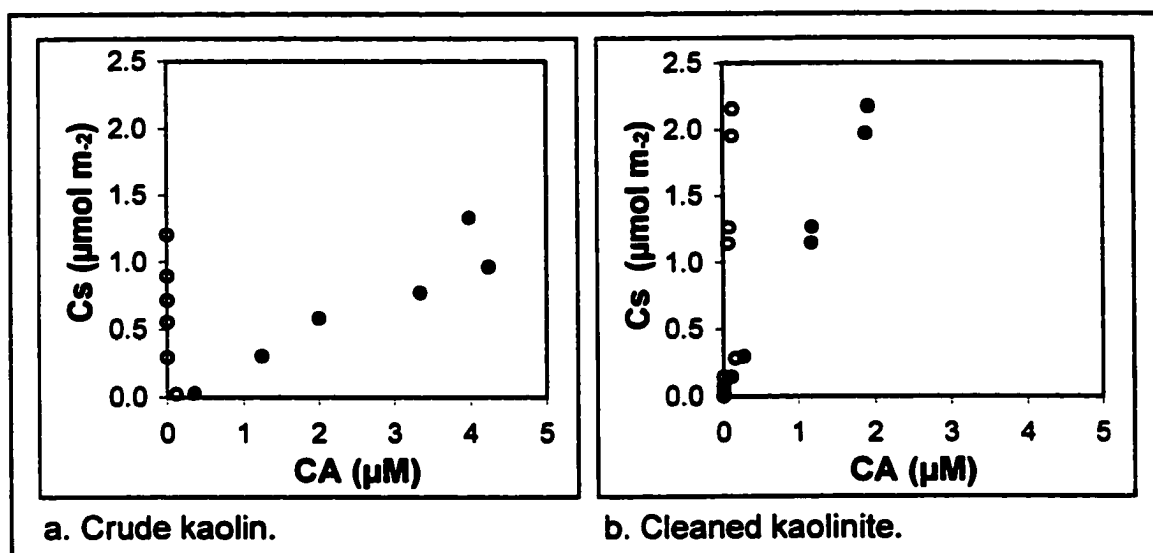


Figure 53. Sorption hysteresis in crude kaolin and cleaned kaolinite. Black circles show adsorption and open circles show desorption.

Natural materials versus bulk goethite. Figures 55 through 57 show the uptake of Cu(II) by the natural materials in comparison to bulk goethite. Of the three natural materials, the subsurface material behaves most like bulk goethite, followed by surface soil. Crude kaolin appears to behave least like bulk goethite. There are a few loadings at which the trends of the SRS materials match bulk goethite, particularly in the high-affinity-site and precipitation-dominated loadings (Figure 55). Also, there are a few places where the materials resemble each other in Cu(II) sorption, such as the similarity between uptake by the surface soil and the subsurface material in the mixed-affinity site region and between soil and crude kaolin in the oligomer formation-dominated region. The subsurface material and crude kaolin do not appear similar at any loading sampled despite qualitative similarities in their N₂ adsorption isotherm shapes (Figures 42 and 47).

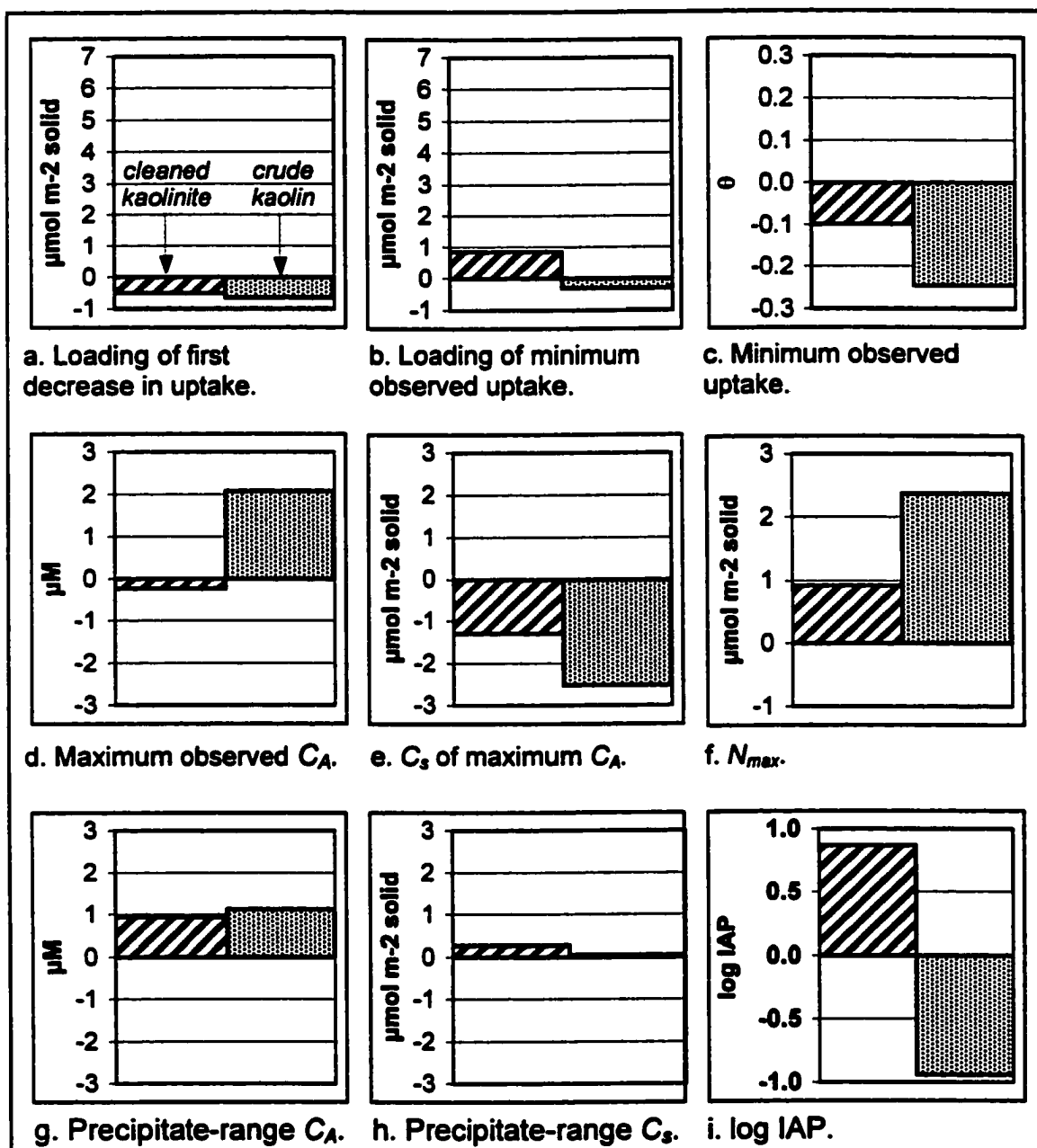


Figure 54. Comparisons of sorption-related quantities for cleaned kaolinite (striped) and crude kaolin (gray) relative to bulk goethite (set to zero).

Figure 56 indicates that all three materials exhibit sorption hysteresis (hysteresis of crude kaolin is shown in Figure 53), but it is less prominent in the SRS materials than in the crude kaolin.

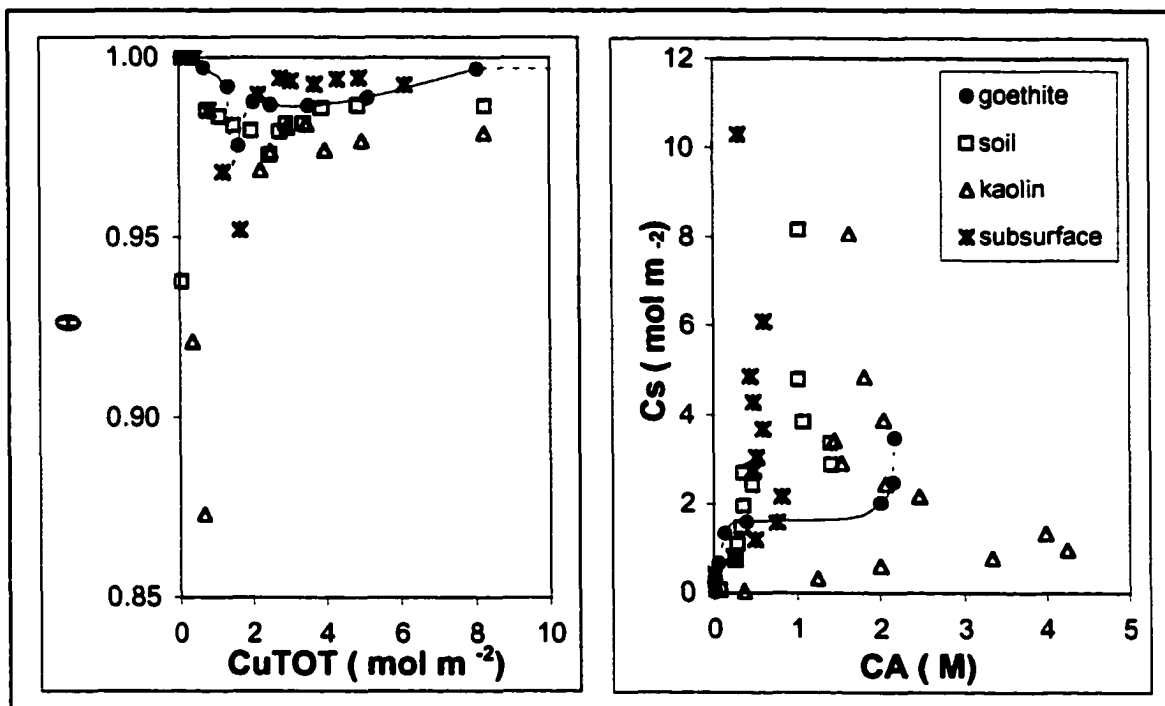
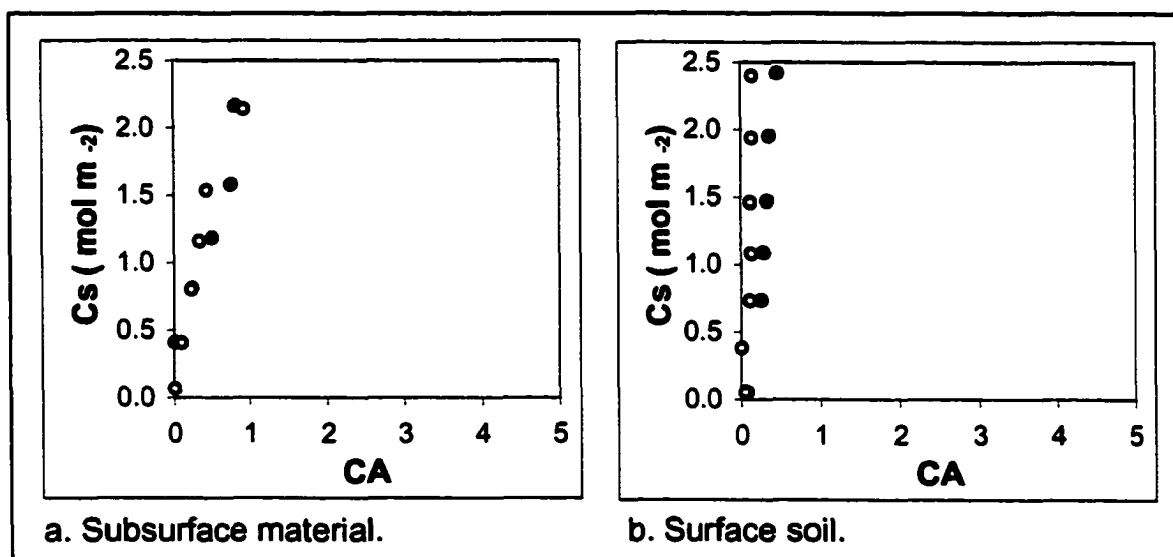


Figure 55. Cu(II) adsorption isotherms and Langmuir plots for natural materials in comparison with bulk goethite. Black line is a spline fit of the goethite data.



a. Subsurface material.

b. Surface soil.

Figure 56. Cu(II) sorption hysteresis in subsurface material and surface soil. Black circles show adsorption and open circles show desorption. Hysteresis in crude kaolin is shown in Figure 53.

Figure 57 shows sorption-related quantities of crude kaolin and cleaned kaolinite to bulk goethite (set to zero). Each solid exhibits a distinct set of similarities to and differences from bulk goethite. In general, crude kaolin is least like bulk goethite, with the exception of precipitation-range C_p , where it is the closest (Figure 57h). It appears to have fewer high-affinity sites (Figure 57a), and oligomer formation begins to become dominant at lower loadings (Figure 57b and f); however, the minimum observed fractional uptake is lower than bulk goethite or either of the SRS materials (Figure 57c). In contrast, it alone has a greater observed maximum C_A than bulk goethite (Figure 57g), supporting a later onset of dominant surface precipitation .

As observed in Figure 55, the subsurface material behaves most like bulk goethite; the exception is the loading of minimum observed uptake (Figure 57b) and N_{max} (Figure 57f). The subsurface material and bulk goethite appear to have similar quantities of high-affinity sites; although mixed-affinity adsorption dominates subsurface sorption at higher loadings than seen for bulk goethite, the minimum observed fractional uptake for subsurface is similar to bulk goethite (Figure 57c). The maximum C_A and corresponding C_p values for the subsurface material are most like bulk goethite as well.

The surface soil is intermediate in its resemblance to bulk goethite. It is most different in its precipitate-range C_p and log IAP values (Figures 56h and i), and most alike in its loading of minimum observed uptake, N_{max} and precipitate-range C_A (Figures 56b and g). Interestingly, its similarity to/difference from bulk goethite is similar to those of the subsurface material at points: specifically, the loading of first observed uptake, minimum observed uptake, maximum observed C_A , and C_p of maximum observed C_A (Figures 56b, d, and e, respectively). Crude kaolin is least like bulk goethite. The only quantity that approaches that of bulk goethite is its precipitation-dominated range C_p value (Figure 55h). Crude kaolin's precipitate-range quantities are somewhat similar to those for the surface soil (Figures 57g, h, and i). Over the rest of the loading range, crude kaolin is generally least like bulk goethite and also relatively dissimilar to the SRS materials. In general, the three solids appear to have lower adsorption site abundances (Figure 57e) and higher values of N_{max} (Figure 57f), as well as lower log IAP values than bulk goethite.

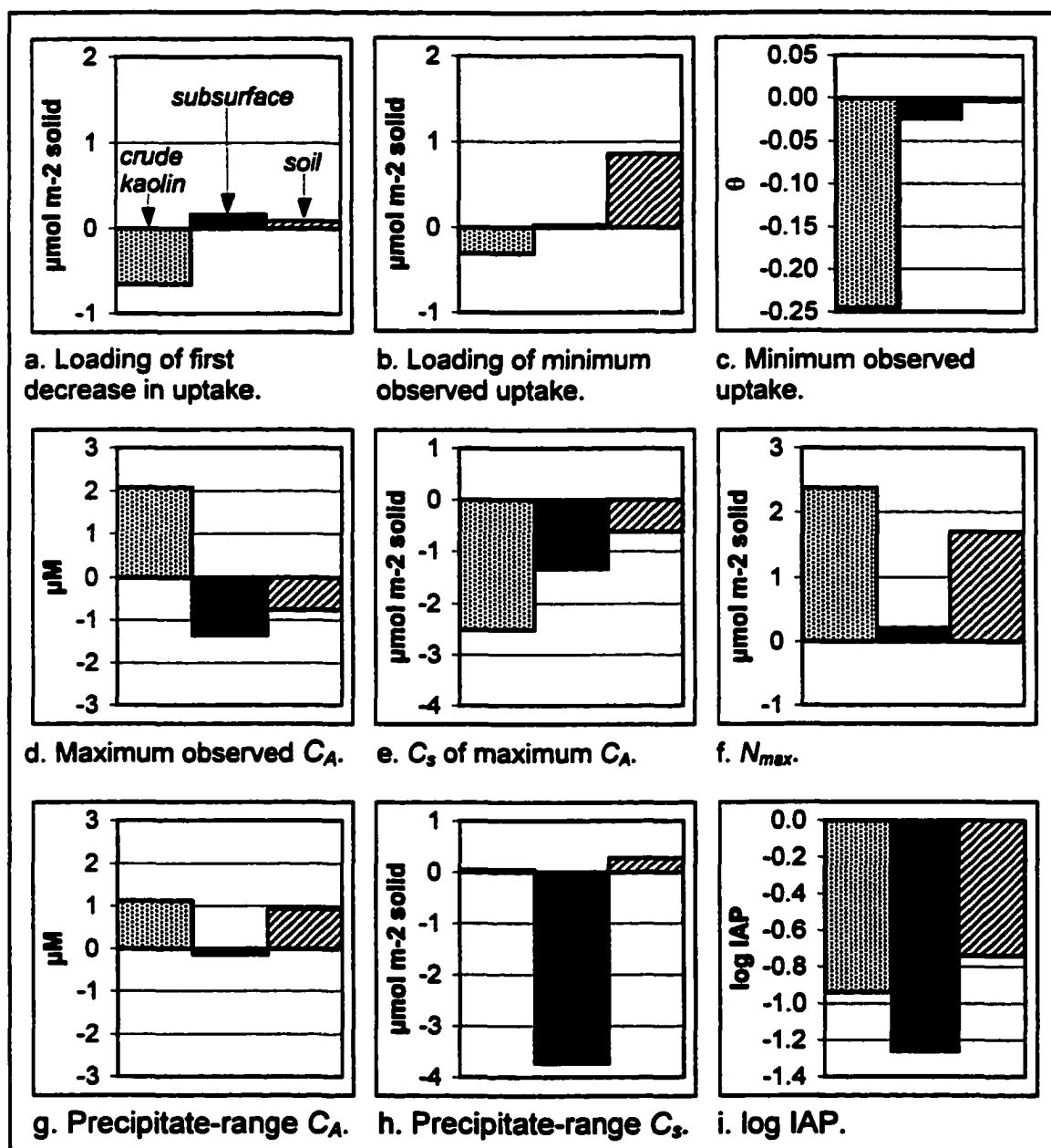


Figure 57. Comparisons of sorption-related quantities for crude kaolin (gray), subsurface material (black), and surface soil (striped) relative to bulk goethite (set to zero).

In these materials, as in the coated solids, there appears to be some delay of dominant oligomer formation and surface precipitation not attributable to a higher abundance of adsorption sites.

Natural materials versus laboratory oxide coatings. Of the five synthetic goethite coated solids studied in Chapters 2 and 3, two matched the sorption behavior of the SRS materials to some extent. Figures 58 and 59 compare the behaviors of the SRS materials to some of the synthetic coated phases and bulk goethite. In Figure 58, the subsurface material is plotted with bulk goethite and the thick chemical coating on kaolinite, Kch-thick. All three match at high-affinity-site adsorption loadings; however, at higher loadings the subsurface material more closely resembles Kch-thick in both adsorption isotherms and Langmuir plots. The transitions between uptake mechanisms take place at similar loadings; the range of fractional uptake is similar; and both take up slightly more Cu than bulk goethite in precipitation-dominated ranges.

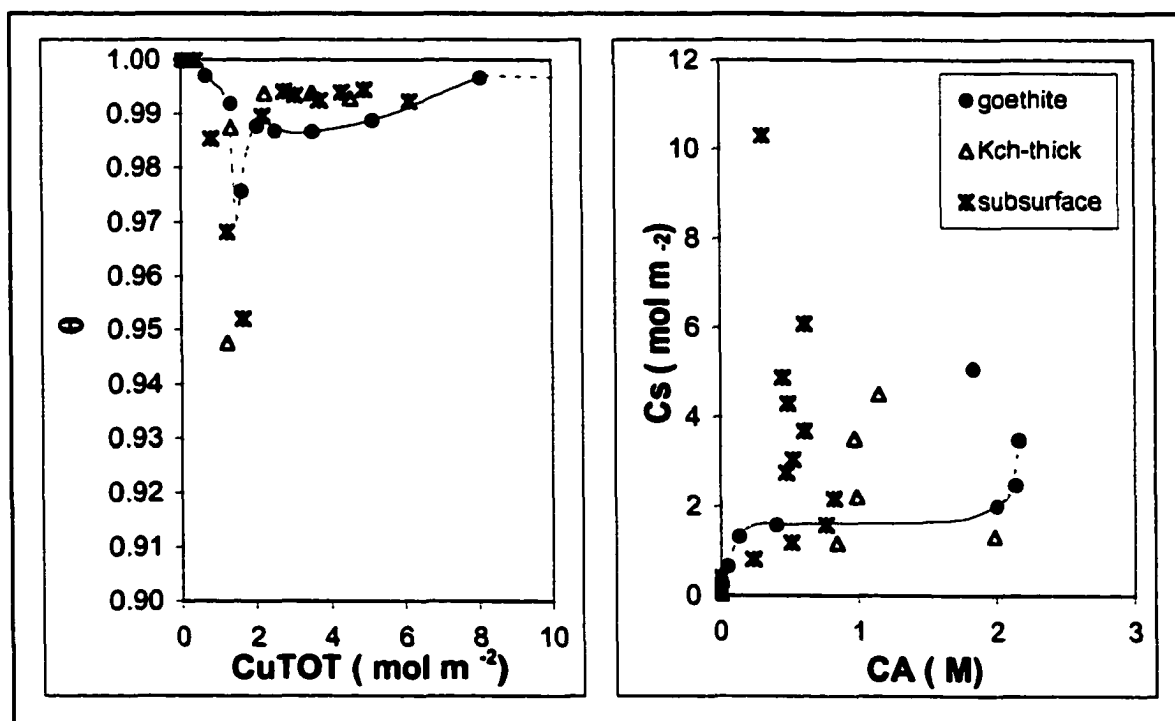


Figure 58. Cu(II) adsorption by subsurface material and Kch-thick in comparison to bulk goethite.

Figure 59 shows sorption by all three natural materials, bulk goethite, and the physical coating on quartz, Q-phys. These plots indicate that the sorption behavior of the

surface soil resembles each of the other materials at different loading regions: all solids in the high-affinity site region, the subsurface material in the mixed-affinity site adsorption region, crude kaolin followed by bulk goethite in the oligomer formation region, and Q-phys in the precipitation region.

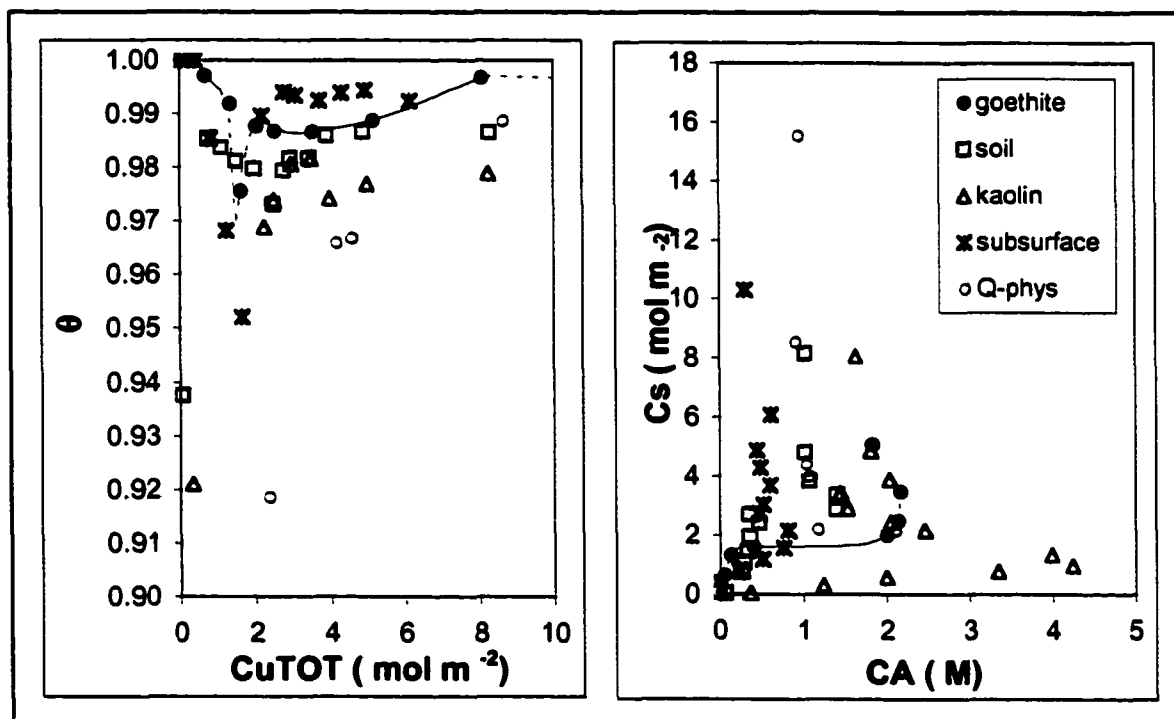


Figure 59. Cu(II) adsorption by natural materials and Q-phys in comparison to bulk goethite.

Discussion

Crude kaolin versus cleaned kaolinite. It is clear that the process of cleaning and purifying the kaolin mined by the Thiele Kaolin Company changes several of its physical and chemical adsorption properties. Since the cleaning techniques have been developed for the express purpose of removing reactive phases such as iron oxides and organic matter, this is not surprising. However, alterations in the reactivity of natural kaolin that may result from cleaning procedures should be kept in mind when using cleaned kaolinite to represent natural soil and sediment components.

Natural materials versus bulk goethite. Like the synthetic coated solids, the natural materials did not closely resemble bulk goethite in their physical and chemical adsorption behavior, except in the high-affinity-site adsorption region. This may be explained to some extent by the presence of other minor mineral phases, and more certainly by the presence of organic matter in the surface soil. Other investigators have asserted that the surface reactivity of the subsurface material is dominated by iron oxide, but that the surface soil also includes a significant amount of organic matter as well as more reactive clay phases such as illite and hydroxy-interlayered vermiculite (Vulava and Seaman, 2000). In addition, the form of the iron oxide in the natural materials may be influencing Cu(II) uptake and release as a function of loading.

Natural materials versus coated solids. Two similarities to synthetic coated solids were observed: the soil behaved like Q-phys (the physical coating on quartz) at precipitation-dominated loadings, and the subsurface material resembled Kch-thick (the thick chemical coating on kaolinite) throughout the entire loading range sampled. Both of these coatings might be expected to occur in the respective natural materials: colloidal goethite associated electrostatically with quartz grains in soil, and thick chemical goethite coatings precipitated onto on kaolinite grains. One way by which the latter might form would be repeated oxygenation of reduced groundwater containing dissolved Fe(II).

Unlike the subsurface material, the surface soil resembled a synthetic goethite-coated solid in only one loading range (precipitation). However, it also matched bulk goethite and the other two natural materials in limited loading ranges. The surface soil may be considered the most complex of the three natural materials (see Table 16). Given the geological relatedness of the three, it is conceivable that elements of the crude kaolin and the subsurface material may be present in the soil, or that weathering and diagenesis processes have worked on the parent materials in each to produce similar phases. The results would be compatible with some phase dominating uptake by the soil material in each loading range. However, the role of the organic matter present in the soil, and absent or nearly absent in the subsurface material and crude kaolin, is not addressed by this speculation. Nevertheless, this result supports further investigation of a composite

approach to modeling sorption by complex aggregates, in which several different types of sorbent phases might together describe net sorption behavior.

The fact that the subsurface material's Cu(II) sorption behavior matched that of the thick chemical coating on kaolinite is somewhat unexpected, given that the subsurface material is composed mainly of quartz (see Table 16). However, it should be kept in mind that even in a sandy aquifer where the quartz grains are described as "extensively coated with Al- and Fe-bearing minerals" (Coston et al., 1995), 90% of the grains sampled had no Fe oxide coating, and of the remaining 10%, 5 to 50% of each grain was coated (Ryan et al., 1999). In contrast, kaolinite in aquifer materials is comprehensively associated with goethite, whether physically or chemically, as individual grains coated with goethite or cemented together with colloidal goethite particles, or as a component, along with goethite and possibly other minerals, in composite coatings on larger grains (see the introductory section of this chapter for more detailed treatment of this topic). It would be reasonable that the resultant precipitation of Fe(III) would preferentially coat clay grains, both because of their higher surface area and their greater affinity for binding Fe. The same high surface area and sorption affinity, especially relative to the largely uncoated quartz surfaces, would help explain a dominance in Cu(II) sorption by a phase resembling the thick chemical coating on kaolinite. In addition, assemblages of clay and Fe/Al oxides have been observed to associate with larger quartz grains in similar subsurface systems (Bertsch and Seaman, 1999); such an association would mask part of the surfaces of the quartz grains, further reducing their influence in net Cu(II) sorption.

These results support the use of more representative forms of reactive coatings in pure-phase studies designed to emulate environmental processes, and indicate that some of the synthetic goethite coatings developed in this study more closely represent those occurring in natural materials. The distinctions observed between crude kaolin and cleaned kaolinite suggest that it might also be prudent to consider the phases removed as impurities during the preparation of laboratory minerals. The resemblance of Cu(II)

sorption by the surface soil to different solids at different loadings suggests that a composite approach to studying sorption in complex phases may be fruitful.

Finally, the fact that the subsurface material and Kch-thick showed similar behavior throughout the entire range of loadings studied is encouraging. This first step in developing more representative surrogates for natural materials succeeded to some extent in producing a pure phase that can describe Cu(II) sorption by a simple natural material better than bulk goethite. Remaining discrepancies could be ascribed to several factors which future research might address, such as the presence in the soil of organic matter and the fact that the grain size distribution was controlled in the synthetic phases but not in the natural materials. In addition, greater success may be achieved using methods for preparing coated synthetic phases refined to more closely emulate environmental conditions and/or a composite approach to account for more than one potentially important sorbent phase in a complex mineral assemblage.

CHAPTER 5: CONCLUSIONS

Human reliance on trace metals has led to the perturbation of trace metal cycling in the environment. In order to make intelligent decisions regarding the potential impact and remediation of trace metal contamination, a thorough understanding of the processes controlling the fate, transport, and bioavailability of trace metals is required. In aquatic systems, solid/water interfaces, such as the surfaces of sedimentary mineral grains, strongly affect the movement of dissolved trace metals. Much research on analogous pure mineral phases has been conducted; however, unfavorably large discrepancies between lab- and field-derived constants describing interfacial processes persist. These discrepancies are believed to arise from the different levels of complexity in field and laboratory systems. This dissertation was designed to investigate one aspect in which field and lab systems differ: the complexity of the solid phases.

The focus of this research was a comparison of the physical and chemical properties of the surfaces of a common reactive mineral phase – goethite (α -FeOOH) – as a function of its form. Although goethite frequently occurs as a coating on other environmental particles, it has traditionally been studied in bulk form in laboratory experiments. The objectives of the study were to compare and contrast the surface properties of bulk goethite to those of several goethite-coated solids prepared in the laboratory, and subsequently to assess how closely the bulk goethite and the laboratory-prepared goethite coatings matched the physical and chemical sorption behavior of field sedimentary materials.

The hypotheses proposed and tested in this dissertation were as follows:

- (1) The surface properties of bulk goethite differ from those of goethite coatings.
Alternate: the surface properties of goethite do not depend on its form.
- (2) The properties of goethite coatings vary with the coating method, substrate, and thickness. Alternate: coating method, substrate, and thickness do not affect the surface properties of goethite.
- (3) Goethite coatings may more closely emulate the sorption behavior of environmental sedimentary materials. Alternate: goethite phases in environmental sedimentary materials may be represented equally well by bulk goethite and goethite coatings.

(1) Physical and chemical characterizations of the goethite-coated solids and bulk goethite confirmed that the surface properties of goethite depend on its form as a coating or bulk particles. N_2 adsorption-desorption experiments indicated that the goethite coatings had higher specific surface areas (SSA) than bulk goethite. In addition, kaolinitic properties such as a lack of porosity were observed in the thin chemical goethite coating on kaolinite (K-chem). In Cu(II) adsorption-desorption experiments, bulk goethite and the five coated solids each exhibited a distinct sorption behavior as a function of Cu(II) loading. All the coated phases had a lower observed minimum fractional uptake of Cu than bulk goethite, and all the thin coatings showed a delay in the onset of oligomer formation as the dominant mechanism of Cu(II) sorption with increased loading. Cu(II) sorption to the thick chemical coating of goethite on kaolinite (Kch-thick) was most like bulk goethite; however, each transition in dominant uptake mechanism – from high-affinity-site adsorption to mixed-affinity-site adsorption, then to oligomer formation, and finally to surface precipitation – occurred at a lower loading than in bulk goethite. In addition, there were suggestions of variability in the properties of the

Cu(II) precipitate forming at high loadings on bulk goethite and each of the goethite-coated solids.

(2) The properties of the goethite-coated solids were also observed to vary as a function of coating method, substrate, and thickness. The kaolinitic N₂ sorption properties exhibited by K-chem were not present in the thicker goethite coating. Neither Kch-thick nor Q-chem showed substrate effects on N₂ sorption; and both shared some characteristics, such as mesoporosity, with bulk goethite. However, examination of the three chemical coatings with SEM/EDS revealed that the Q-chem coating was distributed patchily, while the K-chem and Kch-thick coatings appeared to be distributed evenly across all surfaces of the kaolinite grains. These results confirmed that substrate and thickness influence the properties of the goethite coating.

Cu(II) sorption experiments further supported this hypothesis. As mentioned above, while K-chem experienced the transition from mixed-affinity-site adsorption to oligomer formation at higher Cu loadings relative to bulk goethite, Kch-thick went through all sorption-mechanism transitions at lower loadings than bulk goethite. Q-chem appeared to have a higher abundance of high-affinity sites than either of the other two chemical coatings. In addition, the Cu(II) sorption experiments indicated that coating method also affects the surface properties of goethite coatings. Three of the four thin coatings appeared to have lower adsorption site abundances than bulk goethite; however, K-phys exhibited a higher adsorption site abundance than K-chem (or either of the quartz coatings). In addition, both chemical coatings had markedly lower observed minimum fractional Cu uptake than the corresponding physical coatings, and both chemical coatings had a lower log IAP for the proposed Cu precipitate phase (Cu(OH)₂).

More evidence that the coating method, substrate, and thickness influence the properties of the goethite coating arose from an analysis of the role of physical differences between goethite coatings and bulk goethite. Corrections applied to the Cu(II) sorption data to account for these differences varied in their applicability and success for each of the five coatings. Corrections for changes in surface area-to-volume

ratio were not relevant to the physical coatings, because these did not involve an alteration of the surface area-to-volume ratio of the goethite phases, or to Kch-thick, because it completely masked the kaolinite substrate, so that the measured SSA of the solid was also that of the coating. Similarly, corrections for direct uptake of Cu by exposed substrate surface (i.e., additive modeling of the data) did not apply to either the thick or the thin chemical coatings on kaolinite. However, this correction did appear to improve the fit of Q-chem and K-phys, suggesting the presence of a second non-goethite population of adsorption sites. The remaining discrepancy in Q-chem was interpreted to indicate the formation of a second Fe phase on the quartz surface that went undetected by EDS. The remaining discrepancy in K-phys was hypothesized to arise from the partial blocking of goethite surface area as a result of its binding to the basal planes of the kaolinite particles.

(3) The hypothesis that laboratory-prepared goethite coatings might better be used to represent goethite phases in environmental materials was partially supported by the results of parallel Cu(II) sorption experiments on crude kaolin, a sandy subsurface material, and a surface soil. The first comparison, between the crude kaolin and the cleaned kaolinite used as the substrate for the laboratory goethite coatings (KGa-1b), was intended to explore how important small impurities and coatings may be in controlling the overall sorption behavior of a largely pure and homogeneous material, and conversely, to assess how much the cleaning of mineral materials for use in laboratory studies changes their sorption properties.

Although the crude kaolin came from the same formation as KGa-1b, its N₂ and Cu(II) sorption did not match that of KGa-1b. The crude kaolin was porous and had more than twice the specific surface area as KGa-1b. It bound Cu more strongly, had a lower observed minimum Cu fractional uptake, and reached dominant surface precipitation at a lower Cu loading. The Cu(II) precipitate phase on crude kaolin also appeared to be more soluble. Since it is known that the crude kaolin contains small quantities of goethite, as well as quartz, both of which were removed from KGa-1b, these

differences are not surprising. However, they emphasize the fact that processing minerals for use in laboratory studies may remove phases that, even in small amounts, may substantially affect the net behavior of a mineral phase in a natural material.

Each of the three natural materials also exhibited distinct Cu(II) sorption behavior. The subsurface material behaved most like bulk goethite in terms of Cu(II) sorption, while the surface soil was intermediate and the crude kaolin was least like bulk goethite. Of the five laboratory goethite coatings, two matched the Cu(II) sorption behavior of a natural material as well as or better than bulk goethite. The first was Q-phys, which matched the precipitation-range sorption of the surface soil. This type of coating, the electrostatic binding of goethite to quartz surfaces, is common in natural soils and sediments, and in a soil composed of more than 93% quartz with 0.19% Fe occurring as crystalline Fe oxide, might be expected to play a major role in Cu(II) sorption.

In addition to matching Q-phys at precipitation-dominated loadings, the surface soil also matched the subsurface material at mixed-affinity-site adsorption loadings and the crude kaolin at oligomer formation-dominated loadings. Since all three natural materials occur in the Southeastern Atlantic Coastal Plain sequence and derive from the same parent materials, it may be that similar sorbent phases occur in more than one material; perhaps different phases dominate Cu(II) uptake at different loadings. If this is the case, a composite approach to modeling uptake by natural materials might be fruitful.

The second laboratory goethite coating that matched a natural material better than bulk goethite was Kch-thick, which more closely resembled the subsurface material throughout the entire range of Cu loadings sampled. This agreed to some extent with the N₂ sorption results; in particular, the N₂ adsorption-desorption isotherms for subsurface and Kch-thick showed similar types of hysteresis compared to bulk goethite. This result is also reasonable, even though the subsurface material is composed of more than 95% quartz, since the kaolinite present would be expected to take up Fe(III) oxide deposits preferentially. Periodic recharging of a reduced aquifer would result in the type of iterative chemical coating made using the thick chemical method to produce Kch-thick, and these solids would then be expected to have a higher surface area and greater affinity

for dissolved Cu(II) than analogous coatings on quartz, based on the results of the Cu(II) sorption experiments on Q-chem versus Kch-thick.

An unanticipated, though reasonable, observation was made in the Cu(II) sorption experiments for both the coated solids and natural materials: at very low Cu loadings, where high-affinity-site adsorption is dominant, most of the goethite-coated solids and all three natural materials appeared to match the behavior of bulk goethite. This suggests that bulk goethite is a reasonable surrogate for goethite phases in natural materials in laboratory studies of Cu(II) sorption at very low loadings. The goethite-coated solids and natural materials were also closer to each other and to bulk goethite at precipitation-dominated loadings. The greatest discrepancies occurred in mixed-affinity-site adsorption and oligomer formation loadings for all goethite-coated solids and natural materials.

The surface properties of goethite appear to depend on its form – not only whether it occurs as bulk particles or as a coating, but also the specific form of the coating, as determined by how it formed, how thick it is, and the surface properties of its substrate. Some of the effects appear to derive from physical changes in the goethite, such as surface area-to-volume ratio and partial blocking of goethite surface as a result of its binding to the substrate. There also appear to be variations in the chemical properties of the goethite surface; these may be due to crystal characteristics, such as mean crystal size and dominant crystallographic faces (each of which has a unique population of surface functional groups), or physicochemical properties of the coating such as meso- and microporosity. In some cases, such as the thin chemical coating on kaolinite and quartz, a non-goethite phase may be present.

Future work should include more examination of the crystallinity and mineralogy of the coatings. In addition, mechanistic investigations of the Cu(II) surface complexes would be valuable for confirming the locations of the transitions from one dominant sorption mechanism to another as a function of Cu loading, and thought should be given to methods for assessing the surface area and spatial uniformity of the physical coatings

without altering the coatings or introducing artifacts. Further progress toward an environmental level of complexity in controlled laboratory studies could be sought on two fronts: first, by attempting a composite approach to representing sorption by natural materials using multiple forms of Fe oxide and other reactive mineral coatings; and second, by studying a second class of common, reactive environmental surface coatings: organic matter.

The use of laboratory-prepared goethite coatings as surrogates for goethite phases in natural materials appears to be promising. The observed discrepancies between the crude kaolin and the cleaned kaolinite confirms that even small quantities of reactive phases may influence the net sorption behavior of a material. The improvements in matching the Cu(II) sorption behavior of the subsurface and surface soil materials using goethite coatings as opposed to bulk goethite suggest that substantial gains in improving the similarity of laboratory studies to environmental processes may be made using relatively simple binary phases. The results of this study suggest that quantitative discrepancies between field- and lab-derived systems may be decreased with relatively little effort to foster the development of more accurate and generally applicable models of trace metal cycling in aquatic environments.

APPENDIX 1

Physical adsorption data

Volume of N₂ (g) sorbed at 173K as a function of relative pressure, measured using a Micromeritics Gemini 2375 multipoint surface area analyzer. Pressure increased from 0.05% to 96% of saturation pressure, then decreased to 0.05%. See Physical Characterization Methods for more details.

Goethite

P/Po	Va
0.0500	14.72
0.0900	16.20
0.1300	17.43
0.1690	18.56
0.2090	19.64
0.2490	20.73
0.2880	21.77
0.3280	22.85
0.3670	23.92
0.4070	24.99
0.4470	26.03
0.4860	27.13
0.5260	28.25
0.5650	29.45
0.6050	30.69
0.6440	32.07
0.6840	33.61
0.7230	35.38
0.7630	37.53
0.8020	40.16
0.8420	43.87
0.8810	49.51
0.9210	59.77

P/Po	Va
0.9610	95.83
0.9520	90.75
0.9030	59.17
0.8600	48.57
0.8200	43.06
0.7800	39.30
0.7410	36.63
0.7000	34.61
0.6400	32.08
0.5800	30.04
0.5200	28.16
0.4600	26.42
0.4000	24.60
0.3400	22.93
0.2800	21.28
0.2400	20.17
0.2000	19.05
0.1600	17.91
0.1200	16.72
0.0800	15.42
0.0400	13.76

Quartz

P/Po	Va
0.0505	0.100
0.0899	0.111
0.1296	0.119
0.1693	0.127
0.2090	0.135
0.2487	0.142
0.2884	0.150
0.3283	0.158
0.3680	0.166
0.4078	0.175
0.4473	0.184
0.4871	0.193
0.5268	0.202
0.5663	0.211
0.6060	0.223

P/Po	Va
0.6455	0.236
0.6852	0.251
0.7248	0.270
0.7641	0.291
0.8040	0.318
0.8433	0.354
0.8828	0.405
0.9218	0.488
0.9606	0.695
0.9610	0.707
0.9126	0.476
0.8646	0.386
0.8168	0.334
0.7689	0.298
0.7210	0.271

P/Po	Va
0.6731	0.250
0.6252	0.233
0.5773	0.218
0.5294	0.207
0.4815	0.195
0.4336	0.184
0.3857	0.173
0.3378	0.164
0.2898	0.155
0.2419	0.145
0.1940	0.136
0.1461	0.127
0.0981	0.119
0.0502	0.107

Kaolinite

P/Po	Va
0.0500	1.713
0.0897	1.853
0.1293	1.974
0.1689	2.089
0.2086	2.211
0.2483	2.343
0.2879	2.483
0.3276	2.633
0.3673	2.797
0.4067	2.962
0.4463	3.128
0.4861	3.293
0.5257	3.456
0.5656	3.625
0.6048	3.812
0.6446	4.017
0.6840	4.259
0.7240	4.535
0.7630	4.891
0.8030	5.354
0.8423	5.983
0.8813	6.903

P/Po	Va
0.9207	8.669
0.9603	13.818
0.9511	12.307
0.9025	7.952
0.8605	6.523
0.8206	5.743
0.7805	5.187
0.7404	4.777
0.7005	4.455
0.6406	4.059
0.5805	3.745
0.5205	3.477
0.4605	3.194
0.4005	2.926
0.3404	2.673
0.2804	2.438
0.2404	2.299
0.2003	2.170
0.1603	2.050
0.1203	1.930
0.0802	1.809
0.0402	1.655

GQtzC

P/Po	Va
0.0503	0.187
0.0912	0.215
0.1321	0.231
0.1729	0.251
0.2137	0.270
0.2546	0.288
0.2955	0.305
0.3363	0.315
0.3770	0.329
0.4179	0.345
0.4588	0.361
0.4995	0.376
0.5404	0.395
0.5810	0.413
0.6217	0.428
0.6632	0.449
0.7034	0.468
P/Po	Va
0.7443	0.494

P/Po	Va
0.7848	0.518
0.8259	0.545
0.8665	0.574
0.8865	0.597
0.9076	0.623
0.9336	0.672
0.9658	0.782
0.9876	1.009
0.9819	0.937
0.9355	0.701
0.8904	0.619
0.8505	0.585
0.8004	0.544
0.7404	0.522
0.6704	0.496
0.6005	0.466
0.5605	0.443
0.5205	0.426
0.4805	0.413

P/Po	Va
0.4405	0.375
0.4004	0.345
0.3304	0.315
0.2603	0.286
0.1903	0.256
0.1202	0.233
0.0502	0.195

GKaoC

P/Po	Va
0.0500	4.205
0.0897	4.593
0.1293	4.926
0.1689	5.240
0.2086	5.557
0.2482	5.888
0.2878	6.235
0.3275	6.608
0.3671	7.009
0.4068	7.418
0.4462	7.816
0.4858	8.235
0.5254	8.665
0.5651	9.101
0.6047	9.561
0.6443	10.091
0.6838	10.671
0.7235	11.367

P/Po	Va
0.7631	12.202
0.8027	13.260
0.8421	14.663
0.8814	16.763
0.9209	20.620
0.9604	31.729
0.9510	28.561
0.9026	18.714
0.8606	15.721
0.8206	13.985
0.7806	12.755
0.7406	11.797
0.7006	11.035
0.6406	10.093
0.5805	9.311
0.5205	8.637
0.4605	7.911
0.4005	7.211

P/Po	Va
0.3404	6.589
0.2804	6.015
0.2404	5.662
0.2003	5.332
0.1603	5.002
0.1203	4.670
0.0802	4.330
0.0402	3.892

GKaoC_{thick}

P/P_o	V_a
0.0500	12.367
0.0897	13.722
0.1293	14.823
0.1690	15.811
0.2085	16.760
0.2482	17.700
0.2878	18.625
0.3275	19.562
0.3671	20.510
0.4068	21.493
0.4463	22.501
0.4858	23.561
0.5255	24.697
0.5649	25.901

0.6046	27.180
0.6443	28.610
0.6837	30.185
0.7237	31.953
0.7629	33.974
0.8026	36.332
0.8421	39.389
0.8812	43.447
0.9208	49.530
0.9604	63.477
0.9512	60.391
0.9026	48.083
0.8605	42.507
0.8205	38.973
0.7805	36.165

0.7406	33.872
0.7005	31.875
0.6405	29.274
0.5805	27.046
0.5205	25.022
0.4605	23.119
0.4005	21.262
0.3405	19.729
0.2804	18.246
0.2404	17.262
0.2003	16.285
0.1603	15.275
0.1203	14.208
0.0802	13.013
0.0402	11.482

APPENDIX 2

EDS data

Spot counts for Fe, Si, and Al collected for 100 live seconds at approximately 4,000 counts per second and transformed to relative intensity using automatic standardless ZAF quantitation routine provided with EDS manufacturer's software. See Physical Characterization Methods for more details. In the first column, the numeral indicates the grain sampled (see Figures 18-20); 'f' = face and 'e' = edge. In GQtzC, grains were sampled three times each on one face and one edge; in GKaoC and GKaoC_{thick}, each grain was sampled on a face or an edge. A zero value for Fe indicates that the relative intensity fell below MDL (2 wt %). Low levels of Fe were detected in all samples.

GQtzC

	Pt	Fe	Si	Al
1 ^f	a	0.000 ^b	44.515	1.076
	b	5.840	75.642	0.855
	c	6.088	75.225	0.835
1 ^e	a	0.000	32.429	0.980
	b	0.000	32.396	1.020
	c	10.729	70.660	0.666
2 ^f	a	0.000	41.151	1.076
	b	0.000	42.707	1.128
	c	0.000	52.827	1.085
2 ^e	a	0.000	36.556	0.961
	b	0.000	45.879	1.281
	c	0.000	34.122	1.079
3 ^f	a	0.000	40.033	1.007
	b	0.000	40.957	1.021
	c	0.000	39.560	1.002
3 ^e	a	0.000	30.460	0.901
	b	0.000	29.162	0.806
	c	0.000	51.858	1.129
4 ^f	a	0.000	32.523	0.966
	b	0.000	34.146	0.947
	c	0.000	55.423	1.277
4 ^e	a	0.000	38.316	1.128
	b	0.000	38.529	1.029
	c	2.684	53.025	1.330
5 ^f	a	0.000	69.485	1.406
	b	2.036	58.268	1.238
	c	0.000	62.288	1.284

	Pt	Fe	Si	Al
5 ^e	a	0.000	35.237	1.032
	b	0.000	43.174	1.260
	c	6.009	48.821	1.009
6 ^f	a	0.000	38.367	1.005
	b	0.000	37.871	1.006
	c	0.000	37.782	1.006
6 ^e	a	5.855	34.441	1.158
	b	5.514	48.360	1.127
	c	9.484	32.584	1.166
7 ^f	a	0.000	32.039	0.901
	b	0.000	35.231	0.935
	c	2.529	65.779	1.215
7 ^e	a	3.136	59.343	1.470
	b	7.431	54.323	0.810
	c	0.000	52.308	1.255
8 ^f	a	0.000	39.693	0.954
	b	0.000	34.654	0.925
	c	3.542	52.384	1.021
8 ^e	a	3.092	44.850	1.044
	b	0.000	32.341	0.970
	c	0.000	42.861	1.153
9 ^f	a	0.000	44.913	1.090
	b	0.000	47.155	1.151
	c	2.630	62.687	1.108
9 ^e	a	0.000	31.293	0.895
	b	0.000	32.591	1.084
	c	0.000	51.193	1.202

	Pt	Fe	Si	Al
10f	a	2.101	65.368	1.100
	b	2.542	62.505	0.982
	c	3.931	44.661	0.724
10e	a	0.000	33.254	0.970
	b	0.000	32.819	0.970
	c	0.000	31.364	0.916

GKaoC

	Pt	Fe	Si	Al
1f	a	5.319	10.572	9.925
	b	5.200	10.007	9.710
	c	5.122	12.135	11.331
2f	a	6.093	11.074	9.649
	b	5.687	10.762	9.837
	c	6.282	10.885	10.178
3f	a	6.042	11.309	10.588
	b	6.410	11.791	10.652
	c	6.322	12.150	10.813
5f	a	6.506	11.481	10.545
	b	6.993	12.318	11.436
	c	6.760	12.461	11.678
8f	a	6.367	10.826	10.212
	b	5.714	11.094	9.797
	c	5.484	9.903	9.212
9f	a	6.253	11.459	10.267
	b	6.069	11.292	10.333
	c	5.969	11.007	10.561
11f	a	6.030	11.575	10.465
	b	6.258	10.952	10.254
	c	6.176	10.789	9.928
13f	a	6.336	11.390	10.157
	b	6.871	12.873	12.046
	c	7.115	11.739	10.395
14f	a	5.858	11.037	10.309
	b	5.619	11.115	10.123
	c	6.736	11.747	10.601
20f	a	5.151	10.213	9.635
	b	9.460	18.352	16.148
	c	6.418	13.713	13.147

	Pt	Fe	Si	Al
4e	a	6.636	14.521	14.008
	b	8.101	17.538	16.160
	c	6.453	12.054	11.273
6e	a	5.741	11.573	10.231
	b	6.210	11.748	11.222
	c	6.357	12.237	11.853
7e	a	5.758	10.793	9.575
	b	5.692	11.263	10.403
	c	5.924	11.198	10.292
10e	a	6.049	11.463	10.434
	b	5.401	10.934	10.065
	c	5.714	10.606	10.458
12e	a	6.323	11.652	10.462
	b	6.674	11.887	10.643
	c	6.294	11.000	10.639
15e	a	8.700	12.724	12.005
	b	8.323	11.874	11.096
	c	13.096	17.440	18.408
16e	a	5.916	11.086	10.326
	b	6.014	11.471	10.450
	c	5.821	11.493	10.237
17e	a	4.934	10.226	9.901
	b	5.137	9.437	9.327
	c	7.432	16.889	16.287
18e	a	6.420	11.544	10.517
	b	6.618	13.298	11.919
	c	7.143	12.731	11.947
19e	a	6.014	10.418	10.010
	b	6.064	10.931	9.841
	c	5.350	9.551	8.715

GKaoC_{thick}

	Pt	Fe	Si	Al
1f	a	10.752	24.941	20.700
	b	10.024	22.403	19.472
	c	12.367	26.330	21.658
3f	a	6.825	16.570	14.833
	b	6.667	17.808	15.808
	c	7.838	16.995	15.338
5f	a	7.635	16.238	14.864
	b	8.022	17.559	16.115
	c	8.604	20.259	18.037
6f	a	7.883	20.811	18.026
	b	8.146	21.651	18.764
	c	9.857	23.690	20.345
10f	a	10.884	20.357	17.663
	b	9.183	20.602	17.684
	c	11.610	21.475	18.364
12f	a	6.601	17.318	15.554
	b	8.062	19.922	17.595
	c	8.895	19.535	17.434
13f	a	8.106	20.689	17.752
	b	6.981	20.132	17.505
	c	7.324	21.238	18.118
17f	a	10.054	20.355	17.848
	b	12.763	20.375	17.785
	c	10.175	18.631	17.397
18f	a	4.342	17.311	15.472
	b	4.829	17.658	15.515
	c	4.780	16.173	14.620
19f	a	5.989	17.169	14.926
	b	7.126	17.276	15.490
	c	9.167	18.012	15.775

	Pt	Fe	Si	Al
2e	a	13.927	21.410	18.569
	b	16.777	20.114	17.692
	c	11.600	22.196	18.737
4e	a	5.715	15.893	14.334
	b	6.262	16.998	15.271
	c	7.152	16.931	15.388
7e	a	9.934	18.448	16.599
	b	9.489	17.636	15.670
	c	7.133	16.424	14.914
8e	a	6.082	17.442	15.714
	b	8.194	17.427	15.650
	c	6.446	17.515	15.548
9e	a	5.496	17.733	15.751
	b	6.503	17.472	15.570
	c	6.439	17.031	14.962
11e	a	14.389	23.498	20.723
	b	15.816	23.594	20.411
	c	11.924	20.584	17.879
14e	a	7.236	16.826	14.851
	b	7.414	17.951	15.879
	c	7.620	17.828	15.720
15e	a	14.703	24.871	20.511
	b	12.457	27.915	22.265
	c	7.862	20.324	17.377
16e	a	4.023	20.731	17.910
	b	5.641	21.897	19.252
	c	7.122	21.280	19.048
20e	a	6.459	16.102	14.556
	b	6.204	16.739	15.074
	c	7.021	17.657	15.628

APPENDIX 3

Batch adsorption/desorption data

Batch experiments conducted at constant pH and IS (10‰ synthetic estuarine water) over a range of Cu(II) surface loadings. Cu(II) removal from solution measured by GF-AA and ICP-AES. Experiments stopped by centrifugation after 24 h equilibration. Desorption induced by replacement of the equilibrium adsorption solution with fresh SEW. See Batch Adsorption/Desorption Experiments Methods for more details.

Goethite

Set	Sample	pH _A	g mass1	μM Cu _i	mL volume	μmol Cu _A	μmol Cu _D
STAR99	α1	7.51	0.0249	0.97	50.119	0.000	0.000
STAR99	α2	7.59	0.0249	0.98	50.473	0.000	0.000
STAR99	β1	7.72	0.0031	0.97	50.068	0.000	0.000
STAR99	β2	7.72	0.0032	0.98	50.298	0.000	0.000
STAR99	γ1	7.83	0.0020	0.97	50.212	0.000	0.000
STAR99	γ2	7.85	0.0021	0.97	50.048	0.000	0.000
STAR99	δ1	8.16	0.0173	16.09	50.034	0.005	0.000
STAR99	δ2	7.96	0.0173	16.10	50.026	0.000	0.000
STAR99	ε1	7.89	0.0085	16.14	50.222	0.006	0.000
STAR99	ε2	7.71	0.0086	16.16	50.245	0.007	0.004
STAR99	ζ1	7.64	0.0070	16.09	50.007	0.018	0.005
STAR99	ζ2	7.62	0.0071	16.20	50.364	0.022	0.007
STAR99	η1	8.93	0.0138	155.60	50.437	0.032	0.025
STAR99	η2	8.95	0.0138	154.85	50.525	0.020	0.026
STAR99	θ1	8.96	0.0057	156.70	50.116	0.034	0.043
STAR99	θ2	8.96	0.0058	156.39	50.093	0.035	0.047
pH 1	S1-1	7.3	0.2854	3.94	50.142	0.000	0.000
pH 1	S1-2	7.2	0.2855	3.94	50.126	0.000	0.000
pH 1	γ1	7.3	0.1691	3.95	50.287	0.000	0.000
pH 1	γ2	7.2	0.1693	3.95	50.232	0.000	0.000
pH 1	S2-1	7.3	0.0951	3.96	50.341	0.000	0.000

			g	μM	mL	μmol	μmol
pH 1	S2-2	7.2	0.0953	3.96	50.397	0.000	0.000
pH 1	S3-1	7.3	0.0475	3.93	50.052	0.000	0.000
pH 1	S3-2	7.3	0.0472	3.94	50.073	0.000	0.000
pH 1	S4-1	7.5	0.0319	3.94	50.087	0.000	0.000
pH 1	S4-2	7.4	0.0321	3.94	50.072	0.000	0.000
pH 1	S5-1	7.6	0.0143	3.94	50.127	0.000	0.000
pH 1	S5-2	7.7	0.0140	3.98	50.685	0.000	0.000
fill 1	N3-1	7.3	0.0453	162.00	49.948	0.113	0.021
fill 1	N3-2	7.3	0.0458	162.05	49.942	0.101	0.029
fill 1	M1-1	7.3	0.0326	162.36	50.019	0.120	0.069
fill 1	M1-2	7.4	0.0327	162.77	50.151	0.097	0.067
fill 1	M1-2	7.4	0.0327	162.77	50.151	0.097	0.067
fill 1	M3-1	7.3	0.0567	162.59	50.061	0.115	0.015
fill 1	M3-2	7.2	0.0569	163.55	50.380	0.086	0.018
fill 1	M4-1	7.4	0.0231	163.74	50.412	0.087	0.053
fill 1	M4-2	7.5	0.0226	163.92	50.511	0.098	0.059

Quartz

			g	μM	mL	μmol	μmol
Set	Sample	pH _A	mass1	Cu _i	volume	Cu _A	Cu _D
STAR99	β 1	7.86	0.4672	0.90	50.293	0.031	0.004
STAR99	β 2	7.88	0.4675	0.89	50.228	0.036	0.005
STAR99	γ 1	7.87	0.3116	0.89	50.138	0.034	0.006
STAR99	γ 2	7.91	0.3112	0.89	50.089	0.035	0.006
STAR99	δ 1	7.92	0.1556	0.89	50.102	0.046	0.003
STAR99	δ 2	7.94	0.1554	0.89	50.149	0.043	0.003
STAR99	ϵ 1	7.96	0.0781	0.89	50.027	0.040	0.002
STAR99	ϵ 2	7.92	0.0778	0.89	50.130	0.039	0.004
STAR99	ζ 1	7.97	0.0621	0.89	50.113	0.042	0.002
STAR99	ζ 2	7.96	0.0618	0.90	50.353	0.041	0.002
STAR99	θ 1	7.82	0.0868	14.70	50.050	0.027	0.012
STAR99	θ 2	7.75	0.0868	14.68	50.082	0.023	0.015
STAR99	λ 1	7.82	0.0480	0.89	50.099	0.040	0.002
STAR99	λ 2	7.95	0.0480	0.89	50.016	0.029	0.002
SSRL200	Q4	7.17	0.6002	15.68	49.991	0.216	x
SSRL200	Q5	7.33	0.4798	15.68	49.998	0.065	x
pH 2	S5-2	7.9	0.2406	0.39	50.065	0.011	0.000

Kaolinite

Set	Sample	pH _A	g	μM	mL	μmol	μmol
			mass1	Cu _i	volume	Cu _A	Cu _D
F99	N1-1	7.45	0.0741	0.94	49.979	0.000	0.000
F99	N1-2	7.45	0.0738	0.94	49.986	0.000	0.000
K2	N1-1	7.6	0.1205	0.10	50.282	0.000	0.000
K2	N1-2	7.7	0.1200	0.10	50.146	0.000	0.000
K2	γ1	7.8	0.0177	0.10	50.140	0.000	0.000
K2	γ2	7.9	0.0181	0.10	50.494	0.000	0.000
K2	N2-1	7.9	0.0809	15.74	50.051	0.059	0.003
K2	N2-2	7.9	0.0804	15.70	50.011	0.059	0.003
K2	ε1	7.8	0.0744	15.89	50.589	0.057	0.004
K2	ε2	7.8	0.0748	15.88	50.529	0.063	0.003
K2	λ1	7.8	0.0446	15.76	50.154	0.098	0.006
K2	λ2	7.8	0.0449	15.76	50.158	0.092	0.006
K2	N3-1	7.8	0.0402	15.72	50.052	0.095	0.006
K2	N3-2	7.9	0.0404	15.75	50.104	0.098	0.006
K2	N4-1	7.8	0.0224	15.93	50.725	0.069	0.007
K2	N4-2	8.0	0.0225	15.85	50.429	0.081	0.007
K2	η1	8.0	0.1198	157.22	50.225	0.072	0.005
K2	η2	7.9	0.1197	157.07	50.167	0.086	0.004
pH1	KS4-1	7.5	0.1724	4.00	50.891	0.005	0.000
pH1	KS4-2	7.7	0.1723	4.02	51.171	0.004	0.000
pH1	KS5-1	7.7	0.0775	3.95	50.203	0.013	0.009
pH1	KS5-1	7.7	0.0776	3.95	50.206	0.014	0.007

GQtzC

Set	Sample	pH _A	g	μM	mL	wt%	μmol	μmol
			mass1	Cu _i	volume	%Fe	Cu _A	Cu _D
STAR99	β1	7.90	0.2117	0.97	50.036	0.13	0.000	0.000
STAR99	β2	7.90	0.2115	0.97	50.077	0.13	0.000	0.000
STAR99	γ1	7.88	0.1409	0.97	50.054	0.13	0.000	0.000
STAR99	γ2	7.97	0.1409	0.97	50.029	0.13	0.000	0.000
STAR99	δ1	7.95	0.0706	0.97	50.127	0.13	0.000	0.000
STAR99	δ2	7.97	0.0705	0.97	50.153	0.13	0.000	0.000
STAR99	ε1	7.88	0.0355	0.97	49.985	0.13	0.007	0.000
STAR99	ε2	7.92	0.0356	0.97	50.239	0.13	0.008	0.000
STAR99	ζ1	7.90	0.0281	0.97	50.104	0.13	0.010	0.000
STAR99	ζ2	7.88	0.0280	0.97	50.002	0.13	0.011	0.000
STAR99	η1	7.78	0.0944	16.16	50.201	0.13	0.028	0.012
STAR99	η2	7.71	0.0943	16.16	50.199	0.13	0.027	0.009
STAR99	θ1	7.73	0.0392	16.10	50.006	0.13	0.028	0.009
STAR99	θ2	7.74	0.0394	16.15	50.153	0.13	0.028	0.013
STAR99	κ1	7.80	0.4230	0.97	50.013	0.13	0.000	0.000

			g	μM	mL	wt%	μmol	μmol
STAR99	$\kappa 2$	7.87	0.4229	0.97	50.015	0.13	0.000	0.000
STAR99	S5	7.02	0.4970	39.56	50.234	0.13	0.227	x
pH set 2	S5-1	7.8	0.0994	0.40	50.235	0.13	0.000	0.000
pH set 2	S5-2	7.8	0.0997	0.39	50.105	0.13	0.000	0.000
fill set 1	M2-1	7.6	0.0475	0.97	50.013	0.13	0.007	0.000
fill set 1	M2-2	7.7	0.0475	0.97	50.090	0.13	0.007	0.000
fill set 1	$\lambda 1$	7.6	0.0211	0.97	49.914	0.13	0.013	0.005
fill set 1	$\lambda 2$	7.6	0.0211	0.97	49.992	0.13	0.014	0.004

GKaoC

			g	μM	mL	wt%	μmol	μmol
Set	Sample	pH _A	mass1	Cu _i	volume	%Fe	Cu _A	Cu _D
F99	N1-1	7.4	0.0474	0.99	49.985	1.26	0.000	0.000
F99	N1-2	7.4	0.0472	0.99	49.987	1.26	0.000	0.000
F99	$\gamma 1$	7.1	0.1185	15.84	50.005	1.26	0.018	0.000
F99	$\gamma 2$	7.1	0.1183	15.80	50.132	1.26	0.023	0.000
SSRL00	S1	7.22	0.1998	15.68	49.996	1.26	0.051	x
SSRL00	S5	7.02	0.1248	78.66	124.995	1.26	0.030	x
GK2	N1-1	7.53	0.0473	0.94	50.021	1.26	0.000	0.000
GK2	N1-2	7.41	0.0477	0.95	50.417	1.26	0.000	0.000
GK2	$\gamma 1$	7.74	0.1182	15.77	50.024	1.26	0.000	0.000
GK2	$\gamma 2$	7.77	0.1186	15.77	50.010	1.26	0.000	0.007
GK2	N2-1	7.33	0.0318	16.06	51.075	1.26	0.106	0.017
GK2	N2-2	7.31	0.0316	15.77	50.032	1.26	0.100	0.012
GK2	$\epsilon 1$	7.26	0.0295	15.77	50.065	1.26	0.117	0.012
GK2	$\epsilon 2$	7.28	0.0296	15.96	50.708	1.26	0.121	0.016
GK2	$\lambda 1$	7.25	0.0178	15.80	50.077	1.26	0.149	0.022
GK2	$\lambda 2$	7.22	0.0177	16.01	50.766	1.26	0.170	0.052
GK2	N3-1	7.10	0.0154	15.91	50.532	1.26	0.187	0.022
GK2	N3-2	7.33	0.0155	15.78	50.167	1.26	0.142	0.030
GK2	N4-1	7.33	0.0889	157.34	50.085	1.26	0.122	0.070
GK2	N4-2	7.40	0.0890	157.44	50.047	1.26	0.115	0.055
GK2	$\eta 1$	7.52	0.0473	157.55	50.008	1.26	0.020	0.020
GK2	$\eta 2$	7.62	0.0473	157.43	50.054	1.26	0.027	0.027
pH2	GKS1-1	7.8	0.1000	0.39	50.006	1.26	0.000	0.000
pH2	GKS1-2	7.8	0.1002	0.39	50.017	1.26	0.000	0.000
pH2	GKS2-1	7.8	0.0332	0.40	50.324	1.26	0.000	0.000
pH2	GKS2-2	7.8	0.0332	0.39	50.061	1.26	0.000	0.000
pH2	GKS3-1	7.7	0.1665	0.39	50.024	1.26	0.000	0.000
pH2	GKS3-2	7.7	0.1664	0.40	50.389	1.26	0.000	0.000
pH2	GKS4-1	7.7	0.1111	0.39	50.085	1.26	0.000	0.000
pH2	GKS4-2	7.8	0.1110	0.39	50.022	1.26	0.000	0.000
pH2	GKS5-1	7.8	0.0498	0.39	50.073	1.26	0.000	0.000
pH2	GKS5-2	7.7	0.0501	0.39	50.046	1.26	0.000	0.000

GKaoC_{thick}

Set	Sample	pH _A	g		μM	mL	wt%	μmol	μmol
			mass1	Cu _i	volume	%Fe	Cu _A	Cu _D	
F00	N1-1	7.5	0.0163	0.97	50.254	11.37	0.000	0.000	
F00	N1-2	7.7	0.0162	0.96	50.124	11.37	0.000	0.000	
F00	γ1	7.6	0.0392	15.92	49.985	11.37	0.000	0.000	
F00	γ2	7.5	0.0393	15.93	50.016	11.37	0.000	0.000	
F00	N2-1	7.5	0.0106	15.91	50.031	11.37	0.040	0.009	
F00	N2-2	7.6	0.0108	15.90	49.958	11.37	0.043	0.006	
F00	ε1	7.0	0.0978	157.83	49.929	11.37	0.102	0.022	
F00	ε2	7.1	0.0978	157.86	50.091	11.37	0.096	0.021	
F00	λ1	7.1	0.0589	157.83	50.015	11.37	0.046	0.057	
F00	λ2	7.2	0.0589	158.11	50.114	11.37	0.052	0.046	
F00	N3-1	7.2	0.0527	158.17	50.085	11.37	0.057	0.043	
F00	N3-2	7.2	0.0524	158.02	50.069	11.37	0.103	0.039	
F00	M1-1	7.2	0.0375	157.76	50.047	11.37	0.045	0.039	
F00	M1-2	7.2	0.0373	158.70	50.338	11.37	0.052	0.035	
F00	N4-1	7.2	0.0292	158.36	50.093	11.37	0.066	0.041	
F00	N4-2	7.2	0.0291	159.10	50.366	11.37	0.049	0.041	

GKaoP

Set	Sample	pH _A	g		m ² g ⁻¹	m ²	μM	mL	μmol	μmol
			mass1	mass2	SSA2	SA2	Cu _i	volume	Cu _A	Cu _D
S00	N1-1	7.46	0.0018	0.1985	7.90	1.57	3.92	50.156	0.005	0.005
S00	N1-2	7.51	0.0017	0.1986	7.90	1.57	3.96	50.188	0.004	0.000
S00	γ1	7.57	0.0009	0.1176	7.90	0.93	11.25	49.958	0.013	0.007
S00	γ2	7.60	0.0010	0.1175	7.90	0.93	11.32	50.967	0.012	0.004
S00	N2-1	7.16	0.0012	0.1589	7.90	1.26	80.66	50.163	0.163	0.052
S00	N2-2	7.14	0.0013	0.1589	7.90	1.26	80.36	49.941	0.169	0.050
S00	ε1	7.11	0.0010	0.1470	7.90	1.16	80.50	50.112	0.166	0.067
S00	ε2	7.09	0.0012	0.1467	7.90	1.16	80.38	50.071	0.173	0.060
S00	λ1	7.61	0.0015	0.1763	7.90	1.39	154.32	50.645	0.105	0.125
S00	λ2	7.33	0.0014	0.1761	7.90	1.39	151.93	49.915	0.181	0.110
S00	N3-1	7.16	0.0017	0.1587	7.90	1.25	152.11	50.003	0.224	0.078
S00	N3-2	7.16	0.0013	0.1586	7.90	1.25	152.78	50.212	0.220	0.110
S00	N4-1	7.53	0.0008	0.0829	7.90	0.65	152.60	50.105	0.091	0.185
S00	N4-2	7.60	0.0010	0.0829	7.90	0.65	153.55	50.430	0.092	x
S00	η1	7.23	0.0004	0.0470	7.90	0.37	152.85	50.201	0.206	0.186
S00	η2	7.25	0.0004	0.0475	7.90	0.38	153.16	50.256	0.185	0.262

GQtzP

Set	Sample	pH _A	g	g	m ² g ⁻¹	m ²	μM	mL	μmol	μmol
			mass1	mass2	SSA2	SA2	Cu _i	volume	Cu _A	Cu _D
S00	N1-1	7.56	0.0019	2.3718	0.48	1.14	0.95	125.275	0.000	0.000
S00	N1-2	7.59	0.0019	2.3718	0.48	1.14	0.95	125.111	0.000	0.000
S00	γ1	7.70	0.0013	1.4727	0.48	0.71	3.95	125.049	0.240	0.019
S00	γ2	7.78	0.0012	1.4729	0.48	0.71	3.95	125.222	0.254	0.021
S00	N2-1	7.61	0.0012	1.5881	0.48	0.76	15.78	125.026	0.177	0.019
S00	N2-2	7.74	0.0013	1.5882	0.48	0.76	16.02	126.917	0.149	0.018
S00	ε1	7.61	0.0012	1.4739	0.48	0.71	15.80	125.206	0.219	0.019
S00	ε2	7.45	0.0012	1.4740	0.48	0.71	15.78	125.041	0.306	0.015
S00	λ1	7.69	0.0014	1.7692	0.48	0.85	31.56	125.069	0.135	0.020
S00	λ2	7.70	0.0015	1.7690	0.48	0.85	31.57	125.087	0.134	0.018
S00	N3-1	7.65	0.0013	1.5885	0.48	0.76	31.58	125.146	0.127	0.019
S00	N3-2	7.70	0.0013	1.5889	0.48	0.76	31.19	123.601	0.132	0.020
S00	N4-1	7.73	0.0018	2.2115	0.48	1.06	80.26	125.479	0.123	0.060
S00	N4-2	7.80	0.0017	2.2112	0.48	1.06	81.79	127.198	0.109	0.061
S00	η1	7.80	0.0010	1.1796	0.48	0.57	80.38	125.072	0.109	0.041
S00	η2	7.79	0.0011	1.1797	0.48	0.57	80.51	125.148	0.130	0.084
fill1	κ1	7.9	0.0005	0.4233	0.48	0.20	13.43	50.052	0.051	0.054
fill1	κ2	7.7	0.0005	0.4235	0.48	0.20	13.42	50.051	x	0.053
fill1	S2-1	7.9	0.0005	0.6618	0.48	0.32	13.59	50.658	0.049	0.057
fill1	S2-2	8.0	0.0005	0.6621	0.48	0.32	13.70	51.014	0.049	0.059
fill1	M2-1	7.9	0.0005	0.3972	0.48	0.19	13.43	50.001	0.065	0.055
fill1	M2-2	7.9	0.0005	0.3973	0.48	0.19	13.47	50.191	0.062	0.068

APPENDIX 4

Spline-fit data

Splines were generated to fit the bulk goethite data using the "XIXtrFun" SPLINE add-in function for Microsoft Excel (source: www.netrax.net/~jdavita/XIXtrFun/XIXtrFun.htm). The x-axis range was divided into one or more sets of equal increments and the spline function was calculated using a set of nodes chosen through trial and error. The number of increments and nodes is given in the first table below; the subsequent tables contain the coordinates of the calculated spline points.

Dataset	Number of points	Number of nodes
θ vs. CU_{TOT} (adsorption)	90	23
θ vs. CU_{TOT} (desorption)	88	19
C_s vs. C_A	61	13
C_s vs. C_D	63	5

 C_s vs. C_A

X	Spline pt
0.00	0.0098
0.00	0.0166
0.00	0.0279
0.00	0.0297
0.00	0.0589
0.00	0.0873
0.00	0.2001
0.00	0.2199
0.00	0.3371
0.05	0.6579
0.09	1.0205
0.13	1.2953
0.17	1.4675
0.21	1.5623

X	Spline pt
0.25	1.6056
0.30	1.6180
0.34	1.6121
0.38	1.5999
0.42	1.5929
0.46	1.5948
0.50	1.6005
0.54	1.6059
0.59	1.6105
0.63	1.6143
0.67	1.6173
0.71	1.6198
0.75	1.6217
0.79	1.6231

X	Spline pt
0.84	1.6241
0.88	1.6248
0.92	1.6253
0.96	1.6257
1.00	1.6260
1.04	1.6264
1.08	1.6268
1.13	1.6274
1.17	1.6284
1.21	1.6296
1.25	1.6313
1.29	1.6336
1.33	1.6364
1.38	1.6399

X	Spline pt
1.42	1.6442
1.46	1.6493
1.50	1.6553
1.54	1.6624
1.58	1.6705
1.62	1.6799
1.67	1.6905

X	Spline pt
1.71	1.7024
1.75	1.7177
1.79	1.7426
1.83	1.7832
1.87	1.8371
1.92	1.8982
1.96	1.9605

X	Spline pt
2.00	2.0182
2.04	2.1008
2.08	2.2022
2.12	2.3972
2.16	3.4311
2.17	3.4957

 C_s vs. C_D

X	Spline pt
0.00	0.0098
0.00	0.0166
0.00	0.0279
0.00	0.0297
0.00	0.0589
0.00	0.0873
0.00	0.2001
0.00	0.2199
0.00	0.3371
0.00	0.6579
0.04	1.3309
0.06	1.4024
0.09	1.4726
0.11	1.5405
0.14	1.6049
0.16	1.6656
0.19	1.7232
0.21	1.7784
0.24	1.8321
0.26	1.8849
0.29	1.9376
0.31	1.9909

X	Spline pt
0.34	2.0456
0.36	2.1016
0.39	2.1585
0.41	2.2157
0.44	2.2727
0.47	2.3289
0.49	2.3839
0.52	2.4371
0.54	2.4883
0.57	2.5376
0.59	2.5851
0.62	2.6308
0.64	2.6748
0.67	2.7172
0.69	2.7580
0.72	2.7972
0.74	2.8349
0.77	2.8712
0.79	2.9062
0.82	2.9398
0.84	2.9722
0.87	3.0034

X	Spline pt
0.89	3.0335
0.92	3.0625
0.94	3.0905
0.97	3.1175
0.99	3.1436
1.02	3.1689
1.04	3.1933
1.07	3.2171
1.10	3.2402
1.12	3.2627
1.15	3.2846
1.17	3.3060
1.20	3.3270
1.22	3.3476
1.25	3.3679
1.27	3.3879
1.30	3.4077
1.32	3.4274
1.35	3.4470
1.36	3.4574

θ vs. Cu_{TOT} (adsorption)

X	Spline pt
0.010	1.0000
0.017	1.0000
0.028	1.0000
0.030	1.0000
0.059	1.0000
0.087	1.0000
0.200	1.0000
0.220	1.0000
0.337	1.0000
0.434	0.9997
0.530	0.9991
0.627	0.9983
0.724	0.9974
0.820	0.9964
0.917	0.9955
1.014	0.9949
1.110	0.9944
1.207	0.9928
1.303	0.9921
1.400	0.9800
1.497	0.9700
1.593	0.9734
1.690	0.9791
1.787	0.9831
1.883	0.9858
1.980	0.9874
2.076	0.9882
2.173	0.9885
2.270	0.9885
2.366	0.9882
2.463	0.9877

X	Spline pt
2.560	0.9873
2.656	0.9870
2.753	0.9868
2.850	0.9866
2.946	0.9865
3.043	0.9864
3.139	0.9864
3.236	0.9864
3.333	0.9865
3.429	0.9866
3.526	0.9867
3.623	0.9868
3.719	0.9869
3.816	0.9869
3.912	0.9870
4.009	0.9872
4.106	0.9873
4.202	0.9874
4.299	0.9875
4.396	0.9876
4.492	0.9878
4.589	0.9879
4.686	0.9880
4.782	0.9882
4.879	0.9884
4.975	0.9885
5.072	0.9887
5.169	0.9889
5.265	0.9891
5.362	0.9893
5.459	0.9895

X	Spline pt
5.555	0.9898
5.652	0.9900
5.748	0.9902
5.845	0.9905
5.942	0.9908
6.038	0.9910
6.135	0.9913
6.232	0.9915
6.328	0.9918
6.425	0.9921
6.521	0.9924
6.618	0.9927
6.715	0.9929
6.811	0.9932
6.908	0.9935
7.005	0.9938
7.101	0.9941
7.198	0.9944
7.295	0.9947
7.391	0.9949
7.488	0.9952
7.584	0.9955
7.681	0.9958
7.778	0.9960
7.874	0.9963
7.971	0.9965
8.068	0.9968
8.164	0.9970
19.336	0.9956

θ vs. Cu_{TOT} (desorption)

X	Spline pt
0.010	1.0000
0.017	1.0000
0.028	1.0000
0.030	1.0000
0.059	1.0000
0.087	1.0000
0.200	1.0000
0.220	1.0000
0.337	1.0000
0.660	1.0000
0.756	1.0000
0.853	1.0000
0.950	1.0000
1.046	1.0000
1.143	1.0000
1.240	0.9996
1.336	0.9979
1.433	0.9956
1.529	0.9933
1.626	0.9920
1.723	0.9926
1.819	0.9944
1.916	0.9964
2.013	0.9978
2.109	0.9979
2.206	0.9976
2.303	0.9974
2.399	0.9972
2.496	0.9970
2.592	0.9966

X	Spline pt
2.689	0.9962
2.786	0.9957
2.882	0.9952
2.979	0.9946
3.076	0.9940
3.172	0.9934
3.269	0.9928
3.365	0.9923
3.462	0.9918
3.559	0.9914
3.655	0.9911
3.752	0.9909
3.849	0.9908
3.945	0.9907
4.042	0.9907
4.139	0.9908
4.235	0.9909
4.332	0.9910
4.428	0.9912
4.525	0.9914
4.622	0.9917
4.718	0.9920
4.815	0.9922
4.912	0.9925
5.008	0.9928
5.105	0.9931
5.201	0.9934
5.298	0.9936
5.395	0.9939
5.491	0.9941

X	Spline pt
5.588	0.9943
5.685	0.9945
5.781	0.9947
5.878	0.9949
5.974	0.9951
6.071	0.9952
6.168	0.9954
6.264	0.9955
6.361	0.9956
6.458	0.9957
6.554	0.9958
6.651	0.9959
6.748	0.9960
6.844	0.9961
6.941	0.9962
7.037	0.9963
7.134	0.9963
7.231	0.9964
7.327	0.9964
7.424	0.9965
7.521	0.9965
7.617	0.9966
7.714	0.9966
7.810	0.9966
7.907	0.9967
8.004	0.9967
8.100	0.9967
8.197	0.9968
19.336	0.9942

APPENDIX 5

Derivation of partitioning coefficients for additive models

The partitioning coefficient (K_d) for a metal that may either adsorb to a solid surface or remain in solution is defined as the ratio of adsorbed to dissolved metal:

$$K_d = \frac{C_s}{C_A} = \frac{\{\equiv \text{SOMe}^+\}}{[\text{Me}(\text{aq})]},$$

where $\{\equiv \text{SOMe}^+\}$ represents the sum of all surface species (see Chapter 3 for details). This was chosen for use as a proxy value for the apparent equilibrium coefficient in modeling Cu(II) uptake by the coated solids additively.

The aqueous speciation model MINTEQA2 was used to emulate the subset of the aqueous speciation reactions accounting for adsorption of Cu(II) on the goethite and quartz or kaolinite surface: i.e., the competitive adsorption of aqueous Cu(II) by two "anions" representing goethite surface sites and substrate (quartz or kaolinite) surface sites. For this purpose, three mock components were chosen: Ba^{2+} for Cu^{2+} , and Br^- and F^- for the unoccupied goethite and substrate surfaces, respectively. This selection of unreactive mock components was necessary in order to isolate the surface complexation reactions from other competitive aqueous speciation reactions occurring during the uptake phase of the batch experiments. Several "test" examples with these components present in solution were run through the MINTEQA2 routine in order to verify their suitability for this purpose. Next, two mock species were defined: " BaBr^+ " and " BaF^+ ."

In order to use MINTEQA2 to model additivity, the quantities entered must be expressed in units comparable to molarity (mol L^{-1}). Cu_{TOT} , C_A , and C_s are easily expressed in molar units, and [goethite] and [substrate] were expressed as $\text{m}^2 \text{L}^{-1}$. Using these units, K_d was calculated. It was then necessary to come up with a value for the equilibrium coefficient for each sample loading. Since the precise loadings sampled in the coated solids systems were not replicated in the goethite, quartz, and kaolinite systems, a method for interpolating their values was needed.

K_d was calculated for each goethite, quartz, and kaolinite sample using the equation above. These values were then plotted against Cu_{TOT} (Figure A.1). From established principles of surface chemistry, it was expected that these plots would show a constant and high value for K_d at the lowest Cu_{TOT} where sorption to high-affinity sites is expected to dominate ("HAS"). However, because the solids removed all detectable Cu from solution during high-affinity-site adsorption, K_d values could not be calculated for this region and thus are not shown in these plots (Figure A.1); note that this constant, high- K_d behavior was not seen for quartz, suggesting that HAS sorption never dominates Cu(II) uptake for the range of Cu_{TOT} studied.

The HAS region is followed by one where K_d continually decreases as Cu_{TOT} increases, which corresponds wholly or partially to the MAS regions observed in the Cu(II) uptake plots (i.e., Langmuir and isotherm plots). This in turn is followed by a region of relatively constant K_d in the OLG region in goethite, and in quartz by a region where K_d increased linearly and more gradually in OLG than in MAS. In kaolinite, a change in the slope of decreasing K_d with increasing Cu_{TOT} was observed past the middle

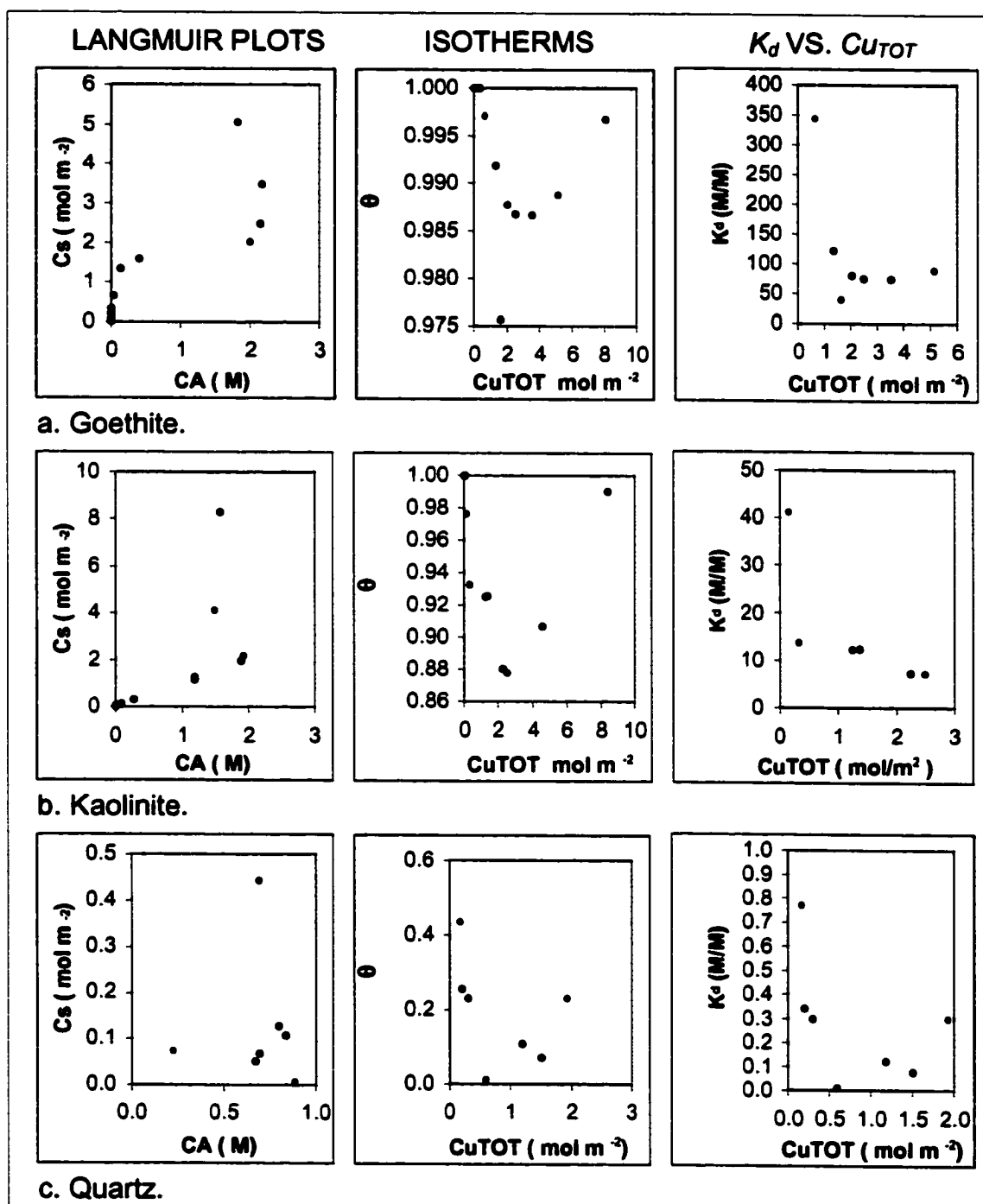


FIGURE A.1. Illustration of how trends in adsorption with loading correspond between the Langmuir plots, isotherms, and K_d vs. Cu_{TOT} plots for goethite, kaolinite, and quartz. Red, blue, and green dots indicate the same samples in each plot for each solid (but do not fall at the same loadings for all three solids).

MAS ranges. Lastly, at the highest loadings, K_d rapidly increases with Cu_{TOT} , reflecting the formation of surface precipitates, and in the case of kaolinite, also the region of oligomer formation (data not shown).

K_d was interpolated within each observed linear range either by using a best-fit linear equation, where the slope was positive or negative, or by calculating an average value for K_d where it appeared to be relatively constant (Figure A.2). For the HAS region for goethite and kaolinite, the value observed for the lowest Cu loading where detectable Cu remained in solution after adsorption was used to derive a minimum value for HAS K_d . The method described in Balistrieri and Murray (1983) for deriving " K_d " (apparent equilibrium coefficient) for Cu(II) uptake on goethite in the HAS region was also applied to the goethite data and yielded comparable results. An interpolated value for K_d was then calculated for each sample loading and used as the apparent equilibrium coefficient for the $Ba^{2+} + Br^- = BaBr^+$ or $Ba^{2+} + F^- = BaF^+$ reactions, as appropriate.

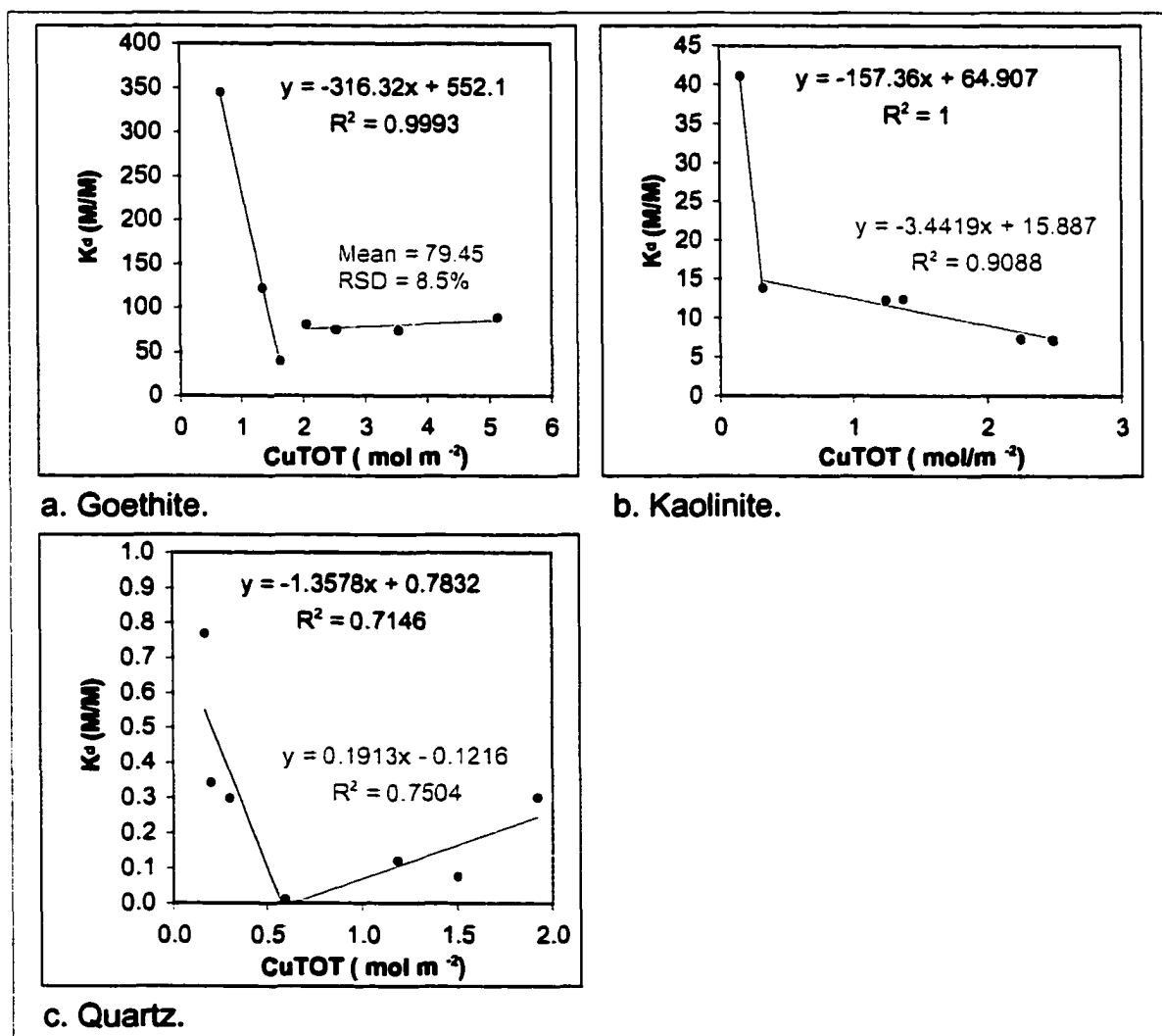


FIGURE A.2. Regions of K_d vs. Cu_{TOT} used to calculate interpolated values for additive modeling of Cu(II) uptake on coated solids.

In order to verify the validity of the derived expressions for K_d , the values for loadings less than $2.50 \mu\text{mol m}^{-2}$ were used to back-calculate values for C_s , C_A and θ for each solid. Differences between the values predicted by K_d and the actual values were calculated and averaged over the data range used in the additivity models in this study ($Cu_{TOT} < 2.50 \mu\text{mol m}^{-2}$). The results are shown in Table A.1. The absolute error is small in all cases. In addition, adsorption Langmuir isotherms constructed from these model K_d functions generally track the data and have the general forms shown in Figure 26 (Chapter 3).

TABLE A.1. K_d -predicted vs. actual values for goethite, quartz, and kaolinite.

Solid		K_d (M/M)	C_s ($\mu\text{mol m}^{-2}$)	C_A (μM)	θ
Goethite	Mean	-0.0629	-0.0008	0.0130	-0.0004
	S.D.	3.4211	0.0016	0.0181	0.0010
Quartz	Mean	0.0069	0.0057	-0.0143	0.0002
	S.D.	0.1245	0.0515	0.0445	0.0672
Kaolinite	Mean	-0.1573	0.0024	-0.0035	0.0002
	S.D.	0.7086	0.0119	0.0980	0.0062

LITERATURE CITED

- Alcacio T. E., Hesterberg D., Chou J. W., Martin J. D., Beauchemin S., and Sayers D. E. (2001) Molecular scale characteristics of Cu(II) bonding in goethite-humate complexes. *Geochimica et Cosmochimica Acta* **65**(9), 1355-1366.
- Allison, J.D.; Brown, D.S.; Novo-Gradac, K.J. MINTEQA2/PRODEFA2, A geochemical assessment model for environmental systems: Version 3.0 users manual: U.S. Environmental Protection Agency: Athens, GA, 1991: EPA/600/3-91/021. Program available at URL www.epa.gov/ceampubl/mmedia/minteq/index.htm.
- Anderson P. R. and Benjamin M. M. (1990) Modeling adsorption in aluminum-iron oxide binary suspensions. *Environmental Science and Technology* **24**, 1586-1592.
- Anderson P. R. and Benjamin M. M. (1990) Surface and bulk characteristics of binary oxide suspension. *Environmental Science and Technology* **24**, 692-698.
- Arias M., Barral M. T., and Diaz-Fierros F. (1993) Effects of iron and aluminum oxides on the colloidal and surface properties of kaolin. *Clays and Clay Minerals* **43**(4), 406-416.
- Baes C. F. I. and Mesmer R. E. (1976) *The Hydrolysis of Cations*. John Wiley and Sons.
- Balistrieri L. S. and Murray J. W. (1982) The adsorption of Cu, Pb, Zn, and Cd on goethite from major ion seawater. *Geochimica et Cosmochimica Acta* **46**, 1253-1265.
- Balistrieri L. S. and Murray J. W. (1983) Metal-solid interactions in the marine environment: estimating apparent equilibrium binding constants. *Geochimica et Cosmochimica Acta* **47**, 1091-1098.
- Balistrieri L. S. and Murray J. W. (1984) Marine scavenging: Trace metal adsorption by interfacial sediment from MANOP Site H1. *Geochimica et Cosmochimica Acta* **48**, 921-929.
- Barrow N. J., Bowden J. W., Posner A. M., and Quirk J. P. (1981) Describing the adsorption of copper, zinc and lead on a variable charge mineral surface. *Australian Journal of Soil Research* **19**, 309-321.
- Benedetti M. F., van Riemsdijk W. H., Koopal L. K., Kinniburgh D. G., Goody D. C., and Milne C. J. (1996) Metal ion binding by natural organic matter: From the model to the field. *Geochimica et Cosmochimica Acta* **60**(14), 2503-2513.
- Benjamin M. M. and Leckie J. O. (1980) Adsorption of metals at oxide interfaces: effects of the concentrations of adsorbate and competing metals. In *Contaminants and Sediments: Analysis, Chemistry, Biology*, Vol. 2 (ed. R. A. Baker), pp. 305-322. Ann Arbor Science Publishers Inc.
- Benjamin M. M. and Leckie J. O. (1981) Multiple-site adsorption of Cd, Cu, Zn, and Pb on amorphous iron oxyhydroxide. *Journal of Colloid and Interface Science* **79**(1), 209-221.

- Bertsch, P.M. and J.C. Seaman (1999) Characterization of complex mineral assemblages: implications for contaminant transport and environmental remediation. *Proc. Nat. Acad. Sci.* **96**, 3350-3357.
- Bourg A. C. M. (1987) Trace metal adsorption modelling and particle-water interactions in estuarine environments. *Continental Shelf Research* **7**(11/12), 1319-1332.
- Boymel P. M., Weiner E. R., and Goldberg M. C. (1981) Solid-solid sorption mechanisms for iron oxide coatings on quartz and kaolinite. U.S. Geological Survey Professional Paper P1275, 150-151.
- Brown G. E., Jr., Henrich V. E., Casey W. H., Clark D. L., Eggleston C., Felmy A., Goodman D. W., Grätzel M., Maciel G., McCarthy M. I., Neilson K. H., Sverjensky D. A., Toney M. F., and Zachara J. M. (1999) Metal oxide surfaces and their interactions with aqueous solutions and microbial organisms. *Chemical Reviews* **99**(1), 77-174.
- Brown G. E., Jr., Parks G. A., and O'Day P. A. (1995) Sorption at mineral-water interfaces: macroscopic and microscopic perspectives. In *Mineral Surfaces* (ed. D. J. Vaughan and R. A. D. Patrick), pp. 129-183. Chapman and Hall.
- Bryan G. W., Gibbs P. E., Hummerstone L. G., and Burt G. R. (1987) Copper, zinc, and organotin as long-term factors governing the distribution of organisms in the Fal Estuary in southwest England. *Estuaries* **10**(3), 208-219.
- Bryan G. W. and Langston W. J. (1992) Bioavailability, accumulation and effects of heavy metals in sediments with special reference to United Kingdom estuaries: a review. *Environmental Pollution* **76**, 89-131.
- Buffle J. and Altmann R. S. (1987) Interpretation of metal complexation by heterogeneous complexants. In *Aquatic Surface Chemistry: Chemical Processes at the Particle-Water Interface* (ed. W. Stumm), pp. 351-383. John Wiley & Sons, Inc.
- Charlet L. and Manceau A. (1992) X-ray adsorption spectroscopic study of the sorption of Cr(II) at the oxide/water interface. II. Adsorption, coprecipitation and surface precipitation on ferric hydrous oxides. *Journal of Colloid and Interface Science* **148**, 25-442.
- Cheah S.-F., Brown G. E., Jr., and Parks G. A. (1998) XAFS spectroscopy of Cu(II) sorption on amorphous SiO₂ and g-Al₂O₃: effect of substrate and time on sorption complexes. *Journal of Colloid and Interface Science* **208**, 110-128.
- Chisholm-Brause C. J., Hayes K. F., Roe A. L., Gordon E. Brown J., Parks G. A., and Leckie J. O. (1990) Spectroscopic investigation of Pb(II) complexes at the g-Al₂O₃/water interface. *Geochimica et Cosmochimica Acta* **54**(7), 1897-1909.
- Chisholm-Brause C. J. (1997) Clay size fractionation and cleanup procedure. Personal written communication. September: Gloucester Point, VA.
- Christl I. and Kretzchmar R. (1999) Competitive sorption of copper and lead at the oxide-water interface: Implications for surface site density. *Geochimica et Cosmochimica Acta* **63**(19/20), 2929-2938.
- Collins C. R., Ragnarsdottir K. V., and Sherman D. M. (1999) Effect of inorganic and organic ligands on the mechanism of cadmium sorption to goethite. *Geochimica et Cosmochimica Acta* **63**(19/20), 2989-3002.

- Conrad C. F., Chisholm-Brause C. J., and Kelley M. J. (2002) Pb(II) sorption onto γ - Al_2O_3 surfaces at the oxide-water interface: a novel approach using planar oxides. *Journal of Colloid and Interface Science* **248**, 275-282.
- Coston J. A., Fuller C. C., and Davis J. A. (1995) Pb²⁺ and Zn²⁺ adsorption by a natural aluminum- and iron-bearing surface coating on an aquifer sand. *Geochimica et Cosmochimica Acta* **59**(17), 3535-3547.
- Cowan C. E., Zachara J. M., and Resch C. T. (1991) Cadmium adsorption on iron oxides in the presence of alkaline-earth elements. *Environmental Science and Technology* **25**, 437-446.
- Davies-Colley R. J., Nelson P. O., and Williamson K. J. (1984) Copper and cadmium uptake by estuarine sedimentary phases. *Environmental Science and Technology* **18**(7), 491-499.
- Davis J. A. (1984) Complexation of trace metals by adsorbed natural organic matter. *Geochimica et Cosmochimica Acta* **48**, 679-691.
- Davis J. A., Coston J. A., Kent D. B., and Fuller C. C. (1998) Application of the surface complexation concept to complex mineral assemblages. *Environmental Science and Technology* **32**(19), 2820-2828.
- Davis J. A. and Gloor R. (1981) Adsorption of dissolved organics in lakewater by aluminum oxide: Effect of molecular weight. *Environmental Science and Technology* **15**, 1223-1229.
- Davis J. A. and Kent D. B. (1990) Surface complexation modeling in aqueous geochemistry. In *Mineral-Water Interface Geochemistry*, Vol. 23 (ed. M. F. Hochella and A. F. White), pp. 177-260. Mineralogical Society of America.
- De Vitre R., Belzile N., and Tessier A. (1991) Speciation and adsorption of arsenic on diagenetic iron oxyhydroxides. *Limnology and Oceanography* **36**(7), 1480-1483.
- Dzombak D. A. and Morel F. M. M. (1990) *Surface Complexation Modeling: Hydrous Ferrous Oxide*. John Wiley & Sons, Inc.
- Edwards M., Benjamin M., and Ferguson J. (1989) New approaches to treatment of metal-bearing wastes. *43rd Industrial Waste Conference*, 389-396.
- Elzinga E. J., Peak D., and Sparks D. (2001) Spectroscopic studies of Pb(II)-sulfate interactions at the goethite-water interface. *Geochimica et Cosmochimica Acta* **65**(14), 2219-2230.
- Goldstein J. I., Newbury D. E., Echlin P., Joy D. C., Romig A. D., Jr., Lyman C. E., Fiori C., and Lifshin E. (1992) *Scanning Electron Microscopy and X-Ray Microanalysis: a Text for Biologists, Materials Scientists, and Geologists*. Plenum Press.
- Gregg S. J. and Sing K. S. W. (1982) *Adsorption, surface area and porosity*. Academic Press, Inc.
- Head P. C. (1985) *Practical Estuarine Chemistry: A Handbook*. Cambridge University Press.
- Hiemenz P. C. and Rajagopalan R. (1997) *Principles of Colloid and Surface Chemistry*. Marcel Dekker, Inc.

- Hiemstra T., Venema P., and Van Riemsdijk W. H. (1996) Intrinsic proton affinity of reactive surface groups of metal (hydr)oxides: the bond valence principle. *Journal of Colloid and Interface Science* **184**, 680-692.
- Holmén B. A. and Gschwend P. M. (1997) Estimating sorption rates of hydrophobic organic compounds in iron oxide- and aluminosilicate clay-coated aquifer sands. *Environmental Science and Technology* **31**, 105-113.
- Honeyman B. D. (1984) Cation and anion adsorption at the oxide-solution interface in systems containing binary mixtures of adsorbents: an investigation of the concept of adsorptive additivity. Ph.D., Stanford University.
- Honeyman B. D., Balistrieri L. S., and Murray J. W. (1988) Oceanic trace metal scavenging: the importance of particle concentration. *Deep-Sea Research* **35**(2), 227-246.
- Honeyman B. D. and Santschi P. H. (1988) Metals in aquatic systems: predicting their scavenging residence time from laboratory data remains a challenge. *Environmental Science and Technology* **22**(8), 862-870.
- Huang C. and Yang Y.-L. (1995) Adsorption characteristics of Cu(II) on humus-kaolin complexes. *Water Research* **29**(11), 2455-2460.
- Ioannou A. and Dimirkou A. (1997) Phosphate adsorption on hematite, kaolinite, and kaolinite-hematite (k-h) systems as described by a constant capacitance model. *Journal of Colloid and Interface Science* **192**, 119-128.
- IXRF Systems Inc. (2002) *EDS 2000 User's Manual*. IXRF Systems, Inc.
- Jackson M. L., Lin C. F., and Zelazny L. W. (1986) Oxides, hydroxides, and aluminosilicates. In *Methods of Soil Analysis, Part I, Physical and Mineralogical Methods* (ed. A. Klute), pp. 101-159. American Society of Agronomy, Inc.
- Jackson T. A., West M. M., and Leppard G. G. (1999) Accumulation of heavy metals by individually analyzed bacterial cells and associated nonliving material in polluted lake sediments. *Environmental Science and Technology* **33**, 3795-3801.
- Johnson P. R., Sun N., and Elimelech M. (1996) Colloid transport in geochemically heterogeneous porous media: modeling and measurements. *30*(3284-3293).
- Jones A. A. and Saleh A. M. (1987) A study of the thickness of ferrihydrite coatings on kaolinite. *Mineralogical Magazine* **51**, 87-92.
- Katz L. E. and Hayes K. F. (1995) Surface complexation modeling I. Strategy for modeling monomer complex formation at moderate surface coverage. *Journal of Colloid and Interface Science* **170**, 477-490.
- Kogel, J.A. (2002). Electronic communication (March 19).
- Kogel, J.A. (2001). Electronic communication (February 19).
- Kretzschmar R., Holthoff H., and Sticher H. (1998): Influence of pH and humic acid on coagulation kinetics of kaolinite: A dynamic light scattering study. *Journal of Colloid and Interface Science* **202**, 95-103.
- Kubicki J. D., Itoh M. J., Schroeter L. M., and Apitz S. E. (1997) Bonding mechanisms of salicylic acid adsorbed onto illite clay: An ATR-FTIR and molecular orbital study. *Environmental Science and Technology* **31**, 1151-1156.
- Lai C. H., Lo S. L., and Lin C. F. (1994) Evaluating an iron-coated sand for removing copper from water. *Water Science and Technology* **30**, 175-182.

- Langmuir D. (1997) *Aqueous Environmental Geochemistry*. Prentice-Hall, Inc.
- Larsen O. and Postma D. (2001) Kinetics of reductive bulk dissolution of lepidocrocite, ferrihydrite, and goethite. *Geochimica et Cosmochimica Acta* **65**(9), 1367-1379.
- Lion L. W., Altmann R. S., and Leckie J. O. (1982) Trace-metal adsorption characteristics of estuarine particulate matter: Evaluation of contributions of Fe/Mn oxide and organic surface coatings. *Environmental Science and Technology* **16**(10), 660-666.
- Lofts S. and Tipping E. (1998) An assemblage model for cation binding by natural particulate matter. *Geochimica et Cosmochimica Acta* **62**, 2609-2625.
- Manceau A., Schlegel M. L., Musso M., Sole V. A., Gauthier C., Petit P. E., and Trolard F. (2000) Crystal chemistry of trace elements in natural and synthetic goethite. *Geochimica et Cosmochimica Acta* **64**(21), 3643-3661.
- Mann K. H. and Lazier J. R. N. (1991) *Dynamics of Marine Ecosystems*. Blackwell Scientific Publications, Inc.
- Mayer L. M. (1999) Extent of coverage of mineral surfaces by organic matter in marine sediments. *Geochimica et Cosmochimica Acta* **63**, 207-215.
- Meng X. and Letterman R. D. (1993) Effect of component oxide interaction on the adsorption properties of mixed oxides. *Environmental Science and Technology* **27**, 970-975.
- Meng X. and Letterman R. D. (1993) Modeling ion adsorption on aluminum hydroxide modified silica. *Environmental Science and Technology* **27**, 1924-1929.
- Millward G. E. and Turner A. (1995) Trace metals in estuaries. In *Trace Elements in Natural Waters* (ed. B. Salbu and S. E.), pp. 223-245. CRC Press, Inc.
- Morel F. M. M. and Hering J. G. (1993) *Principals and Applications of Aquatic Chemistry*. John Wiley & Sons, Inc.
- Morra M. J., Fendorf S. E., and Brown P. D. (1997) Speciation of sulfur in humic and fulvic acids using X-ray absorption near-edge structure (XANES) spectroscopy. *Geochimica et Cosmochimica Acta* **61**(11), 2223-2235.
- Müller B. and Sigg L. (1990) Interaction of trace metals with natural particle surfaces: comparison between adsorption experiments and field measurements. *Aquatic Science* **52**(1), 74-92.
- Murphy E. M., Zachara J. M., Smith S. C., Phillips J. L., and Wietsma T. W. (1994) Interaction of hydrophobic organic compounds with mineral-bound humic substances. *Environmental Science and Technology* **28**, 1291-1999.
- Nelson Y. M., Lo W., Lion L. W., Shuler M. L., and Ghiorse W. C. (1995) Lead distribution in a simulated aquatic environment: effects of bacterial biofilms and iron oxide. *Water Research* **29**(8), 1934-1944.
- O'Day P. A., Carroll S. A., and Waychunas G. A. (1998) Rock-water interactions controlling zinc, cadmium, and lead concentrations in surface waters and sediment, U.S. tri-state mining district. 1. Molecular identification using X-ray absorption spectroscopy. *Environmental Science and Technology* **32**, 943-955.
- O'Day P. A., Chisholm-Brause C. J., Towle S. N., Parks G. A., and Brown G. E., Jr. (1996) X-ray adsorption spectroscopy of Co(II) sorption complexes on quartz (α -SiO₂) and rutile (TiO₂). *Geochimica et Cosmochimica Acta* **60**(14), 2515-2532.

- Oakley S. M., Nelson P. O., and Williamson K. J. (1981) Model of trace-metal partitioning in marine sediments. *Environmental Science and Technology* 15(4), 474-480.
- Padmanabhan E. and Mermut A. R. (1996) Submicroscopic structure of Fe-coatings on quartz grains in tropical environments. *Clays and Clay Minerals* 44(6), 801-810.
- Powell, D.C. (1999). Personal communication.
- Randall S. R., Sherman D. M., Ragnarsdottir K. V., and Collins C. R. (1999) The mechanisms of cadmium surface complexation on iron oxyhydroxide minerals. *Geochimica et Cosmochimica Acta* 63(19/20), 2971-2987.
- Ransom B., Bennett R. J., Baerwald R., and Shea K. (1997) TEM study of in situ organic matter on continental shelf margins: occurrence and the "monolayer" hypothesis. *Marine Geology* 138, 1-9.
- Riedel G. F., Sanders J. G., and Osman R. W. (1997) Biogeochemical control on the flux of trace elements from estuarine sediments: water column oxygen concentrations and benthic infauna. *Estuarine, Coastal, and Shelf Science* 44, 23-38.
- Rietra R. P. J. J., Hiemstra T., and Van Riemsdijk W. H. (1999) The relationship between molecular structure and ion adsorption on variable charge minerals. *Geochimica et Cosmochimica Acta* 63(19/20), 3009-3015.
- Robertson A. P. and Leckie J. O. (1997) Cation binding predictions of surface complexation models: effects of pH, ionic strength, surface complex, and model fit. *Journal of Colloid and Interface Science* 188(2), 444-472.
- Robertson A. P. and Leckie J. O. (1998) Acid/base, copper binding, and $\text{Cu}^{2+}/\text{H}^+$ exchange properties of goethite, an experimental modeling study. *Environmental Science and Technology* 32, 2519-2530.
- Rule J. H. and Alden R. W. (1992) Partitioning of Cd in geochemical fractions of anaerobic estuarine sediments. *Estuarine, Coastal, and Shelf Science* 34, 487-499.
- Ryan J. N., Elimelech M., Ard R. A., Harvey R. W., and Johnson P. R. (1999) Bacteriophage PRD1 and silica colloid transport and recovery in an iron oxide-coated sand aquifer. *Environmental Science and Technology* 33, 63-73.
- Ryan J. N. and Gschwend P. M. (1992) Effects of iron diagenesis on the transport of colloidal clay in an unconfined sand aquifer. *Geochimica et Cosmochimica Acta* 56, 1507-1521.
- Saleh A. M. and Jones A. A. (1984) The crystallinity and surface characteristics of synthetic ferrihydrite and its relationship to kaolinite surfaces. *Clay Minerals* 19, 745-755.
- Salomons W., de Rooij N. M., Kerdik H., and Bril J. (1987) Sediments as a source for contaminants? *Hydrobiologia* 149, 13-30.
- Schindler P. W. and Stumm W. (1987) The surface chemistry of oxides, hydroxides, and oxide minerals. In *Aquatic Surface Chemistry: Chemical Processes at the Particle-Water Interface* (ed. W. Stumm), pp. 83-109. John Wiley & Sons, Inc.
- Schmitt J., Gu B., Shorer M., Flemming H.-C., and McCarthy J. J. (1996) The role of natural organic matter as a coating on iron oxide and quartz. *Archives of Hydrobiology Special Issues in Advanced Limnology* 47, 315-322.

- Schulthess C. P. and Huang C. P. (1990) Adsorption of heavy metals by silicon and aluminum oxide surfaces of clay minerals. *Soil Science Society of American Journal* **54**, 679-688.
- Schwertmann U. and Cornell R. M. (1991) *Oxides in the Laboratory: Preparation and Characterization*. VCH.
- Seaman J. C. (1998) Retardation of fluorobenzoate tracers in highly weathered soil and groundwater systems. *Soil Science Society of America Journal* **62**(2), 354-361.
- Seaman J. C. (2000) Thin-foil SEM analysis of groundwater colloids: reducing instrument and operator bias. *Environmental Science and Technology* **34**, 187-191.
- Seaman J. C., Bertsch P. M., and Strom R. N. (1997) Characterization of colloids mobilized from southeastern coastal plain sediments. *Environmental Science and Technology* **31**, 2782-2790.
- Steele H. M., Wright K., and Hillier I. H. (2002) Modelling the adsorption of uranyl on the surface of goethite. *Geochimica et Cosmochimica Acta* **66**(8), 1305-1310.
- Stumm W. and Morgan J. J. (1996) *Aquatic Chemistry: Chemical Equilibria and Rates in Natural Waters*. John Wiley & Sons, Inc.
- Summerhayes C. P., Ellis J. P., and Stoffers P. (1985) Estuaries as sinks for sediments and industrial wastes -- a case history from the Massachusetts coast. In *Contributions to Sedimentology*, Vol. 14 (ed. H. Fuchlbaum, A. P. Lesitzyn, J. D. Milliman, and E. Siebold). E. Schweizerbart'sche Verlagsbuchhandlung (Nägele u. Obermiller).
- Sung W. (1995) Some observations on surface partitioning of Cd, Cu, and Zn in estuaries. *Environmental Science and Technology* **29**, 1303-1312.
- Swartz C. H. and Gschwend P. M. (1998) Mechanisms controlling release of colloids to groundwater in a southeastern coastal plain aquifer sand. *Environmental Science and Technology* **32**, 1779-1785.
- Swartz C. H., Ulery A. L., and Gschwend P. M. (1997) An AEM-TEM study of nanometer-scale mineral associations in an aquifer sand: Implications for colloid mobilization. *Geochimica et Cosmochimica Acta* **61**(4), 707-718.
- Takahashi K. and Tanaka K. (1986) Adsorption of copper ion and alkyldithiocarbonate at silica by a molecular orbital method. *Journal of Colloid and Interface Science* **113**(1), 21-31.
- Tessier A. (1993) Sorption of trace elements on natural particles in oxic environments. In *Environmental Particles*, Vol. 2 (ed. J. Buffle and H. P. van Leeuwen), pp. 425-453. Lewis.
- Tessier A., Couillard Y., Campbell P. G. C., and Auclair J. C. (1993) Modeling Cd partitioning in oxic lake sediments and Cd concentrations in the freshwater bivalve *Anodonta grandis*. *Limnology and Oceanography* **38**(1), 1-17.
- Tessier A., Fortin D., Belzile N., DeVitre R. R., and Leppard G. G. (1996) Metal sorption to diagenetic iron and manganese oxyhydroxides and associated organic matter: narrowing the gap between field and laboratory measurements. *Geochimica et Cosmochimica Acta* **60**(3), 387-404.

- Tipping E. (1984) Humic substances and the surface properties of iron oxides in freshwaters. In *Transfer Processes in Cohesive Sediment Systems* (ed. W. R. Parker and D. J. J. Kinsman), pp. 31-47. Plenum Press.
- Tipping E., Griffith J. R., and Hilton J. (1983) The effect of adsorbed humic substances on the uptake of copper(II) by goethite. *Croatica Chemica Acta* 56(4), 613-621.
- Truesdail S. E., Lukasik J., Farrah S. R., Shah D. O., and Dickinson R. B. (1998) Analysis of bacterial deposition on metal (hydr)oxide-coated sand filter media. *Journal of Colloid and Interface Science* 203, 369-378.
- Turner A., Millward G. E., Hale A. J., and Morris A. W. (1993) Application of the K_D concept to the study of trace metal removal and desorption during estuarine mixing. *Estuarine, Coastal and Shelf Science* 36, 1-13.
- Vulava V. M. and Seaman J. C. (2000) Mobilization of lead from highly weathered porous material by extracting agents. *Environmental Science and Technology* 34, 4828-4834.
- Warren L. A. and Haack E. A. (2000) Biogeochemical controls on metal behavior in freshwater environments. *Earth-Science Reviews* 54, 261-320.
- Waychunas G. A., Davis J. A., and Reitmeyer R. (1998) Aqueous Fe^{3+} sorption on silica surfaces, pp. 350-352. Stanford Linear Accelerator Center.
- Waychunas G. A., Davis J. A., and Reitmeyer R. (1999) GIXAFS study of Fe^{3+} sorption and precipitation on natural quartz surfaces. *Journal of Synchrotron Radiation* 6, 615-617.
- Waychunas G. A., Davis J. A., and Reitmeyer R. (1999) Initial $Fe(III)$ hydroxide precipitation processes on quartz surfaces. *American Chemical Society National Meeting*.
- Waychunas G. A., Rea B. A., Fuller C. C., and Davis J. A. (1993) Surface chemistry of ferrihydrite: Part 1. EXAFS studies of the geometry of coprecipitated and adsorbed arsenate. *Geochimica et Cosmochimica Acta* 57, 2251-2269.
- Webb P. A. and Orr C. (1997) *Analytical Methods in Fine Particle Technology*. Micromeritics Instrument Corporation.
- Williams T. P., Bubb J. M., and Lester J. N. (1994) Metal accumulation within salt marsh environments: a review. *Marine Pollution Bulletin* 28(5), 277-290.
- Xia K., Bleam W., and Helmke P. A. (1997) Studies of the nature of Cu^{2+} and Pb^{2+} binding sites in aquatic and soil humic substances using X-ray absorption spectroscopy. *Geochimica et Cosmochimica Acta* 61(11), 2211-2221.
- Xia K., Mehadi A., Taylor R. W., and Bleam W. (1997) X-ray adsorption and electron paramagnetic resonance studies of $Cu(II)$ sorbed to silica: surface-induced precipitation at low surface coverages. *Journal of Colloid and Interface Science* 185, 252-257.
- Yao W. and Millero F. J. (1996) Adsorption of phosphate on manganese dioxide in seawater. *Environmental Science and Technology* 30, 536-541.
- Zachara J. M., Ainsworth C. C., Cowan C. E., and Resch C. T. (1989) Adsorption of chromate by subsurface soil horizons. *Soil Science Society of America Journal* 53, 418-428.

Zachara J. M., Resch C. T., and Smith S. C. (1994) Influence of humic substances on Co^{2+} sorption by a subsurface mineral separate and its mineralogic components. *Geochimica et Cosmochimica Acta* 58(2), 553-566.

Zhuang J. and Yu G.-R. (2002) Effects of surface coatings on electrochemical properties and contaminant sorption of clay minerals. *Chemosphere* 49, 619-628.

VITA**KEA U. DUCKENFIELD**

Born in Colorado Springs, Colorado, 3 September, 1969. Graduated from Fountain Valley School in 1987. Earned B.A. in geology from Carleton College in 1991. Received M.A. in classics from the University of Iowa in 1994. Entered doctoral program at the College of William & Mary, School of Marine Science, in 1995.